MITIGATION, MONITORING, AND GEOMORPHOLOGY RELATED TO GULLY EROSION OF CULTURAL SITES IN GRAND CANYON

Joel L. Pederson[1], Paul A. Petersen[1,2], William W. Macfarlane[2],
Mark F. Gonzales[3], Keith Kohl[3]

[1]Department of Geology, Utah State University
[2]GEO/Graphics Incorporated
[3]Grand Canyon Monitoring and Research Center, Southwest Biological Science Center

November 2003

Report in fulfillment of cooperative agreement 01WRAG0074 and modifications
between Utah State University and the U.S. Geological Survey,
Grand Canyon Monitoring and Research Center

ACKNOWLEDGMENTS

This report is derived from the Master's Thesis of Paul Petersen through the Department of Geology, Utah State University. Additional funding was provided to Paul Petersen by the Geological Society of America, the Colorado Scientific Society, and the USU Department of Geology. John Schmidt, David Chandler, and Kristin Brown reviewed and edited a draft, and we thank Jen Dierker, Lisa Leap, Kristin Brown, Jay Norton, Stacy Petersen, Sammie Macfarlane, Isaac Larsen, Jesse Allen, and Scott Cragun for field assistance and supplementary data. Finally, we are grateful to Grand Canyon National Park for granting a research permit and access to study sites.

ABSTRACT

Gully erosion has been damaging cultural sites in Grand Canyon over the last several decades, and there is a need to protect these features through monitoring, mitigating, and continuing to improve our understanding of the erosion. The goals of this study were to assess the performance of erosion-control structures, to determine the accuracy and utility of aerial photogrammetry for monitoring gullies, and to build our geomorphic understanding of the erosion. We performed total-station surveys, obtained detailed aerial photographs, and collected several types of geomorphic field data in February and October of 2002 at nine different sites; four in eastern and five in western Grand Canyon. Study sites included 22 gullies with 113 erosion-control structures and two ungullied control sites. Data reduction included photogrammetric remote sensing, survey comparisons and terrain analyses in a geographic information system (GIS), and statistical analysis of survey and field data.

Results indicate the erosion-control structures are generally successful in slowing erosion or causing deposition of sediment. Analogous gullies with no treatments exhibited greater erosion compared to those with rock linings or brush checkdams. Treatments are more prone to be breached or flanked by flow when they are located in reaches of relatively high gradient, and damaged erosion-control structures were less effective than intact structures, apparently increasing erosion in cases. Initial data suggest brush checkdams are more effective in causing sediment deposition and staying intact than rock linings.

Aerial photogrammetry was performed on four sites in western Grand Canyon before and after the summer 2002 monsoon season with 1:1600 scale photographs in order to assess the accuracy and utility of this remote sensing tool for monitoring gully erosion. Accuracy of the photogrammetry was assessed by comparing the photogrammetry data to conventional survey data. Mean vertical error for individual datasets ranged from 6-10 cm, depending upon the degree of data interpolation, and less than 50% of gully knickpoints 10-30 cm in relief could be detected. Likewise, with the compounded error of repeat data collection at sites for successive monitoring, accurracy

was inadequate to identify most decemeter-scale erosion features. Primary sources of error include obstruction of aerial photography by vegetative canopy or shadows, and error across a site also increases with topographic ruggedness and decreases with greater density of photogrammetric data. Considering spatial variation in topographic ruggedness, we calculate the density of photogrammetric data needed to minimize error at sites. Such an optimal data collection in the future could reduce mean error to ~5 cm for individual datasets at this photographic scale.

Improving our understanding of the geomorphology of gully erosion along the Colorado River corridor is required in order to indisputably identify its causes. Repeat ground surveys show that gully erosion is concentrated at knickpoints and that new knickpoints tend to form in relatively steep reaches. Initial field data suggest soil shear strength and infiltration capacity vary significantly with sediment texture, vegetation, and soil crusts. An empirical slope-area erosion threshold for study gullies was successfully applied in a preliminary GIS-based model to identify locations exceeding this threshold, which are hypothetically sensitive to gully erosion.

Based on these results, we recommend that the placement, monitoring, and maintenance of erosion-control structures continue in Grand Canyon as further research is done to test our initial findings, including that brush checkdams are superior to rock linings. Though aerial photogrammetry is not yet suitable for monitoring erosion at sites, it may be at some point in the future with continuing technological advances. In the meantime, human visitation at sites clearly increases erosion and other remote sensing tools need to be explored for monitoring. Finally, future GIS numerical modeling incorporating field-geomorphic data would be a powerful tool for cultural site management and protection, and it is probably the only way to identify the relative importance of different controls on the erosion, including baselevel.

CONTENTS

PREFACE

Gullies in Grand Canyon are eroding a series of middle-to-late Holocene alluvial terraces along the Colorado River corridor and are damaging cultural sites in the process. Monitoring of these sites indicates that the erosion has increased over the last two decades, and it has been hypothesized that the operations of Glen Canyon Dam contribute to this problem (Hereford et al., 1993; Thompson and Potochnik, 2000). Lower-impact methods of monitoring sites need to be explored, and current efforts to reduce gully erosion require evaluation. The goals of this research were to assess the effectiveness of erosion-control structures, test aerial photogrammetry as a tool for monitoring gully erosion, and continue investigating the geomorphology of the gully erosion. Protection of cultural sites in Grand Canyon is the overall theme of the three facets of this research.

Chapter 1 focuses on stone and brush erosion-control structures that have been placed in gully channels over the last several years. The purpose of these structures is to reduce flow velocity and stabilize the channel, but their effectiveness in these tasks has never been formally examined. An analysis of the effectiveness of erosion-control structures is achieved through total-station surveys and field observations of trends in the erosion of treated gullies over the 2002 monsoon season.

Chapter 2 is an account of testing aerial photogrammetry as a method to detect decimeter-scale gully features and to monitor change of these features over time. Conventional ground surveys are precise and relatively accurate, but require intensive site visitation with associated damaging effects. Aerial photogrammetry has the potential to measure detailed topography of an area with minimal impact. We evaluate its success over two data collections using 1:1600 aerial photography, likely near the maximum scale feasible in this setting.

Chapter 3 builds upon previous work by exploring aspects of the geomorphology of gully erosion through a combination of field data collection and GIS topographic analysis. We show that the terrain models produced from our photogrammetry help predict gully-prone areas through GIS modeling. In the future, an improved model parameterized by field data would be a powerful tool for protecting and monitoring cultural sites and identifying the causes of the erosion.

CHAPTER 1: EROSION-CONTROL STRUCTURES

INTRODUCTION

Erosion due to gullying can be an acute problem, and the search for inexpensive, durable, low-maintenance techniques to control gully erosion has proven elusive (Heede, 1966; Gellis et al., 1995; Norton et al., 2002). Many cultural sites that lie along the Colorado River corridor of Grand Canyon National Park are being eroded by gullies (Hereford et al., 1993; Fairley et al., 1994), and erosion-control structures have been installed at many sites to reduce or prevent further erosion, but their performance is uncertain. Our goal has been to provide the first formal evaluation of the effectiveness of these erosion-control structures in Grand Canyon by evaluating their performance in slowing erosion and by evaluating the conditions under which they tend to fail.

BACKGROUND

Gully Erosion in Grand Canyon

Most cultural sites are located in deposits Hereford and others (1993,1996) called the "striped alluvium" and the "alluvium of Pueblo II age", which date from 2500 BC – 300 AD and 700 – 1200 AD, repectively, and consist of fine-grained fluvial sand locally interbedded with eolian sand and gravelly colluvium. Gullies in Grand Canyon have also formed in these same Holocene stream terraces, eolian deposits, and at the toes of hillslopes along the Colorado River corridor. The study gullies are relatively small, ranging from ~20-200 m in thalweg length, and from ~0.2-2.5 m in channel width. They may extend below the older prehistoric terraces associated with cultural sites to younger prehistoric and historic sandy flood deposits, and may terminate on any of the terraces, in side-canyon washes, or the Colorado River itself.

Field observations indicate erosion is driven primarily by infiltration-excess overland flow, is also influenced locally by piping, and is associated with both knickpoint retreat and channel widening from bank undercutting and failure (Appendix B). These processes are common in semi-arid to arid landscapes such as Grand Canyon that feature infrequent, high-intensity precipitation events, low vegetation density, and bedrock exposure.

Hereford et al. (1993) and Thompson and Potochnik (2000) concluded gully incision increased dramatically between 1973 and 1984 based on repeat photographs of sites in both eastern and western Grand Canyon. Hereford et al. (1993) studied changes in daily precipitation and proposed that a period of more intense precipitation from the late 1970s through the 1990s has driven accelerated erosion, but these studies also raised the idea that increased erosion is linked to Glen Canyon Dam. They hypothesized that in the pre-dam era relatively frequent flood deposition prevented gullies from reaching the river, and that the lack of flood deposition in post-dam time has allowed some gullies to reach the Colorado River, reducing their baselevel 3-4 m. These studies document increased gully erosion, yet its causes are still debated.

Professional archaeologists began studying cultural features in Grand Canyon National Park in the early 1950s. The first recognition of the erosion of cultural sites came during increased monitoring immediately after the unexpected July 1983 flood release from Glen Canyon Dam. A complete archaeological inventory was completed along a 410-km-long segment of the Colorado River corridor from the base of Glen Canyon Dam to Separation Canyon in May 1991 (Fairley et al., 1994). One product of this survey was an evaluation of site conditions and impacts, including gully erosion; and monitoring indicated that some form of action was necessary to impede destruction of archaeological sites (Dierker et al., 2002). The Bureau of Reclamation and the NPS conferred with geologists, geomorphologists, archaeologists, trail crew personnel, and Native American tribal members, and decided to construct traditional Zuni-style checkdams of both rock and brush at severely eroding sites. Since September 1995, the National Park Service and the Zuni Conservation Program have installed, monitored, and maintained rock and brush linings, checkdams, and water-diversion structures at 29 different sites along the Colorado River corridor (Dierker et al., 2002). Although some of these structures have remained intact, many need frequent maintenance or have been destroyed.

Erosion-Control Methods

Many attempts have been made to control gully erosion by building dams of concrete, stone, or wood (Heede, 1976). The purpose of checkdams from an engineering

perspective is to locally dissipate flow energy and reduce channel gradient (Jaeggi and Zarn, 1999). Erosion occurs when the driving forces in the flow exceed the resisting forces of the channel boundary. Reducing channel gradient or flow depth proportionally decreases the boundary shear stress driving erosion and acting against the weight and cohesion of sediment in the flow and along the gully channel. The number and height of checkdams needed for engineered erosion control depends on the stable, equilibrium gradient of the sediment being transported and deposited upstream of structures. Checkdams, in effect, are an attempt to adjust the channel gradient to this lower value, which varies with sediment size and channel hydraulic geometry (e.g. Kaetz and Rich, 1939; Hack, 1957). Studies suggest this lower equilibrium gradient may typically be 0.7 times that of the pre-gullied channel (Woolhiser and Lentz, 1965; Heede, 1976). Following this, Heede (1976) used a formula to calculate the required spacing of checkdams:

$$S = H / K \tan\alpha \cos\alpha \quad (1)$$

where S is the spacing (meters), H is the dam height (meters), α is the channel gradient, and K is a constant (0.3 for gradients less than or equal to 0.2, and 0.5 for gradients greater than 0.2). The lower post-gullying equilibrium gradient causes the influence of checkdams to extend only a limited distance upstream (Kaetz and Rich, 1939; Leopold and Bull, 1979). Given time, checkdams are often bypassed or undermined, and it is important to recognize that they do not remedy the basic cause of gully erosion.

Typical erosion-control methods rely on rigid concrete, stone, or log checkdams. Brush structures are also used in some places, for example, by the Zuni Indians in the southwestern United States. These brush structures reduce the erosive power of flows because the high permeability and roughness of woody debris dissipates the power of flows and allows greater time for infiltration (Norton et al., 2002). Brush dams are also cost-effective and take little time to construct. In an assessment on the Zuni Reservation, Gellis et al. (1995) noted 1/3 fewer repairs needed in brush checkdams compared to stone checkdams. Norton et al. (2002) also found that traditional Zuni brush structures were effective, specifically in retarding erosion, reducing scour, and causing deposition of sediment.

Some of the erosion-control structures in Grand Canyon are wood or stone checkdams, but the majority are low-profile rock linings. Many of these rock linings were originally constructed as larger rock and rock-and-brush checkdams, but were reduced by maintenance to the linings in order to prevent future breaching (Dierker et al., 2002). These rock linings serve to armor the channel and increase roughness, hopefully preventing loss of channel and bank material. Fischenich (2001) noted that such armoring can cause local scour where flow is constricted and of higher velocity between clasts. Also, the effects of armoring are not expected to influence the area beyond the structure itself. Unfortunately, little evaluation of rock linings in gullies has been performed, since brush and stone checkdams are more common, especially in larger gullies and arroyos.

METHODS

Cultural sites in two reaches of the river corridor were selected for study with the guidance of National Park Service personnel (Fig. 1.1). All feature one or more gullies, and a total of 22 gullies with 116 erosion-control structures were studied (Table 1.1). This represents 47% of all structures in Grand Canyon National Park, and over 90% are rock linings (Fig. 1.2). Three sites are in eastern Grand Canyon: 60-mile (four gullies), Palisades (four gullies), and Basalt Cliffs (four gullies). 60-mile and Palisades have a history of active erosion, whereas the Basalt Cliffs site had no active knickpoints as of the beginning of this study. Four sites are in western Grand Canyon: Indian Canyon (one gully), Arroyo Grande (four gullies), Granite Park (one gully), and 223-mile (four gullies). 60-mile, Palisades, Arroyo Grande, and 223-mile are also "checkdam control sites," in that they include one eroding gully without any erosion-control features. The study sites are representative of a range of geomorphic settings, degrees of erosion, and erosion-control efforts.

Field data collection occurred in February and October 2002 to bracket the erosional changes associated with the 2002 monsoon precipitation season. Visual assessment and repeat photography of damage to structures from runoff was undertaken, as well as conventional topographic surveys to measure thalweg profiles, channel gradients, planview areas of structures, and drainage areas of entire gullies and areas

above individual erosion-control structures. These survey data were used to compare normalized channel longitudinal profiles for both February and October datasets to determine if treatments trapped sediment or prevented erosion and to explore relations between the condition of erosion-control structures, local channel gradient (gradient <2 m upstream of each erosion treatment), and contributing drainage area. In addition to these surveys, several types of field data were collected to gain an understanding of the catchment properties influencing erosion, including vegetation transects, soil descriptions, geomorphic descriptions, and soil strength and permeability tests.

Summer 2002 Rainfall

Grand Canyon receives ~50% of its yearly rainfall in relatively short, intense thunderstorms during the monsoon season, which generally spans from mid-June until mid-September (Western Regional Climate Center, 2003). These thunderstorms can be highly localized. For example, the largest storm during the study was on September 8, when rangers at Lees Ferry reported 4.6 cm of rainfall in 35 minutes, while the Phantom Ranch weather station recorded only 0.18 cm of precipitation in 24 hours (Table 1.2). Runoff and erosion during the study period was relatively intense at the eastern study sites compared to western sites (Appendix G), and thus eastern sites provide much of the data in our assessment of erosion-control treatments.

RESULTS

Integrity of Erosion-Control Structures

Of the 116 erosion-control structures assessed, 51 (45%) were damaged by erosion at the time of the second data collection in October of 2002. Based on all sites but Palisades (incomplete data), 23% of these damaged structures were intact at the beginning of the research in February of 2002 (Appendix D). Most of those that were already damaged at the beginning of this research underwent further erosion during the study. Of the damaged erosion-control structures, 47% were flanked (eroded at its side; Fig. 1.3), 22% were breached (damaged in the middle; Fig. 1.4), and 31% were both flanked and breached.

The majority of this erosion and damage is interpreted as caused by infiltration-excess overland flow discharging through gully channels. Piping caused measurable headcutting and channel widening over the study period at only the Palisades study site, where it undermined structures and caused bank collapse (Fig. 1.5). A salt pan comprising much of the upper catchment of the Palisades gully system generates high runoff due to its unusually low infiltration capacity (Appendix E), and also encourages piping due to its sodium-rich (dispersive), silty sediment and the macroporosity provided by its desiccation-cracked surface (Appendix B).

Morphometric data of gradient and contributing drainage area immediately above each of the 116 erosion-control structures can be analyzed for correlations to the damage of treatments. Drainage area is a common surrogate for discharge that is especially appropriate in infiltration-excess-dominated settings, and gradient controls the shear stress applied by a given depth of flow from this discharge. Mean gradients of reaches within 2 m of intact structures are 0.11, in contrast to 0.17 for damaged structures (Fig. 1.6A), which is significantly different at $\alpha = 0.1$. Damaged structures exhibit a greater variance in both gradient and contributing area than intact structures (Fig. 1.6). The large variance in contributing drainage area for damaged structures skews the mean to higher values, whereas medians between intact and damaged structures are relatively similar in value, and the drainage area dataset fails a Mann-Whitney U-test for significance (data fail a Kolmogorov-Smirnov normality test). Despite differences in drainage area not being strictly significant, a plot of gradient-drainage area product shows distinct trends between damaged and intact structures (Fig. 1.7). Slope-area product is commonly used as a simple erosivity index because of its similarity to stream power. The trend line representing damaged structures is higher and both trend lines have a negative slope, indicating that structure damage is associated to some degree with both higher gradients and larger contributing drainage areas.

Effectiveness of Erosion-Control Structures

Overall Trends

We tested the effectiveness of structures in trapping sediment and reducing erosion by comparing thalweg longitudinal profiles measured in February and October

2002 at sites in eastern Grand Canyon that underwent measurable erosion during the study period. One "control" gully or reach with no erosion control was included at each site. Relative to the overall gully channel, ~60% of the areas at and immediately above rock linings and brush checkdams were associated with lower denudation or even deposition (Appendix D, summary in Table 1.3). Most of the control gullies denuded more than adjacent, treated gullies or reaches. The exception is the 70-mile site, where the high denudation of the east gully was associated with the failure of five of its six stone linings during the course of this study (Table 1.3). Intact structures were sometimes associated with deposition (Fig. 1.8). In contrast, structures damaged before or during the study denuded more than intact structures at all sites, and they were associated with greater local denudation than the mean of their overall channel (Appendix D). These data are normally distributed, and a t-test indicates that denudation at intact vs. damaged structures is significantly different at the 95% level. Thus, intact erosion-control structures reduce erosion and promote deposition, but when damaged they appear to enhance erosion locally.

60-mile

A tributary gully at the 60-mile site with no erosion-control structures incised, on average, more than either of the two gullies with treatments (Fig. 1.9, Table 1.3). The main gully aggraded slightly in the central, treated reach of the channel, despite this reach being relatively steep. Most of the denudation of the main channel was located in the untreated upper reaches or downstream, not upstream, of erosion-control treatments.

Palisades

The Palisades site is the most complex to assess. Its drainage area and gully dimensions are an order of magnitude larger than most other study sites, and, as mentioned above, its catchment has a very low permeability compared to the other sites and piping is an active process in the upper catchment (Appendix E). In general, the channels of treated gullies at Palisades underwent incision comparable to the other treated gullies at the 60-mile and Basalt Cliffs sites (2–5 cm; Figs. 1.10, 1.11). Two exceptions were a tributary of the south-main Palisades arroyo, with an average incision of ~10 cm

(Fig. 1.10C), and the mouth of the south-main gully (Fig. 1.10A). The incision of the south-main Palisades gully was associated with the headward advance of an existing knickpoint and the formation of another in the steep reach near the gully mouth. This gully also had distinct erosion patterns above and below its confluence with a major tributary (Fig. 1.10A). Only three of the nine erosion-control structures upstream of the confluence with a large tributary were in need of repair, whereas six of the seven structures downstream of the confluence were damaged or obliterated. Average incision upstream of the confluence was less than 4 cm; downstream of the confluence it was nearly 13 cm. Average gradient upstream of the confluence is 0.015, but downstream it is 0.04, and drainage area increases from 61,000 m^2 to 85,000 m^2 at the confluence. The greatest erosion in the north tributary gully is also in its lower, steeper reach (Fig 1.11B).

Basalt Cliffs

All four gullies at the Basalt Cliffs site have similar gradients and drainage areas, but differ in erosion treatment. Brush checkdams at the Basalt Cliffs site were relatively effective at staying intact and in trapping sediment (Figs. 1.12C,D and see Fig. 1.14). The benefits of these structures are localized, however, and most denudation was associated with knickpoints formed between and downstream of the checkdams, especially rock linings. The rock linings that remained intact were successful to a lesser degree in stabilizing the channel (Figs. 1.12A,B), but were not associated with deposition as much as the brush checkdams were (Fig. 1.12C,D). Like the 60-mile and Palisades sites, the treated parts of the Basalt Cliffs gullies fared better than the untreated segments. For example, a gully with only one checkdam aggraded an average of 3 cm upstream of the structure, but eroded an average of 4 cm on the untreated reach downstream of the dam (Fig. 1.12D).

DISCUSSION

Erosion-Control Structure Failure and Maintenance

Our data indicate erosion-control structures worked to slow erosion or, in some cases, cause deposition in comparison to untreated areas over the course of the 2002 monsoon season. But our observations also indicate that structures in relatively steep

gully reaches tend to fail and require maintenance, especially at reach gradients over ~0.2. These damaged features, in turn, exacerbate erosion. Of course, erosion-control structures in Grand Canyon have been placed over steep knickpoints in order to slow erosion, but these structures are then susceptible to damage due to this high gradient. Rock linings seem to be particularly vulnerable, probably because their relatively immobile clasts deflect and concentrate the flow, causing local scour. The key point based the data thus far is that the current erosion-control efforts seem to work to slow erosion, if maintained. Without sustained monitoring and maintenance, structures in high-gradient locations will eventually fail and contribute to the erosion. Installation of checkdams and then their maintenance are two necessary components to erosion control, and existing research suggests low-impact treatments inherently require maintenance (e.g. Norton et al., 2002). Likewise, these efforts can only be expected to slow down the pace or temporarily stop longer-term cycles of gully erosion.

Continued monitoring is also valuable because of the possibility of building a record and tracking these gullies through predictable erosional changes. A discontinuous gully's geometry at a single location can be expected to go through a sequence of changes in form, including initial knickpoint incision, then widening, and finally deposition ahead of the next migrating knickpoint (e.g. Gellis et al., 1991; Elliot et al., 1999). Erosion-control structures should be prone to breaching or flanking if the local channel is in the stage of active deepening or widening, and the lower reach of the Palisades south-main arroyo is a current example of this, which may be particularly difficult to mitigate.

It is well established that, for a given contributing drainage area, there is a threshold topographic gradient associated with gully erosion (Schumm and Hadley, 1957; Patton and Schumm, 1975). Our data in Grand Canyon are consistent with this, indicating that local channel gradient and, to a lesser degree, contributing drainage area are effective in predicting where knickpoints form, where erosion happens, and where erosion-control structures will fail. The relatively poor correlation of drainage area to structure failure is probably due to the fact that ephemeral drainages commonly do not increase with drainage area because of infiltration into the streambed (Leopold and Bull, 1979). Also, lower reaches of gullies have higher width-to-depth ratios (Fig. 1.13), and

therefore discharge in the lower catchment may not be deeper (higher in shear stress) than in upper gully reaches. But with more data, the area-slope relation illustrated in figure 1.7 could potentially be used to define a failure threshold for erosion-control structures. This could be used to identify existing structures that are vulnerable to damage, but variation will exist in this due to details of construction and maintenance, as indicated by the scatter in this plot.

Brush Checkdams versus Rock Linings

The Basalt Cliffs site has five erosion-control structures made of woody debris along with stone structures and untreated areas, all in a setting with uniform geomorphic characteristics, which allows for comparison of treatment types. Brush dams fared better than the neighboring rock linings in terms of both damage and erosion control. Repeat observations indicated that all of the brush structures stayed intact and were not associated with local scour (Fig. 1.14). Over half of the rock structures in similar gullies at the same site were destroyed by runoff during the study period (Appendix D). Logically, the more-uniform permeability of brush checkdams slow flow but still let water through without concentrating it, causing deposition and creating a more resilient dam. Our initial observations indicate that, unlike a stone structure, brush structures that are damaged tend to stay somewhat intact or remain effective roughness elements after washing some distance down the channel.

Several studies suggest that woody debris is effective in causing sedimentation and reducing erosion. The majority of these studies were performed in larger, perennial streams in wetter settings than the small gullies studied here, but the general hydraulic qualities of woody debris may be applicable. The fraction of a flow's energy available to move sediment is a function of total channel roughness, which includes in-channel obstructions such as woody debris (Montgomery and Buffington, 1993; Fetherston et al., 1995). Manga and Kirchner (2000) determined that woody debris accounted for nearly 50% of the total flow resistance in a spring-dominated stream in the central Oregon Cascades, despite covering less than 2% of the total streambed, and Fetherston et al. (1995) found that woody debris was responsible for up to 87% of sediment storage in a New Hampshire stream.

Our observations that brush erosion-control structures may be superior to stone are also supported by studies from the region. In New Mexico, Gellis (1996) observed 23 brush structures, only five of which were damaged, compared to our 50% of stone structures and 0% of our five brush checkdams. Norton et al. (2002) found that the Zuni-made brush piles and checkdams in larger gullies and arroyos successfully endured flows up to the magnitude of the 25-year recurrence interval. Larger floods tended to move and redeposit the material in a large debris jam down the channel, which was still beneficial. The intact structures caused large amounts of deposition, and the washed-out structures coalesced to form debris jams, causing upstream deposition. Traditional Zuni approaches simply place as much material as possible in the channels with little reinforcement, negating the hydraulics and scour sometimes attributed to rigid, relatively impermeable rock structures (Norton et al., 2002). Extensive lengths of channel could be treated in such a way rapidly and efficiently.

More study is needed to test this initial finding that brush checkdams may be a better mitigation strategy than stone linings. But if slowing erosion and the destruction of cultural features is the goal, this first round of data indicate that consistently maintained checkdams of woody debris are the best low-impact option.

CHAPTER 1

FIGURES AND TABLES

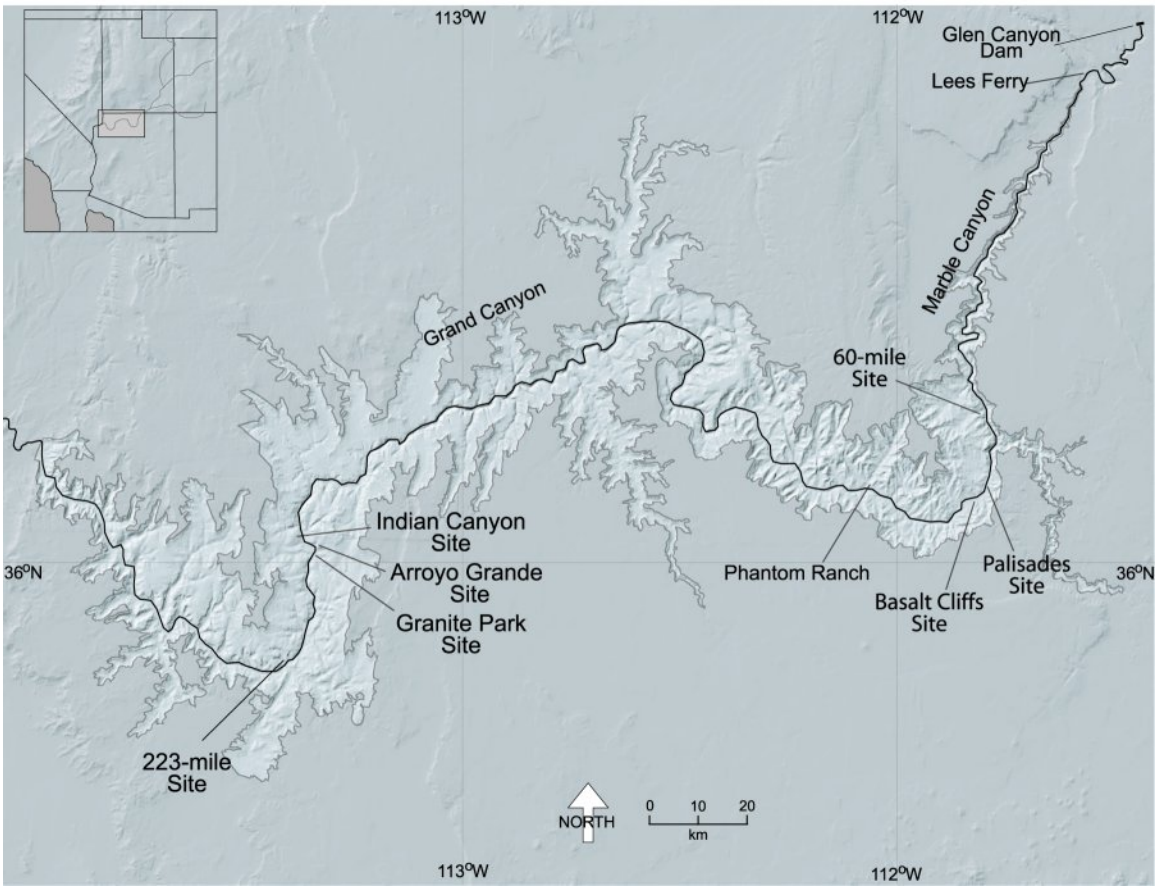

Figure 1.1. Locations of erosion-control study sites.

TABLE 1.1. EROSION-CONTROL STUDY SITE DESCRIPTIONS

Site Name	Mitigation	Geomorphic Setting[1]	Gully	Gradient	Drainage Area (ha)
60-mile	13 rock linings	Bright Angel shale in upper catchment to eolian sand	B1	0.22	0.05
		to termination in side canyon	B2	0.22	0.04
			B3	0.24	0.02
			B4	0.23	NA
Palisades	42 rock linings;	low-relief, large distal debris fan/"playa" catchment to	C1	0.03	8.28
	2 rock checkdams	ap[2] terrace to termination near Colorado River	C2	0.03	0.95
			C3	0.06	0.89
			C4	0.04	0.35
Basalt Cliffs	9 rock linings;	large alluvial fan catchment; drains across toe of fan	D1	0.09	0.36
	5 brush checkdams	to termination on ap terrace	D2	0.08	0.26
			D3	0.08	0.37
			D4	0.08	NA
Indian Canyon	5 rock linings	talus catchment to eolian, ap, and termination on pda[3] sand	F1	0.19	0.05
Arroyo Grande	9 rock linings	basement rock and debris fan catchment to	G1	0.12	0.18
		termination on ap/eolian sand	G2	0.10	0.04
			G3	0.20	0.05
			G4	0.28	0.02
Granite Park	15 rock linings;	Bright Angel bedrock catchment to eolian, slopewash,	H1	0.06	0.16
	1 rock checkdam	and Pleistocene gravel pile to termination on debris fan			
223-mile	15 rock linings	talus/debris fan catchment to eolian/ap sand to	I1	0.26	0.08
		termination in side canyon or on terrace	I2	0.27	0.06
			I3	0.40	<0.01
			I4	0.24	<0.01

[1] Describes up to downslope catchment characteristics

[2] Alluvium of Pueblo II Age (Hereford et al., 1996)

[3] Pre-Dam Alluvium (Hereford et al., 1996)

Figure 1.2. Rock lining erosion-control structures typical of treatments in Grand Canyon.

TABLE 1.2. MAJOR PRECIPITATION EVENTS[1]

Date	Lee's Ferry2	Phantom Ranch2
7/18/2002	2.57	0.00
7/19/2002	0.00	0.08
8/4/2002	1.50	0.25
9/7/2002	0.33	1.32
9/8/2002	4.57	0.18
9/9/2002	0.13	0.25
9/10/2002	0.00	1.27

[1] Units are cm

[2] See Fig. 1.2 for station locations

Figure 1.3. Example of a flanked rock lining at Palisades site.

A

B

Figure 1.4. Rock lining at Basalt Cliffs sites undercut by knickpoint and close to being fully breached. A) February, at the start of research; B) October, at end of study period.

Figure 1.5. Piping along channel side with rock lining at Palisades.

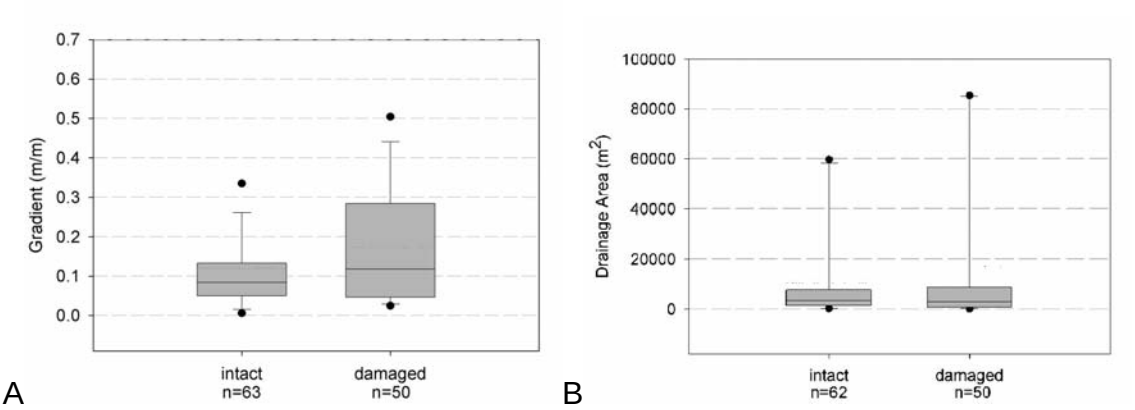

Figure 1.6. Box-and-whisker plots of intact and damaged structures for A) gradient, and B) contributing drainage area. Boxes show 1st (25%), 2nd (median), and 3rd (75%) quartiles, whiskers show outliers at 90%, and dots show outliers at 95%.

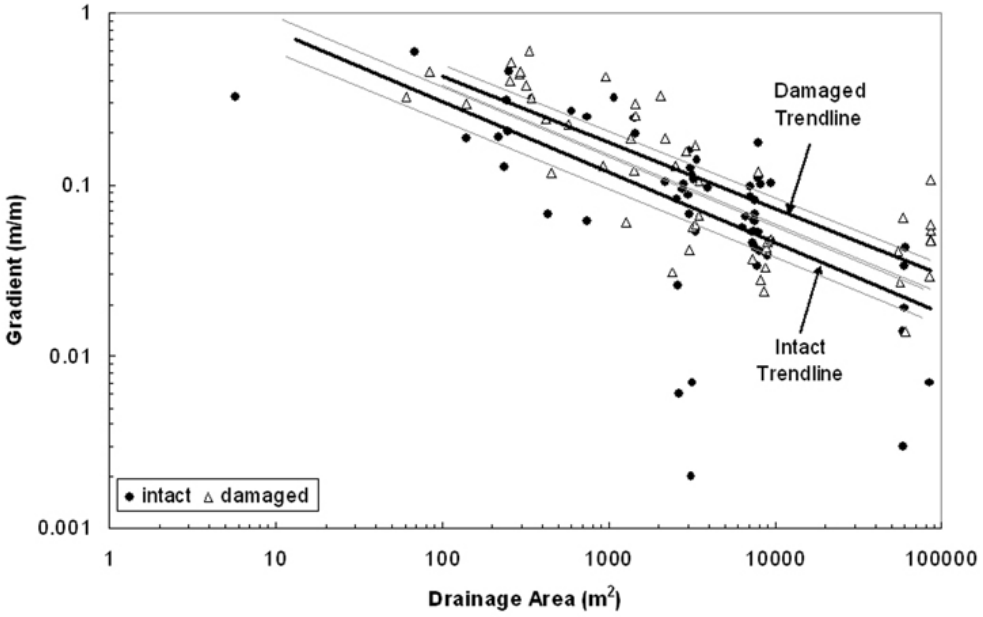

Figure 1.7. Local gradient vs. contributing drainage area for intact and damaged structures. 90% confidence intervals shown by dotted lines.

TABLE 1.3. LOCAL EFFECTS OF EROSION-CONTROL STRUCTURES

Gully	n	% Intact	Channel Denudation (m)[1,3]	Structure Denudation (m)[1,4]	Overall Gully Gradient
60 (west)	2	50	0.014	-0.008	0.211
60 (main)	10	40	-0.020	-0.038	0.212
60 (w trib)[2]	0	0	0.049	na	0.236
palisades (s main)	16	44	0.079	0.030	0.027
palisades (n main)	7	71	0.048	0.045	0.062
palisades (s trib)	8	13	0.045	0.055	0.029
palisades (n trib)	10	80	0.030	0.034	0.054
palisades (small trib)[2]	0	0	0.100	na	0.066
70 (east)	6	17	0.061	0.034	0.070
70 (e most)	3	67	0.032	0.058	0.073
70 (w most)	1	100	0.018	-0.044	0.087
70 (west)	4	100	0.034	-0.006	0.061
70 (untreated reach)[2]	0	0	0.038	na	

[1] Positive numbers represent denudation, negative numbers represent deposition

[2] Control gullies

[3] Mean denudation of the entire channel

[4] Mean denudation within and ~1 m above the erosion control structures

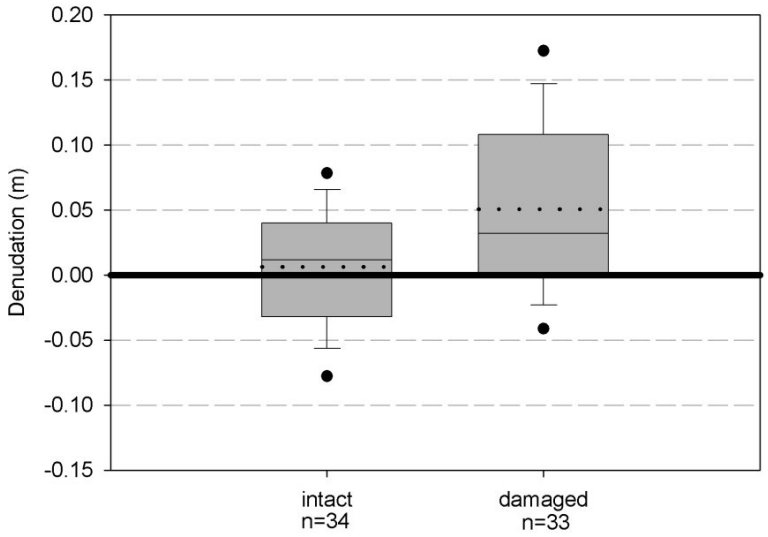

Figure 1.8. Box-and-whisker plot depicting differences in denudation for intact and damaged structures during the study period. Dotted lines show mean, dots show outliers at 5 and 95%. In many, but not all, cases, damaged structures can promote increased local denudation.

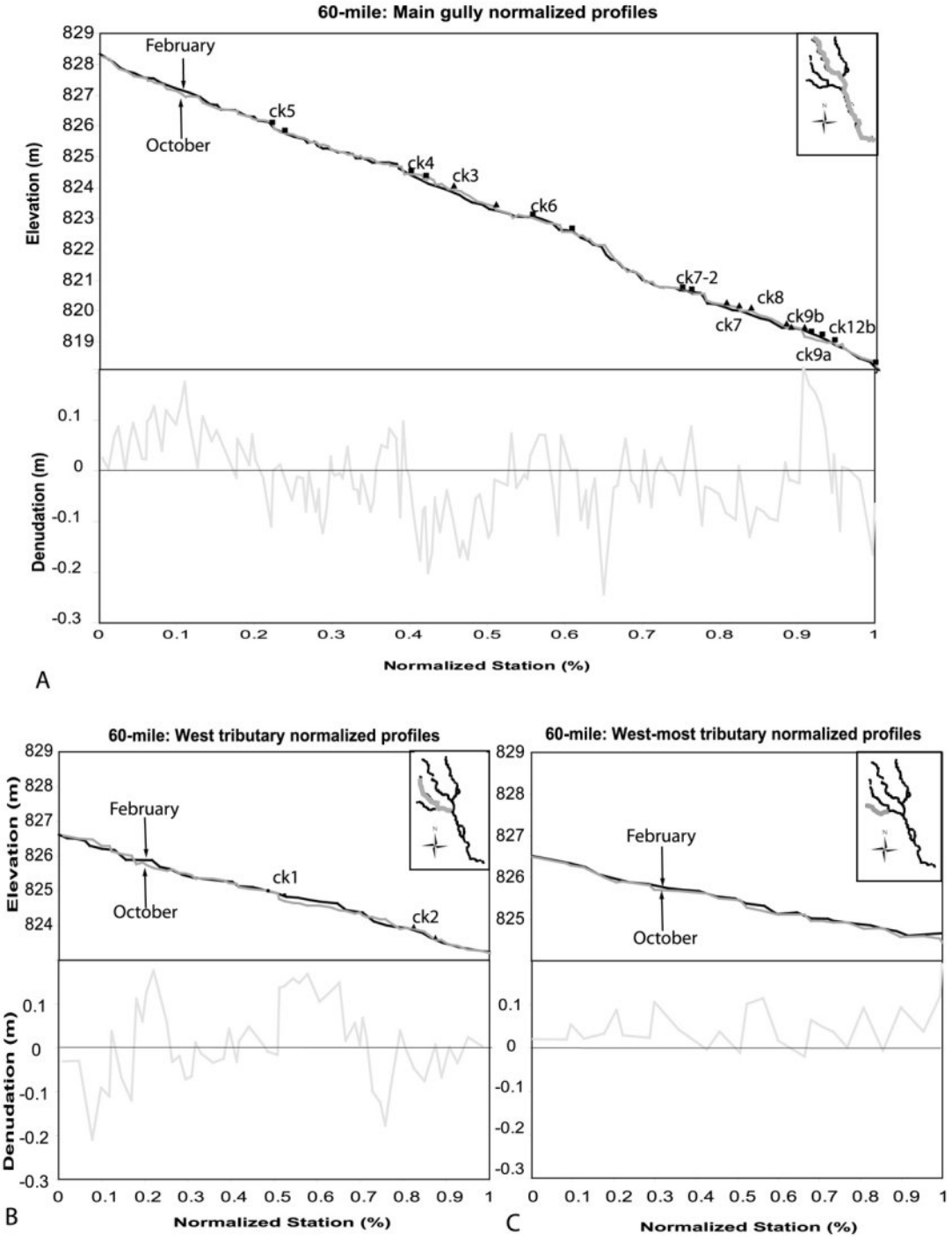

Figure 1.9. February and October normalized longitudinal profiles of 60-mile gullies. A and B contain erosion-control structures and aggraded slightly in places between the two surveys, whereas C has no structures and incised between the two surveys. Squares represent failed structures, triangles represent intact structures.

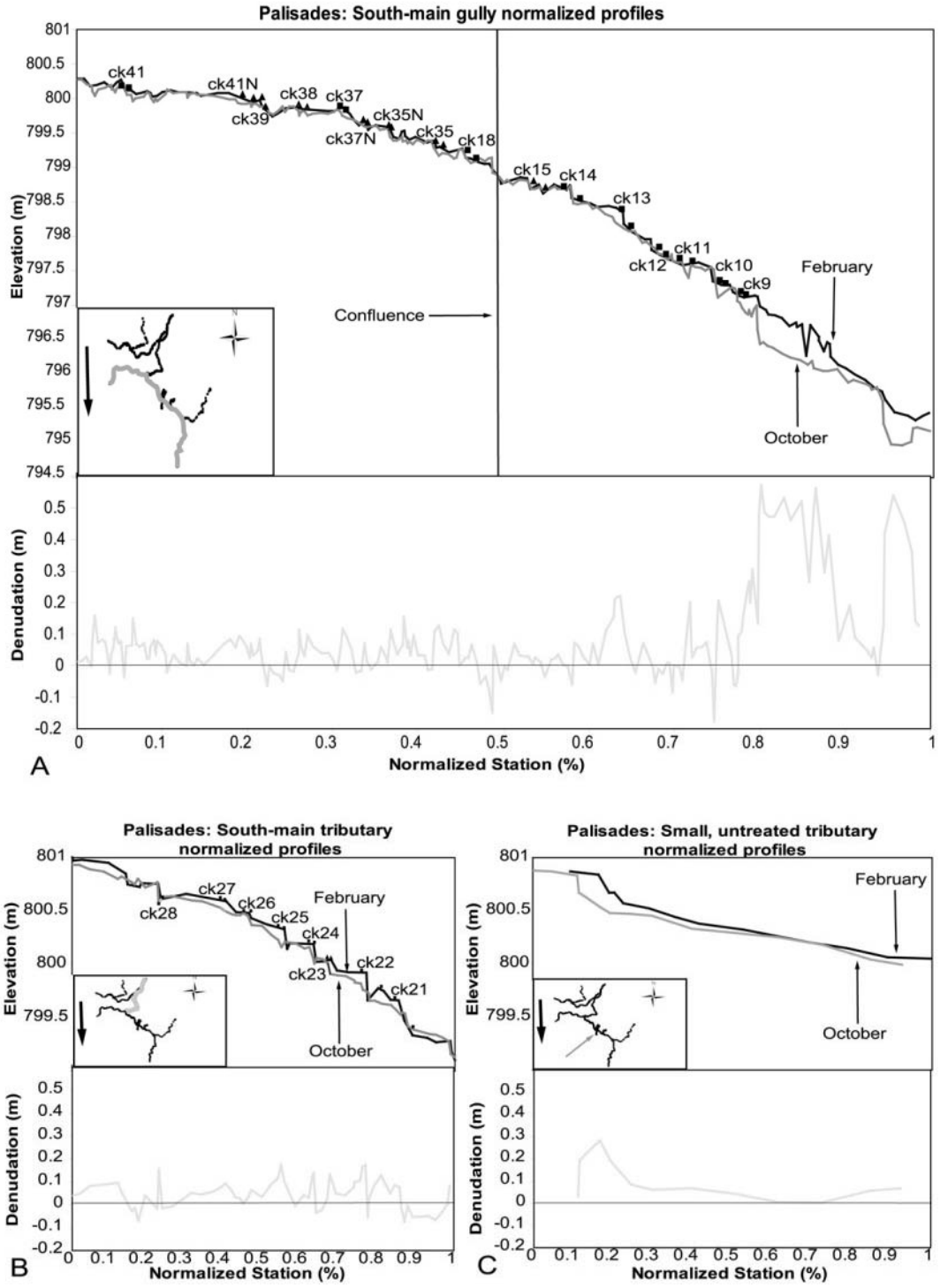

Figure 1.10. February and October normalized longitudinal profiles of south-Palisades gullies. Squares represent failed structures, triangles represent intact structures.

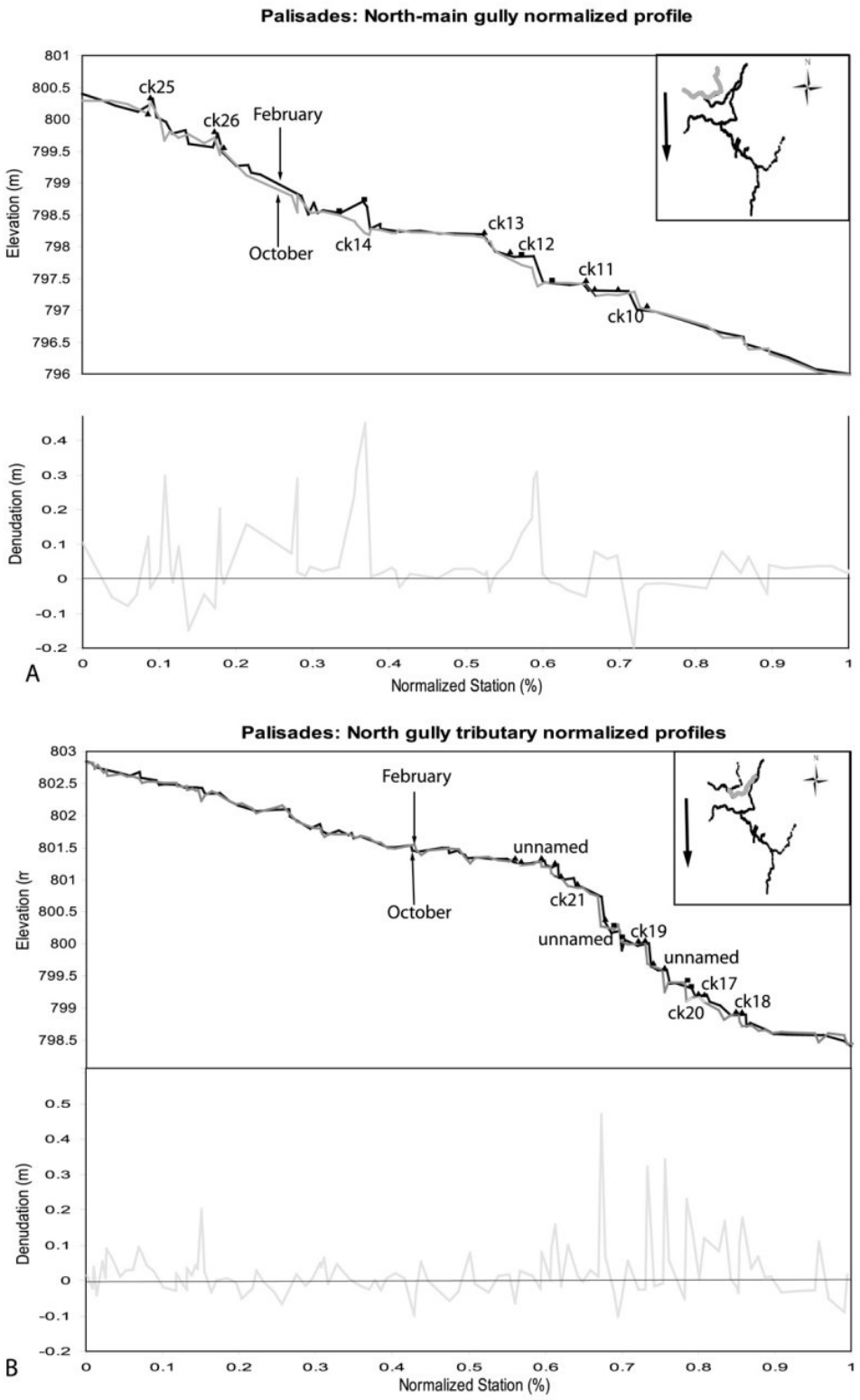

Figure 1.11. February and October normalized longitudinal profiles of north-Palisades gullies. Squares represent failed structures, triangles represent intact structures. Note erosion spikes at damaged structures in A.

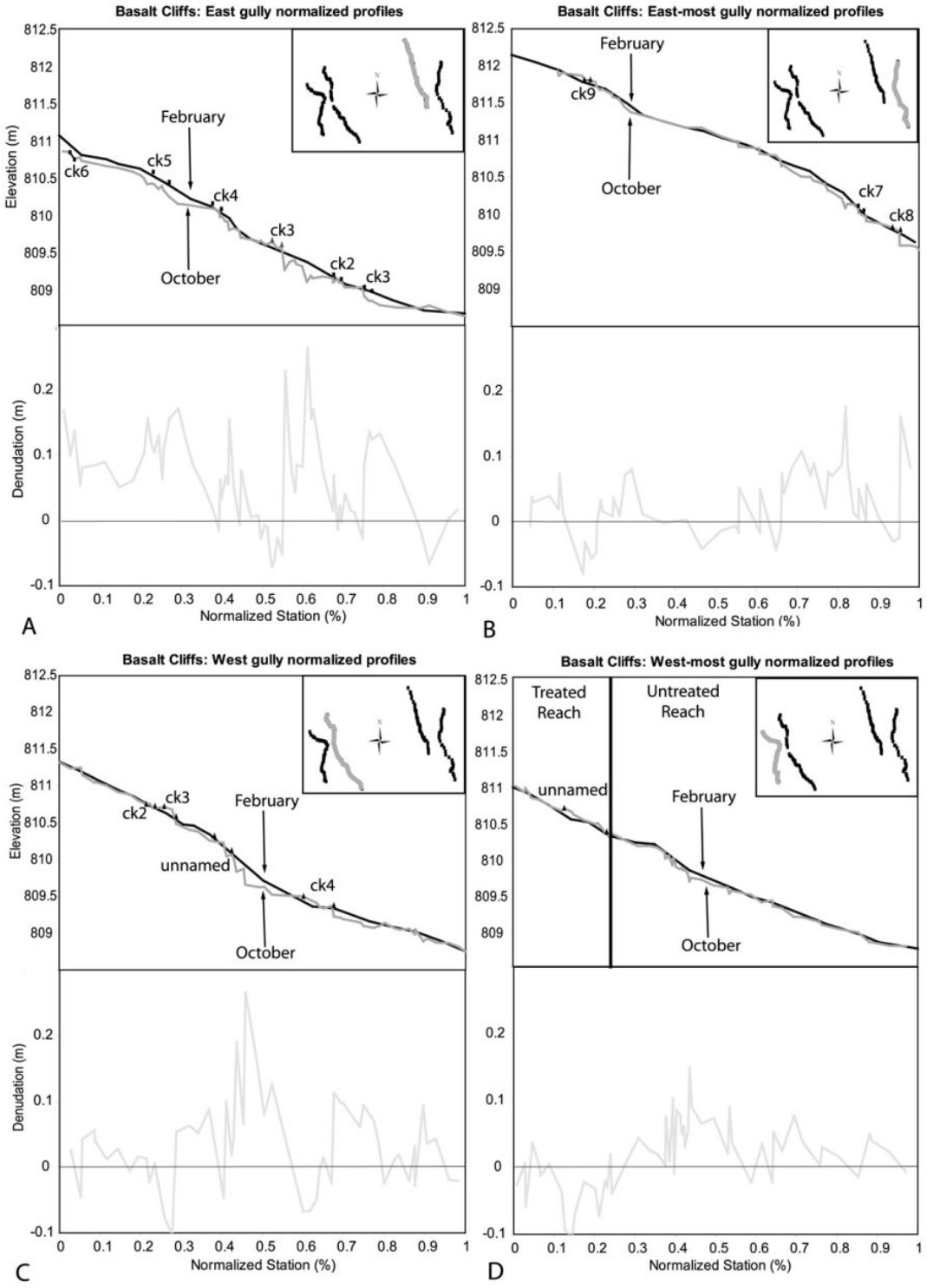

Figure 1.12. February and October normalized longitudinal profiles of Basalt Cliffs gullies. Squares represent failed structures, triangles represent intact structures. Note higher erosion of untreated reach in D. A and B are gullies with only rock linings, whereas C and D feature only brush checkdams.

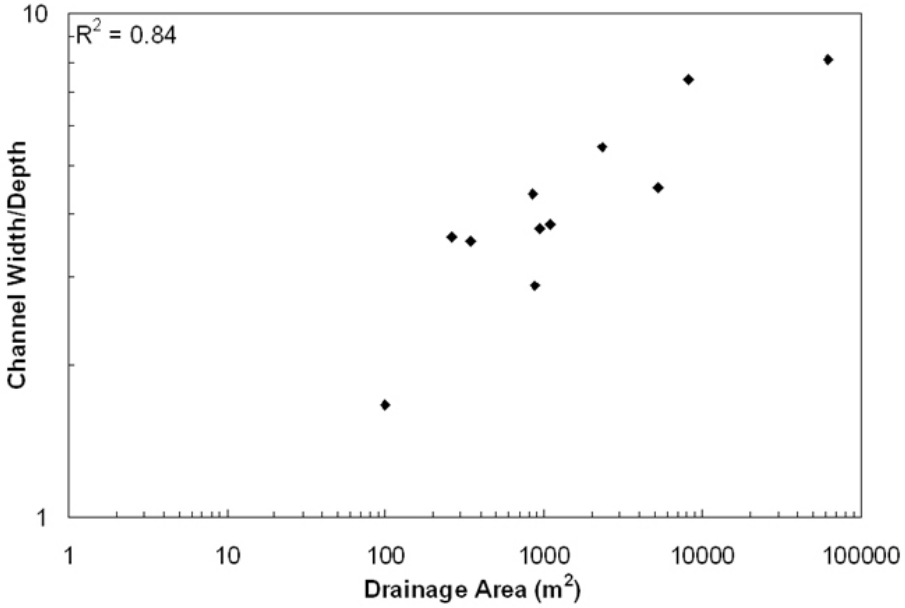

Figure 1.13. Log-log relation between channel width-to-depth ratio and drainage area.

A

B

Figure 1.14. Repeat photographs of brush checkdams at the Basalt Cliffs site. A) February, 2002; B) October, 2002, filled in with sediment. Notebook for scale.

CHAPTER 2: UTILITY OF PHOTOGRAMMETRY IN MONITORING

INTRODUCTION

Gully erosion along the Colorado River corridor in Grand Canyon National Park has increased in magnitude and frequency in the last few decades, and cultural sites are being damaged as a consequence (Hereford et al., 1993; Fairley et al., 1994; Thompson and Potochnik, 2000). Monitoring erosion at cultural sites is essential, but traditional total-station surveys can further risk resources through human trampling and disturbance. Aerial photogrammetry, which derives topography through analysis of stereo photographs, is a promising remote sensing technology that could be used to monitor erosion without ground disturbance. The purpose of this study is to determine the accuracy and the change-detection utility of the current technology in high-resolution aerial photogrammetry as applied in this setting.

Accuracy and detail of photogrammetry are partly controlled by photographic scale. 1:1600 photographs were taken for this research, and this scale is likely near the limit of what is possible in Grand Canyon National Park, considering the impact of low-flying aircraft. Two key elements of our research design are: 1) accuracy of photogrammetry was determined through comparison to conventional ground survey; and 2) separate data collections took place before and after the 2002 summer monsoon runoff-and-erosion season in order evaluate photogrammetry's ability to detect decimeter-scale topographic change.

BACKGROUND

Previous Work

Photogrammetry is a method of measurement using photographic images that was invented in 1851 and is still widely used to model topography. The development of digital photogrammetry has revolutionized the method over the past decade, making it possible to process higher-resolution imagery faster and at a lower cost (Baldi et al., 2002; Heipke, 1995). Several recent studies have applied photogrammetry in

geomorphic and monitoring studies, such as detecting erosion and deposition in mountainous terrain (Oka, 1998; Baldi et al., 2002), shorelines (Hapke and Richmond, 2000; Adams and Chandler, 2002), and stream channels and floodplains (Heritage et al., 1998; O'Brien et al., 2000).

The most recent studies that compare aerial photogrammetry to ground-survey data resulted in mean absolute vertical errors of several decimeters at best (O'Brien et al., 2000; Adams and Chandler, 2002; Baldi et al., 2002), which was sufficient for their respective studies. Several variables have been shown to account for error in photogrammetry, most notably topographic gradient and irregularity (Heritage et al., 1998; Adams and Chandler, 2002; O'Brien et al., 2000; Baldi et al., 2002). Heritage et al. (1998) also showed that photogrammetric point density is correlated to accuracy, and suggested that point density should increase with topographic irregularity. Adams and Chandler (2002), for example, took the important step of using their total methodological error to determine the amount of photogrammetry-detected topographic change needed to be considered genuine geomorphic change rather than measurement uncertainty.

Although terrestrial (ground-based) photogrammetry has achieved very high resolution and accuracy for drainages (Barker et al., 1997; Heritage et al., 1998), to our knowledge no research has attempted to detect decimeter-scale, high relief features such as the gullies we study here using aerial photogrammetry. O'Brien et al. (2000) is the only other study to test the application of photogrammetry in Grand Canyon. They used pre-existing aerial photographs to reconstruct topography of Colorado River sandbars at different time periods using digital photogrammetry, and comparison of these models to ground survey measurements showed that photogrammetry was not as accurate as ground-based topographic surveys. They recommended methods to obtain higher photogrammetric accuracy, which include use of ground-control panels distributed throughout the study sites, smaller scale, higher resolution photographs taken expressly for photogrammetric study, improved methods of image correlation, and more than one study reach. Our research followed these recommendations.

Setting

We studied gully erosion at cultural sites along the Colorado River corridor associated with a suite of Holocene sandy stream deposits and terraces (Hereford et al., 1996). These gullies are relatively small, ranging from 20-200 m in length and 0.2-2.5 m in channel width. Centimeter-to-meter-high knickpoints are common and up-drainage knickpoint migration results in substantial erosion. Gullies on Grand Canyon terraces often feature near-vertical knickpoints with plunge pools, and can retreat over a meter during an intense rainstorm. Most of the study knickpoints are 10-30 cm in height, so it is imperative to test the capability of photogrammetry in achieving decimeter-scale vertical accuracy.

Four sites in western Grand Canyon were selected for photogrammetric study: Indian Canyon, Arroyo Grande, Granite Park, and 223-mile (Fig 2.1). The gullies and associated catchments at these sites span a range of geomorphic settings, but most are characterized by an upper catchment in talus or bedrock at the toe of escarpments, and a middle-lower drainge that is gullied through alluvium or eolian sand (Table 2.1).

METHODS

Ground-Control Survey

Conventional topographic and ground-control-point surveys were performed in late February and mid October 2002, 1-7 days immediately before the respective photogrammetry flights on March 1 and October 15 to ensure no change in elevation between the ground survey and photogrammetry datasets. The purpose of the ground surveys was to: a) conduct a ground-control-point survey, and b) create detailed digital-terrain models (DTMs) of the gullies for both February and October data collections. Individual points and two types of DTMs, triangulated-irregular networks (TINs) and digital-elevation models (DEMs), were used to assess the vertical accuracy of the corresponding photogrammetric data by comparing elevations for specific points of interest, as well as the general elevation agreement of the entire terrain models. Total-station ground surveys followed methods employed in previous Grand Canyon Monitoring and Research Center (GCMRC) research for capturing detailed terrain features by high density data collection and defining slope breaklines, and thalweg

longitudinal profiles to characterize gullies (e.g. Yeatts, 1996; Hazel et al., 2000). Surveys included catchment topography, but focused primarily on recording gullies in detail.

Ground surveys were tied into the GCMRC survey department river-control network. Collected survey data were processed in reference to ellipsoid values to ensure accurate coordinates and good repeatability, rather than orthometric heights, which necessitates the use of a poorly constrained local geoid. The quality of these ground-survey data are key to this research since they are considered the true position that photogrammetry data are measured against. Opening and closing benchmark shots on all surveys were within 2 cm of documented elevations, and we estimate overall conventional-survey error to be ± 5.4 cm considering compounded control, sideshot, centering, and measuring errors. Variability in survey-rod positioning can lead to additional horizontal error up to a few centimeters, but lower vertical error. A preview of our results is assuring, in that comparison of February and October survey data for repeated topographic and control points indicates a vertical median error of < 2 cm (Table 2.3).

A related ground-control point survey for photogrammetry was conducted at the same time as the overall topographic survey. Ten to thirteen black and white, 30 x 30 cm, hourglass-shaped ground-control panels were positioned at each site and then surveyed, and these were used to precisely locate the ground-control points (GCPs) on the photos during the laboratory triangulation process. These panels were evenly distributed over as much of the anticipated photo exposure area as possible.

Photogrammetry

Aerial photography for this research took place on March 1, 2002, and October 15, 2002, by Bechtel Nevada Corporation. Black and white, 1:1600 scale photographs were taken using a Wild RC30 photogrammetric camera with a focal length of 152 mm from a Bell 412 helicopter flying at an average height of 240 m. Many photos were taken at each site, and two photos with 60-80% overlap were selected for each of the four study sites resulting in one stereopair per site. Film negatives were scanned on a VEXCEL VX-4000 photogrammetric scanner, which is a device capable of high image quality and

excellent positional accuracy, at 12.5 microns (2032 dpi) resulting in an image resolution of 2-2.5 cm per pixel.

Aerial triangulation is the process of establishing mathematical relations between aerial photography, the camera, and the ground surface. This information is required as input for the creation of digital stereopairs, DTMs, and orthophotography. We used ERDAS™ IMAGINE OrthoBASE Pro Version 8.5 digital photogrammetry software for all these processes.

The first step in the aerial triangulation process is to perform interior orientation by manually defining the location of fiducial ticks on the photography based on the fiducial locations in the camera calibration report. Our root-mean-square error in this was < 0.3 pixels, ensuring an accurate solution. The next step in aerial triangulation is exterior orientation, which defines the position and angular orientation of the camera when the photos were taken by relating GCPs from ground surveys to their locations on the photography. 150-300 additional tie points common to both photos in a stereopair were used in this process to improve image correlation. A triangulation solution is then developed by the software using the "least-squares bundle block adjustment" algorithm. This process minimizes and distributes the errors associated with the imagery, image measurements, GCPs, and tie points. Before the triangulation solution was accepted, the standard deviation of unit weight (a global indicator of the quality of the triangulation) was less than the pixel size of the original photography. Control points not used in the triangulation process were used as checkpoints for additional quality control, and the triangulated coordinates of these points were computed and compared against their surveyed coordinates.

After the aerial triangulation process was complete, photogrammetric TINs were produced using a semi-automated and a manual approach. In the semi-automated process, the software uses an extraction algorithm that maximized the number of ground-surface points collected while keeping collection on vegetated surfaces to a minimum, and these points were manually edited to remove anomalies. Elevations were collected on a 20-25 cm grid, which is ten times the pixel resolution of the photographs. In the manual process, stereo goggles are used to view stereo pairs on-screen, and a floating cursor is used to estimate elevation of ground surfaces based on where it appears to "set" on a

surface. Manual data collection used ERDAS™ IMAGINE Stereo Analyst, with the color anaglyph mode for the March photos, and with the upgraded to quad-buffered-stereo mode for October photos. Elevations were collected with a point density similar to that of ground surveys, typically 1000-1500 per site. The manual approach ensures collection of topographic breaklines and other channel features, such as knickpoints and channel banks.

Orthorectification, the process of removing the geometric errors in the photography, was completed by using the aerial triangulation solution and the newly derived DTMs to remove the effects of topographic-relief displacement.

Accuracy Assessment

Lateral or planview accuracy in this study is high due to the small pixel size and optimal ground control, but photogrammetry is limited by vertical accuracy, which is the focus of this work. Three levels of investigation were used to assess vertical accuracy: point-to-point, point-to-model, and model-to-model comparisons (Table 2.2). Point-to-point assessment compared photogrammetry elevations for the two data collections to the ground-survey data. Common points from survey and photogrammetry datasets were taken from gullies exhibiting no evidence of change in the field. Points between two datasets that lay within 2.5 cm of each other laterally (our assumed error for survey-rod placement) were located in ArcGIS and their elevations were directly compared. Another point-to-point comparison was the identification of knickpoints using the criteria of decimeter-scale segments of the channel that have gradients over 100%. Planview position of tops of all knickpoints were identified and recorded both in the field with the ground survey and with photogrammetry, and the success of photogrammetry in detecting these was investigated.

Survey point-to-photogrammetry model comparisons were also conducted at each site for both semi-automated and manual photogrammetry collection. These comparisons allowed a more robust accuracy analysis than the point-to-point assessment because of the order-of-magnitude higher number of data comparisons possible and the greater discretion of datapoint location. On the other hand, it involved interpolation of model data between actual collected photogrammetry points. For semi-automated DTMs, we

imported ground-survey points into the Accuracy Assessment Module of ERDAS™ IMAGINE OrthoBASE Pro in order to generate residuals between them and the photogrammetry DTM to calculate vertical accuracy. Accuracies of manual photogrammetric TINs were calculated by importing the ground survey points as an Arc/Info point coverage, and then interpolating the photogrammetry elevations for those points from the manual photogrammetric TINs using the Arc/Info *tinspot* command. This allowed point-specific elevation comparison between the ground surveys and photogrammetry DTMs for entire channels as well as longitudinal profiles.

Model-to-model comparisons involve the most interpolation and have the greatest error, but three-dimensional change detection necessitates the use of terrain models. Photogrammetric and ground-survey TINs were rasterized into 0.2 m grids (a spacing based on gully scale and point density, and matching automatic photogrammetry collection density) and clipped to show only the channels. Model-to-model accuracy was then determined by subtracting ground-survey DEMs from photogrammetric DEMs at each site. *Focalstd* and *pointdensity* commands in Arc/Grid were used to measure terrain irregularity and density of photogrammetry points, respectively, and the relation of these to vertical error was explored.

Model-to-model analyses were also performed in two dimensions through interpolated cross sections. Likewise, this is not expected to be as accurate as point-to-point comparisons, but is also a useful and common exercise for monitoring. At least one cross section was chosen in each gully at locations that featured both high survey and photogrammetry point density, which tended to be in the vicinity of checkdams and knickpoints. Points were created in Terramodel and elevations were extracted from ground-survey and photogrammetry datasets in Arc/Info using *tinspot*.

All data comparisons were in terms of both raw difference (higher or lower in elevation) and absolute value of that difference. Raw differences help in show the full range of data and any preference in the positive or negative direction, whereas absolute values indicate magnitude of difference and are valuable for representing probable error of a single point.

RESULTS

Point-to-Point

Point-to-point elevation comparisons of February and October ground-survey datasets at sites with no observed erosion or deposition yield a normal distribution with a mean and median of zero and an absolute-value mean of 3 cm (Table 2.3, Fig. 2.2A). Analogous comparison of repeat March and October manual photogrammetry points show significantly greater deviation (mean error 9.2 cm) than repeat ground-survey points (Fig. 2.2B). This error distribution is skewed negative by the Granite Park site, but by eliminating the consistently higher October Granite Park data, the March-October photogrammetry error distribution also has a mean and median near zero.

March and October manual photogrammetry points were compared to common ground-survey points from their respective data collections to determine vertical error of the photogrammetry. Means and medians of these comparisons are also near zero, indicating lack of systematic error overestimating or underestimating elevation during manual collection (Fig. 2.2C,D. Absolute mean error for March is 6.6 cm, and for October is 7.6 cm (Table 2.3).

Overall, photogrammetric data collection was able to detect 29% and 25% of knickpoints identified during February and October ground surveys, respectively (Table 2.4). Only four individual knickpoints were resolved at both time intervals, indicating that the repeatability of photogrammetry data at this scale is poor. Photogrammetry was more effective in resolving the locations of knickpoints in planview than in profile view (Table 2.5), but the method was still only able to locate ~50% of surveyed features on average. 26 of 33 (78%) individual knickpoints identified in March were detected again in October. Simply identifying knickpoint position with photogrammetry is somewhat more effective and repeatable than modeling them along the gully profile and obtaining their height and elevation. Detection percentages at each site are consistent between successive surveys, suggesting that the accuracy of photogrammetry is site-variable.

Point-to-model

Semi-automated

Semi-automated photogrammetry collects vast amounts of elevation points in a short time, but does not offer the discretion of manual photogrammetry or ground survey. Residual statistics from the comparison of ground-survey points to semi-automated DTMs show that the March models are more accurate than October, with an absolute mean error for the respective datasets of 8 and 10 cm (Tables 2.6). Semi-automated error distributions are shifted slightly positive, and this is true even when the especially high elevations from the Granite Park October photogrammetry are removed, suggesting that semi-automated photogrammetry data tend to overestimate elevation (Fig. 2.3).

Manual

With manually-collected photogrammetry data, we compared gully longitudinal profiles as well as entire-channel DTMs. Longitudinal-profile comparisons measured the difference between ground-surveyed thalweg elevations and manually-collected photogrammetry elevations interpolated from the channel DTM at the same locations. Again, the March photogrammetry dataset was more accurate than the October dataset (Table 2.7), with absolute-value mean errors of 6 and 9 cm, respectively. Most interpolated profiles represent the form of the true survey profile well (Fig. 2.4A), although clusters of anomalous points that result in higher error exist in reaches that are steep or have overhanging vegetation inhibiting photogrammetric point collection (Fig. 2.4B).

Accuracy of manually collected photogrammetry compared to survey points was also determined by comparing all survey points collected in gullies to elevations extracted from the DTMs in the same locations. Absolute-value mean and standard deviation of error for both March and October datasets are ~10 cm (Table 2.8, Appendix I). Histograms of point-to-model datasets combined for all sites show that the error is normally distributed around zero for the March manual DTMs (Fig. 2.5A). The mean October error is skewed positive at 2 cm (overestimation), but when the Granite Park site is removed the October error drops to zero (Fig. 2.5B,C). Manual collection, unlike

semi-automated, is free of systematic error, with the exception of the consistently high October Granite Park photogrammetry results.

Model-to-Model

Channel DTMs and channel cross sections from photogrammetry were directly compared to those models from ground–survey data in the final phase of accuracy assessment. Ground-survey grids of 20 cm cell size were subtracted from corresponding manual photogrammetry grids for each site and for both March and October data. Complete statistics and spatial trends of grid comparison are in Appendix I. All combined model-to-model comparisons yielded a mean absolute-value error of 10 cm, with a standard deviation of 10 cm (Table 2.9), approximately the same accuracy as point-to-model comparisons (Table 2.8), though the maximum DTM errors of model-to-model comparison (249 cm) tended to be higher than maximum errors resulting from point-to-model (97 cm). This general similarity in error between types of assessment is to be expected since the photogrammetry DEMs used here are direct grid representations of the previously used TINs, and the ground-survey DEMs were derived from TINs constructed with ground points. Thus, little actual interpolation was done. Figure 2.6 illustrates that the spatial distribution of error at a site, and between sites, is very uneven. Channel thalwegs, constrained by abundant data points, have lower error than channel banks with fewer data.

At least one cross section was extracted from both photogrammetry and ground survey TINs of each gully channel for both March and October datasets (Appendix L). These were placed in areas with high ground-survey and photogrammetry point density, such as above erosion-control structures or knickpoints. Accuracy of photogrammetric channel cross-sections compared to ground-survey cross sections was slightly better than that just reported for entire DTMs. Mean absolute-value error for both March and October datasets was 9 cm, standard deviation was <9 cm, and maximum error was <45 cm, respectively, for each time interval (Table 2.10). Since the cross sections were placed in regions of high-density datapoints, fairly accurate representations of the channel could be extracted (Fig. 2.7). As expected, higher-relief cross sections extracted from areas of low data density are less reliable (Fig. 2.7).

Minimizing Photogrammetry Error

One of the themes of our error assessment thus far is the influence of surface ruggedness and point density on DTM data quality, as recognized by others (e.g. Heritage et al., 1998). These trends can be used to map the photogrammetry data density required to minimize error for a given topography in future use of this technology. Standard deviation of surface elevations (SDSE) based on ground survey DEMs was used to quantify and map local topographic ruggedness using the ARC/INFO Grid module function *focalstd* set at 1 x 1 m rectangles across each site (Fig. 2.8). Density of the manual photogrammetric sampling was also quantified using the *pointdensity* function in Grid, which calculates within a moving window the number of elevation points per m^2 (Fig. 2.9). The ratio between photogrammetric sampling density and topographic ruggedness can be used as a topographic index related to the potential photogrammetry error. Dividing the density grid by the SDSE grid creates a map of this index relative to photogrammetry point errors (Fig. 2.10).

An easier evaluation of the relations between these values can be gained by extracting SDSE and density values from these grids at each survey point using *latticespot* to compare to point-to-model error (Fig. 2.11). Tremendous scatter and very large amounts of data exist in these relations, and the general trend can be identified by using a log-bin average. The data indicate a positive relation between the SDSE and associated error (Fig. 2.11A) and a negative relation between photogrammetric sample density and associated error (Fig. 2.11B). By comparing the combined index of point density/SDSE to error for each point, an overall negative relation is apparent (Fig. 2.11C). Importantly, though absolute error steadily decreases with increasing density/SDSE values, this trend ceases when the ratio exceeds ~40 (Fig. 2.11C). This indicates that photogrammetry data collection at densities beyond that needed to provide a local index value of ~40 will result in little or no improvement in accuracy for the terrain of the Grand Canyon study sites. Recognizing this, we can map the minimum photogrammetric sampling density needed to for the most accurate results in a given topography (e.g. Heritage et al., 1998). In this case, multiplying the SDSE grid of a

location by 40 will result in a map of the required density of photogrammetry data (Fig. 2.12, Appendix M).

Detecting Erosion between March and October

Field evidence and repeat photography during the October survey and nearby gauge data indicate at least one substantial runoff and erosion event occurred during the study period in eastern Grand Canyon. However, little to no runoff and erosion occurred in our four study sites in western Grand Canyon, and only two of the 10 gullies studied for photogrammetry exhibited change: Indian Canyon and one gully at 223-mile. Repeat photography and survey-profile comparison show that the upper reach of the Indian Canyon gully incised and widened by several centimeters (Fig. 2.13), and the lower reach of the Indian Canyon gully aggraded slightly. The upper reach of the easternmost 223-mile gully was the site of up to 20 cm of eolian sand deposition (Fig. 2.14). These two gully reaches will be the primary focus of our change detection, and their relatively subtle changes are well-suited for testing the utility of photogrammetry for realistic monitoring.

Before investigating whether this observed change was detected, the uncertainty we have quantified for our tool must be considered. That is, the topographic change we are monitoring must be greater than the inherent error of the photogrammetry in order to detect that change with statistical certainty. Recent studies have done this by using their survey accuracy assessments to calculate the threshold of topographic change needed for true detection (Brasington et al., 2000; Adams and Chandler, 2002). We have shown in the previous section that photogrammetry DTM error varies spatially with topographic ruggedness and the density of data points collected, and it is therefore illogical to assume a single threshold of change detectable across an entire site or even an entire gully. Where the topography is gentle and/or the DTM dense with points, there will be a lower detection threshold than where the gully is deeply incised and DTM points sparse.

It is likewise important in change detection between two datasets to propagate the error of each in calculating the combined error E, as:

$$E = [(e_1)^2 + (e_2)^2]^{0.5} \quad (1)$$

where e_1 and e_2 are the two standard deviation (2σ) error distributions of each dataset (Squires, 1968).

To calculate a spatially variable detection threshold for our sites, density/SDSE grids (like that in Fig. 2.10) were created for both March and October with 0.2 m cell size. From these, grids of the 2σ variance in error were calculated for both March and October data collections, based on linear regression of the point-to-model errors (Fig. 2.15). This variance is an appropriate error threshold because we have shown the error for these data to be centered about a mean of zero. Our 2σ error threshold line for March is:

$$0.55(\text{density/SDSE})^{-0.33} \quad (2)$$

and 2σ error threshold for October is:

$$0.64(\text{density/SDSE})^{-0.31} \quad (3)$$

These power functions illustrate again that the October data are not as accurate as the March data at a given density/SDSE value (Fig. 2.15).

Error of these October and March 2σ error grids was combined by applying Equation 1 to create a critical-error grid. This combined error is also a very conservative representation of the spatially distributed threshold amount of erosion that can be detected with successive photogrammetry datasets. The thresholds of erosion detection for the Indian Canyon and 223-mile sites are several decimeters when density/SDSE is low (< 20) and are ~20 cm when density/SDSE is 40 or higher, and Fig. 2.15 illustrates this for all four sites combined. This means that, in this setting and at this photographic scale, even optimized photogrammetry with minimized error can only confidently detect topographic changes of 20 cm or greater with repeat monitoring.

A map of elevational change in simplified terms of erosion, deposition, and no change, was created by subtracting gridded October photogrammetry elevations from March photogrammetry elevations at each of the two sites of interest. A query was then performed to identify values in this change grid that exceed the values of the threshold-detection grid and assign them as either positive (erosion) or negative (deposition). Grid cells that do not exceed the critical values were considered to show no change (Figs. 2.16B, 2.17B). These photogrammetric-detected change maps can be compared to analogous ground-survey detection maps, which we made by subtracting October from February ground-survey elevation grids and using a conservative, fixed detection

threshold of 10 cm (compounded 2σ ground-survey variance of 7.2 cm, Table 2.3) (Figs. 2.16A, 2.17A).

The erosion observed in the upper reach of the Indian Canyon gully (Fig. 2.13) is evident in the ground-survey comparison, but was undetected by repeat photogrammetry, strictly speaking (Fig. 2.16). The lower reach of the same channel is lower in gradient and less incised, and a limited amount of deposition was detected in both photogrammetry and ground-survey change grids. Only 12 cells in the eastern-most 223-mile gully that had eolian deposition with enough vertical change to be detected by photogrammetry (Fig. 2.17). The <20 cm of aggradation observed in the field in the upper reach of this gully is not quite in the range of detectable change.

Comparison of repeat gully longitudinal profiles is an exercise that would commonly be used to illustrate geomorphic change along a gully, and the most dense photogrammetry DTM data are along the thalweg. Each photogrammetry long-profile data point has an associated density/SDSE ratio and error, which can be applied to change detection at each point. The photogrammetry profiles will show significant change where the difference of the March and October elevations at each point exceeds the error associated with the density/SDSE, as outlined above. Profiles from the Indian Canyon gully have only four points of significant change between the two photogrammetry DTMs, all of which were deposition (Fig. 2.18), whereas survey data indicate several places along the profile with >10 cm detection threshold erosion and only one location of deposition. The 223-mile eastern-most gully profiles for photogrammetry seem to indicate overall deposition, but not enough to be considered truly detectable (Fig. 2.19), whereas ground-survey data detected significant deposition in upper reaches. In summary, our photogrammetry generally failed to confidently monitor the moderate-to-subtle changes observed in the field.

DISCUSSION

Semi-Automated and Manual Photogrammetry Accuracy

The accuracies associated with the manual approach to photogrammetry data collection are a bit higher than the semi-automated collection accuracies. The manual approach is also superior in modeling particular features, in that the semi-automated

method did not necessarily collect data points in areas of interest such as gully walls, thalwegs, and knickpoints. This phenomenon is partly due to the fact that many gully features are in sandy, low-contrast areas of images making it difficult for the automatic extraction algorithm to collect points on these features. Manual collection was performed specifically to define knickpoints, thalwegs, channel sides, and other breaklines, resulting in a better DTM. O'Brien et al. (2000) found the opposite in their sandbar monitoring study. More systematic error was present in their manual collection, but they studied low-relief, broadly convex topography, rather than the sharp declivities of our gullies.

Semi-automated collection also falls short because of its tendency to overestimate elevation due to the lack of control in capturing the true shape of gullies; in particular, vertical gully walls. Vegetation probably also contributes to overestimation in semi-automated in areas near or under the canopy of shrubs and cacti (Fig. 2.20). Many of the automatic DTM points are preferentially collected along the periphery and within vegetation, due to their high tonal contrast. Consequently, points that end up being collected on top of the vegetation contribute to the positive error. To remedy this, a particular set of DTM extraction parameters may be selected to limit the collection of points in vegetated areas, but this results in low point density and the increased error inherent with greater interpolation. Also, the greater positive error of the October semi-automated DTMs (Fig. 2.3) is partly the result of a fully leaved plant canopy during October relative to March. The Arroyo Grande site had the most vegetation obstructing surveyed gullies, driving the relatively high semi-automated and manual error for October (Fig 2.21B).

Poor October photo quality is another factor influencing photogrammetric accuracy. We observed that the October flight photos were blurry compared to the March photos. This lower photo quality was due to greater cloudiness and high helicopter velocity during October photography (55 knots). This combination caused the shutter to remain open longer with excessive movement over a pixel during exposure (Philip A. Davis, USGS, personal communication, 2002). This blurriness caused greater difficulty in collecting precise photogrammetry data.

Our highest errors in manual photogrammetry data collection consistently occurred in highly vegetated or high-relief, shadowed areas, and attempts to collect points through the vegetation or shadow obstruction often resulted in 1-2 m errors (Fig. 2.21). We found that it was actually better to collect as few points as possible in these shadowy or shrubby regions where the ground is obscured. Relatively low accuracy in steep or topographically irregular areas was also observed by Heritage et al. (1998), O'Brien et al. (2000), Baldi et al. (2002), and Adams and Chandler (2002). Analyzing photogrammetry error in terms of point density and SDSE indirectly factors in the error from vegetation and shadows. These sources of error are captured in the density and ruggedness analysis, since steep, high-relief channels that cast shadows have a high SDSE, and surfaces that are obstructed by shadows or vegetation tend to have low manual DTM point density.

Absolute-value mean and standard deviations of error of individual datasets ranged between 6 cm for point-to-point accuracy assessment, to 11 cm for model-to-model. In terms of types of analyses typical for monitoring, using a DTM is advantageous in that elevations can be interpolated at any location and the site can be visualized completely. But if the number of data points in the model is not enough to represent landscape ruggedness, the model will be inaccurate. The profile and cross sections extracted from DTMs were more accurate than the overall DTMs, and consistently exhibited sub-decimeter error. Lowest DTM errors tend to be along the axis of the gully channel, which is usually flat (low SDSE), and highest errors tend to be on channel banks and other high-relief features.

Point-to-point comparisons give the best estimate of strict vertical accuracy for each dataset. As a rule-of-thumb, photogrammetric accuracy is often thought of as twice the pixel resolution of the original photographs. Our pixel resolution is about 2.5 cm, and so it might be predicted that our best possible accuracy is ~5 cm, and this is about right. Our mean point-to-point error for March is 6.6 cm, for October it is 7.6 cm, and mean accuracy peaks at about 5 cm for March and 6.5 cm for October when the density/SDSE reaches a value of ~40. Under ideal circumstances an error magnitude of ~5 cm may be obtained if a density/SDSE value of 40 is reached throughout a site, but real-world monitoring is usually less than ideal. This density/SDSE threshold of 40 at our sites will

vary with different applications and locations, but it is useful for future monitoring in Grand Canyon in that one can save time and money by using resultant maps to predetermine the required point density for a desired accuracy.

Although we have used the best methods practically available, direct georeferencing, the real-time measurement of the position and orientation of the camera and photographs, was not available. The ideal georeferencing method uses an integrated system consisting of a Global Positioning System (GPS) and an Inertial Measurement Unit (IMU) to calculate the exterior orientation parameters. The airborne GPS provides position information (i.e., X, Y, and Z) about where the camera is at the time of image capture, whereas the IMU provides orientation information (i.e., Ω, Φ, and K) for the camera. Onboard GPS and IMU may improve model quality relative to aerial triangulation, which estimates exterior orientation parameters using ground-control-point data. The greatest benefit to direct georeferencing is the elimination of ground control, which would reduce costs and lower even further the site impacts in places such as Grand Canyon.

A strong control on accuracy that also controls cost is the scale of photography. Our results indicate an accuracy of 5-7 cm for 1:1600 aerial photogrammetry, but accuracy is also dependent on image quality, use of ground-control panels, accuracy of GCPs, shadows, vegetation, topography, point density, and the ability of the photogrammetrist. Figure 2.22 shows the accuracy of photogrammetric terrain models in this and other studies derived from different scales of aerial photography. The scatter in this is due to differences in these other factors besides photographic scale, and also complications arising from comparing studies with different methods of reporting accuracy. Other studies use mostly DTMs, and the error they report is analogous to our point-to-model or model-to-model values. Because of this, we place the accuracy from this study at 10 cm to be consistent with the other studies. Given these caveats, figure 2.22 may be broadly useful in future decisions about the scale of photography needed to achieve a given accuracy and change-detection threshold.

Photogrammetric Change Detection

Repeat photogrammetry failed to consistently detect 10-20 cm changes in elevation observed in the field and detected with ground surveys, partially due to the effects of error propagation. Obtaining density/SDSE values near 40 throughout these Grand Canyon sites should result in consistent detection of change greater than ~20 cm. Our purpose here was to try to detect gully channels and knickpoints at a smaller, centimeter-to-decimeter scale. The aerial photogrammetric method in its present technology, although obtaining very high accuracies relative to previous work, appears to be just below the threshold of resolution and change detection needed for yearly monitoring and rigorous geomorphic study of gully erosion in Grand Canyon.

Photogrammetry also falls short for change detection due to its inability to consistently identify knickpoints due to obstruction by shadows, vegetation, and vertical gully walls. For example, knickpoints in the Arroyo Grande site were covered by the overhanging vegetation (Figure 2.21B), causing this site's very low detection percentage of 8% (Table 2.4). The low-gradient, low-relief, relatively non-vegetated gully at the Granite Park site accommodated the best knickpoint detection, but ~50% of the knickpoints still were not identified. The poor detection and repeatability with respect to knickpoints is of concern, since tracking a knickpoint over time is a basic goal of monitoring these sites.

Despite its present shortcomings, aerial photogrammetry could have a future in monitoring gullies in Grand Canyon. Improvements to the technology, including the broader use of aircraft IMU-GPS, may eventually improve accuracy and efficiency to an acceptable level in terms of both the detail of data and elevation of flight required. Photogrammetry could be useful now to detect larger features. For example, the significant erosion recorded by ground surveys at the Palisades site of eastern Grand Canyon (Chapter 1) could confidently be detected. We have concentrated on vertical accuracy, but photogrammetry's relatively high planview accuracy may be useful for present monitoring. For example, the subtle incision observed at Indian Canyon was not detectable or measurable in the vertical dimension, but the creation of this newly formed knickpoint could be documented and its position recorded with high accuracy.

CHAPTER 2

FIGURES AND TABLES

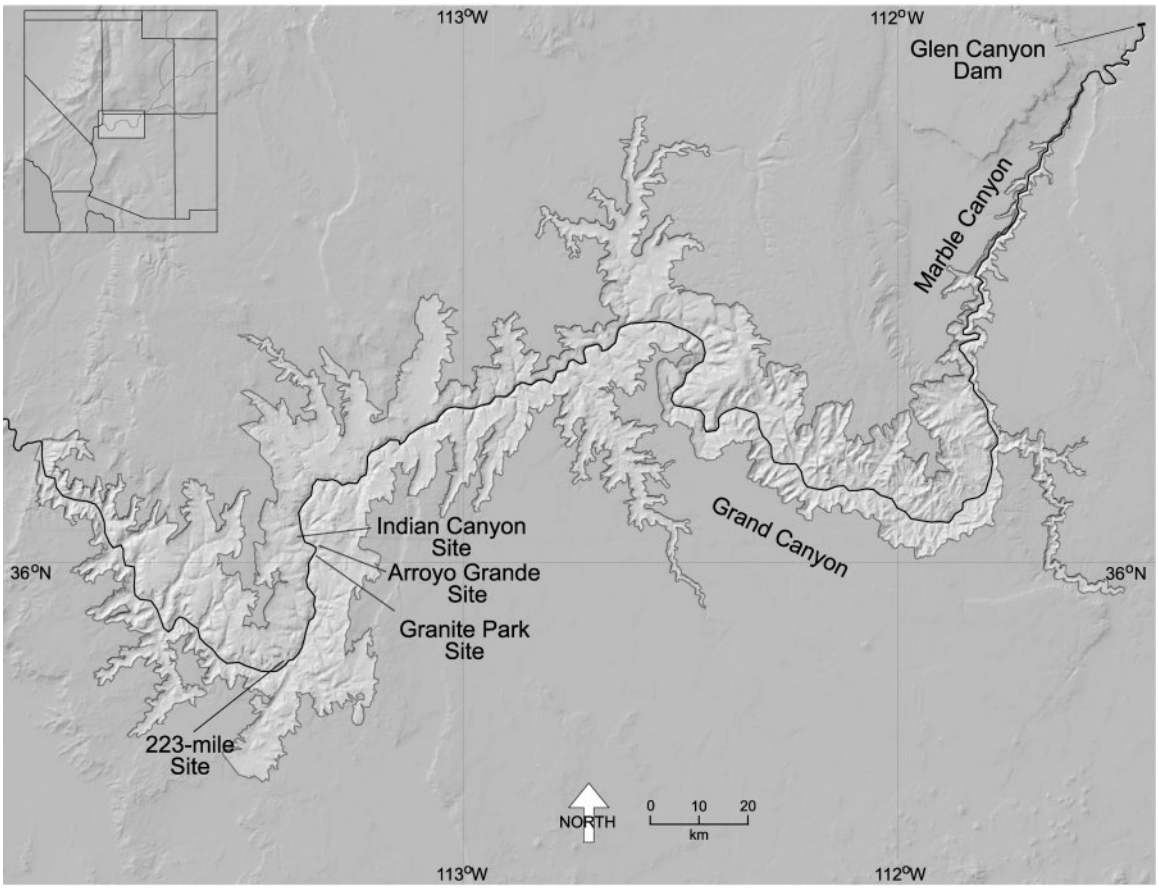

Figure 2.1. Photogrammetry study sites in western Grand Canyon.

TABLE 2.1. PHOTOGRAMMETRY STUDY SITE DESCRIPTIONS

Site Name	Mitigation	Geomorphic Setting[1]	Gully	Gully Relief (m)	Gully Length (m)	Gradient (m/m)
Indian Canyon	5 rock linings	talus catchment to eolian, ap2, and termination on pda3 sand	F1	27	140	0.19
Arroyo Grande	9 rock linings	basement rock and debris fan catchment to termination on ap/eolian sand	G1	26	207	0.12
			G2	12	117	0.10
			G3	5	23	0.20
			G4	5	18	0.28
Granite Park	15 rock linings; 1 rock checkdam	Bright Angel bedrock catchment to eolian, slopewash, and Pleistocene gravel pile to termination on debris fan	H1	11	190	0.06
223-mile	15 rock linings	talus/debris fan catchment to eolian/ap sand to termination in side canyon or on terrace	I1	12	45	0.26
			I2	9	33	0.27
			I3	6	15	0.40
			I4	9	37	0.24

[1] Describes up to downslope catchment characteristics
[2] Alluvium of Pueblo II Age (Hereford et al., 1996)
[3] Pre-Dam Alluvium (Hereford et al., 1996)

TABLE 2.2. LEVELS OF ACCURACY ASSESSMENT

Level	Data Compared	Products
Point-to-Point	Survey points -TO- Manual photogrammetry points	Determines accuracy without interpolation, knickpoint detection and repeatability
Point-to-Model	Survey points -TO- Semi-automated and manual photogrammetry TINs	Accuracy of channel DTMs, accuracy of long profiles
Model-to-Model	Survey TINs and DEMs -TO- Manual photogrammetry TINs and DEMs	Spatial analysis of error, accuracy of cross sections, change detection

TABLE 2.3. ABSOLUTE VALUE ELEVATION DIFFERENCES OF COMMON POINTS

	n	mean	stdev	min (q0)	q1	median (q2)	q3	max (q4)
Feb-Oct Survey Sets[1]	199	0.030	0.036	0.000	0.008	0.018	0.039	0.233
Feb-Oct Photogram Sets[1]	36	0.092	0.104	0.001	0.028	0.073	0.107	0.529
March Photogram Error[2]	84	0.066	0.069	0.003	0.029	0.044	0.079	0.481
Oct Photogram Error[2]	77	0.076	0.078	0.000	0.020	0.053	0.105	0.451

[1] Calculated as [(February ground-survey points) - (October ground-survey points)]

[2] Calculated as [(manual-photogrammetry points) - (ground-survey points)]

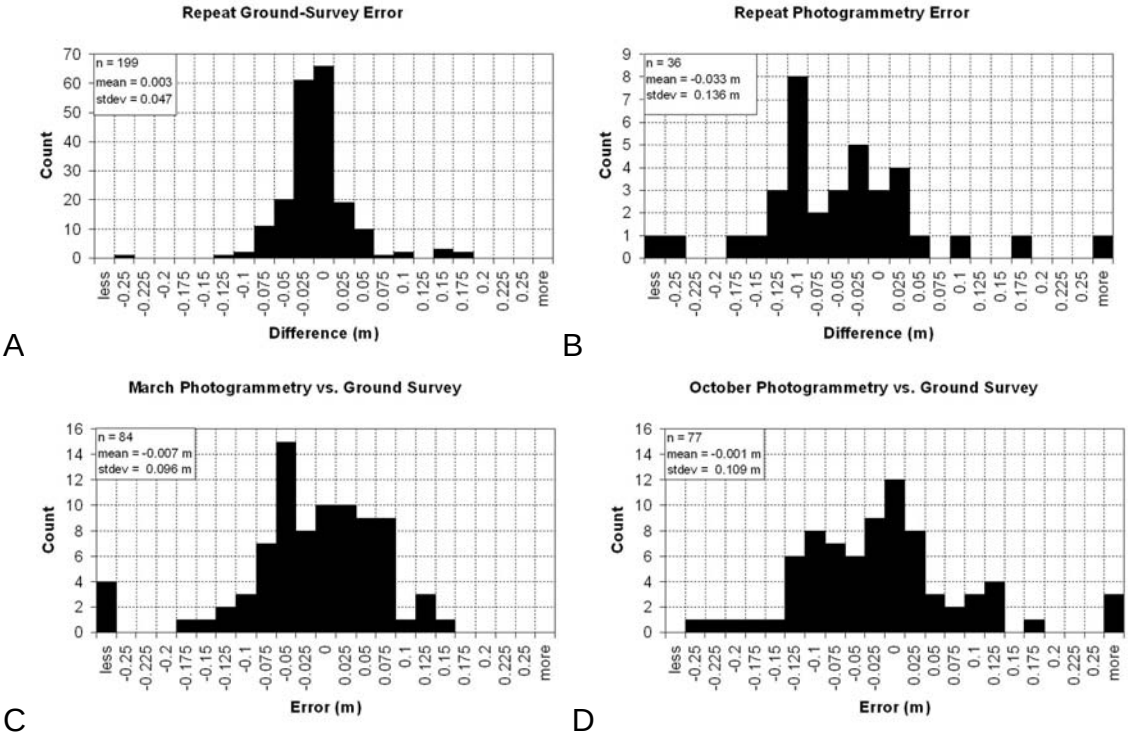

Figure 2.2. Histograms showing point-to-point difference distributions summarized in Table 2.3. A) February-October ground surveys; B) March-October photogrammetric surveys; C) March photogrammetry compared to February ground surveys; D) October photogrammetry compared to October ground surveys.

TABLE 2.4. PROFILE KNICKPOINT DETECTION

Site	February Survey (#)	March Photogrammetry (#)	Percent Detected	October Survey (#)	October Photogrammetry (#)	Percent Detected
Indian Canyon	13	5	38	16	6	38
Arroyo Grande	24	2	8	24	2	8
Granite Park	15	7	47	15	4	27
223-mile	16	6	38	13	5	38
Total	68	20	29	68	19	27

TABLE 2.5. PLANVIEW KNICKPOINT DETECTION

Site	February Survey (#)	March Photogrammetry (#)	Percent Detected	October Survey (#)	October Photogrammetry (#)	Percent Detected
Indian Canyon	13	8	62	16	9	56
Arroyo Grande	24	10	42	24	9	38
Granite Park	15	9	60	15	7	47
223-mile	16	6	38	13	5	38
Total	68	33	49	68	30	44

TABLE 2.6. SEMI-AUTOMATED PHOTOGRAMMETRY ABSOLUTE VALUE ERROR (M)[1,2]

March site	n	mean	stdev	min (q_0)	q_1	median (q_2)	q_3	max (q_4)
Indian Camp	1138	0.09	0.09	0.00	0.03	0.06	0.11	0.83
Arroyo Grande	1464	0.07	0.09	0.00	0.02	0.04	0.08	0.67
Granite Park	1073	0.04	0.05	0.00	0.01	0.03	0.06	0.54
223-mile	1261	0.13	0.16	0.00	0.03	0.07	0.16	1.22
All Sites	4936	0.08	0.11	0.00	0.02	0.05	0.10	1.22
October site	n	mean	stdev	min (q_0)	q_1	median (q_2)	q_3	max (q_4)
Indian Camp	733	0.08	0.12	0.00	0.02	0.03	0.07	1.33
Arroyo Grande Overall	1122	0.12	0.11	0.00	0.05	0.10	0.16	0.71
Granite Park	930	0.10	0.07	0.00	0.05	0.09	0.13	0.66
223-mile	758	0.10	0.11	0.00	0.02	0.06	0.12	0.74
All Sites	3636	0.10	0.10	0.00	0.03	0.08	0.13	1.33

[1] See Appendix B for site maps

[2] Calculated as [(manual-photogrammetry DTMs) - (ground-survey points)]

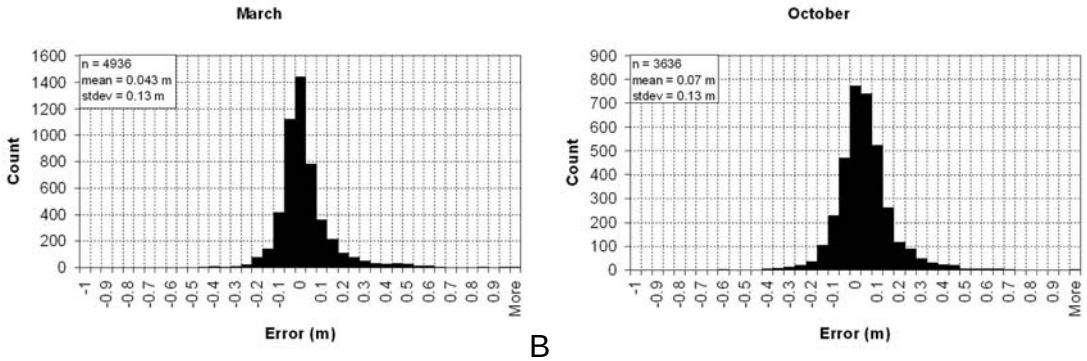

A B

Figure 2.3. Error distributions for semi-automated DTMs. Both have means and medians that are shifted positive, the October dataset (B) more than the March dataset (A).

TABLE 2.7. MANUAL PHOTOGRAMMETRY PROFILE ABSOLUTE VALUE ERROR (M)[1]

March site	n	mean	stdev	min (q_0)	q_1	median (q_2)	q_3	max (q_4)
Indian Camp	227	0.07	0.06	0.00	0.03	0.06	0.10	0.34
Arroyo Grande	282	0.06	0.06	0.00	0.02	0.04	0.09	0.39
Granite Park	247	0.04	0.04	0.00	0.01	0.03	0.06	0.20
223-mile	227	0.07	0.08	0.00	0.02	0.05	0.09	0.45
Overall Sites	983	0.06	0.06	0.00	0.02	0.04	0.09	0.45
October site	n	mean	stdev	min (q_0)	q_1	median (q_2)	q_3	max (q_4)
Indian Camp	227	0.07	0.06	0.00	0.03	0.05	0.09	0.47
Arroyo Grande	282	0.10	0.08	0.00	0.04	0.08	0.13	0.43
Granite Park	247	0.09	0.05	0.00	0.06	0.09	0.12	0.38
223-mile	227	0.10	0.09	0.00	0.03	0.06	0.14	0.59
Overall Sites	983	0.09	0.07	0.00	0.04	0.07	0.12	0.59

[1] Calculated as [(manual-photogrammetry DTMs) - (ground-survey points)]

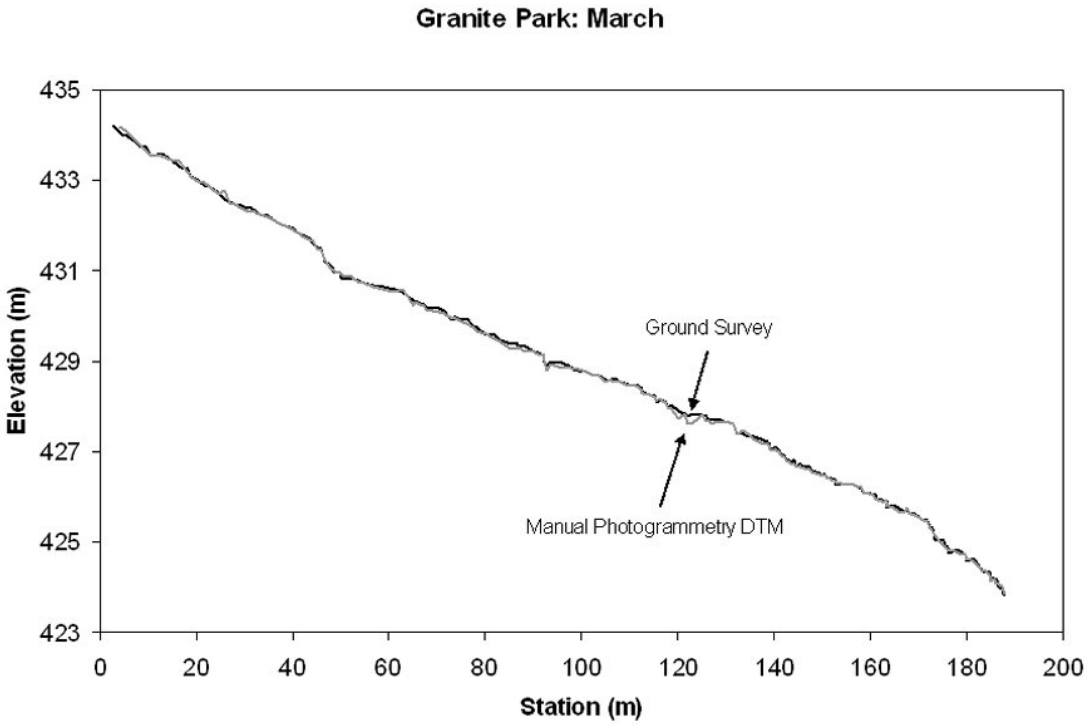

A

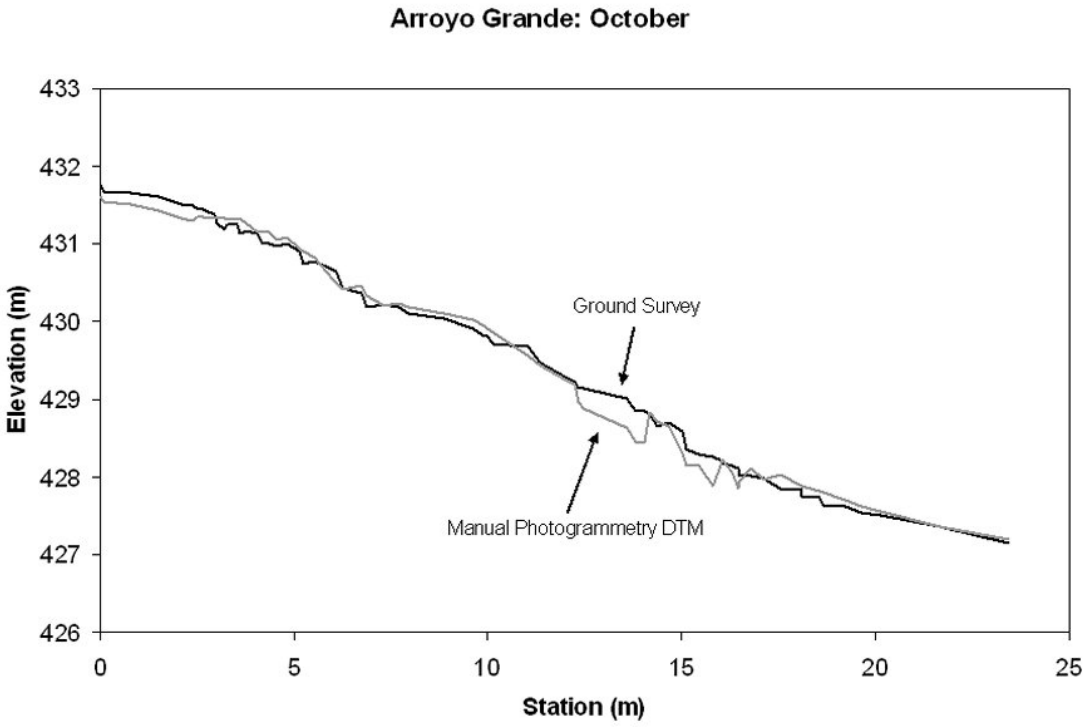

B

Figure 2.4. Example longitudinal profiles of gully thalwegs. A) gully with a relatively accurate manual photogrammetry profile; B) gully with inaccurate photogrammetry profile likely due to vegetation obstruction.

TABLE 2.8. MANUAL PHOTOGRAMMETRY DTM ABSOLUTE VALUE ERROR (M)[1]

March site	n	mean	stdev	min (q_0)	q_1	median (q_2)	q_3	max (q_4)
Indian Camp	1094	0.10	0.10	0.00	0.03	0.07	0.12	0.81
Arroyo Grande	1481	0.09	0.12	0.00	0.03	0.06	0.12	0.97
Granite Park	1072	0.05	0.05	0.00	0.02	0.04	0.07	0.40
223-mile	1797	0.10	0.12	0.00	0.03	0.06	0.13	0.93
All Sites	5444	0.09	0.10	0.00	0.03	0.06	0.11	0.97
October site	n	mean	stdev	min (q_0)	q_1	median (q_2)	q_3	max (q_4)
Indian Camp	747	0.08	0.09	0.00	0.02	0.05	0.09	0.75
Arroyo Grande	1177	0.11	0.11	0.00	0.04	0.08	0.14	0.77
Granite Park	945	0.09	0.06	0.00	0.05	0.08	0.12	0.53
223-mile	872	0.09	0.09	0.00	0.03	0.06	0.12	0.59
All Sites	3741	0.10	0.10	0.00	0.03	0.07	0.12	0.77

[1] Calculated as [(manual-photogrammetry DTMs) - (ground-survey points)]

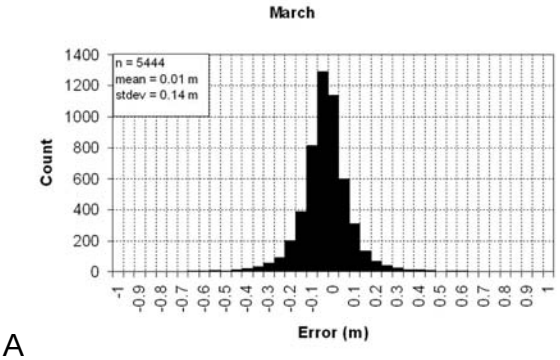

A

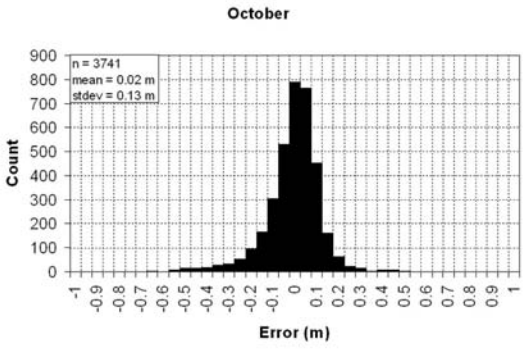

B

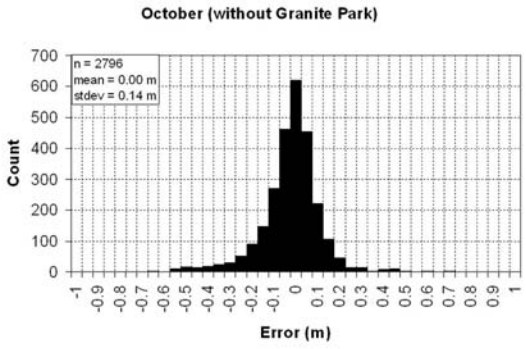

C

Figure 2.5. Point-to-model error distributions [(manual-photogrammetry DTM – ground-survey points)] for March (A) and October (B, C) manual photogrammetric DTMs.

TABLE 2.9. MANUAL PHOTOGRAMMETRY DEM ABSOLUTE VALUE ERROR (M)[1]

March site	n[2]	mean	stdev	min (q_0)	q_1	median (q_2)	q_3	max (q_4)
Indian Camp	5493	0.12	0.11	0.00	0.04	0.09	0.16	0.89
Arroyo Grande	3777	0.13	0.15	0.00	0.03	0.07	0.16	1.17
Granite Park	7343	0.07	0.06	0.00	0.02	0.05	0.09	0.54
223-mile	3617	0.11	0.12	0.00	0.03	0.07	0.14	2.49
All Sites	20230	0.10	0.10	0.00	0.03	0.07	0.13	2.49
October site	n	mean	stdev	min (q_0)	q_1	median (q_2)	q_3	max (q_4)
Indian Camp	4904	0.12	0.15	0.00	0.03	0.07	0.14	2.16
Arroyo Grande	3749	0.11	0.12	0.00	0.03	0.07	0.14	0.82
Granite Park	7315	0.09	0.07	0.00	0.04	0.08	0.12	0.68
223-mile	3456	0.09	0.10	0.00	0.03	0.06	0.12	0.76
Overall Sites	19424	0.10	0.11	0.00	0.03	0.07	0.13	2.16

[1] Calculated as [(ground-survey DEM from TIN) - (manual photogrammetry DEM from TIN)]

[2] n represents number of grid cells used in comparison

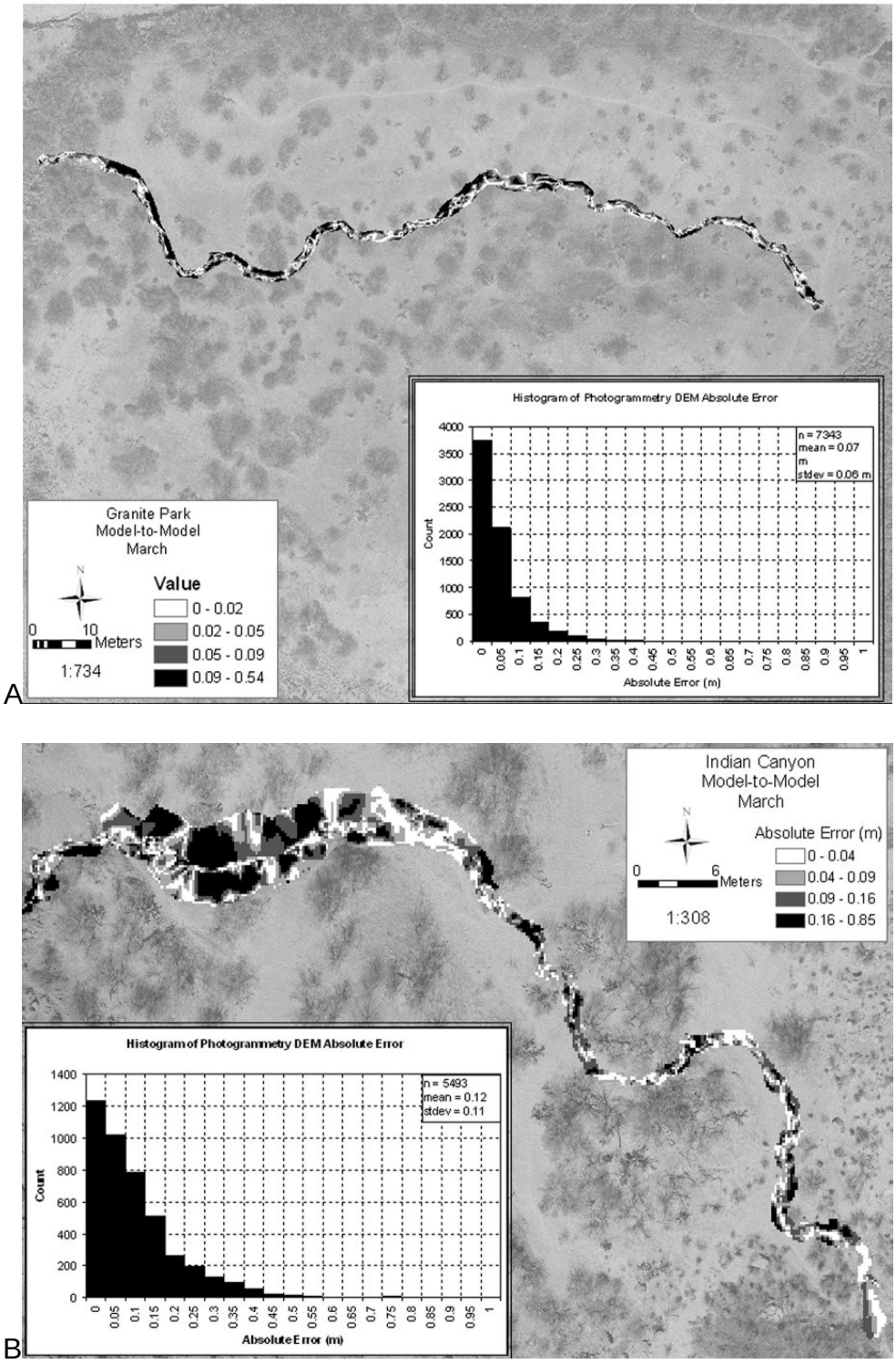

Figure 2.6. Example model-to-model comparison showing A) relatively low photogrammetry DTM vertical error for Granite Park and B) relatively high error for Indian Canyon in March, both having highly variable spatial distribution of error. Legend shows error in terms of quartiles. Background is reduced-contrast aerial photograph of site.

TABLE 2.10. MANUAL PHOTOGRAMMETRY CHANNEL CROSS SECTION ABSOLUTE VALUE ERROR (M)[1]

March site	n[2]	mean	stdev	min (q_0)	q_1	median (q_2)	q_3	max (q_4)
Indian Canyon (1 xsection)	17	0.08	0.06	0.00	0.04	0.04	0.12	0.20
Arroyo Grande (4 xsections)	77	0.06	0.04	0.00	0.03	0.06	0.08	0.17
Granite Park (1 xsection)	14	0.06	0.05	0.00	0.03	0.05	0.11	0.14
223-mile (5 xsections)	100	0.13	0.11	0.00	0.05	0.09	0.18	0.44
All Sites (11 xsections)	207	0.09	0.09	0.00	0.04	0.07	0.13	0.44
October site	n	mean	stdev	min (q_0)	q_1	median (q_2)	q_3	max (q_4)
Indian Canyon (1 xsection)	17	0.05	0.04	0.01	0.03	0.04	0.07	0.17
Arroyo Grande (4 xsections)	77	0.08	0.06	0.00	0.03	0.05	0.14	0.21
Granite Park (1 xsection)	14	0.07	0.05	0.01	0.04	0.06	0.09	0.18
223-mile (5 xsections)	100	0.10	0.09	0.00	0.04	0.07	0.14	0.35
All Sites (11 xsections)	207	0.09	0.07	0.00	0.03	0.06	0.14	0.35

[1] Calculated as [(ground-survey TIN cross-section points) - (manual photogrammetry TIN cross-section points)]

[2] n represents total number of points in each cross section

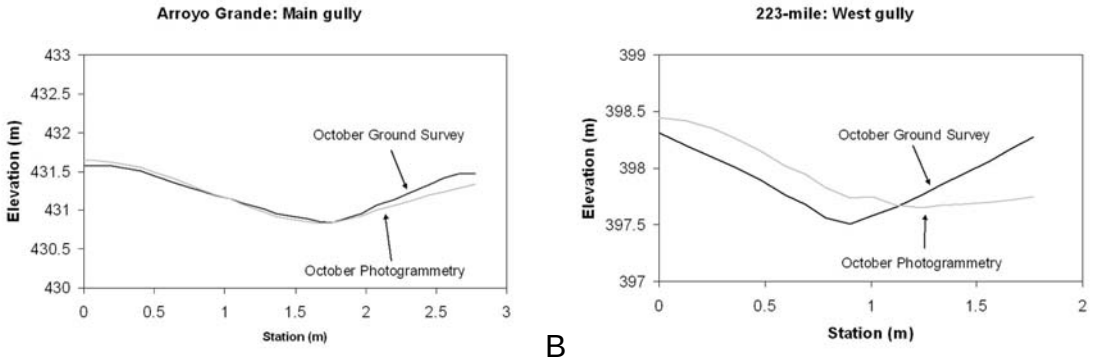

A B

Figure 2.7. Examples of channel cross sections extracted from DTMs. A) one of the most accurate photogrammetry-derived cross sections; B) one of the least accurate.

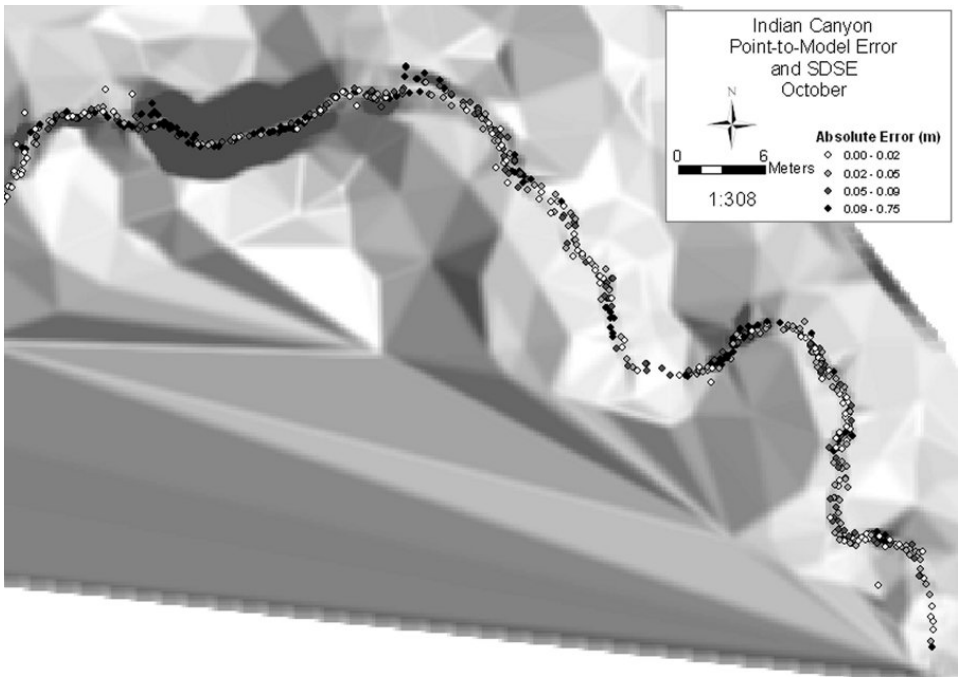

Figure 2.8. Example of a SDSE grid. High SDSE values (dark shades) tend to coincide with higher error (black dots)

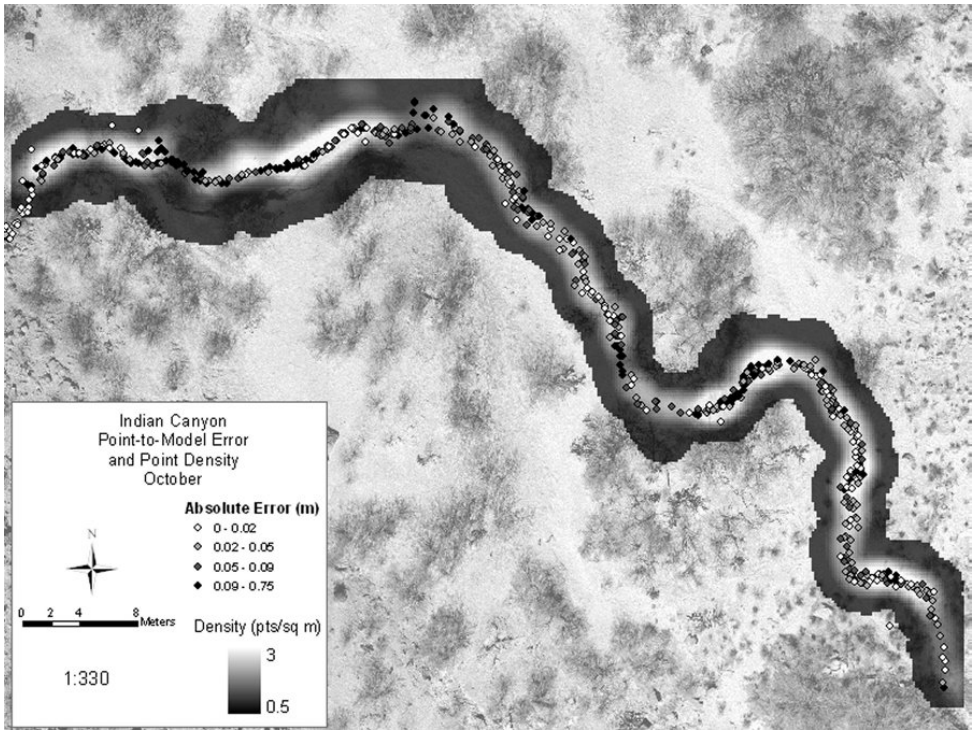

Figure 2.9. Example of a point density grid from the same dataset as Fig. 2.8. Background is aerial photograph of site. Low density values (dark shades) tend to coincide with high errors (black dots).

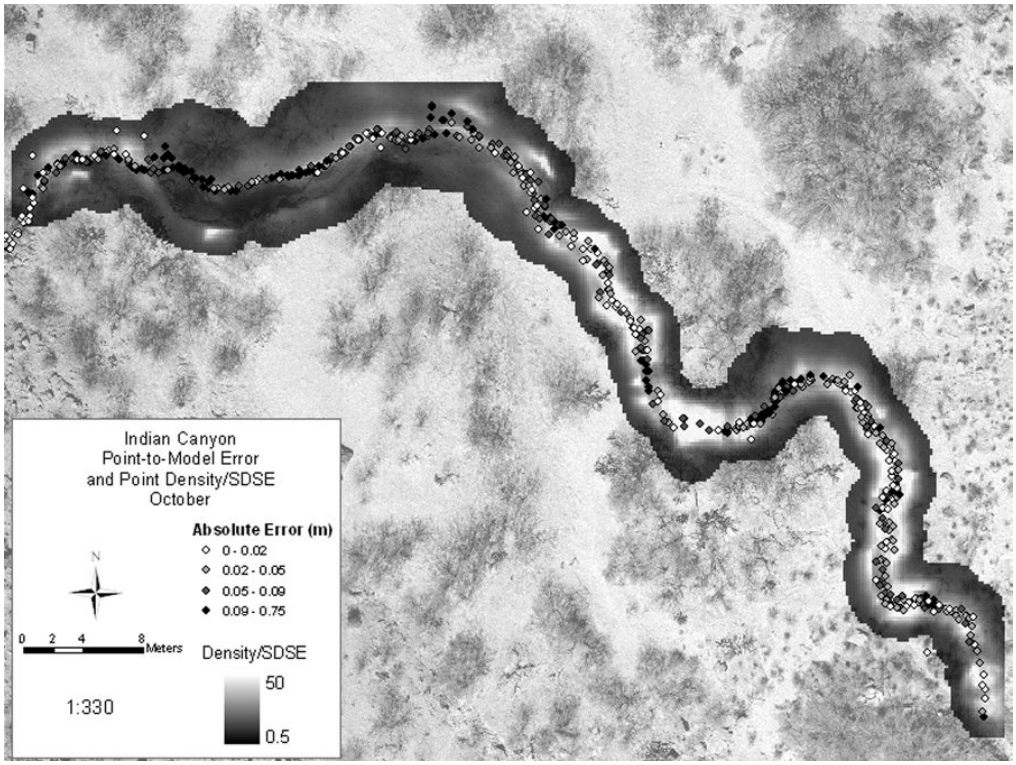

Figure 2.10. Point density/SDSE grid from the same dataset. This was created by dividing the density grid in Figure 2.8 by the SDSE grid in Figure 2.9. Low density/SDSE values (dark shades) tend to coincide with high errors (black dots).

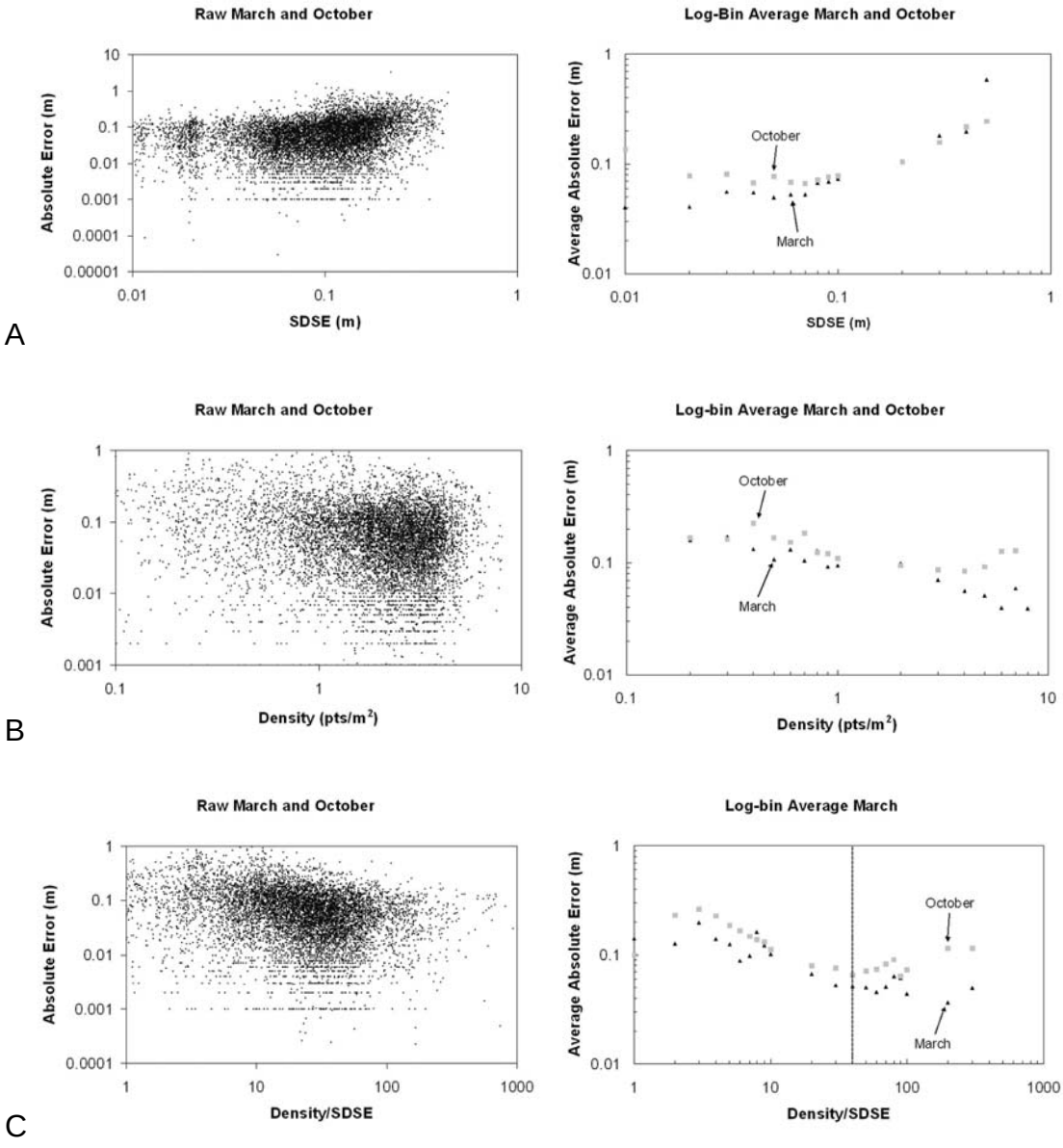

Figure 2.11. Raw and log-bin average plots for March and October showing the relation between A) standard deviation of surface elevation (terrain irregularity) and absolute error; B) photogrammetry sample density and absolute error; C) density/SDSE ratio and absolute error. Note that average error values in C steadily decrease until a ratio of 40, then appears to level out (shown by dotted line). Obtaining a ratio of higher than 40 would not necessarily result in higher quality data.

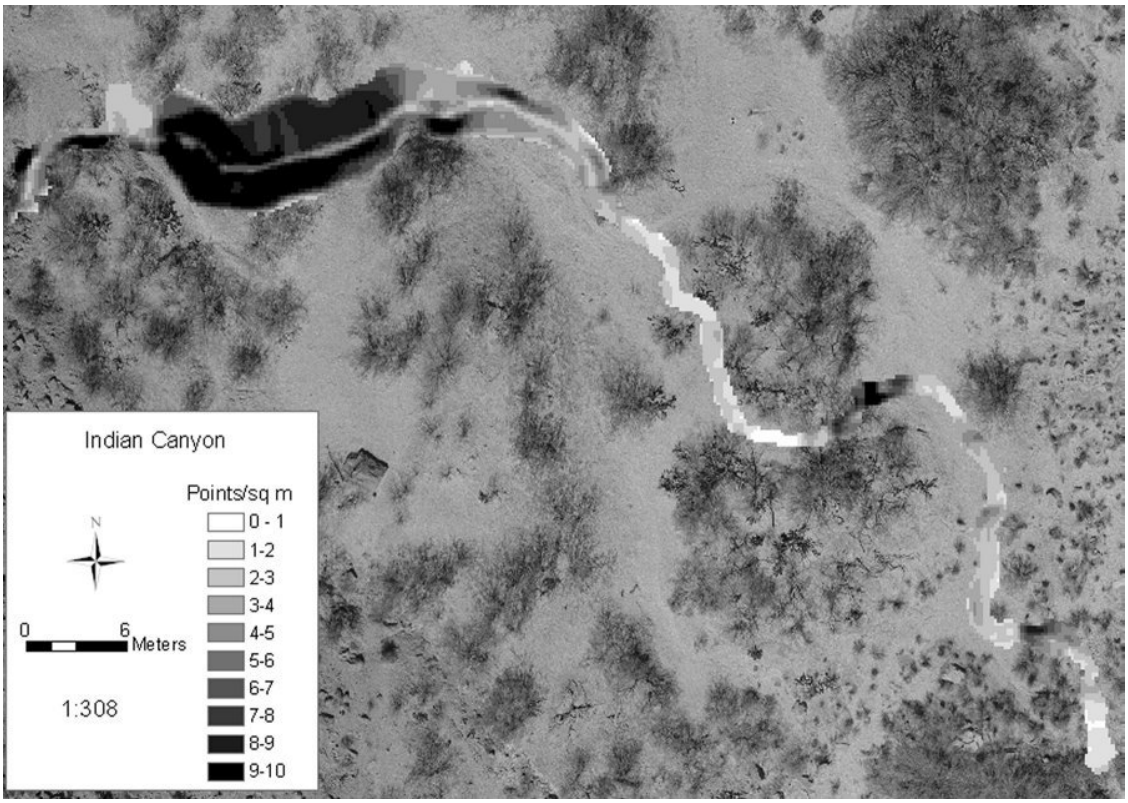

Figure 2.12. Calculated photogrammetry point density (pts/m^2) required to achieve optimal vertical accuracy (density/SDSE = 40) for the topography at Indian Canyon. Values vary by an order of magnitude. Maps such as these could be used during manual photogrammetric collection to ensure minimal error and labor.

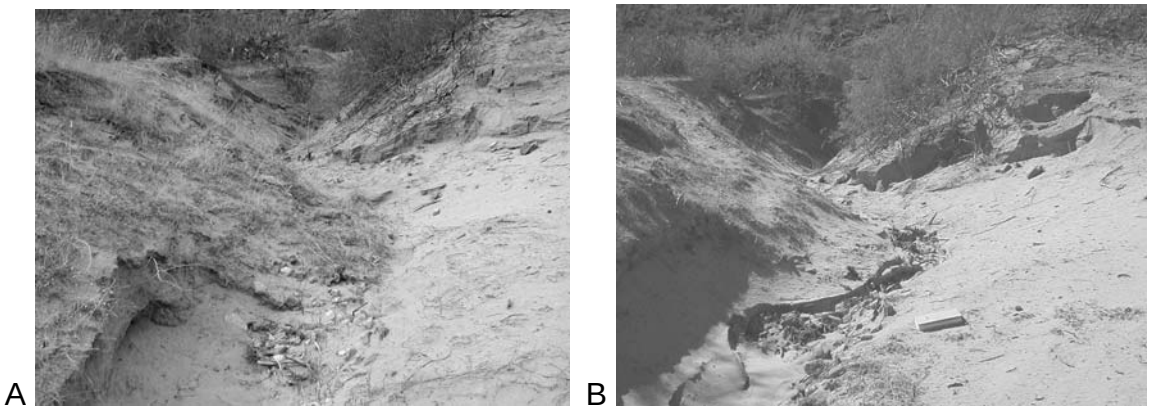

Figure 2.13. Channel incision and widening in the upper Indian Canyon gully between (A) February and (B) October.

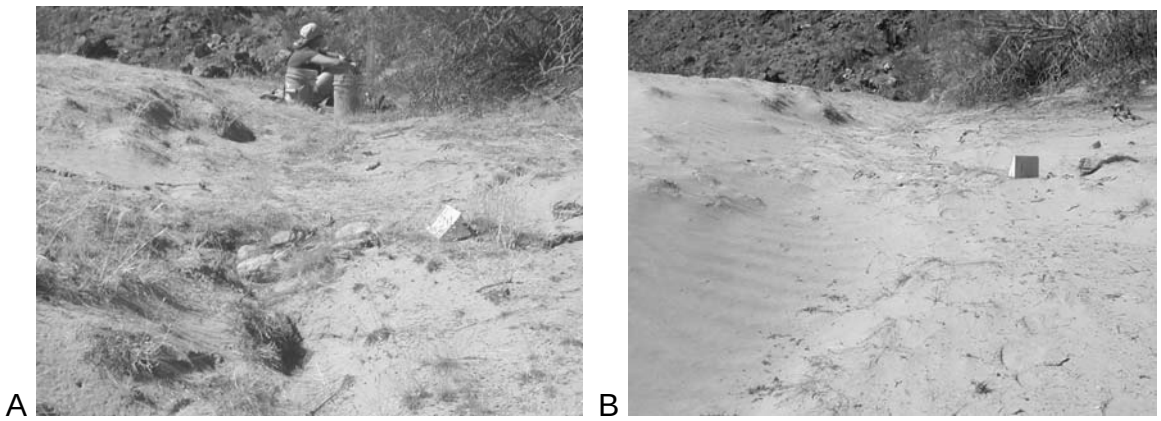

Figure 2.14. Eolian infilling in the east-most 223-mile gully between (A) February and (B) October. Rocks and vegetation in middle of February photo are buried in October.

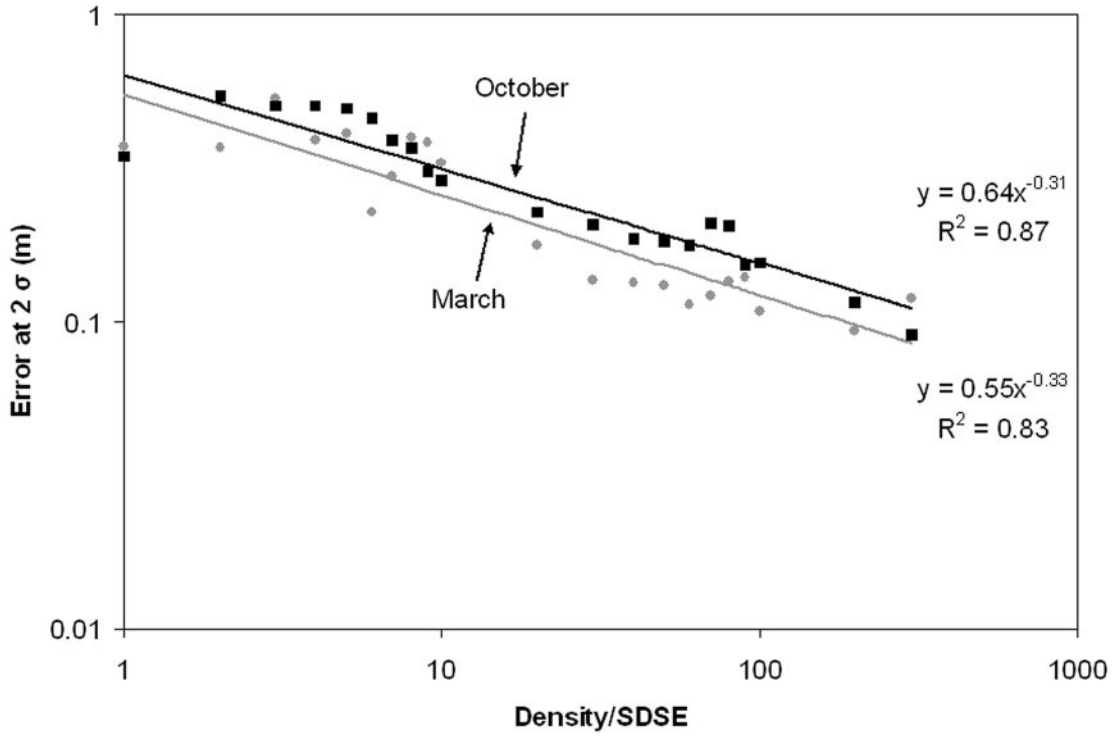

Figure 2.15. Plot of density/SDSE vs. 2σ variance in point-to-model accuracy assessment of all four study sites. October data are black squares, March data are gray circles. Power equations of regression lines were used to represent error for any density/SDSE value.

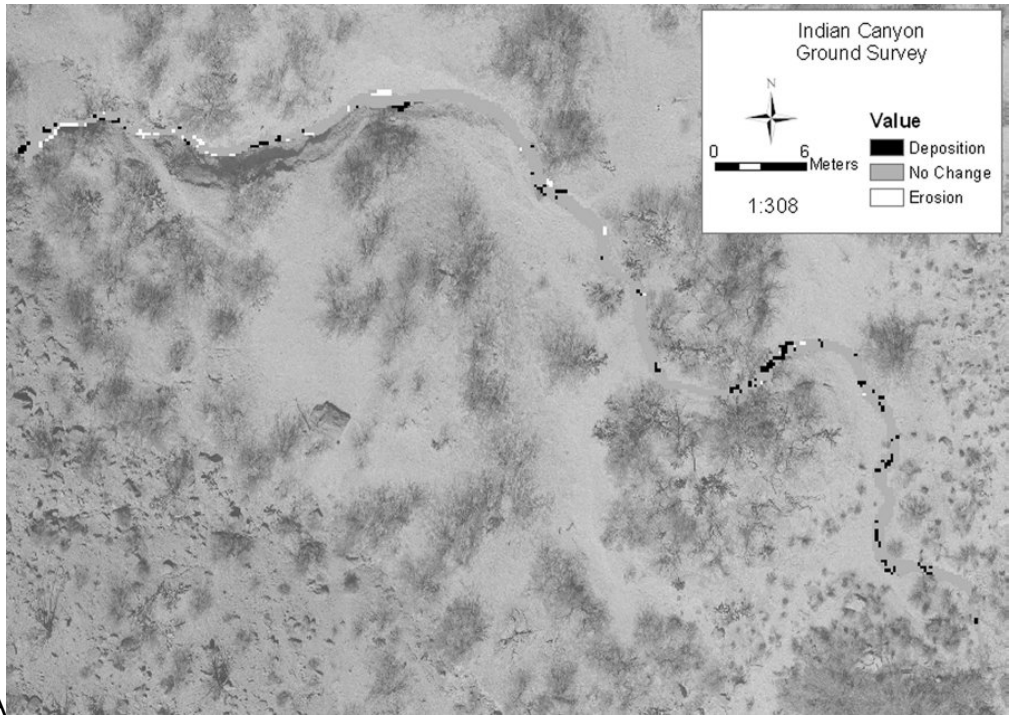

A

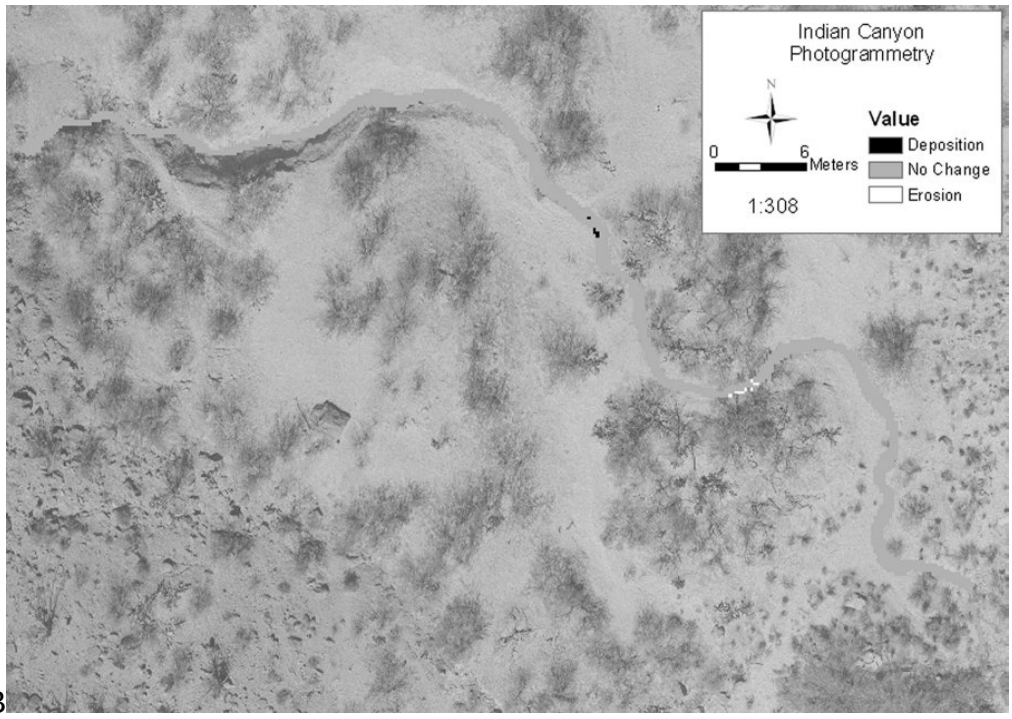

B

Figure 2.16. Change-detection maps of Indian Canyon gully bottom. (A) The ground survey change map is based on a 10-cm compounded error detection threshold and shows erosion in the upper reach and deposition in the lower reach; (B) using a spatially variable detection threshold based on the density/SDSE topographic index, none of this change is of a magnitude large enough to be detected by photogrammetry in the upper reach, and very little change can be detected in the lower reach.

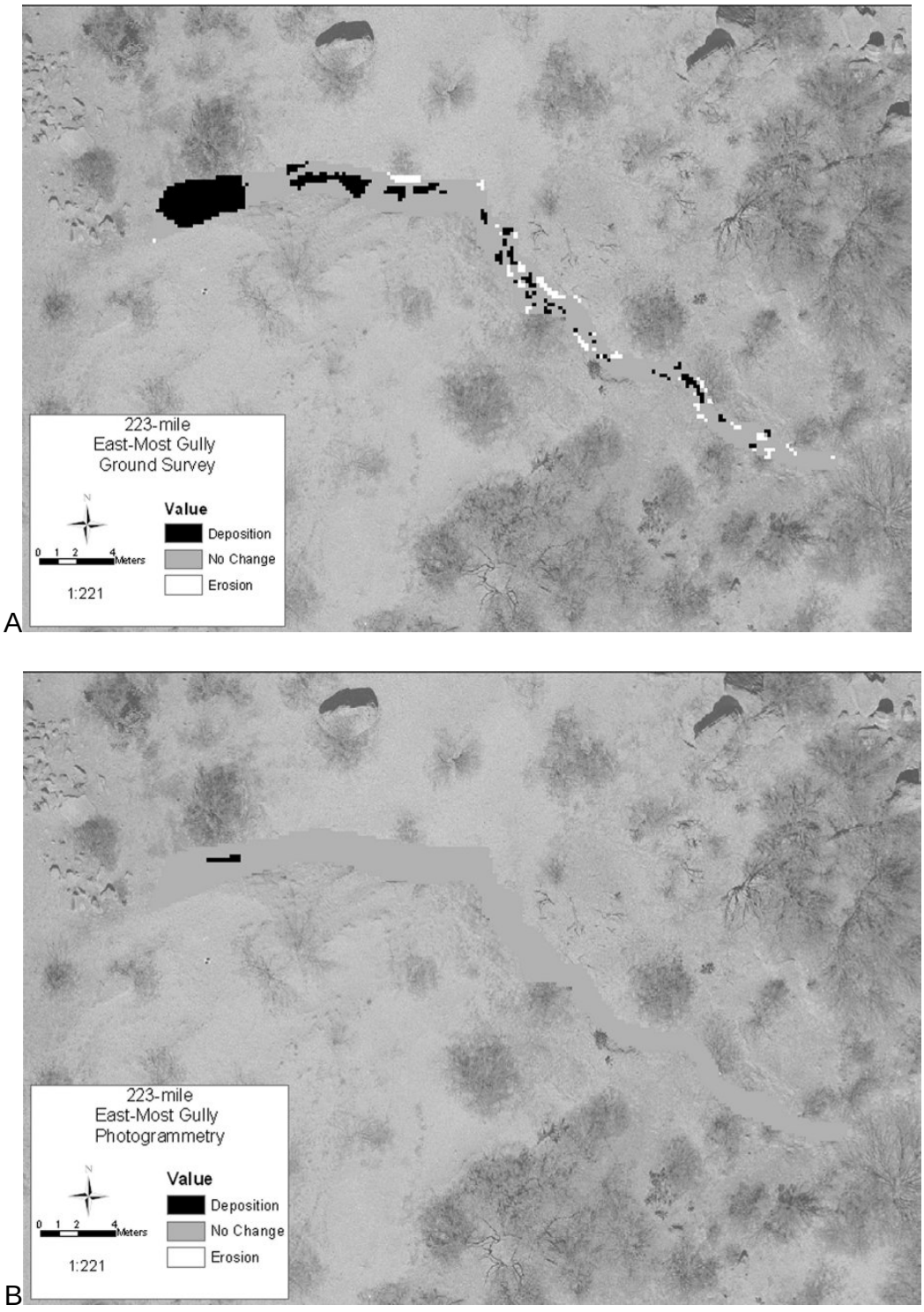

Figure 2.17. Change-detection maps of east-most 223-mile gully. (A) The ground survey change map is based on a 10-cm compounded error detection threshold and shows several areas of deposition throughout the gully, especially in the upper reach; B) using a spatially variable detection threshold based on the density/SDSE topographic index, very little of this deposition is of a magnitude large enough to be detected by photogrammetry.

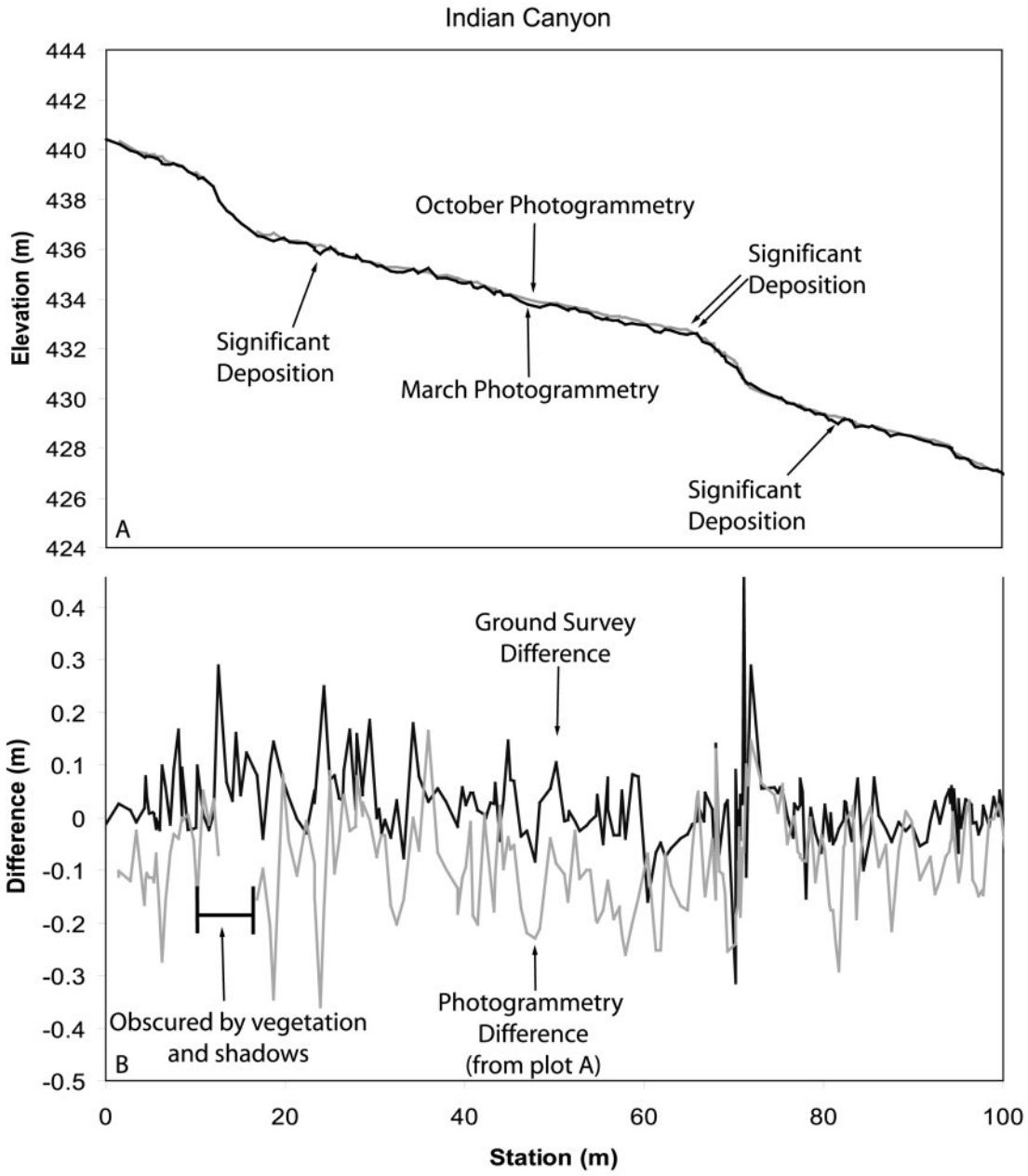

Figure 2.18. A) Indian Canyon photogrammetry gully-long profiles with four locations of deposition great enough to confidently be detected using variable threshold; B) difference plots (March – October data points) indicating ground-survey profiles show significant erosion in several places. Positive difference is denudation, negative difference is deposition. Ground-survey profiles not shown.

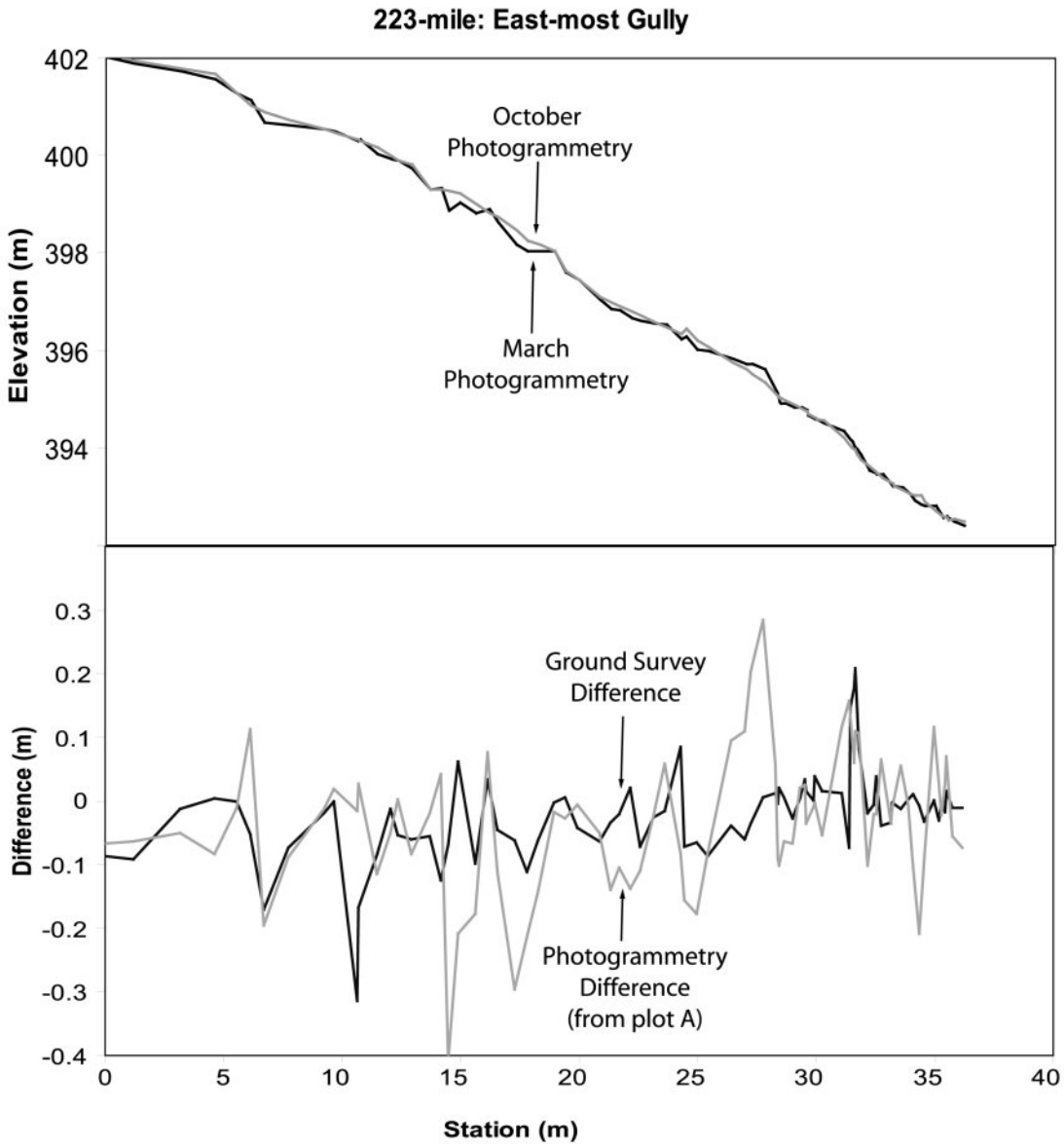

Figure 2.19. (A) 223-mile photogrammetry profiles; (B) difference plots (March – October data points). Although the profile reveals areas of deposition, no elevation change was great enough be considered significant, but ground survey had three locations of detectable deposition in upper gully. Positive difference is denudation, negative difference is deposition.

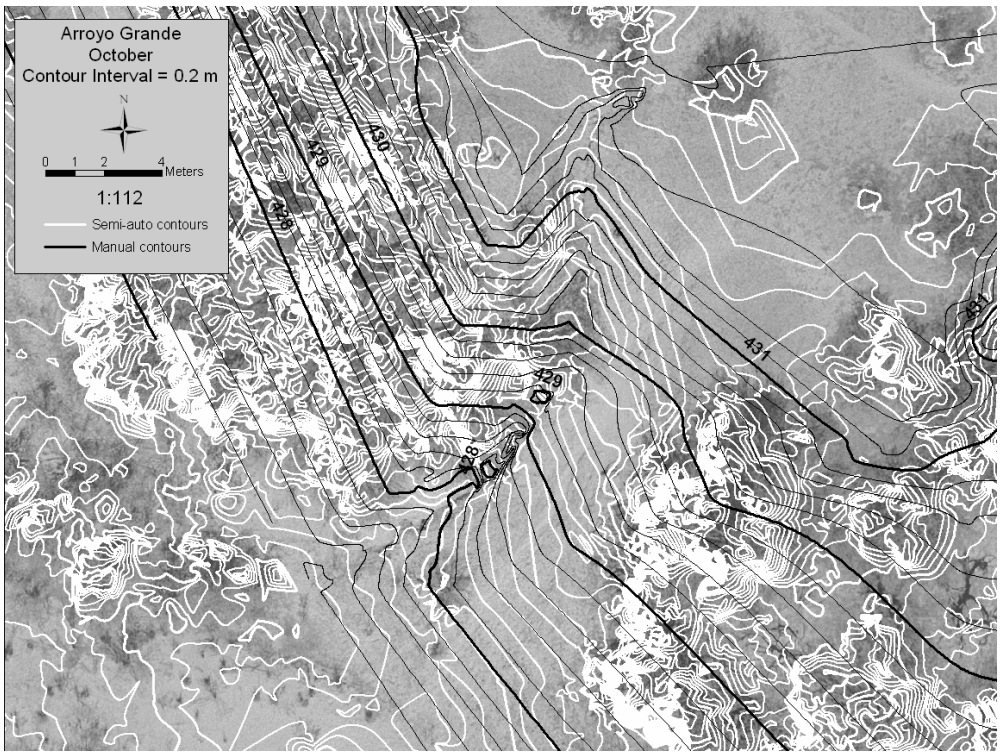

Figure 2.20. Contours derived from manual and semi-automated photogrammetry data points in example of Arroyo Grande October data. The contrast provided by vegetation attracts erroneous detail in semi-automated collection that contributes to overestimates of elevation.

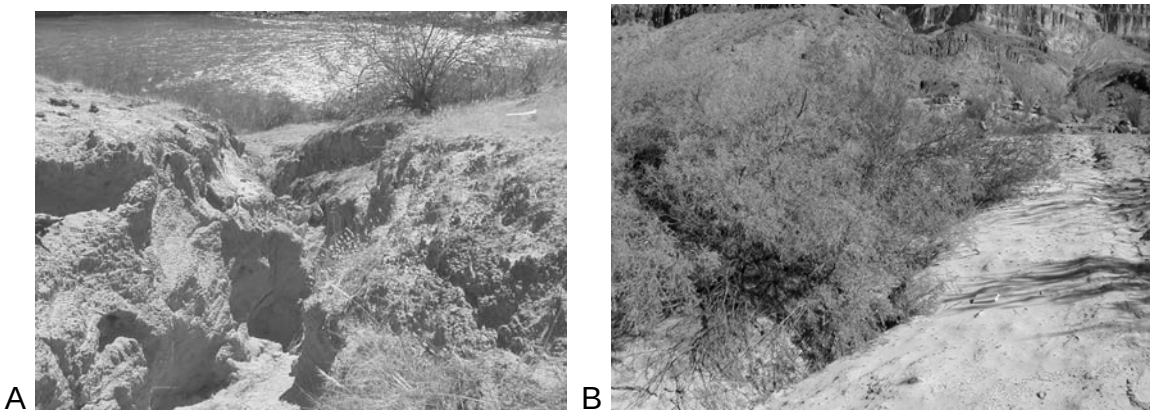

Figure 2.21. A) Example of high-relief, vertical banks with shadows at 223-mile and B) complete obstruction of the channel by vegetation at Arroyo Grande, which obstructs and impedes photogrammetric detection of eight knickpoints.

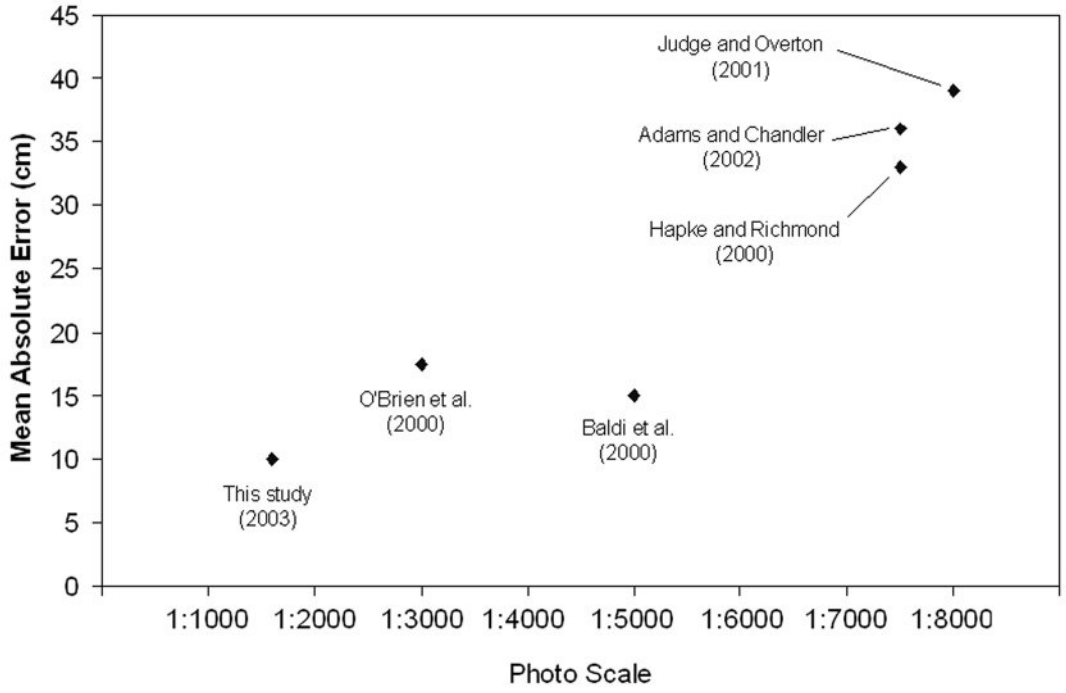

Figure 2.22. Mean photogrammetry error synthesized from previous studies. Error is related to scale of photography, but also results from many other factors.

CHAPTER 3: GEOMORPHOLOGY RELATED TO GULLY EROSION

INTRODUCTION

Gullies are watercourses marked by steep, high relief channel walls, a stepped profile, and often an abrupt channel head (Higgins, 1990; Knighton, 1998). Though they are prevalent in drylands, gullies are often thought of as indicating disturbance and accelerated erosion brought about by changing climate or land-use. Gully erosion increases sediment yield, removes fertile agricultural soil, destabilizes hillslopes, and can lower the water table of alluvial aquifers (e.g. Patton and Schumm, 1975; Karlstrom, 1988; Gellis, 1996; Bull, 1997; Elliot et al., 1999; Norton et al., 2002). In Grand Canyon, cultural sites along the Colorado River corridor are being damaged by the incision and widening of gullies (Hereford et al., 1993; Fairley et al., 1994). A complete understanding of the geomorphology of this erosion is important for protecting cultural resources and for identifying the causes of erosion, including the potential role of Glen Canyon Dam. As a step towards this goal, the purpose of this study is to increase our knowledge of the geomorphic processes and properties related to gully erosion in Grand Canyon.

BACKGROUND

Setting

The gullies of interest in Grand Canyon form on a suite of Holocene stream terraces underlain by sandy alluvium, as well as on eolian deposits and on colluvium at the toes of hillslopes. Hereford and others (1993,1996) studied the Holocene alluvial stratigraphy of the river corridor and found that most cultural sites are located in deposits they called the “alluvium of Pueblo II age” and the “striped alluvium.” (Fig. 3.1). The striped alluvium dates from 2500 BC to 300 AD, consists of interbedded slopewash deposits and fluvial sand, and is found mostly in eastern Grand Canyon. The alluvium of Pueblo II age has been dated from 700 – 1200 AD and consists of fine-grained fluvial sand locally interbedded with eolian sand and gravelly slopewash deposits. These middle-late Holocene deposits generally have not been inundated by historic pre-dam

flows of the Colorado River. The "upper mesquite" and "lower mesquite" terraces are composed of silty sand and are distinguished by the presence of mature mesquite trees on the upper terrace and younger mesquite on the lower terrace (Fig. 3.1). Deposition of upper mesquite sediment began ~1400 AD, perhaps during an episode of enhanced flooding, whereas the lower mesquite deposit probably was not formed until a late 19th century flood event (Fairley and Hereford, 2002).

Climate and the precipitation that drives erosion varies strongly with elevation in this setting. Mean annual precipitation (MAP) is 647 mm and mean annual temperature (MAT) is 6.3^{o}C at the north rim, whereas at the bottom of the canyon MAP is 213 mm and MAT 20.4^{o}C (Western Regional Climate Center, 2003). The Southwestern monsoon, typically between June 15 – October 15, produces ~50% of Grand Canyon's yearly rainfall. Most flood and runoff events in the region are initiated during this time through intense, isolated thunderstorms (Hereford and Webb, 1992), but also some of the largest runoff events have occurred in during long-duration, low-intensity, late fall or winter storms (Griffiths et al., 1996).

The study gullies are relatively small, ranging from ~20-200 m in thalweg length, and from ~0.2-2.5 m in channel top width. The channels typically have near-vertical knickpoints with plungepools, and can have either gradual or abrupt channel heads. Abrupt channel heads may be similar in form to knickpoints, but are differentiated as being the upstream boundary of the channel, whereas knickpoints lie within the channel.

Previous Work in Grand Canyon

Hereford et al. (1993) and Thompson and Potochnik (2000) concluded gully incision has increased since 1973 and increased most dramatically between 1973 and 1984 based on repeat photographs of sites in both eastern and western Grand Canyon. Hereford and Webb (1992) noted that most years between the mid-1930s and late 1970s were very dry, but were followed by several unusually wet years of higher storm frequency. Hereford et al. (1993) studied changes in daily precipitation and proposed that this same period of more intense precipitation from the late 1970s through the 1990s has driven accelerated erosion. These studies also raised the idea that increased erosion is linked to Glen Canyon Dam. They suggest that, although unusually high runoff drove

the erosional process, lowered baselevel due to dam operations increased the depth of erosion and caused knickpoint retreat throughout some catchments. They hypothesized that in the pre-dam era flood deposition prevented gullies from reaching the river (Fig. 3.1), and that the lack of flood deposition in post-dam time allowed some gullies to reach the Colorado River, reducing their baselevel 3-4 m. Hereford et al. (1993) suggest that, as a result, gully incision may have intensified relative to pre-dam conditions in the ~25% of catchments terminating at the Colorado River or on its terraces.

Thompson and Potochnik (2000) attempted to test Hereford and others' (1993) baselevel hypothesis. They compared gullied terraces in Grand Canyon to those in Cataract Canyon upstream, which experiences relatively natural flooding and sediment loads. They suggested that the relative absence and small size of gullies in Cataract Canyon supports the idea that flood deposition by the mainstem river is effective in maintaining a higher baselevel and reducing incision. They also suggested that the redistribution of flood sand onto higher terraces and gully infilling by wind may be a critical process that also potentially has been altered by Glen Canyon Dam.

Our research does not address the potential influence of Glen Canyon Dam, nor is it a test of these previous ideas. Our goal is to contribute to our knowledge of the processes and conditions of this problematic gully erosion, setting a groundwork for future research on the relative importance of different controlling factors in the erosion.

Geomorphic Concepts

Erosion Thresholds

Several empirical studies have related gully erosion to topographic thresholds. For example, upslope contributing drainage area and local channel gradient have been used in simple models to predict the initiation, location, and soil loss caused by gully erosion through both saturation overland flow and infiltration-excess overland flow (e.g. Patton and Schumm, 1975; Begin and Schumm, 1979; Foster, 1986; Merkel et al., 1988; Thorne et al., 1986; Auzet et al., 1993; Montgomery and Dietrich, 1994). The rationale for this approach is that the location of gully initiation in a drainage and the amount of subsequent erosion is primarily controlled by the generation of surface runoff of sufficient depth and velocity to exceed a critical shear stress of grain entrainment. Since

runoff-discharge data are not available for most drainages, upslope contributing area is substituted, assuming that runoff volume increases downslope proportional to increasing catchment area. This should be true in places like Grand Canyon where infiltration-excess overland flow results from high-intensity precipitation events falling on sparsely-vegetated catchments.

We take the initial steps in this study towards a numerical model of gullying at Grand Canyon study sites. The rationale for a complete model is based on a threshold relation between contributing area and local gradient, but includes other empirical parameters (e.g. Montgomery and Dietrich, 1994). If one assumes steady-state rainfall intensity (R) and turbulent flow of runoff over a loose-sediment substrate with uniform infiltration capacity (I), discharge per unit contour length (q) may be determined by:

$$q = (R - I)a \tag{1}$$

where a is the drainage area per unit contour length. A second independent method of estimating unit discharge is through flow depth and a version of the Manning equation, which approximates mean flow velocity:

$$q = (1/n)h^{5/3}S^{1/2} \tag{2}$$

where n is the Manning roughness coefficient, h is flow depth, and S is water surface slope. The driving forces of this discharge must overcome a critical shear stress (τ_{cr}) in order to entrain particles:

$$\tau_{cr} = \rho_w g(hS)_{cr} \tag{3}$$

where ρ_w is the density of water and g is gravitational acceleration. The critical discharge that matches this (q_{cr}) can then be expressed by rearranging (3) in terms of h and substituting it into (2):

$$q_{cr} = \tau_{cr}^{5/3}/[(\rho_w g)^{5/3} n S^{7/6}] \tag{4}$$

Equating (4) and (1) and solving for the critical unit-width drainage area required for erosion by surface runoff yields:

$$a_{cr} = \tau_{cr}^{5/3}/[(R - I)(\rho_w g)^{5/3} n S^{7/6}] \tag{5}$$

This expresses that the contributing drainage area required to cause erosion is nearly inversely proportional to the local gradient, and that the additional factors needed to

actually calculate an area-slope threshold are bed roughness and critical shear stress (resisting forces), rainfall intensity, and infiltration rate, all which are variable in space and time. A larger drainage area would be required for erosion if there was an increase in resisting forces or infiltration capacity of the soil; a smaller drainage area is needed with an increase in precipitation intensity or decrease in roughness, infiltration, or critical shear stress.

The initial work we do here with a relatively simple area-slope threshold is similar to the classic empirical study of Patton and Schumm (1975), who collected data on contributing area and slope above channel heads of entrenched gullies in small, semi-arid catchments of northwest Colorado. They used a line fit at the base of their data scatter in a slope vs. area plot to represent a critical slope-area erosion threshold. Measuring slope and contributing areas of existing gullies can provide a rough predictive tool for identifying potentially unstable locations in a drainage. The advent of GIS and use of raster datasets of elevation (DEMs) has enhanced this sort of threshold analysis. Vandaele et al. (1996), like Patton and Schumm, compiled analog data sets of slope and upstream drainage area measured just above gully heads, and delineated a threshold line below which there was no incision in their study area, expressing it as a power function:

$$S_{cr} = aA^{b} \tag{6}$$

where S_{cr} is the critical slope, A is the drainage area (in hectares), and the values of *a* and *b* are empirically established from their data sets of gully heads. Using a GIS, they then subtracted the calculated critical gradient (S_{cr}) from the actual local gradient (S_{ac}) for each cell within a DEM of their study catchment, predicting that in cells where $S_{ac} - S_{cr} > 0$, gullying is likely to occur, whereas if $S_{cr} \leq 0$ gullying is unlikely. They found good agreement between the predicted and observed locations of ephemeral gullies using this technique. Desmet et al. (1999) quantified the success of the method in predicting gully locations in three catchments in central Belgium using 5-m DEMs, where ~80% of the cells with observed gullying were predicted by the model.

These studies focus on channel heads, with the assumption that gullies will extend down-drainage from this upper limit of channelization. Yet gullies are discontinuous, and distinct from this are knickpoints along the channel below the head that initiate and

move independent of the channel head. Regardless, area-slope thresholds provide information as to the predicted extent of gullying. Future, more-detailed modeling of the potential maximum extent of current gully channels and the predicted locations of new channels on a site-by-site basis could aid managers in identifying and protecting at-risk resources.

Baselevel

Baselevel defines the potential for erosion by a drainage, and baselevel change has an elusive and complicated effect on gully erosion that depends upon the time and space scales that the processes of interest are acting upon. Baselevel fall and rise have distinct effects, with baselevel fall being one way of forming knickpoints and baselevel rise causing upstream deposition for a distance that varies with several factors. Knickpoints, places along a drainage profile where gradient increases abruptly, concentrate and deepen flow and increase its velocity, resulting in greater basal shear stress. Thus, erosion rates at knickpoints are higher, driving upslope knickpoint migration. Substrate character defines the longevity and form of knickpoints (Brush and Wolman, 1960; Holland and Pickup, 1976; Leopold and Bull, 1979; Gardner, 1983). Grand Canyon gully knickpoints can retreat several meters during an intense rainstorm, but it is unknown how quickly individual knickpoints in Grand Canyon diffuse from their steep initial form during headward migration.

Studies generally show that on human to short-geologic timescales baselevel rise and baselevel fall have only a limited effect on upstream deposition and erosion (Leopold and Bull, 1979; Schumm, 1993; Schumm and Rea, 1995; Harvey, 1994; Florsheim et al., 2001). In terms of baselevel fall, Graf (1982) explained that knickpoint erosion decays with distance upstream until the signal disappears (the knickpoint height approaches zero). A baselevel fall may propagate bed incision for greater distances through a positive feedback if the sediment is cohesive or has a resistant layer at its upper lip that is maintained through time (Leopold and Bull, 1979; Gardner, 1983; Schumm, 1993). However, knickpoints will eventually dissipate and flatten, especially outside of bedrock channels, and the rate of knickpoint migration decreases over time and distance from the outlet (Begin et al., 1980; Graf, 1982; Gardner, 1983; Florsheim et al., 2001). The

influence of baselevel fall is also dependent upon whether baselevel is lowered abruptly or gradually, whether changes in channel morphometry (for example, sinuosity) can accommodate the change, and, importantly, the gradient over which baselevel is lowered. If baselevel falls over a slope shallower than the gradient of the upstream drainage, no effective fall is produced at all (Schumm, 1993).

One of the most relevant studies to the situation and scale of the gullying in Grand Canyon is by Harvey (1994), who studied the linkage between eroding gullies and baselevel changes at their confluence with a stream in northwest England. The mouths of gullies were episodically scoured by the river, lowering effective baselevel, but Harvey concluded this caused only local incision near the gully mouths. He related erosion further upslope to catchment hydrologic processes and not to downslope baselevel effects.

For the purposes of this study, Grand Canyon gullies drain to some "effective baselevel", the point where the gullies terminate, which defines their erosional potential or the total relief of the drainage. Changes in this baselevel are effective to the degree that they influence the specific processes active at seasonal-yearly timescales in this setting. Effective baselevel differs from "ultimate baselevel," which is sea level, and from "local baselevel," which can be any point along a drainage controlling erosion and deposition immediately upslope (Powell, 1875; Gilbert, 1877; Leopold and Bull, 1979). Ultimate baselevel is pertinent at large geologic time (10^6 yrs) and space scales, whereas local baselevel is relevant on single-event time and individual-grain space scales not applicable here. This effective baselevel is certainly one of the controls on gully erosion in Grand Canyon, but where it lies will vary from gully to gully. Importantly, the gradient over which changes in this baselevel occur and the degree of linkage between gullies and the mainstem Colorado River will also vary from site to site.

METHODS

Nine cultural sites having a total of 22 gullies and exhibiting a range of geomorphic settings were selected for study (Fig. 3.2). Four sites are in eastern Grand Canyon: Kwagunt, 60-mile (four gullies), Palisades (four gullies), and Basalt Cliffs (four gullies). These eastern sites are within 23 river km of each other and are all ~800 m

elevation. Kwagunt is an "control" site, in that it is a relatively stable, ungullied drainage. Five sites are in western Grand Canyon: Parashant (control site); Indian Canyon (one gully), Arroyo Grande (four gullies), Granite Park (one gully), and 223-mile (four gullies). These western sites are all within 40 river km of each other and are at ~400 m elevation. Eastern Grand Canyon sites underwent much more erosion than western sites over the course of this study, and so we focus our discussion on them (Table 3.1).

To gain a better understanding of catchment geomorphic properties at each site, vegetation cover was measured along multiple transects with an 8-pin frame, soil-surface shear strength of different surface types was measured with a torvane, sediment samples were collected for laboratory measurement of texture by standard hydrometer methods, and infiltration tests were performed with a tension-disk infiltrometer on different ground-cover types. Infiltration tests were converted to saturated hydraulic conductivity to represent minimum infiltration rate (Reynolds and Elrick, 1991).

Total-station ground surveys at all the sites in February and October bracketed the 2002 summer monsoon precipitation season, and for geomorphic purposes we collected longitudinal profiles of each gully, defined catchment areas, and measured gradient above each gully head and knickpoint. Denudation along the gully thalwegs of nine eastern Grand Canyon gullies was identified by normalizing longitudinal channel profiles from February and October and comparing elevations at each profile point. Magnitude of denudation was then compared to the local slope-contributing area product along the gully profile. Gully long profiles were also compared and analyzed in terms of knickpoint height and spacing.

The gradient and contributing drainage area above each gully head and each knickpoint were measured in the field and with a GIS, respectively, in order to investigate topographic thresholds associated with gully erosion in Grand Canyon. This was then applied in a GIS to predict areas sensitive to gullying at the western Grand Canyon sites. We were able to produce 10-cm cell-size terrain models from spline-tension interpolation of combined photogrammetry and ground-survey data at these sites, and slope and drainage area grids for this predictive model were derived from each DEM using the $D\infty$ algorithm (Tarboton, 1997). We evaluated the accuracy of the model results by the

number of predicted cells that correspond to the location of the gullies recorded in the field.

One of the original intentions of this study was to employ previous surveys from the past five years in order to evaluate longer-term gully change and erosion-control structure impacts. Most of these data came from 1997-1998 and were not included in the present analysis, mostly because previous data required correction due to an updating of the Grand Canyon survey-control system. After applying correction factors, uncertainty for these datasets was still too high for accurate erosion monitoring at our scale of interest. For example, the adjusted 1998 profile of the Palisades south-main arroyo showed about 0.3 m of degradation along the entire thalweg over the past four years, which does not agree with photographic evidence and is probably a result of coordinate-system conversion errors. Still, the gradient of the 1998 profile should be accurate and is used here to show change in the form of the important south-main Palisades gully.

RESULTS

Basic Geomorphic Data

The geomorphic setting of sites can be characterized by three zones from the top to the base of catchments. The upper catchments are typically steep (gradient > 0.5) and underlain by bedrock or colluvium (Fig. 3.3). Gully heads are usually near the base of the steep, upper catchment. Drainage basins below the upper catchment are relatively narrow and increase in contributing area very little downslope to the gully terminus. All field evidence at the sites indicates erosion is dominantly caused by infiltration-excess overland flow. Infiltration along macropores and then the return of this flow to the surface by piping is an important erosion process locally, particularly at the Palisades site where unusually sodium-rich (dispersive), silty sediment combines with a desiccation-cracked upper catchment (Appendix B). At most sites, observations and survey data indicate the studied channels erode by both knickpoint retreat and channel widening through undercutting and failure of banks (Appendices B and G).

Below the upper catchment, gullies are formed mostly in sandy-loam alluvial deposits, although better-sorted with a somewhat coarser eolian deposits blanketing the alluvial terraces are entrentched by gullies locally (Appendix C, texture data). Median

soil-surface shear strength varies with groundcover type, increasing from 0.4 for soil disturbed by human trampling or gullying, to 0.7 for soil with rainsplash crust, to 1.1 kg/cm^2 for cryptobiotic crust (Fig. 3.4, Appendix D). These data highlight the effect of disturbances like trampling on the resistance of soil to erosion, with cryptobiotic cover being nearly three times as strong as soil without crusts.

Saturated permeability also varies with cover type, but in an unexpected way. Mean permeability is 0.008 cm/s for bare ground and 0.007 cm/s for cryptobiotic crust, but then drops significantly to 0.003 and 0.004 cm/s beneath shrubs and grass, respectively (Fig 3.5A, Appendix E). This contrasts with most settings, where studies have shown that permeability beneath plants tends to be significantly higher due to macroporosity of roots (e.g. Dunne et al, 1991). This needs more study, but if this trend holds true, it would suggest that runoff at the study sites may be exacerbated by thicker ground cover. Another pattern evident in the data is that saturated permeability tends to increase with distance down the catchment, from a median of 0.003 cm/s for upper catchments, to 0.006 near gully heads, and then 0.009 cm/s near gully mouths (Fig. 3.5B, Appendix E). This is consistent with a system where runoff is readily produced in the upper, steep catchment with more resistant ground, this runoff erodes the weaker substrate of lower catchments despite the higher permeability materials there. A final interesting distinction in the permeability data is related to the properties of eolian sediment. Splitting bare ground into eolian and non-eolian subsets reveals that median infiltration of eolian sediment (0.037 cm/s) is six times higher than that of alluvium or colluvium (median = 0.006 cm/s) (Fig. 3.5C, Appendix E), reducing the relative amount of runoff eolian sand generates and increasing the amount it absorbs.

Profile Analysis

Comparison of gully profiles through time is useful for tracking knickpoint erosion and its patterns, but this study is limited by having only eight months between surveys. Profile comparisons over longer time is available for the south-main Palisades gully because of the previous work done there, but problems with survey corrections made it impossible to confidently track denudation. Despite this, comparison of profiles indicates two new, large knickpoints near the mouth of the gully since 1998 (Fig. 3.6).

The first (February) survey for this study indicates little net erosion since 1998, except for a single relatively low-gradient knickpoint near the mouth. Only eight months later, this knickpoint had enlarged and advanced several meters and another ~80 cm high knickpoint had formed near the mouth. Along with two smaller knickpoints upstream, these resulted in more net erosion in eight months than over the previous five years (Fig. 3.6). Gradient of this lower reach below a major confluence increased from 0.03 in 1998 to 0.04 in October of 2002, and erosion of the lower reach was much higher than the upper reach over the course of our study.

February-October 2002 Data

Channel longitudinal profiles of Grand Canyon gullies tend to be irregular and either straight or convex in overall shape (Figs. 3.6, 3.7, 3.8, Appendix N). Some of the broadly convex gully profiles imitate the cross-sectional shape of the terraces they form on, as in the Palisades gullies. Many profiles are generally straight, regardless of surrounding topography. Straight profiles are not unusual for dry environments where effective discharge does not necessarily increase downstream because of infiltration into the channel substrate (Leopold and Bull, 1979), and this is also consistent with our results that measured infiltration rates generally increase down catchment. Thus, the shapes of gully profile may reflect adjustment to infiltration-discharge characteristics across the catchments rather than disequilibrium or disturbance.

Denudation along channel profiles is discontinuous, with maximum values corresponding to knickpoints and relatively-steep reaches (Figs. 3.7, 3.8, Appendix N). The sections of the profiles with overall higher and more variable slope-area erosion index based on February profiles match up relatively well with reaches that had the highest denudation, suggesting that erosion correlates to the power of runoff locally. Individual denudation peaks do not correspond to individual erosion-index peaks partly because of the spacing of data, but this simple erosion index is a useful means to identify reaches along a profile with anomalously high gradient that are susceptible to knickpoint formation or retreat.

Gullies at the Basalt Cliffs site were devoid of knickpoints during the February survey but underwent substantial erosion and knickpoint formation over the study period

(Fig. 3.8). These knickpoints tended to form in places that were relatively steep but ungullied to begin with, and this suggests topographic control of gully initiation. The slope-area index of this February profile predicts erosion in five places with high index values, and this roughly matches what happened (Fig. 3.8). Reaches of anomalously high gradient and erosion vulnerability like this may be evident in the field, but the combined influence of contributing area and relatively subtle gradient variations is much more likely to be identified through modeling of an area-slope threshold for erosion using survey data.

Knickpoint Metrics

It may be useful to understand any patterns associated with knickpoint metrics such as spacing and height for the purposes of future monitoring and mitigation. The combined data for all study gullies that have four or more knickpoints indicates mean knickpoint spacing for a given channel is inversely and exponentially correlated to gradient ($r^2 = 0.92$) (Fig. 3.9):

$$D = 20e^{-9.7s} \quad (7)$$

where D is average spacing and s is mean channel gradient. This confirms intuition that steeper drainages have more knickpoints that are more closely spaced. Similarly, we may expect that a steeper gully would have taller knickpoints. Yet our data indicate no apparent correlation between steeper gullies and taller knickpoints (Fig. 3.10A). Likewise, we might anticipate that the taller knickpoints would be formed at locations with a high slope-area product, and there is a weak positive correlation ($r^2 = 0.17$) (Fig. 3.10B).

Slope-Area Analysis

The final metric related specifically to knickpoints is a plot of the relation between local gradient and contributing drainage areas above knickpoints (Fig. 3.11A). The channel gradient required to form a knickpoint generally decreases as drainage area increases, but there is a lot of scatter in this relation ($r^2 = 0.33$). Such a plot is more usefully viewed as defining a topographic threshold for erosion. A trend line with a negative slope can be drawn at the base of this scatter to represent a threshold, with the

area above the line representing drainage topography where knickpoints tend to form and the area below the threshold being topography where they do not.

Closely related to this, and having a very similar trend, is a more common type of slope-area plot using the slope immediately above channel heads rather than above downstream knickpoints (Fig. 3.10B). Not all channel heads are necessarily steep knickpoints, but they mark the boundary in the landscape between the hillslope and drainage geomorphic processes where runoff becomes concentrated enough to form drainages through erosion. There are fewer data points, but the negative relation is stronger between contributing area and local gradient ($r^2 = 0.75$). The position of a threshold line for this plot was chosen by moving a line with the same slope as the linear regression through the data to the bottom limit of the main scatter (Vandaele et al., 1996). Referring back to Equation 6, we empirically derive *a* to be 0.017 and *b* to be -0.47 for the Grand Canyon gully data here. Three points in Figure 3.10B plot below the threshold line, and are considered non-representative outliers. One point is from the faint head of a small, inactive drainage at the Kwagunt control site. The two other points are from active gully heads at the atypical Palisades site. The relatively large, unusually impermeable catchment at Palisades creates anomalously high runoff for a given contributing area in this setting.

The relation in figure 3.11B, though relatively simple, is useful for identifying areas in a landscape that are susceptible to channel processes over somewhat longer time periods and are therefore at risk of gully erosion. To do this, the detailed photogrammetry DEMs available for each of the four western Grand Canyon sites were used to make a grid of contributing drainage area. Multiplying this by 0.017 and taking this product to the -0.47 power (Eq. 1) produced grids with cell values representing critical gradients that must be exceeded for channel erosion to occur. Maps predicting areas vulnerable to gullying were then constructed by identifying locations where the actual gradient in the landscape exceeds this spatially variable critical threshold grid (Appendix O). This preliminary model showed good general ability to predict channel erosion in the places where we recorded gullies in the field (Table 3.2), but it also predicted potential gullies in many areas where none existed in the field (Fig. 3.12). These false positives probably represent places that are unincised but susceptible to

erosion, but also places where the model fails to capture the complexity of real processes at the sites.

DISCUSSION

Erosion-Threshold Predictive Model

Previous research by Thompson and Potochnik (2000) proposed the use of a predictive equation for site vulnerability that is pieced together from several sub-equations and semi-quantitative modifying factors. Their vulnerability calculations are limited by the generalization of inputs to a one-dimensional equation, and the use of several semi-quantitative factors rather than the basic few types of empirical data that control erosion. They use the equation to estimate the vulnerability of a hypothetical ungullied landform at the hillslope-terrace intersection. That is, their exercise does not actually model existing gully drainage systems and is unable to capture the essential spatial variability in controlling factors and conditions. This includes the key factor we have identified here—the sub-meter scale, site specific topographic changes that trigger incision.

Our initial GIS-based gully prediction model is distinct from Thompson and Potochnik's in several ways. It is a full three-dimensional computer model that utilizes detailed terrain models of actual sites to route and calculate the energy of the overland flow that does the work of erosion. Most importantly, it could accommodate the input of several key types of spatially variable field data that control runoff and erosion, thus allowing it to simulate actual sites with complex and variable ground conditions. In this way, our initial exercise here represents the groundwork for a more complete and useful computational tool in the future.

Results of our initial GIS effort to identify locations at sites that exceed an empirically derived area-slope erosion threshold are encouraging, and the model does well in predicting even small, discontinuous gullies that exist at sites. For example, 89% of knickpoints at the four photogrammetry study sites correspond to cells that exceed the erosion threshold in our predictive model. Cells that exceed the threshold but do not correlate to present-day gullies in the field (false positives) potentially reflect two conditions: 1) an area is near the erosion threshold and vulnerable to gullying in the

future; or 2) varying geomorphic conditions at the site prevent gullying where it would otherwise occur. The potential utility of a model such as this is its ability to identify locations that exceed a theoretical erosion threshold but that are not yet incised. If a storm produces high runoff, the "false-positive" cells could predict where the next new gully may erode, or how far an existing gully may expand.

The second potential reason for false positive predictions plays an important role in Grand Canyon, and points out how the model can be improved with further work. Many cells in our model are in areas with geomorphic properties different than the trend of the dataset used to construct the model, as illustrated by the scatter in the empirical plots (Fig 3.11). Slope-area points in figure 3.11B were primarily taken from typical gullies formed in non-cohesive sandy-loam substrate, so the threshold and any model derived from it will only apply to that average set of geomorphic conditions. In particular, infiltration rates and soil strength vary immensely over a site. For example, eolian deposits may have a sufficient slope and contributing drainage area to be sensitive to gully erosion in the model, but in reality its infiltration capacity is too high to sustain runoff. Similarly, many areas underlain by talus or by cryptobiotic crust may have the topography to exceed the erosion threshold, but its substrate is too resistant to be entrained by runoff that would erode the bare silty sand of typical gullies.

Not only do the parameters that affect the threshold of gully erosion vary with distance across a site, but they also vary through time. Montgomery and Dietrich (1994) note that channel head locations are dynamic through time and will migrate up or down slope in response to changes in climate and infiltration that affect the erosion threshold. The modeled threshold represents gullies that are predicted to form under the prevailing climate and soil conditions under which gullies have recently formed in Grand Canyon. Changes in climate, vegetation, and soil properties all vary at seasonal, decadal, and geologic time scales, and even relatively small changes can have an effect on erosion (e.g. Rogers and Schumm, 1991). For example, a decadal climate change to generally more intense precipitation, and/or less vegetative cover would result in lower infiltration, more runoff, and channel expansion—effectively decreasing the threshold for erosion. Alternatively, an increase in eolian activity could increase infiltration at sites and increase

the threshold for erosion. The static initial model we have at this point would fail to identify these expanded or contracted areas susceptible to erosion.

A more sophisticated model that includes not only topographic information but also represents geomorphic processes should be able to capture these effects of changing surface processes and be more flexible and useful for predictive purposes. Such a model would have as input parameters empirical data like those we have collected here for infiltration, soil strength, and vegetative cover, and could have the flexibility to model, for example, the expected erosion resulting from a precipitation event of prescribed magnitude and intensity. The application of such a model, in combination with detailed DTMs, could aid land managers in identifying cultural features that are at risk in Grand Canyon.

Controls on Grand Canyon Gully Erosion

Baselevel defines the potential for erosion, but erosion is actually driven by running water. The effect of a change in erosional potential on the hydrologic processes that cause erosion hinges on whether gradient is changed by the shift in baselevel. Though the pertinent geomorphic literature is consistent in its findings that baselevel is a relatively weak control on erosion and deposition at the scale of the gullies in Grand Canyon, the actual influence of a baselevel fall on upstream erosion in Grand Canyon gullies cannot be confidently known without site-specific analysis. First, the degree to which the Colorado River is the effective baselevel for the gullies is unclear, but this can be documented and measured in the field. Compounded on this, whether or not an effective baselevel fall would actually translate into a steepening of gradient near the gully mouth depends upon the the topography of individual sites. Without focused study on the site-by-site geomorphology of gullies in Grand Canyon, interpretations of the importance of different controlling factors is premature.

Future work investigating the relative roles of baselevel, infiltration characteristics, topography, and soil strength in gully erosion in Grand Canyon would be most effective if they involve both collection of field data and numerical modeling. Results thus far indicate that such research has the potential to identify the causes of this erosion and to aid in protecting cultural resources.

CHAPTER 3

FIGURES AND TABLES

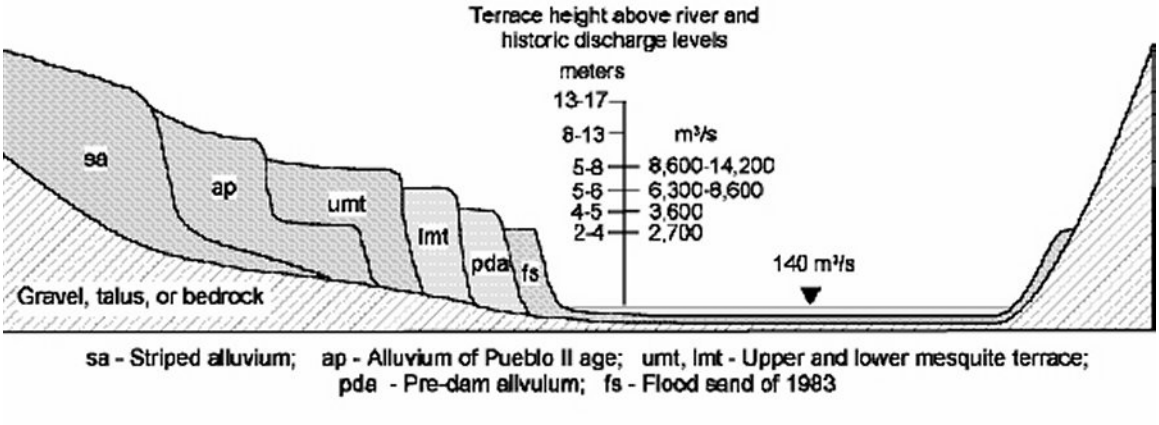

Figure 3.1. Holocene alluvial stratigraphy along the mainstem Colorado River corridor (from Fairley and Hereford, in press). Most cultural sites subject to gully erosion are associated with the striped alluvium (sa) and alluvium of Pueblo II age (ap) units.

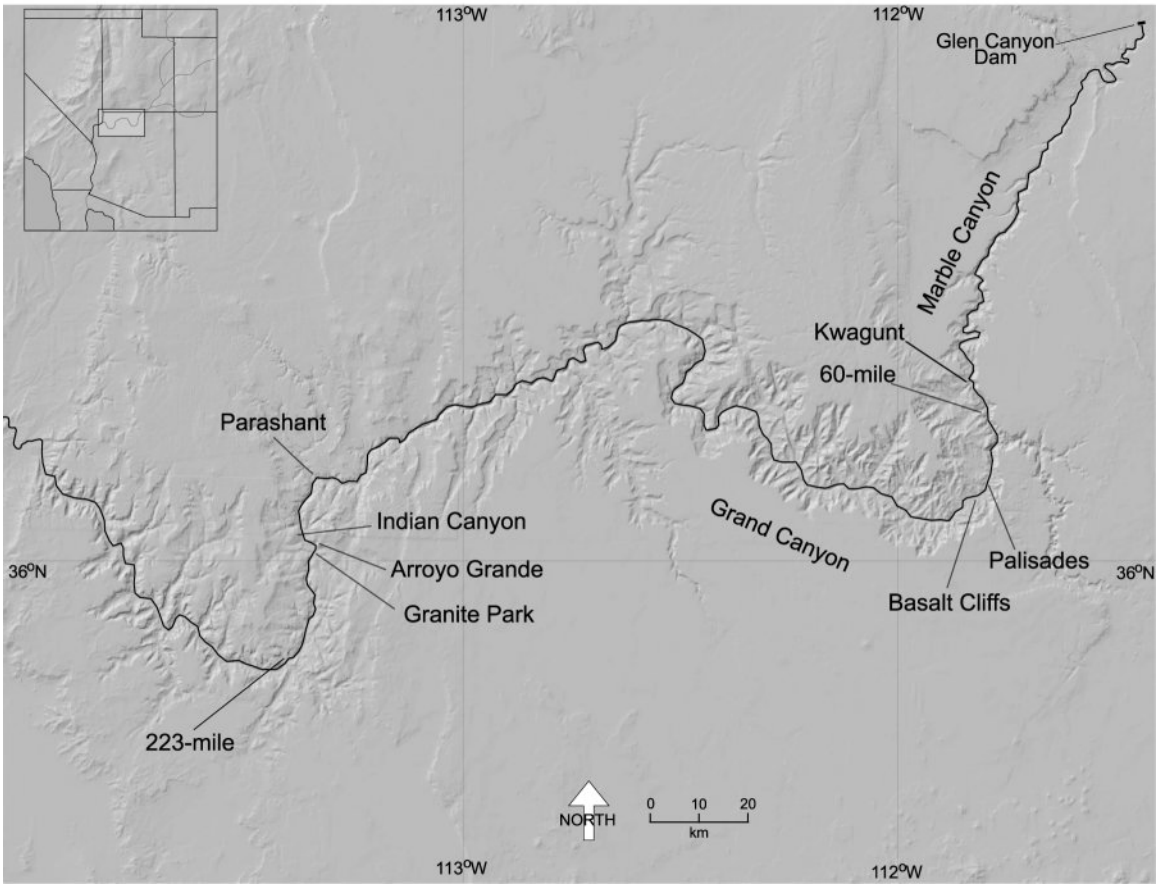

Figure 3.2. Geomorphology study site locations.

TABLE 3.1. GEOMORPHOLOGY STUDY SITE DESCRIPTIONS

Site Name	Geomorphic Setting[1]	Gully	Gradient (m/m)	Drainage Area (ha)
Kwagunt (control)	talus catchment to termination on eolian and ap2 sand	A1	0.12	0.03
60-mile	Bright Angel shale in upper catchment to eolian sand	B1	0.22	0.05
	to termination in side canyon	B2	0.22	0.04
		B3	0.24	0.02
		B4	0.23	NA
Palisades	low-relief, large distal debris fan/"playa" catchment to	C1	0.03	8.28
	ap2 terrace to termination near Colorado River	C2	0.03	0.95
		C3	0.06	0.89
		C4	0.04	0.35
Basalt Cliffs	large alluvial fan catchment; drains across toe of fan	D1	0.09	0.36
	to termination on ap terrace	D2	0.08	0.26
		D3	0.08	0.37
		D4	0.08	NA
Parashant (control)	talus catchment to termination on flat, silty, mainstem ap terrace	E1	0.17	0.08
Indian Canyon	talus catchment to eolian, ap, and termination on pda3 sand	F1	0.19	0.05
Arroyo Grande	basement rock and debris fan catchment to	G1	0.12	0.18
	termination on ap/eolian sand	G2	0.10	0.04
		G3	0.20	0.05
		G4	0.28	0.02
Granite Park	Bright Angel bedrock catchment to eolian, slopewash, and Pleistocene gravel pile to termination on debris fan	H1	0.06	0.16
223-mile	talus/debris fan catchment to eolian/ap sand to	I1	0.26	0.08
	termination in side canyon or on terrace	I2	0.27	0.06
		I3	0.40	<0.01
		I4	0.24	<0.01

[1] Describes up to downslope catchment characteristics

[2] Alluvium of Pueblo II Age (Hereford et al., 1996)

[3] Pre-Dam Alluvium (Hereford et al., 1996)

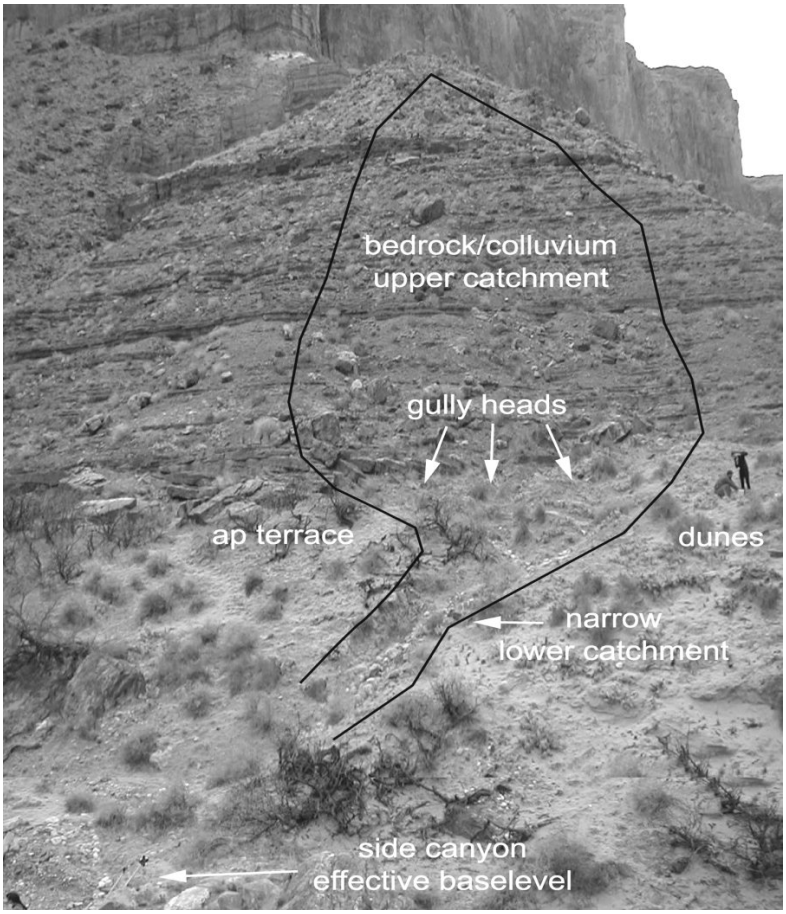

Figure 3.3. Overview of 60-mile gully catchment, which is typical geomorphic setting for several Grand Canyon gullies studied. Note people for scale at right center edge of photograph.

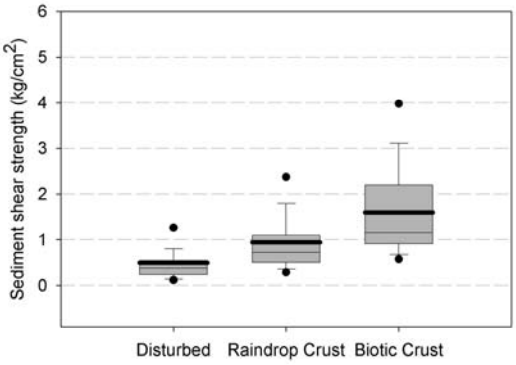

Figure 3.4. Box-and-whisker plots showing distributions of sediment shear strength data for three cover types. Dark black lines show means, lower lines of gray boxes mark the first quartile (q_1), middle lines are q_2 (or the median), and upper lines of boxes are q_3 (75%); whiskers show outliers up to 90%; dots show outliers at 95%.

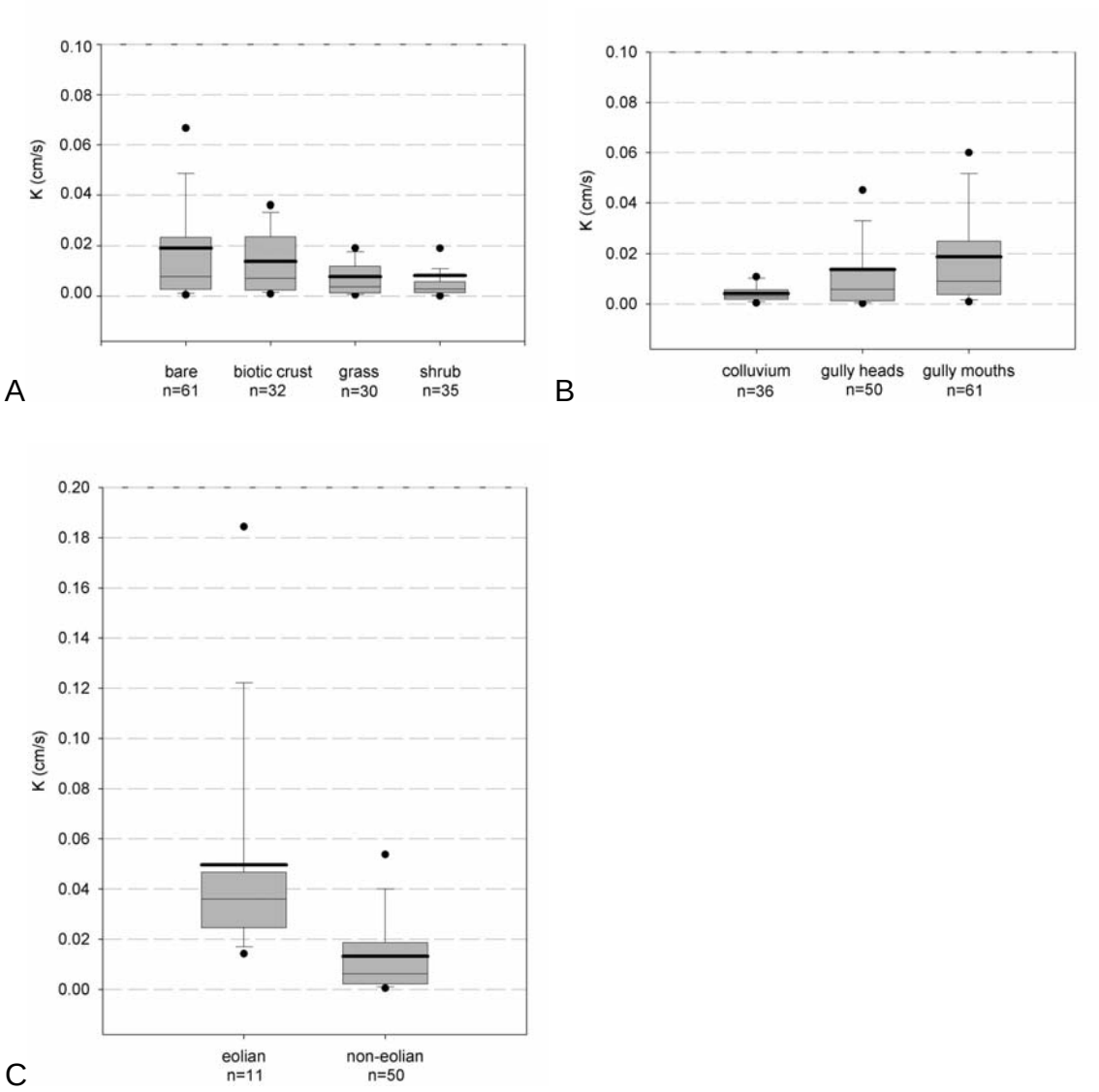

Figure 3.5. Box-and-whisker plots showing range of saturated hydraulic conductivity. A) bare ground, biotic crust, grass, and shrub cover types; B) the three catchment zones; C) eolian and non-eolian subsets of bare ground.

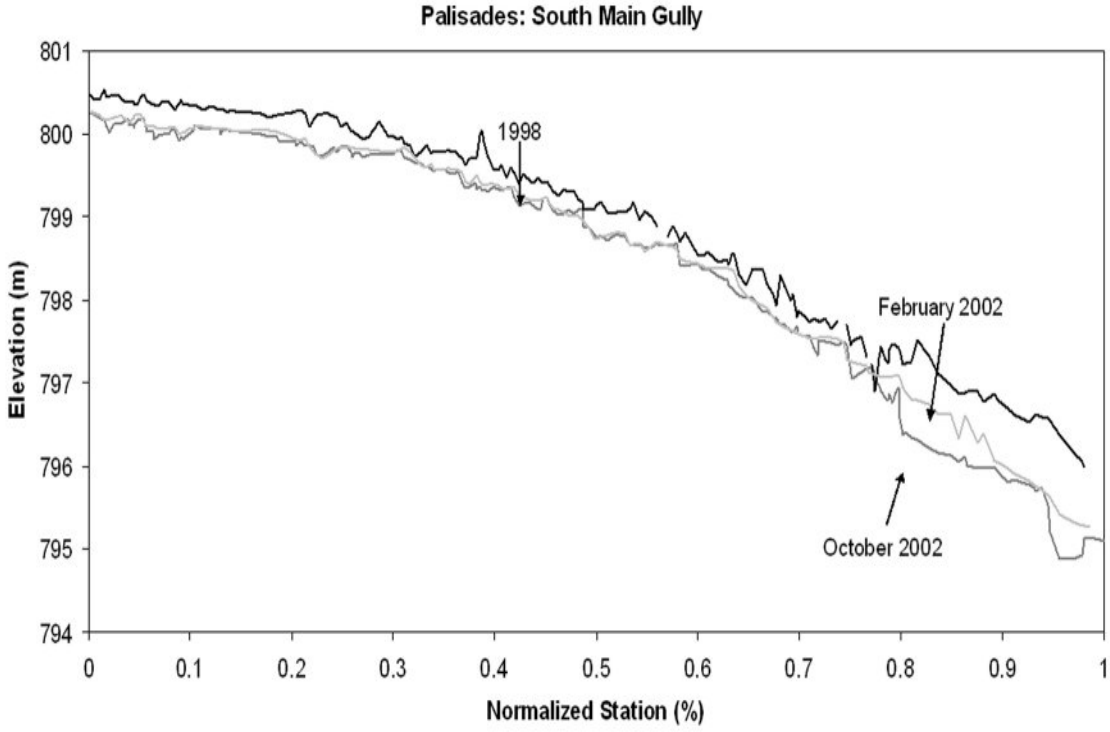

Figure 3.6. South main Palisades gully 1998 profile (Brode study) compared to the February (gray) and October (light gray) profiles of this study. normalized for. Offset of 1998 profile (~30 cm higher) is due to systematic data conversion errors (see methods).

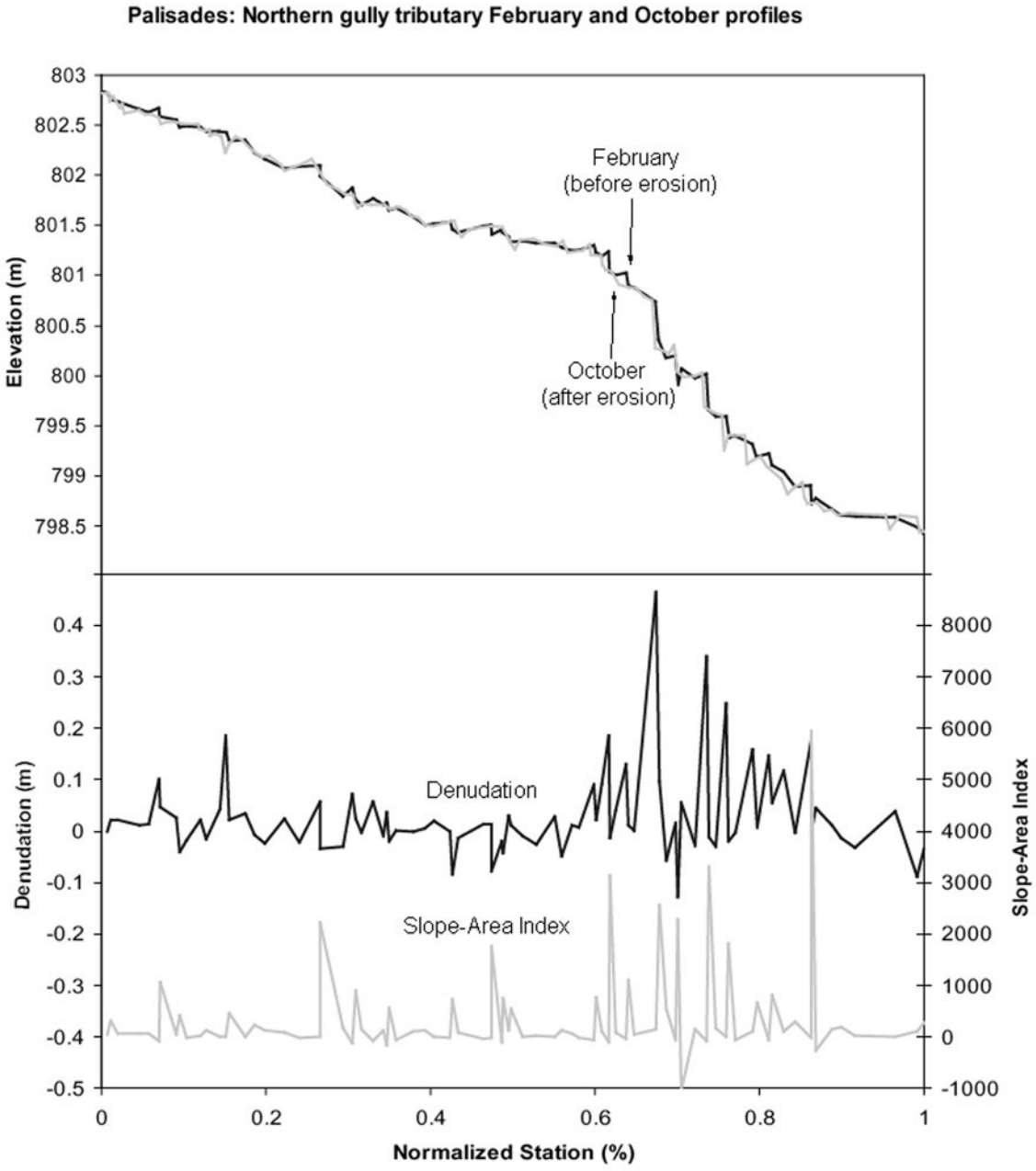

Figure 3.7. Example of the distribution of erosion along profile of northern Palisades gully. Peaks in denudation correspond to knickpoints that retreated during the study in the steeper lower reach of channel. A topographic erosion index based on the February profile is consistent with more erosion in this lower reach.

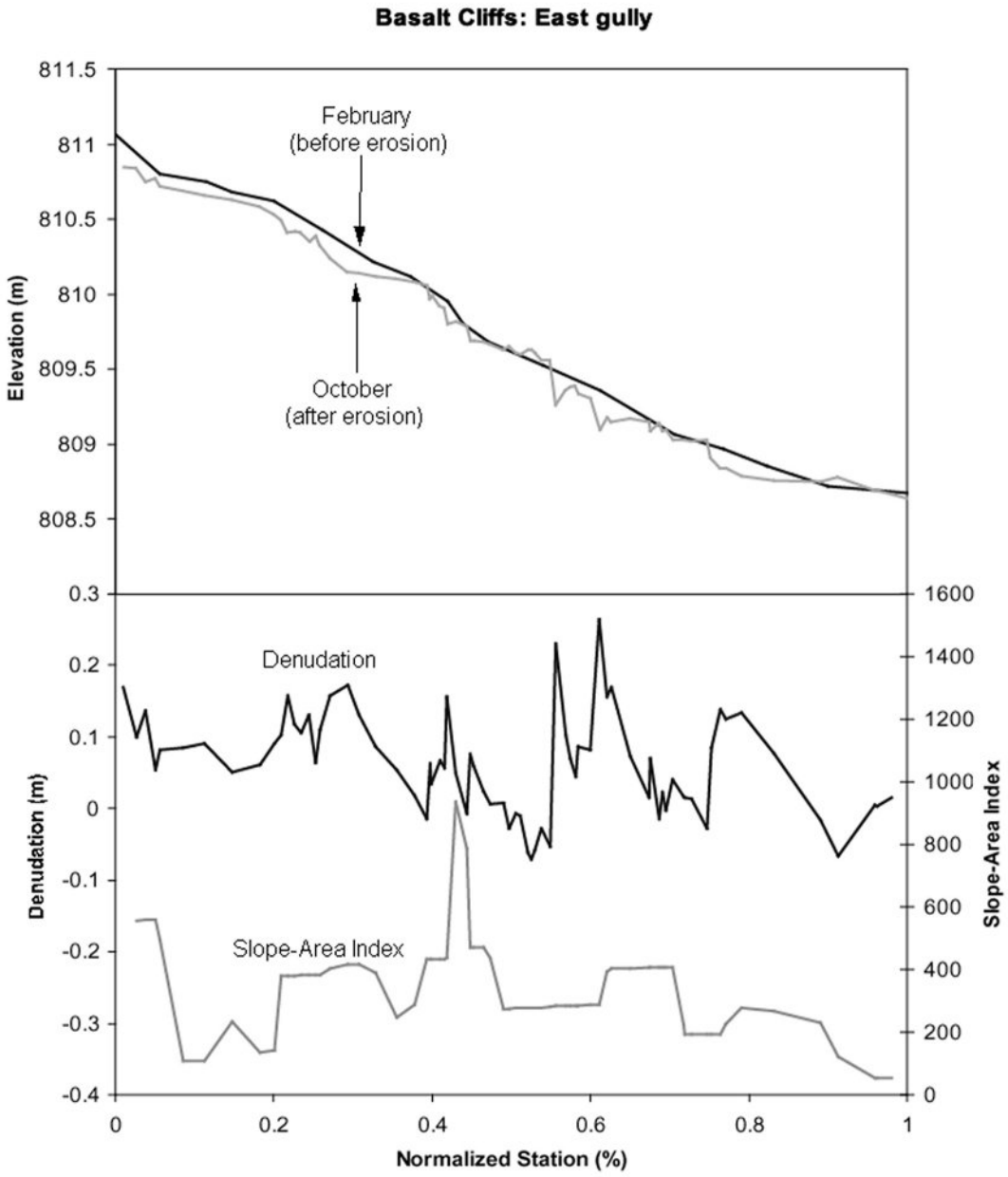

Figure 3.8. Example of profiles, denudation, and topographic erosion index along the east Basalt Cliffs gully, which did not have any knickpoints at the beginning of the study.

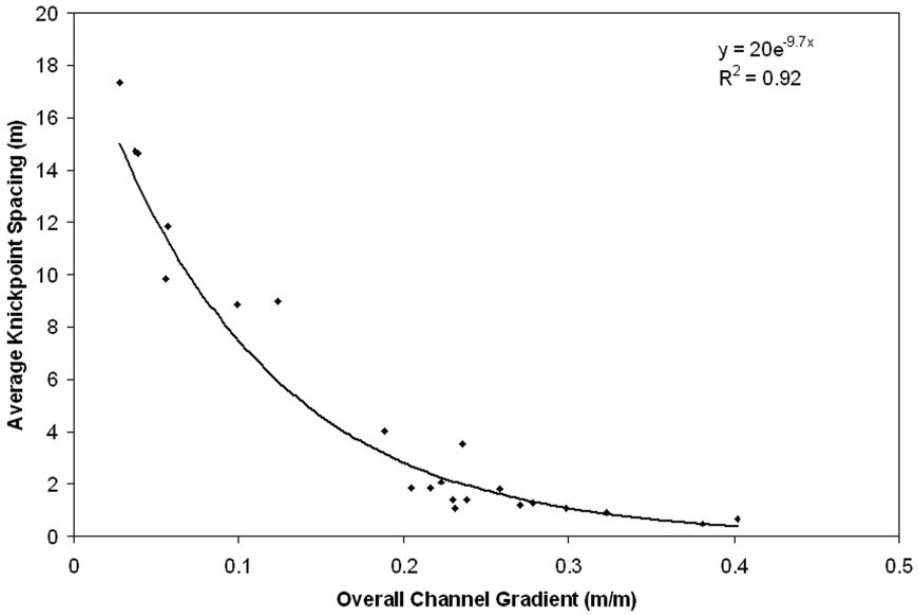

Figure 3.9. Comparison of average knickpoint spacing in a gully to the average gradient of the same gully.

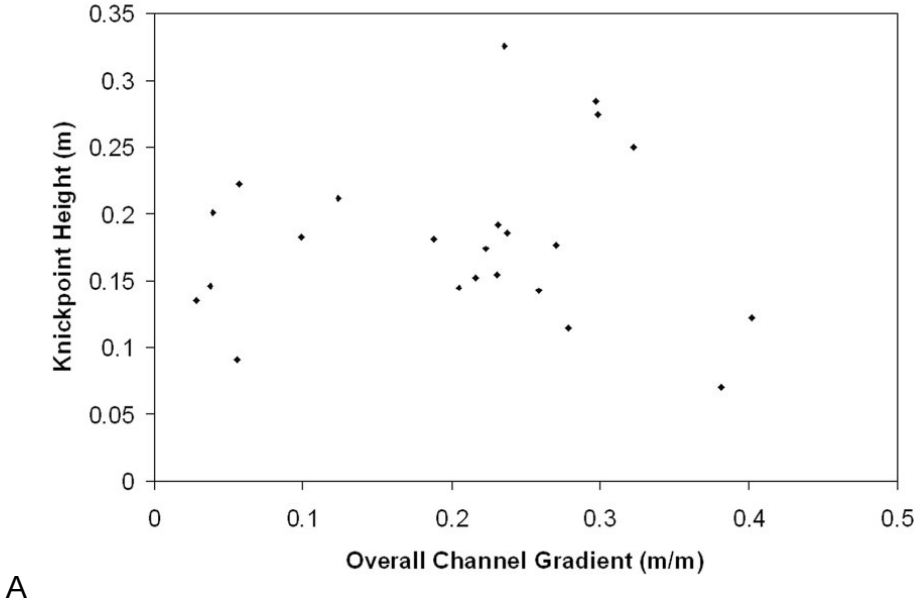

A

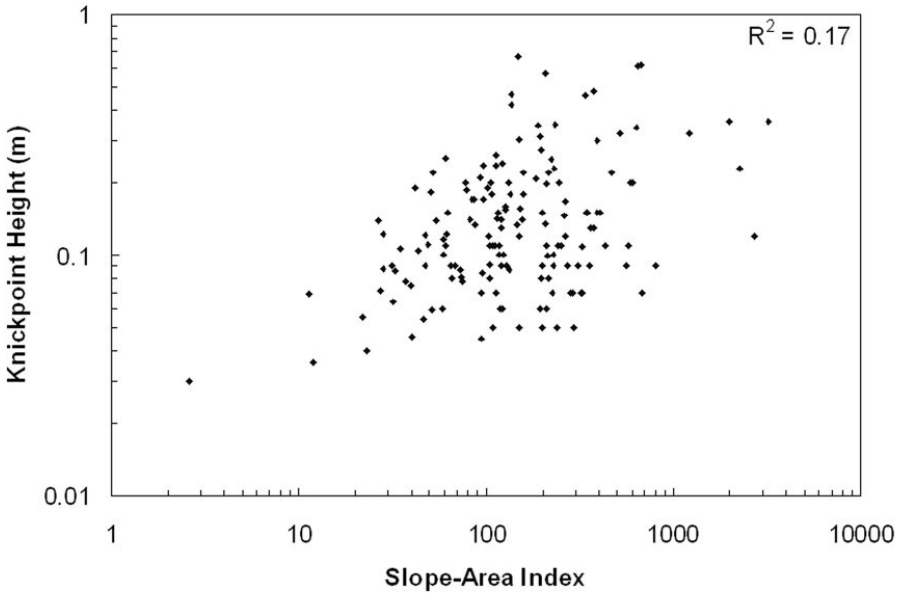

B

Figure 3.10. Comparison of knickpoint height to A) mean gradient of channel, and B) slope-area index immediately above knickpoints.

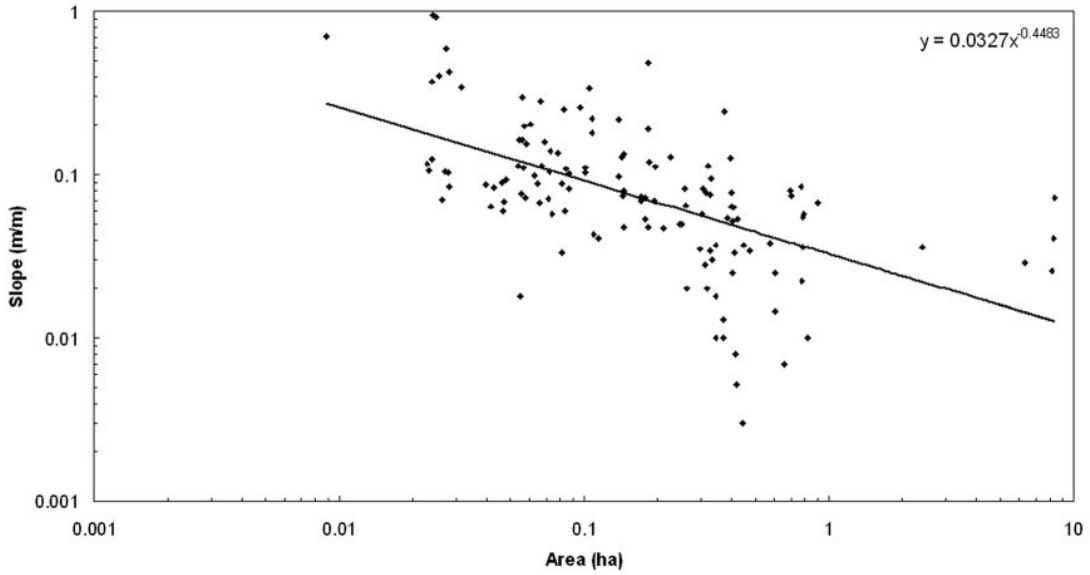

A

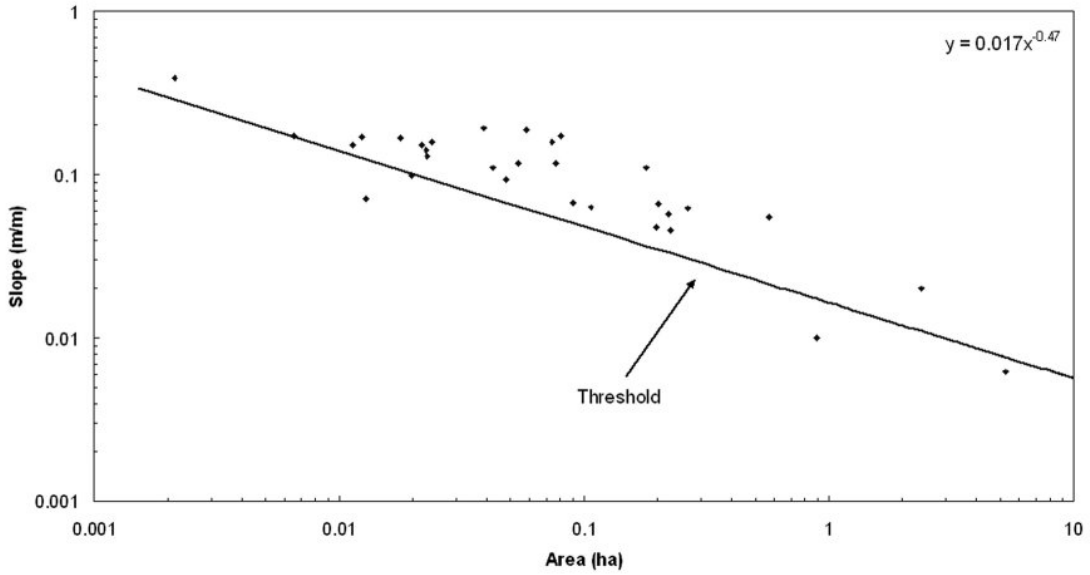

B

Figure 3.11. Slope-area plots for A) points in drainages immediately above knickpoints, and B) channel heads.

TABLE 3.2. MAPPED AND MODELED GULLIES

Site	Gullies Mapped	Represented in Model
Indian Canyon	10	10
Arroyo Grande	19	18
Granite Park	19	18
223-mile	20	20
Total	68	66

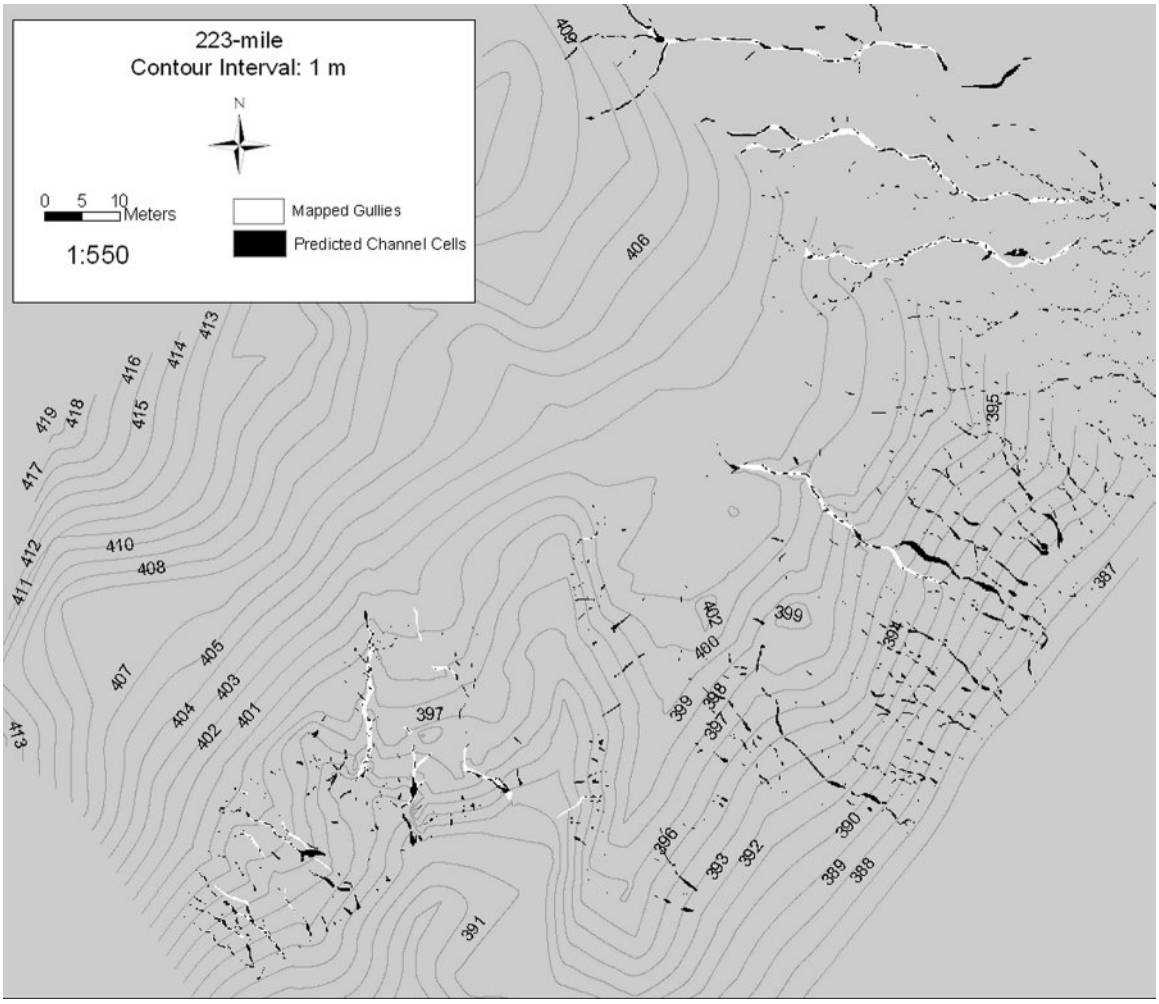

Figure 3.12. Example of predicted channel map for 223-mile site. "Predicted" cells (black) are those that have an actual slope-contributing area product that exceeds the critical value for channelization according to the threshold defined in Fig. 3.11B.

CONCLUSIONS AND RECOMMENDATIONS

The main *conclusions* from our study of erosion-control structures, photogrammetric monitoring techniques, and the geomorphology of gullies in Grand Canyon can be summarized as follows:

1) *Erosion control*: The erosion-control structures emplaced in Grand Canyon are generally successful in slowing erosion or causing deposition of sediment compared to gullies without treatments. Structures in steeper locations tend to be damaged, and damaged structures appear to exacerbate erosion and therefore need consistent maintenance. Initial data suggest brush checkdams are significantly more effective than rock linings.

2) *Aerial photogrammetry for monitoring*: Individual datasets based on 1:1600 photography had absolute-mean vertical accuracies of 6-10 cm depending upon level of interpolation. Combined successive datasets had a vertical accuracy of ~20 cm, which is larger than some of the erosion features that need to be measured. Error can be minimized with numerical guides, but vegetation, shadows, weather, photographic quality, and cost are other problems. The tool is not yet suitable to quantify erosion or track knickpoints in small channels. Advances could make aerial photogrammetry a viable option in the future.

3) *Geomorphology of gully erosion*: Erosion is happening by the processes of infiltration-excess overland flow, knickpoint retreat, and minor piping. Locally steep gradients, unexpected infiltration patterns, and varying soil strength across sites all play roles in the initiation and extent of erosion. An initial GIS-based slope-area numerical model indicates gully erosion in this setting can likely be modeled for management and scientific purposes, given a greatly expanded model parameterized with field data.

Based on these conclusions, we make the following *recommendations*:

1) Continue monitoring, construction, and especially maintenance of erosion-control structures. If it is desirable to slow the pace of erosion for site protection, then it should be recognized that low-impact erosion-control measures need to be coupled with sustained maintenance. Research should be continued to test our single-season

evaluation of erosion-control, particularly the effectiveness of brush relative to stone structures.

2) Though photogrammetry at 1:1600 scale is not yet appropriate for full monitoring, it could be useful for particular tasks including tracking larger gullies and detecting changes in planview. Photogrammetry could be reconsidered in the future as the technology advances, but other remote-sensing techniques should be pursued in the meantime.

3) Continue geomorphic studies, including monitoring of knickpoint initiation and behavior, gathering empirical data on topography, soil infiltration, soil strength, site-by-site measurement of effective baselevel, and documenting the functional relation between precipitation magnitude and intensity and resultant erosion. These field data should be combined with an expanded numerical model for use as a management tool. In addition, such a model is probably the only way to unequivocally answer questions about the causes and controls of erosion in this specific setting.

REFERENCES CITED

Adams, J.C., and Chandler, J.H., 2002, Evaluation of lidar and medium scale photogrammetry for detecting soft-cliff coastal change: Photogrammetric Record, v. 17, n. 99, p. 405 - 418.

Auzet, V., Boiffin, J., Papy, F., Ludwig, B., and Maucorps, J., 1993, Rill erosion as a function of the characteristics of cultivated catchments in the North of France, Catena: v. 20, p. 41-62.

Baldi, P., Bonvalot, S., Briole, P., Coltelli, M., Gwinner, K., Marsella, M., Puglisi, G. and Remy, D., 2002, Validation and Comparison of Different Techniques for the Derivation of Digital Elevation Models and Volcanic Monitoring (Vulcano Island, Italy): International Journal of Remote Sensing, v. 22, p. 4783 - 4800.

Barker, R., Dixon, L., and Hooke, J., 1997, Use of terrestrial photogrammetry for monitoring and measuring bank erosion: Earth Surface Processes and Landforms, v. 22, p. 1217-1227.

Begin, Z.B. and Schumm, S.A., 1979, Instability of alluvial valley floors: a method for its assessment: Transcriptions of the American Society Agricultural Engineers, n. 23 (4), p. 347-350.

Brasington, J., Rumsby, B.T., and McVey, R.A., 2000, Monitoring and modeling morphological change in a braided gravel-bed river using high resolution GPS-based survey: Earth Surface Processes and Landforms, v. 25, p. 973-990.

Brush, L.M., and Wolman, M.G., 1960, Knickpoint behavior in noncohesive material: a laboratory study: GSA Bulletin, v. 71, p. 59-74.

Bull, W.B., 1997, Discontinuous ephemeral streams: Geomorphology, v. 19, p. 227-276.

Desmet, P.J.J., Poesen, J., Govers, G., and Vandaele, K., 1999, Importance of slope gradient and contributing area for optimal projection of the initiation and trajectory of ephemeral gullies: Catena, v. 37, p. 377-392.

Dierker, J.L., Leap, L.M., and Andrews, N.B., 2002, Fiscal year 2002 archaeological site monitoring and management activities along the Colorado River in Grand Canyon National Park, RCMP Report #87, Flagstaff, AZ (submitted to the US Bureau of Reclamation, Salt Lake City, UT, Acquisition no. 99-AA-40-2340.

Dunne, T., Zhang, W., Aubrey, B.F., 1991, Effects of rainfall, vegetation, and microtopography on infiltration and runoff: Water Resources Research, v. 29, p. 2271-2285.

Elliot, J.G., Gellis, A.C., and Aby, S.B., 1999, Evolution of arroyos: incised channels in the Southwestern United States, *in* Darby, S.E. and Simon, A., eds., Incised River Channels, John Wiley & Sons Ltd., p. 153-185.

Fairley, H.C., Bungart, P.W., Coder, C.M., Huffman, J., Samples, T.L., and Balsom, J.R., 1994, The Grand Canyon River Corridor Survey Project: Archaeological Survery along the Colorado River between Glen Canyon Dam and Separation Canyon. Cooperative Agreement No. 9AA-40-07920, Grand Canyon National Park.

Prepared in cooperation with the Bureau of Reclamation, Glen Canyon Environmental Studies, Flagstaff.

Fairley, H.C. and Hereford, R., 2002, Geoarchaeological research along the Colorado River in Grand Canyon, Arizona, *in*, Philips, B.P., ed., Papers in honor of Robert C. Euler, 10 ms p. 4 figs.

Fetherson, K.L., Naiman, R.J., and Bilby, R.E., 1995, Large woody debris, physical processes, and riparian forest development in montane river networks of the Pacific Northwest: Geomorphology v. 13, p. 133-144.

Fischenich, C., 2001, Impacts of stabilization measures: Water Operations Technical Support Program Special Report ERDC TN-EMRRP-SR-32, Vicksburg, MS.

Florsheim, J.L., Mount, J.F., and Rutten, L.T., 2001, Effect of baselevel change on floodplain and fan sediment storage and ephemeral tributary channel morphology, Navarro River, California: Earth Surface Processes and Landforms, v. 26, p. 219-232.

Foster, G.R., 1986, Understanding ephemeral gully erosion, *in* National Research Council, Board of Agriculture, Soil Conservation: Assessing the National Research Inventory, National Academy Press, Washington, D.C., n. 2, p. 90-118.

Gardener, T.W., 1983, Experimental study of knickpoint and longitudinal profile evolution in cohesive, homogeneous material: GSA Bulletin v. 94, p. 664-672.

Gellis, A.C., 1996, Gullying at the Petroglyph National Monument, New Mexico: Journal of Water Soil Conservation, v. 51, n. 2, p. 155-159.

Gellis, A.C., Cheama, A., Laahty, V., and Lalio, S., 1995, Assessment of gully-control structures in the Rio Nutria Watershed, Zuni Reservation, New Mexico: Water Resources Bulletin, v. 31, n. 4, p. 633-646.

Gellis, A.C., Hereford, R., Schumm, S.A., and Hayes, B.R., 1991, Channel evolution and hydrologic variations in the Colorado River Basin—factors influencing sediment and salt loads: Journal of Hydrology, v. 124, p. 307-314.

Gilbert, G.K., 1877, Geology of the Henry Mountains (Utah): U. S. Geographical and Geological Survey of the Rocky Mountains Region: Washington D.C., U. S. Government Printing Office, 170 p.

Graf, W.L., 1982, Distance decay and arroyo development in the Henry Mountains regions, Utah: American Journal of Science, v. 282, n. 11, p. 1541-1554.

Griffiths, P.G., Webb, R.H. and Melis, T.S., 1996, Initiation and frequency of debris flows in Grand Canyon, Arizona: U.S. Geological Survey Open-File Report 96-491, 35 p.

Hack, J.T., 1957, Studies of longitudinal stream profiles in Virginia and Maryland: United States Geological Survey Professional Paper, 294B.

Hapke, C., and Richmond, B., 2000, Monitoring beach morphology changes using small-format aerial photography and digital softcopy photogrammetry: Environmental Geosciences, v. 7, n. 1, p. 32-37.

Harvey, A.M., 1994, Influence of slope/stream coupling on process interactions on eroding gully slopes: Howgill Fells, northwest England, *in* Kirkby, M.J., ed., Process Models and Theoretical Geomorphology, John Wiley & Sons Ltd, p. 247-270.

Hazel, J.E., Kaplinski, M., Manone, M., and Parnell, R., 2000, Monitoring arroyo erosion of pre-dam river terraces in the Colorado River ecosystem, 1996-1999, Grand Canyon National Park, Arizona: Draft Final Report to the Grand Canyon Monitoring and Research Center, Flagstaff, AZ, 29 p.

Heede, B.H., 1966, Design, construction, and cost of rock check dams: U.S. Forest Service Research Paper RM-20, 24 p.

Heede, B.H., 1976, Gully development and control: U.S. Department of Agriculture Research Paper RM-169, 40 p.

Heipke, C., 1995, State-of-the-art of digital photogrammetric workstations for topographic applications: Photogrammetric Engineering and Remote Sensing, v. 61, p. 49-56.

Hereford, R., Fairley, H.C., Thompson, K.S., and Balsom, J.R., 1993, Surficial Geology, Geomorphology, and Erosion of Archaeological Sties along the Colorado River, Eastern Grand Canyon, Grand Canyon National Park, Arizona: U.S. Geological Survey Open-File Report 93-517.

Hereford, R., and Webb, R.H., 1992, Historic variation in warm season rainfall on the Colorado Plateau, USA: Climatic Change, v. 22, p. 239-256.

Hereford, R, Thompson, K.S., Burke, K.J., and Fairley, H.C., 1996, Tributary debris fans and the late Holocene alluvial chronology of the Colorado River, eastern Grand Canyon, Arizona, v. 108, n. 1, p. 3-19.

Heritage, G.L., Fuller, I.C., Charlton, M.E., Brewer, P.A., and Passmore, D.P., 1998, CDW photogrammetry of low relief fluvial features: accuracy and implications for reach-scale sediment budgeting: Earth Surface Processes and Landforms, v. 23, p. 1219-1233.

Higgins, C.G., 1990, Gully development, with a case study by Hill, B.R., and Lehre, A.K., *in* Higgins, C.G. and Coates, D.R., eds., Groundwater Geomorphology; The role of subsurface water in Earth-surface processes and landforms: Boulder, Colorado, Geological Society of America Special Paper 252.

Holland, W.N., and Pickup, G., 1976, Flume study of knickpoint development in stratified sediment: GSA Bulletin, v. 87, p. 76-82.

Jaeggi, M., and Zarn, B., 1999, Stream channel Restoration and erosion control for incised channels in alpine environments, *in* Darby, S.E. and Simon, A., eds., Incised River Channels, John Wiley & Sons Ltd., p. 343-369.

Kaetz, A.G., and Rich, L.R., 1939, Report of surveys made to determine grade of deposition above silt and gravel barriers: U.S. Soil Conservation Scr., Albuquerque, N.M., mineogr.

Karlstrom, T.N.V., 1988, Alluvial chronology and hydrologic change of Black Mesa and nearby regions, *in* Gummerman, G.J., ed., The Anasazi in a changing environment: New York, Cambridge University Press, p. 45-91.

Knighton, D., 1998, Fluvial Forms and Processes, John Wiley & Sons Ltd., p. 30-32.

Leopold, L., and Bull, B., 1979, Baselevel, aggradation, and grade: Proceedings of the American Philosophical Society, v. 123, n. 3, p. 168-202.

Manga, M., and Kirchner, J.W., 2000, Stress partitioning in streams by large woody debris: Water Resources Research, v. 36, p. 2373-2379.

Merkel, W.H., Woodward, D.E., and Clarke, C.D., 1988, Ephemeral gully erosion model (EGEM), *in* Modelling Agricultural, Forest and Rangeland Hydrology, Proc. 1988 Int. Symp. 12-13 December 1988, p. 315-323.

Montgomery, D.R., and Buffington, J.M., 1993, Channel classification, prediction of channel response, and assessment of channel condition, Report to the Sediment, Hydrology, and Mass Wasting Committee of the Washington State Timber/Fish/Wildlife Agreement, Department of Geological Sciences and Quaternary Research Center, University of Washington, Seattle, 83 p.

Montgomery, D.R., and Dietrich, W.E., 1994, Landscape dissection and drainage area-slope thresholds, *in* Kirkby, M.J., ed., Process Models and Theoretical Geomorphology, John Wiley & Sons Ltd, p. 221-246.

Norton, J.B., Bowannie Jr., F., Peynetsa, P., Quandelacy, W., and Siebert, S.F., 2002, Native American methods for conservation and restoration of semiarid ephemeral streams: Journal of Soil and Water Conservation, v. 57, n. 5, p. 250-258.

O'Brien, L.E., Coleman, A., Blank, B.L., Grams, P.E., and Schmidt, J.C., 2000, Testing the application of digital photogrammetry to monitor topographic changes of sandbars in the Colorado river ecosystem: Final Report to the Grand Canyon Monitring and Research Center, Flagstaff, AZ, 32 p.

Oka, N., 1998, Application of photogrammetry to the field observation of failed slopes: Engineering Geology, v. 50, p. 85-100.

Patton, P.C., and Schumm, S.A., 1975, Gully erosion, Northwestern Colorado: a threshold phenomenon: Geology, v. 3, p. 83-90.

Powell, J.W., 1875, Exploration of the Colorado River of the west and its tributaries: Smithsonian Institute Annual Report, 291 p.

Reynolds, W.D., and Elrick, D.E., 1991, Determination of hydraulic conductivity using a tension infiltrometer: Soil Science Society of America Journal, v. 55, n. 3, p. 633-639.

Rogers, R.D., and Schumm, S.A., 1991, The effect of sparse vegetative cover on erosion and sediment yield: Journal of Hydrology, v. 123, p. 19-24.

Schumm, S.A., 1993, River response to baselevel change: implications for sequence stratigraphy: Journal of Geology, v. 101, p. 279-294.

Schumm, S.A. and Hadley, R.F., 1957, Arroyos and the semi-arid cycle of erosion: American Journal of Science, v. 225, p. 161-174.

Schumm, S.A., and Rea, D.K., 1995, Sediment yield from disturbed earth systems: Geology, v. 23, n. 5, p. 391-394.

Squires, G.L., 1968, Practical Physics, McGraw-Hill: London.

Tarboton, D., 1997, A new method for the determination of flow directions and contributing areas in grid digital elevation models: Water Resources Research, v. 33, n. 2, p. 309-319.

Thompson K.S., and Potochnik, A.R., eds., 2000, Development of a Geomorphic Model to Predict Erosion of pre-Dam Colorado River Terraces Containing Archaeological Resources: Cultural Resources Report No. 99-257 prepared for the Grand Canyon Monitoring and Research Center by SWCA, Inc., Environmental Consultants, Flagstaff, AZ, 130 p. plus appendices.

Thorne, C.R., Zevenbergen, L.W., Grissinger, E.H., and Murphey, J.B., 1986, Ephemeral gullies as sources of sediment, Proc. Fourth Federal Interagency Sedimentation Conf., Las Vegas, Nevada, 1, p. 3.152-3.161.

Vandaele, K., Poesen, J., Gover, G., and van Wesemael, B., 1996, Geomorphic threshold conditions for ephemeral gully incision: Geomorphology, v. 16, p. 161-173.

Western Regional Climate Center, 2003, Arizona Climate Summaries: http://www.wrcc.dri.edu/summary/climsmaz.html.

Woolhiser, D.A., and Lenz, A.T., 1965, Channel gradients above gully-control structures: Journal of the Hydraulics Division, Proceedings of the American Society of Civil Engineers, Paper 4333, p. 165-187.

Yeats, M., 1996, High elevation sand deposition and retention from the 1996 spike flow: An assessment for cultural resources stabilization: Report on file at the Grand Canyon Monitoring and Research Center, Flagstaff, AZ, 32 p.

Appendix A. Site Maps
(Naming and showing locations of gullies, erosion-control structures, infiltration stations, vegetation transects, and cross-section lines)

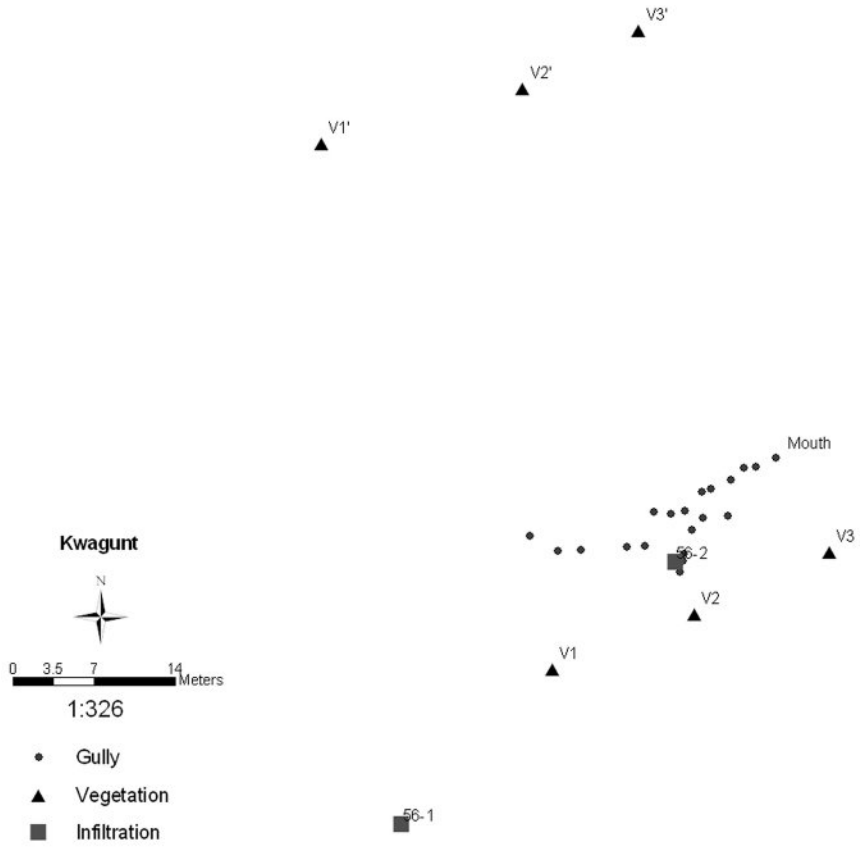

Figure A.1. Kwagunt site map (no base photography available).

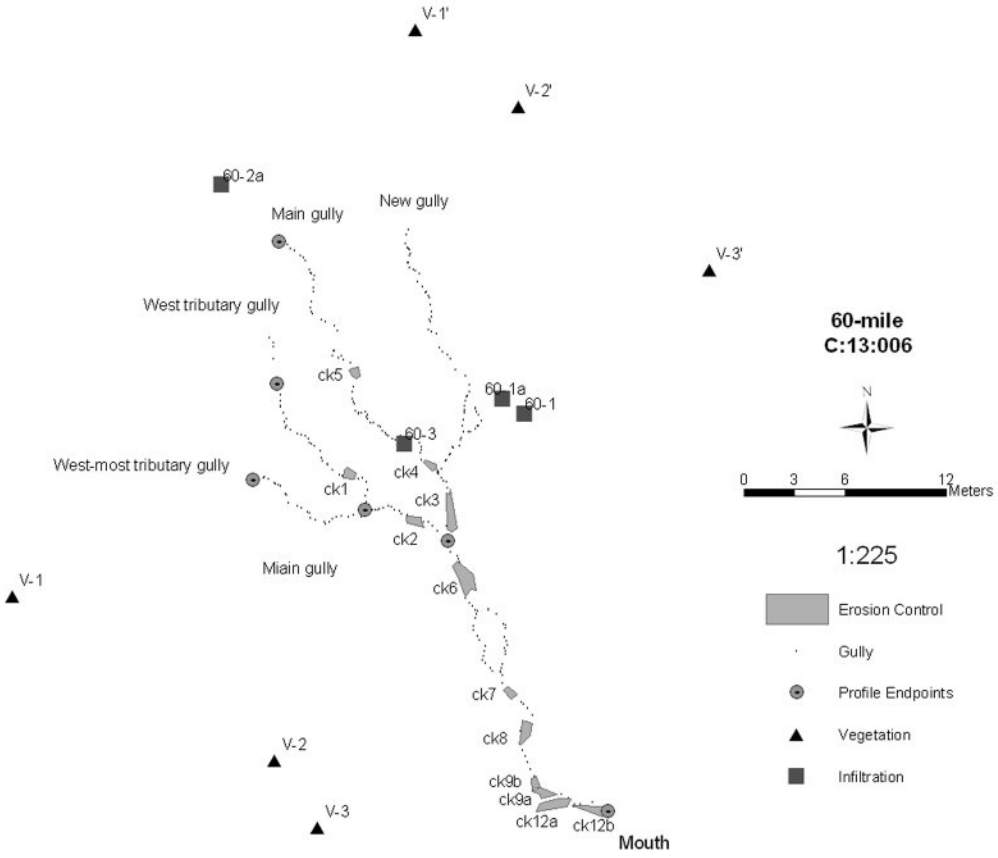

Figure A.2. 60-mile site map (no base photography available).

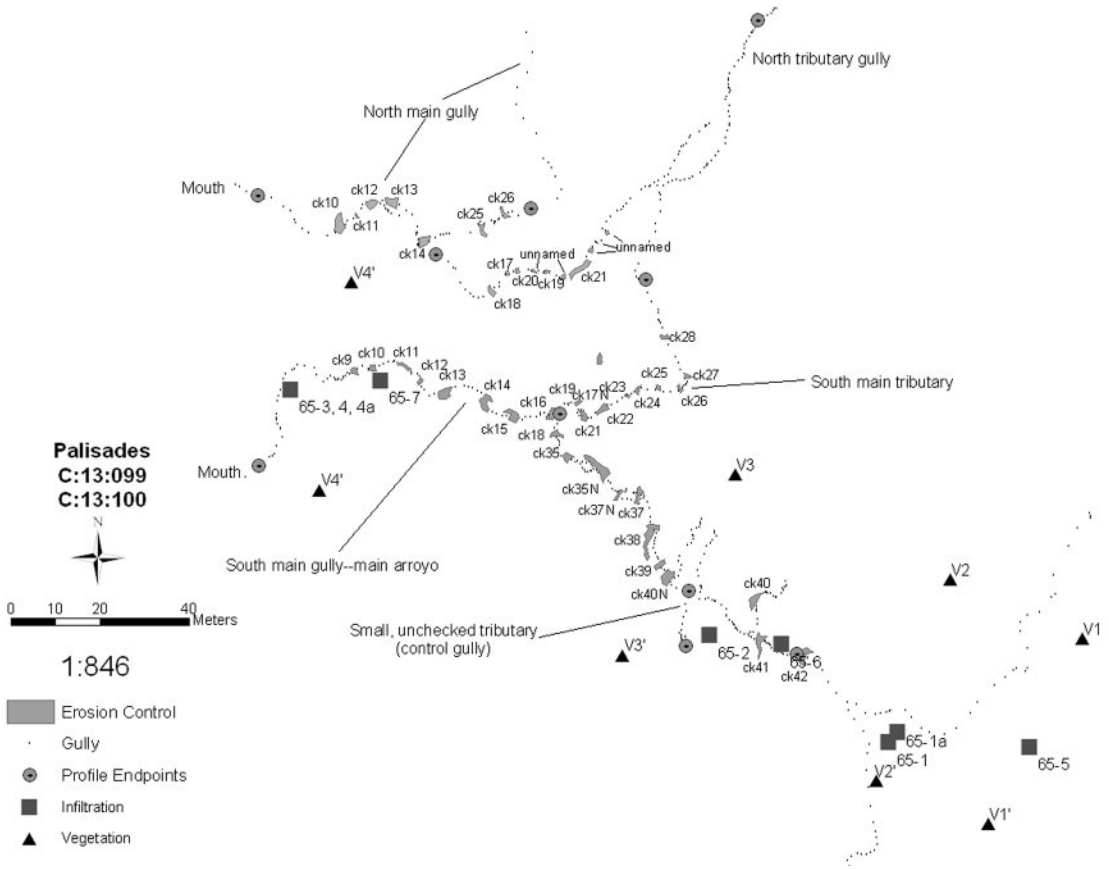

Figure A.3. Palisades site map (no base photography available).

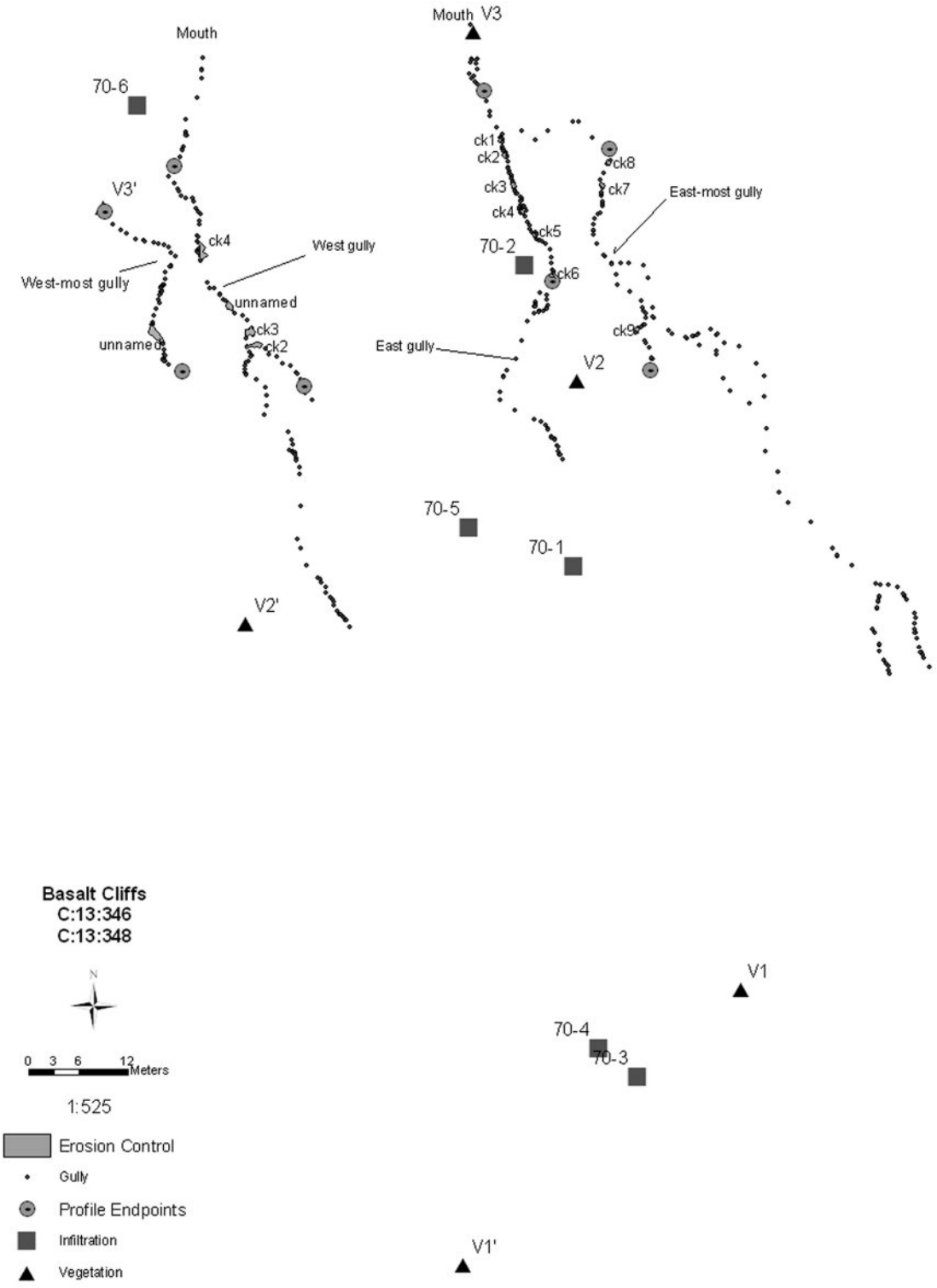

Figure A.4. Basalt Cliffs site map (no base photography available).

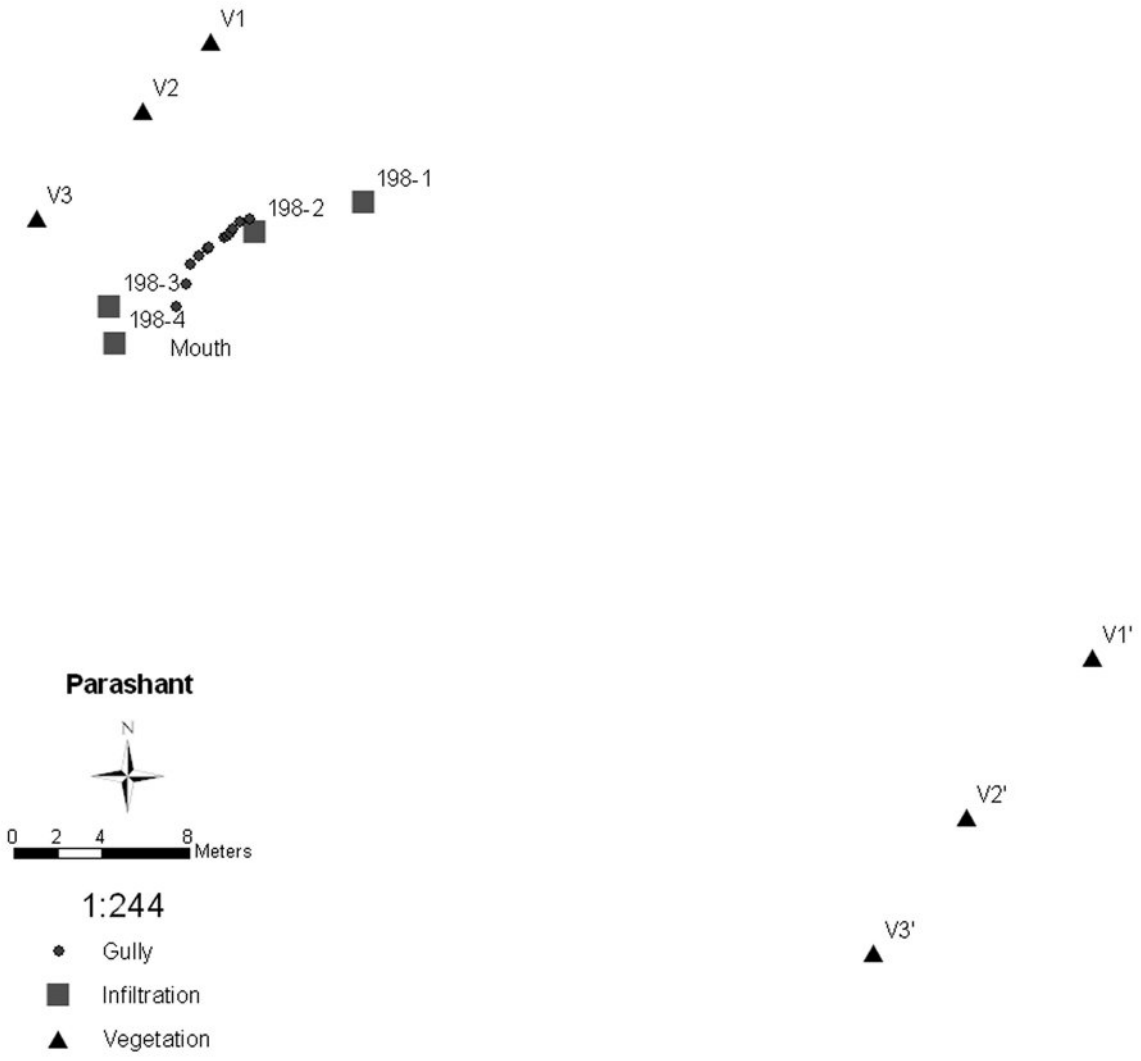

Figure A.5. Parashant site map (no base photography available).

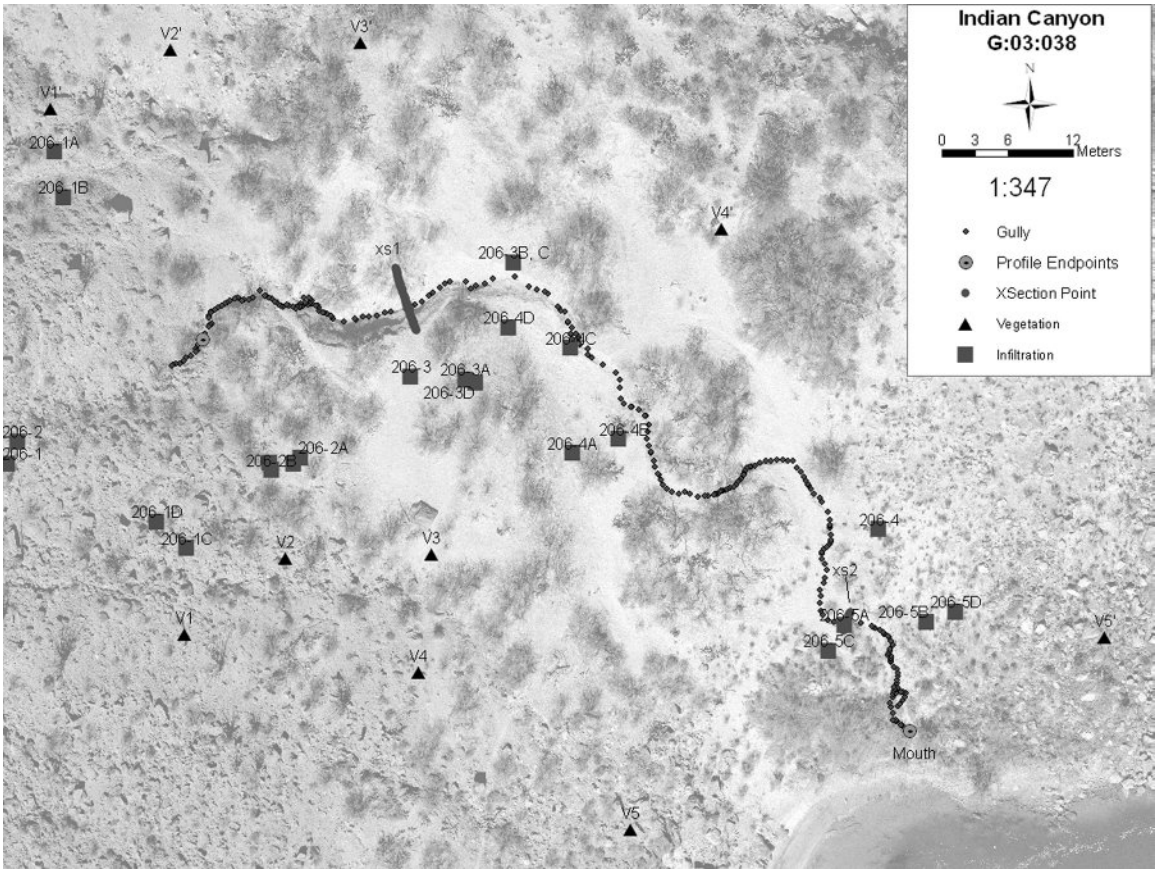

Figure A.6. Indian Canyon site map.

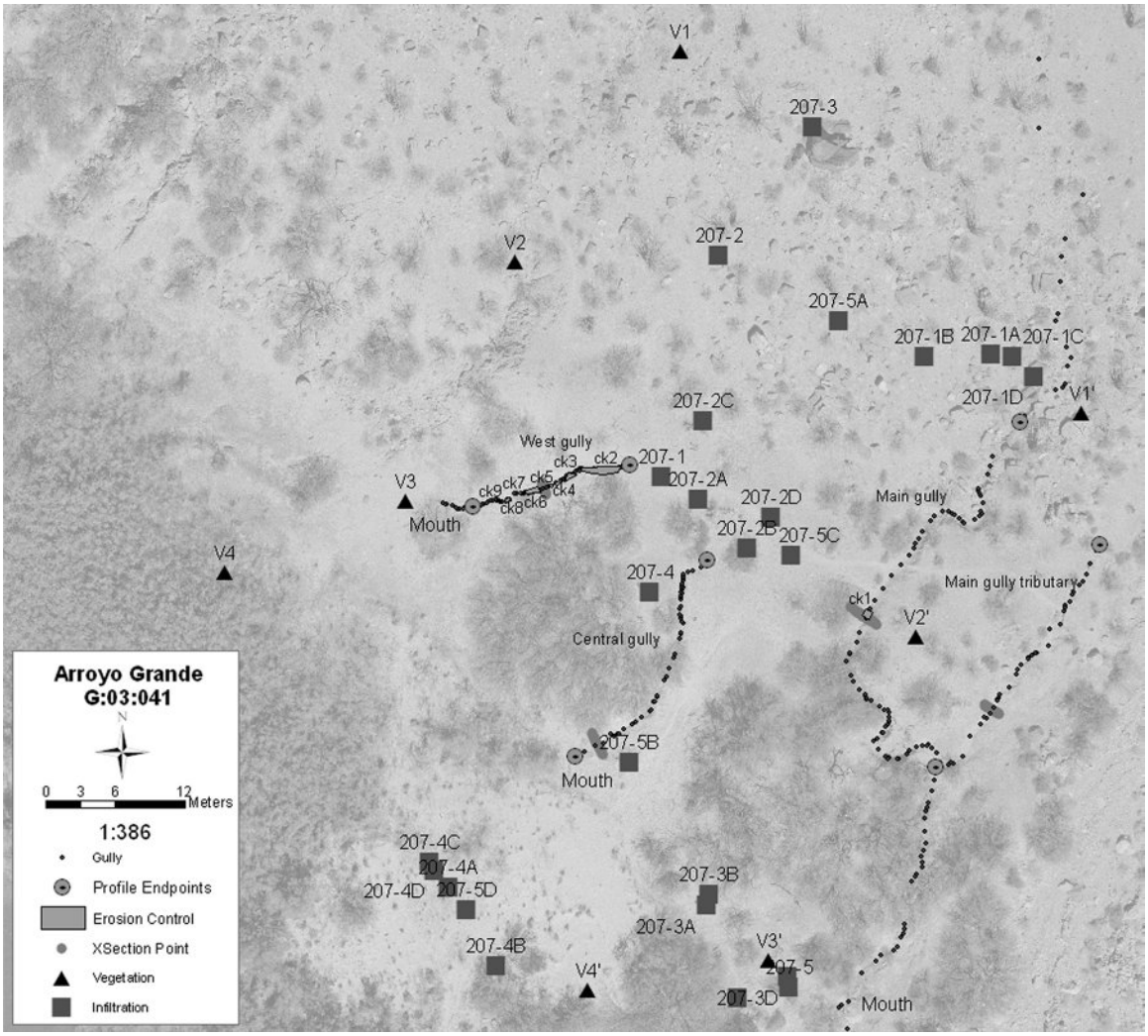

Figure A.7. Arroyo Grande site map.

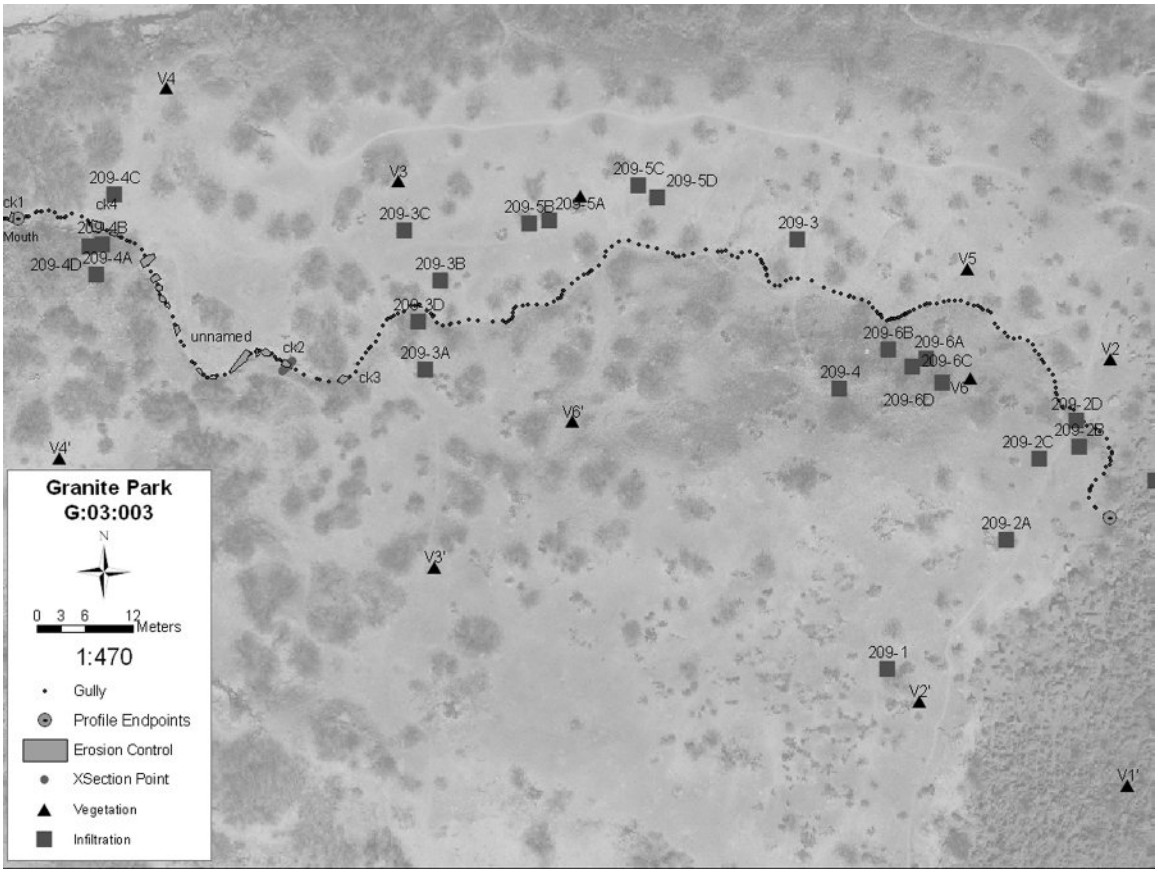

Figure A.8. Granite Park site map.

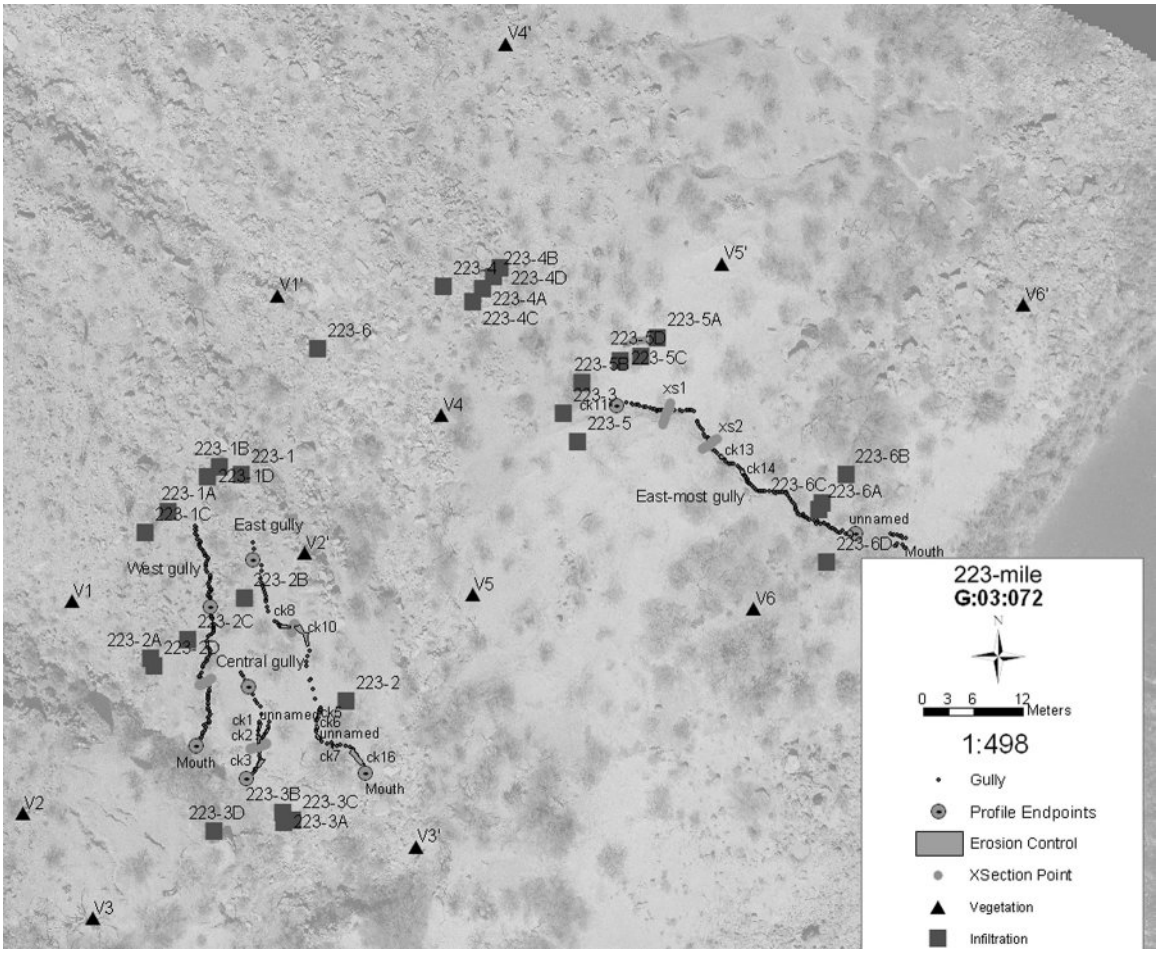

Figure A.9. 223-mile site map.

Appendix B. Site Descriptions
(Overview of catchment geomorphology)

Kwagunt

Kwagunt serves as an erosion-control site; there is no active gully erosion endangering archaeological features. There are two very small gully channels, neither of which features any knickpoints. The catchment is very small (~0.03 ha) and the channel gradients are ~12%. Both channels appear to be old and inactive, and are probably experiencing infilling. The northern channel experienced runoff during the study period, but did not show signs of channel incision or widening. The upper catchment faces the northeast and is set in talus boulders derived from Redwall limestone, Muav limestone, and Bright Angel shale. The small gully features exist at the toe of the talus, where there is still relatively steep gradient, and drains within the ap terrace. A major trail trends parallel to the hillslope near the site. The archaeological site itself lies between the talus toe and a large foredune to the east. All dunes and eolian activity exist to the east of the study site. Vegetation is dominated by cryptobiotic crust, grass and forbs, brittle brush, salt brush, and mesquite. The abundance of grass and forbs and organic detritus relative to other sites is notable.

Figure B.1. Overview of Kwagunt site. Photograph taken on dune, facing southwest. Person standing on boulder for scale.

60-mile

The 60-mile site features one active gully with four notable tributary branches; archaeological sites are endangered and are actively being destroyed. The catchment is small (0.12 ha) and the main gully drops nearly 11 m over the length of 46 m (24% slope). All of the gully channels feature many abrupt, steep knickpoints, and most contain stone erosion-control structures. Channels widened and incised during the summer of 2002, and the east-most tributary is entirely new. The upper catchment is south-facing and is composed of Bright Angel shale bedrock. The gullies begin in the bedrock, and incise through a dune-dominated ap terrace, and drain to a tributary to the Colorado River. The site has experienced trailing on the dune near the gullies, but this path is becoming less visible due to Park Service efforts. Eolian activity is high and the site is very sensitive to impacts due to its dune setting. Vegetation is dominated by cryptobiotic crust, grass and forbs, mesquite, cholla, prickly pear, saltbrush, and fedra. Raindrop erosion and crusts are readily visible. Infiltration-excess overland flow dominates the runoff regime, creating knickpoints and plunge-pools.

Figure B.2. Overview of 60-mile catchment. Photo taken facing north. Main gully trends through lower middle portion of photo.

Palisades

The Palisades site features two very large active gullies, each with a high density of tributaries; archaeological sites are endangered and are actively being destroyed. The catchments are large (~2 ha) and the two gullies drop 5 and 7 m over the length of 185 and 180 m (4 and 5% slope), respectively. All of the gully channels feature many abrupt, steep knickpoints, and most contain stone erosion-control structures. Channels widened and incised during the summer of 2002. The upper catchment faces the west and is composed of Dox sandstone and Cardenas basalt bedrock and talus. The middle catchment consists of a virtually impermeable, flat, cracked, salt-crusted "playa." The gullies begin in this playa area, and incise through an expansive mainstem alluvial ap terrace, draining in or near the Colorado River. The site has experienced trailing on both upper and lower sections. Eolian activity is present. Vegetation is dominated by cryptobiotic crust, grass and forbs, mesquite, prickly pear, saltbrush, and arroweed. Salt crusts are prevalent on the upper gully reaches. Piping causes substantial channel initiation, widening, and headward retreat in the upper reaches, and bank caving caused by lateral scour promotes further channel widening. Pipe collapse into small tributary rills is common in the upper reaches. Drainage density decreases in the lower reaches, as the influence of piping diminishes, sediment is more permeable, and vegetation increases. Overall the site can be divided into three gully reaches: 1) upper: unvegetated playa catchment with high drainage density; 2) middle: piping zone with moderate vegetation and hard soil crust; 3) lower: relatively vegetated incised zone with eolian influence.

Figure B.3. Talus upper catchment

Figure B.4. Overview of entire site, looking west from talus slope. Playa in foreground.

Figure B.5. Playa. Note mudcracks and sparse vegetation.

Basalt Cliffs

The Basalt Cliffs site features four medium-sized gullies and several small tributaries that are separated into eastern and western archaeological sites. Artifacts exist near several of the channels. The catchment is a large north-facing alluvial fan that extends from Dox sandstone in the distance, and the gullies begin in variable locations on the alluvial fan and primarily incise through the steep fan toe. The catchment drains to the dune-dominated ap terrace immediately below, where flow disperses and channelization ceases. The combined catchment for the gully system is large (~0.5 ha) and the two eastern gullies drop 7 m over 84 and 100 m (8 and 7% slope), respectively, in comparison to the two western gullies, which drop 2.3 and 3.2 m over 28 and 42 m (8% slope), respectively. All gullies were inactive and without knickpoints before summer of 2002, but channels widened and incised during the summer of 2002 and now feature many abrupt, steep knickpoints. Stone erosion-control structures are present in the eastern gullies, and brush checkdams are established in the western channels. The site

has experienced no trailing. Eolian piles are active throughout the site, near gully heads and below gully mouths. Vegetation is dominated by cryptobiotic crust, annual grasses and forbs, mesquite, prickly pear, and iodine brush. Grasses were particularly abundant during the February visit, as well as organic detritus in the channels. Overland flow dominates the runoff regime and creates prominent plungepools, but piping is not present. The alluvial fan catchment is sandier and much more permeable than the rocky talus catchments of other sites.

Figure B.6. Alluvial fan catchment. Photo taken facing south.

Figure B.7. North-facing view from mid-fan.

Figure B.8. Gully incising through toe of fan. Photographer standing at baselevel.
Parashant

Parashant is an erosion-control site where no archaeological sites are being destroyed or endangered by active gullies. The catchment is small (0.08 ha) and one very small gully drops 1 meter over 8 m (0.17% slope). The entire gully channel features only one small knickpoint and contains no erosion-control structures. There appeared to be no change between the February and October, 2002 trips. The upper catchment faces the southwest and is composed of talus derived from the Muav limestone. The gully begins at the lower talus slope break, and drains to a flat, silty, mainstem ap terrace, where flow disperses and channelization ceases. The site has experienced extensive trailing below the gully mouth. Eolian activity was not noted. Vegetation is sparse, dominated by shrubs such as creosote, and mesquite, as well as cryptobiotic crust, and prickly pear. What little runoff occurs is due to overland flow, and piping is not present.

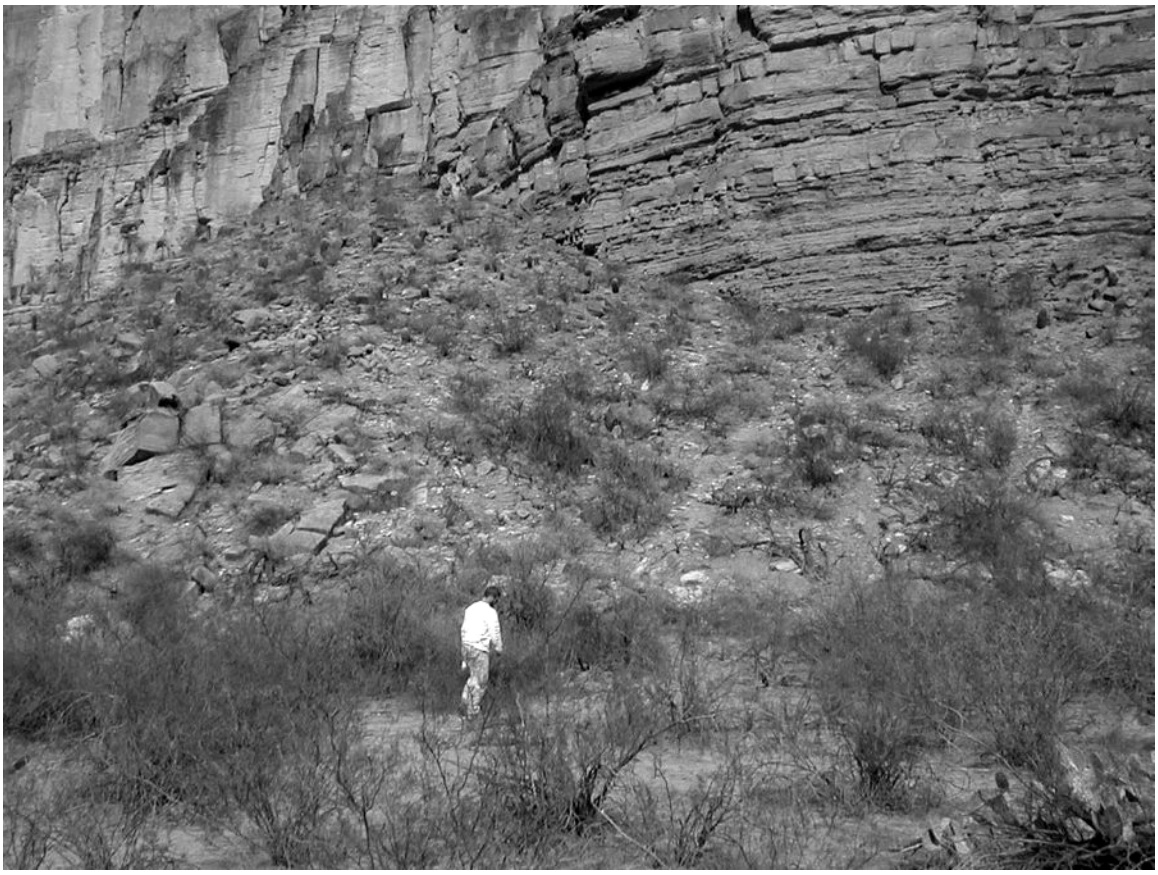

Figure B.9. Talus catchment, Muav source. Photo taken facing northeast.

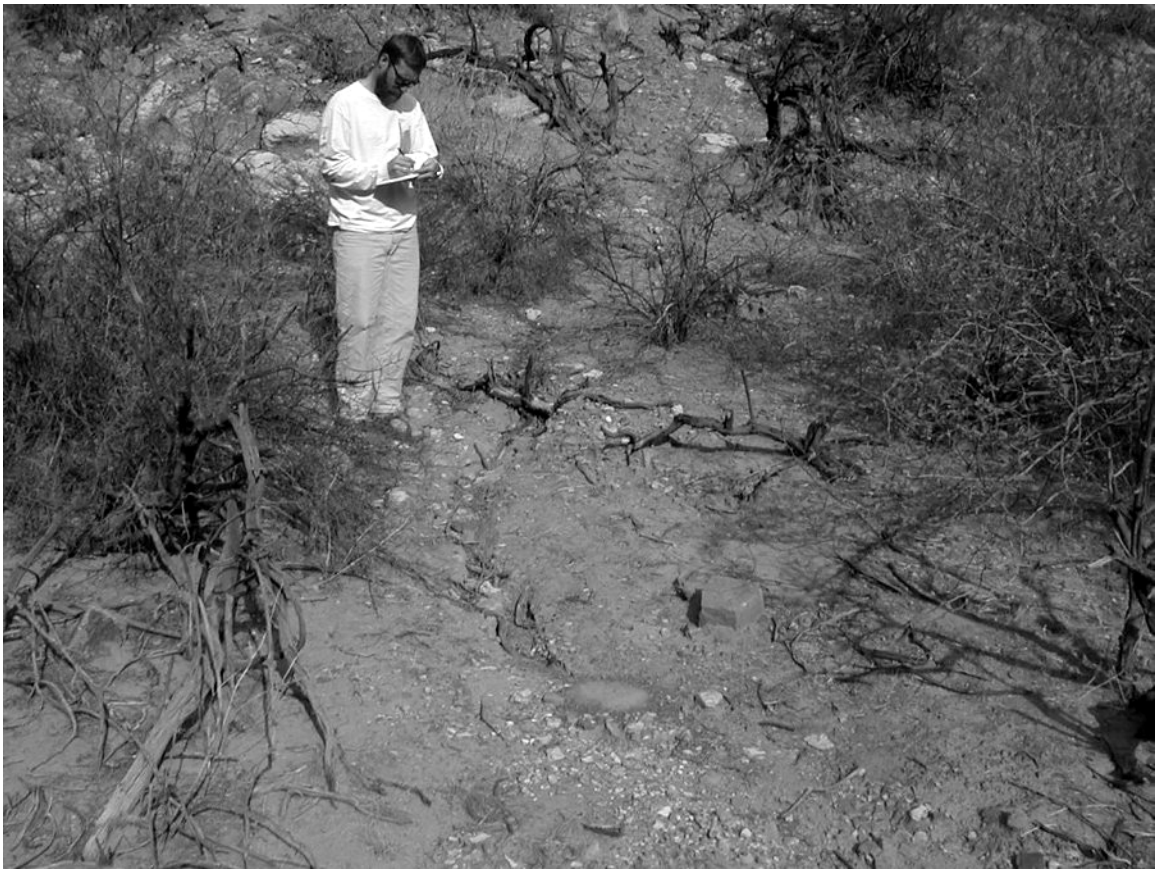

Figure B.10. Small gully. Knickpoint exists near root across channel.

Indian Canyon

The Indian Canyon site features one large active gully, along with several small, rill-like tributaries and small, discontinuous gullies; archaeological sites are actively being destroyed. The catchment is medium-sized (~0.05 ha) and the main gully drops 26 m over the length of 140 m (19% slope). The gully channel has many abrupt, steep knickpoints, and contains several failed stone erosion-control structures. The channel widened and incised slightly in the upper reach during the summer of 2002. The upper catchment faces the east and consists of talus derived from Bright Angel shale and Muav limestone. The gully begins in the lower talus, incises deeply immediately upon entering the softer, coppice dune-dominated ap terrace, especially through two steep terrace risers, and becomes discontinuous near the bottom before it terminates on 1983 flood sand near the river. The site experiences little visitation, but study impacts and trampling were

large due to the sensitive eolian nature of the site. Most dunes are sufficiently vegetated and feature raindrop seals, but several areas exhibit loose sand available for transport. Vegetation is not extremely dense, and is dominated by cryptobiotic crust and creosote, as well as sparse grass, barrel cactus, ocotillo, brittle brush, mormon tea, and blackbrush. Piping contributes to the erosion in places, but overland flow is the dominant runoff process.

Figure B.11. Talus upper catchment. Photo taken facing west.

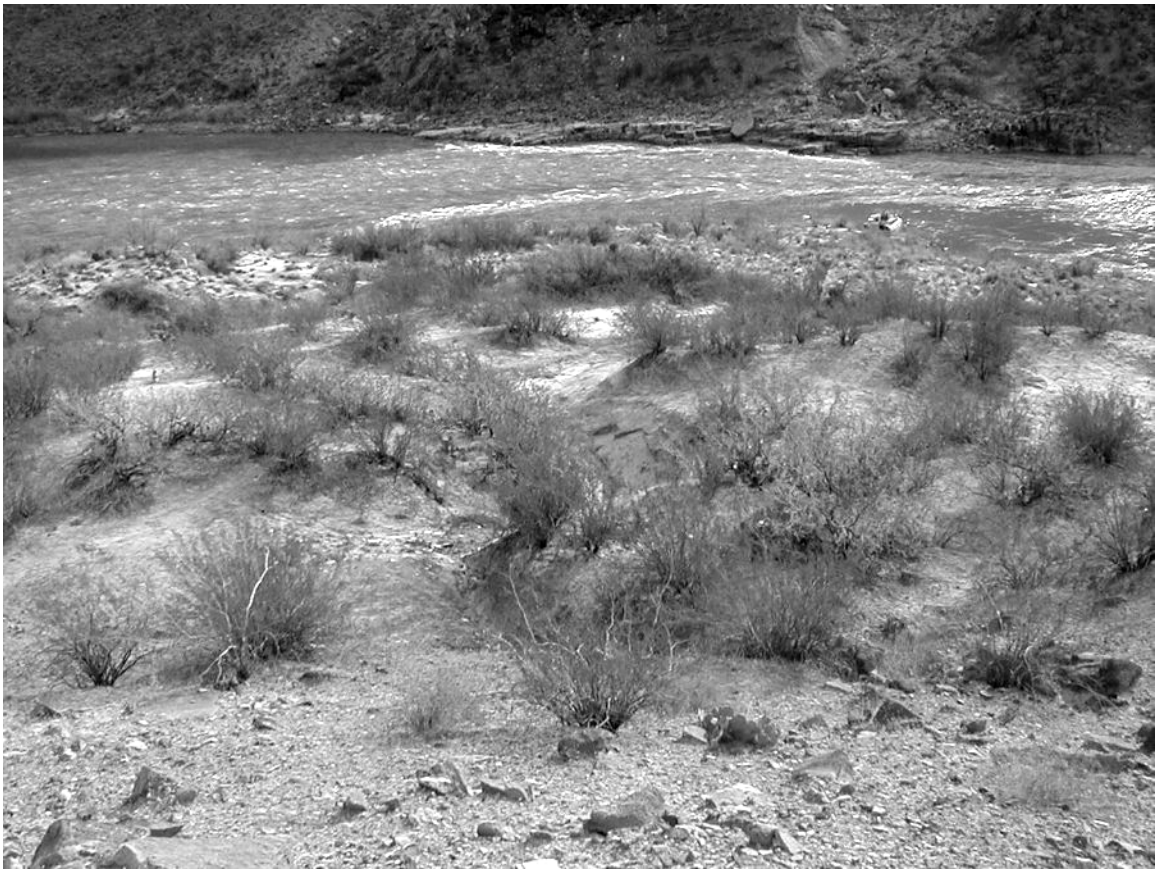

Figure B.12. View of site from talus slope. Gully is in middle of photo.

Arroyo Grande

The Arroyo Grande site features two small gullies and one large gully with a small tributary, all are active; several archaeological sites are endangered and are being damaged. Two of the gullies feature stone erosion-control structures, while one has no erosion treatments. The catchments range in size with each gully (~0.02-0.18 ha) and the three gullies drop 25, 5, and 5 m over the length of 200, 23, and 18 m (12, 20, 28% slope), respectively. All of the gully channels feature several abrupt, steep knickpoints. Channels changed very little between February and October, 2002, and perhaps infilled with eolian sediment slightly in places. A raindrop seal had formed over the soil between visits; apparently there had not been enough flow to initiate runoff. The upper catchment faces the southwest and is composed of Pleistocene debris-flow material with small outcroppings of Precambrian pegmatite bedrock. The smaller gullies begin on a small ap terrace, incise through the oversteepened terrace riser, and drain to a more expansive

Holocene terrace, where flow disperses and channelization ceases. The larger gully begins in the lower talus, incises through the ap terrace, becomes discontinuous, and drains to a Holocene debris flow several tens of meters from the mainstem Colorado River. The site has experienced trailing near the small gully heads, crossing over the largest gully. Eolian activity appears to have a small impact in healing the gullies, and source dunes are present below the ap terrace. Vegetation is dominated by cryptobiotic crust, mesquite, creosote, grasses, ocotillo, prickly pear, and barrel cactus. Piping catalyzes substantial erosion in smaller rills, but the gullies exhibit classic plunge-pools derived from overland flow.

Figure B.13. Quaternary debris flow upper catchment, with ap terrace top in foreground. Photo facing the northeast.

Figure B.14. Modern debris-flow deposit to which large main gully (right foreground) drains.

Granite Park

The Granite Park site features one relatively long gully and many small, rill-like tributaries; archaeological sites are endangered by several of these small tributaries. The catchment is large (~0.16 ha) and the gully drops 11 m over a length of 190 m (6% slope). The gully channel is not very incised or well-defined, but features a few small knickpoints, and many stone erosion-control structures. Little or no change occurred between the February and October, 2002 surveys, and it is doubtful there was any runoff during the study period. The upper catchment faces the west and is composed of Bright Angel shale and Muav limestone bedrock and talus. The gully head is immediately below the talus slope, at the beginning of an expansive, fine-grained ap terrace with superimposed dunes. The main gully channel trends west, winding through an easily-defined catchment comprised of a convex north-facing and south-facing hillslope set.

The north-facing slope is dominated by grass and shrubs and has no erosional features, while the south-facing slope features only cryptobiotic crust, sparse shrubs, and bare ground, and has several small, erosive tributaries draining to the main gully. The gully dissipates at the boundary between the ap terrace and a bouldery modern tributary debris-flow deposit, about 100 m from the mainstem Colorado River. The site has experienced trailing on the far-east side, perpendicular to the gully head, and on the crest of the south-facing hillslope, parallel to the main gully. Dunes are present throughout the ap terrace, and an eolian mantle lies over the most of the terrace. Vegetation is dominated by cryptobiotic crust, grass, creosote, brittle brush, prickly pear, barrel cactus, ocotillo, and some mesquite. Piping plays a small role on the crusted, south-facing hillslope of the catchment, but overland flow dominates as the main process.

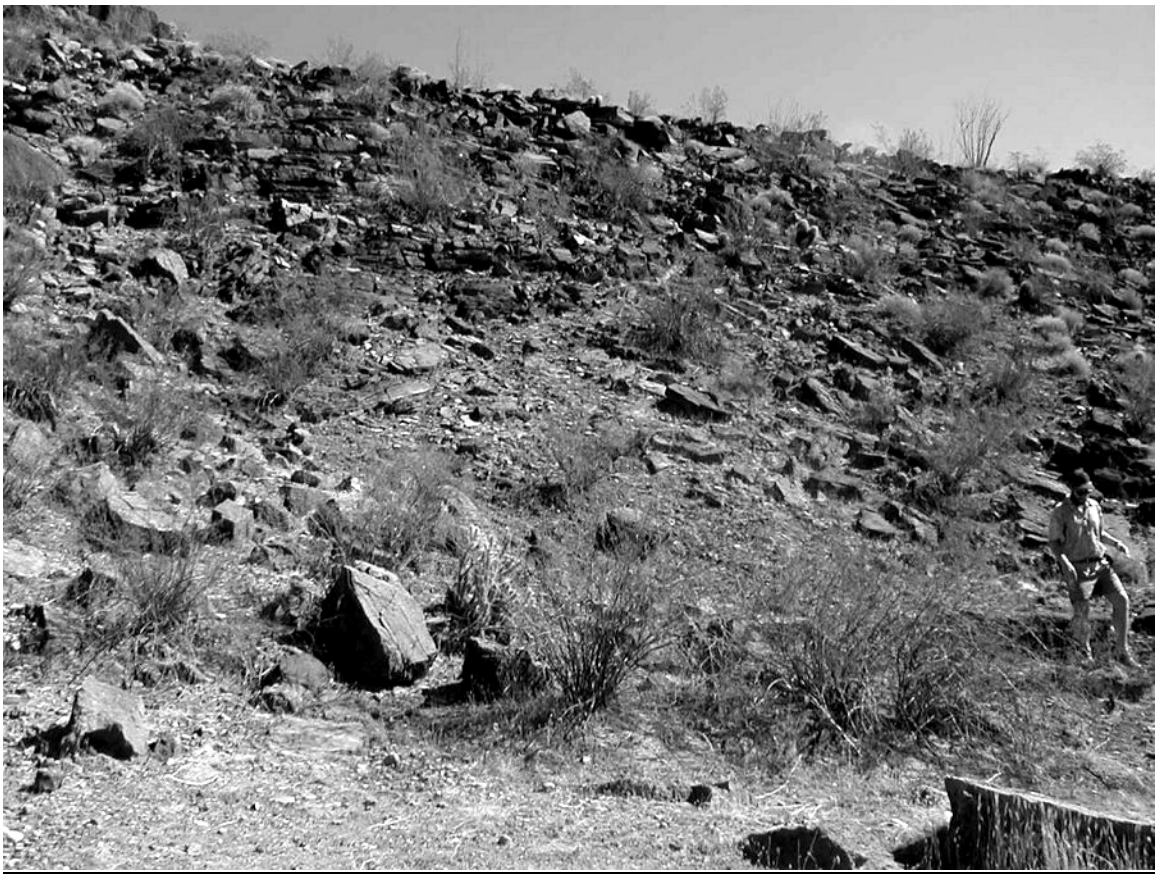

Figure B.15. Upper catchment: talus and bedrock. Photo taken facing east.

Figure B.16. View of entire site from talus/bedrock slope. Note vegetated N-facing slope (on left) and bare S-facing slope (right). Trails trend both perpendicular and parallel to gully.

Figure B.17. Thick vegetation where gully terminates. Photo taken from debris-flow deposit, facing east (upcatchment).

223-mile

The 223-mile site features four active study gullies, as well as several other unstudied gullies and smaller tributaries; several archaeological sites are endangered and are actively being destroyed. The study site can be divided into two sub-sites: east and west. The catchments in the west site are very small to medium (~0.002 to 0.06 ha) and the three gullies drop 6, 9, and 9 m over the length of 15, 33 and 37 m (40, 27, and 24% slope), respectively. All of the western gullies feature a few small knickpoints, and channelization is often discontinuous. Two of the three channels exhibit stone erosion-control structures. None of the channels changed or experienced runoff between the February and October surveys. The eastern gully has a medium-sized catchment (~0.075 ha) and drops 12 m over the length of 45 m (26% slope). This gully features a multitude of large, near-vertical knickpoints, and is deeply incised. Erosion-control structures are present, but are washed out and have not been maintained. Although this gully did not experience runoff or erosion during the monitoring period, significant eolian infilling from a nearby dune occurred, "washing out" several of the upper knickpoints. The upper catchment for all gullies faces the southeast and consists of Pleistocene debris flow deposits, with Tapeats sandstone outcrops above. The western gullies all originate at the top of the ap terrace, and erode through the oversteepened terrace toe, draining to mainstem tributary washes. The eastern gully is longer, beginning on a deflating dune at the terrace top break in slope and becoming discontinuous near the bottom before terminating in thick vegetation some tens of meters from a mainstem cobble beach. The site has experienced little visitation and trailing. Eolian activity differs immensely between the eastern and western sub-sites. The western sub-site general has a more compacted, crusted substrate with little eolian influence, whereas the eastern sub-site is much sandier and dominated by dunes. Vegetation is characterized by cryptobiotic crust, creosote, mesquite, grasses, prickly pear, ocotillo, and barrel cactus. Some piping is present, but overland flow is evident as the dominant runoff type, especially in the eastern gully, which features a multitude of knickpoint-plungepool sets.

Figure B.18. Debris-flow upper catchment for western gullies. Photo taken facing north.

Figure B.19. Debris-flow upper catchment for east-most gully. Photo taken facing north.

Figure B.20. Ephemeral wash to which western gullies drain. Photo taken facing east.

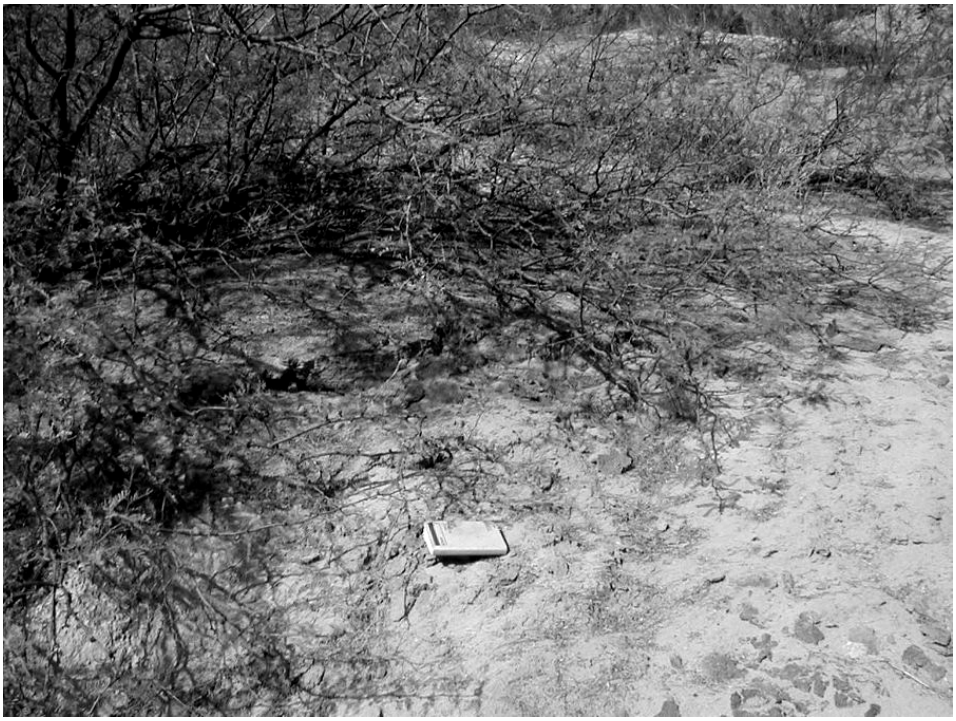

Figure B.21. Mouth of east-most gully (terminates in the vegetation)

Appendix C. Soil Descriptions
(see Fig. C.1 for sample datasheet; terminology and abbreviations from Jorgenson, 1989)

Soil Description: Location ____

Site No. _____ Date _________ Time ___________ Vegetation ______________________________________

Elevation __________ Slope ___________ Aspect _________ Geomorphic Surface ______________________________

Parent Material(s) ________________________________ Described by _________________________________

Depth (cm)	Horizon	Color moist / dry	Structure	Gravel %	Consistence Wet	Consistence Moist	Consistence Dry	Texture	pH	Clay films	Boundaries	notes
		....	m vf gr sg f pl 1 m pr 2 c cpr 3 vc abk sbk	0 50 <10 75 10 >75 25	so po ss ps s p vs vp	lo vfr fr fi vfi efi	lo so sh h vh eh	S SiCL LS SiL SL Si SCL SiC L C CL SC		v1 f pf 1 po 2 d br 3 co p cobr	a s c w g i d b	
		....	m vf gr sg f pl 1 m pr 2 c cpr 3 vc abk sbk	0 50 <10 75 10 >75 25	so po ss ps s p vs vp	lo vfr fr fi vfi efi	lo so sh h vh eh	S SiCL LS SiL SL Si SCL SiC L C CL SC		v1 f pf 1 po 2 d br 3 co p cobr	a s c w g i d b	
		....	m vf gr sg f pl 1 m pr 2 c cpr 3 vc abk sbk	0 50 <10 75 10 >75 25	so po ss ps s p vs vp	lo vfr fr fi vfi efi	lo so sh h vh eh	S SiCL LS SiL SL Si SCL SiC L C CL SC		v1 f pf 1 po 2 d br 3 co p cobr	a s c w g i d b	
		....	m vf gr sg f pl 1 m pr 2 c cpr 3 vc abk sbk	0 50 <10 75 10 >75 25	so po ss ps s p vs vp	lo vfr fr fi vfi efi	lo so sh h vh eh	S SiCL LS SiL SL Si SCL SiC L C CL SC		v1 f pf 1 po 2 d br 3 co p cobr	a s c w g i d b	
		....	m vf gr sg f pl 1 m pr 2 c cpr 3 vc abk sbk	0 50 <10 75 10 >75 25	so po ss ps s p vs vp	lo vfr fr fi vfi efi	lo so sh h vh eh	S SiCL LS SiL SL Si SCL SiC L C CL SC		v1 f pf 1 po 2 d br 3 co p cobr	a s c w g i d b	
		....	m vf gr sg f pl 1 m pr 2 c cpr 3 vc abk sbk	0 50 <10 75 10 >75 25	so po ss ps s p vs vp	lo vfr fr fi vfi efi	lo so sh h vh eh	S SiCL LS SiL SL Si SCL SiC L C CL SC		v1 f pf 1 po 2 d br 3 co p cobr	a s c w g i d b	
		....	m vf gr sg f pl 1 m pr 2 c cpr 3 vc abk sbk	0 50 <10 75 10 >75 25	so po ss ps s p vs vp	lo vfr fr fi vfi efi	lo so sh h vh eh	S SiCL LS SiL SL Si SCL SiC L C CL SC		v1 f pf 1 po 2 d br 3 co p cobr	a s c w g i d b	
		....	m vf gr sg f pl 1 m pr 2 c cpr 3 vc abk sbk	0 50 <10 75 10 >75 25	so po ss ps s p vs vp	lo vfr fr fi vfi efi	lo so sh h vh eh	S SiCL LS SiL SL Si SCL SiC L C CL SC		v1 f pf 1 po 2 d br 3 co p cobr	a s c w g i d b	
		....	m vf gr sg f pl 1 m pr 2 c cpr 3 vc abk sbk	0 50 <10 75 10 >75 25	so po ss ps s p vs vp	lo vfr fr fi vfi efi	lo so sh h vh eh	S SiCL LS SiL SL Si SCL SiC L C CL SC		v1 f pf 1 po 2 d br 3 co p cobr	a s c w g i d b	
		....	m vf gr sg f pl 1 m pr 2 c cpr 3 vc abk sbk	0 50 <10 75 10 >75 25	so po ss ps s p vs vp	lo vfr fr fi vfi efi	lo so sh h vh eh	S SiCL LS SiL SL Si SCL SiC L C CL SC		v1 f pf 1 po 2 d br 3 co p cobr	a s c w g i d b	

Figure C.1. Sample soil properties data sheet.

Kwagunt

Talus Mantle (0 - 5 cm)
Texture: ratio of sand/silt/clay = 52/42/6 (sandy loam)
Sodium absorption ratio: 1.4
Horizon: Av
Dry Color: 2.5Y 6/3
Structure: 1-f-sbk
Gravel %: 50
Wet consistence: so-ps
Dry consistence: lo
Notes: slightly vesicular, but due to rooting; not pavement; effervesces

Talus Matrix (50 cm)
Texture: ratio of sand/silt/clay = 52/42/6 (sandy loam)
Sodium absorption ratio: 1.6
Horizon: C
Dry Color: 10YR 6/3
Structure: 1-f-sbk
Gravel %: >75
Wet consistence: so-ps
Dry consistence: lo
Notes: rooted; structure very weak, not pedogenic; effervesces

Toe (0 – 5 cm)
Texture: ratio of sand/silt/clay = 58/36/6 (sandy loam)
Sodium absorption ratio
Horizon: A
Dry Color: 2.5Y 5/3
Structure: 1-f-sbk
Gravel %: 25
Wet consistence: so-ps
Dry consistence: lo
Notes: more sand than talus matrix; structure slightly more; parent material pebbly (angular) sandy silt (slopewash, not talus)

Misc. soil notes: Talus parent deposit is clast-supported, angular, cobble-boulder "breccia," uncemented, probably original open-framework (rockfall), no visible fabric; clasts are limestone, rare sandstone.

60-mile

Bedrock catchment regolith (0 – 4 cm)
Texture: ratio of sand/silt/clay = 66/18/16 (sandy loam)
Sodium absorption ratio: 4.6

Horizon: Av/C
Dry Color: 5YR 4/3 (deep red from bedrock)
Structure: 1-m-abk
Gravel %: 25
Wet consistence: s-po
Dry consistence: so
Notes: sweet pavement; 1-2 cm of Av; effervesces

Representative eolian
Texture: ratio of sand/silt/clay = 45/50/5 (silt loam/sandy loam)
Sodium absorption ratio: 1.6
Horizon: na
Dry Color: 2.5Y 6/3
Structure: 1-f-sbk
Gravel %: 0
Wet consistence: so-po
Dry consistence: so
Notes: pseudo-structure; effervesces

Misc. soil notes: parent material sediment of eolian: massive rooted vf-f sand;

thin Av over bedrock regolith: pebbled-sized sandstone and shale chips, clear slope parallel fabric, in areas seems quite stable, clasts varnished; these pavements protect areas from rainsplash (seen elsewhere); HOF hitting bedrock above has already created gullies at midslope

Palisades

Red muddy local playa
Texture: ratio of sand/silt/clay = 37/39/24 (loam)
Sodium absorption ratio: 83
Horizon: na
Dry Color: 7.5YR 5/3
Structure: 2-c-sbk
Gravel %: 0
Wet consistence: s-p
Dry consistence: h
Notes: structure not pedogenic; has “flaky” texture; laminated, small (2 mm) salt modules; red/tan color varies on laminae-scale; vesicular throughout; flakiness may be due to geochem characteristics/dispersion or smectites

Sandy overbank mainstem playa
Texture: ratio of sand/silt/clay = 76/17/7 (sandy loam/loamy sand)
Sodium absorption ratio: 164
Horizon: na

Dry Color: 2.5Y 6/3
Structure: 1-m-sbk
Gravel %: 0
Wet consistence: so-po
Dry consistence: sh
Notes: clean, well-sorted, vfU sand; ripple cross-stratification (subcritical) and few thin low-angle crossbed strata; paleocurrents variously directed, including both up and downstream relative to mainstem

Sandy coppice dunes
Texture: ratio of sand/silt/clay = sand (field)
Sodium absorption ratio: na
Horizon: na
Dry Color: na
Structure: sg/1-m-sbk
Gravel %: 0
Wet consistence: so-po
Dry consistence: so
Notes: vfU-fU sand, rooted; biotic crust in areas

Misc. soil notes: "eolian" coppice dunes actually largely trapped flood sand (pda and mesquite terrace), only minor eolian reworking and capture at crest of coppices; as much or more evidence for deflation as is for deposition

Basalt Cliffs

Early Holocene (?) alluvial fan—mid (0-1 cm)
Texture: ratio of sand/silt/clay = 86/7/7 (loamy sand/sand)
Sodium absorption ratio: 1.4
Horizon: Av
Dry Color: na
Structure: sg
Gravel %: 10
Wet consistence: so-po
Dry consistence: lo/so
Notes: not vesicular, but trapped silty vf-f sand

Early Holocene (?) alluvial fan—mid (1-20 cm)
Texture: ratio of sand/silt/clay = 76/17/7 (sandy loam/loamy sand)
Sodium absorption ratio: 1.4
Horizon: C
Dry Color: 5YR 4/3
Structure: m/sg
Gravel %: >75
Wet consistence: ss-po

Dry consistence: sh
Notes: fine, flaky, chippy, pebbly gravel; angular fragments→2 cm; matrix silty vf-f sand; in channels, pebbles clearly imbricated, in deposit imbricated and slope parallel; no pedogenics seen, but not a good soil profile, just cutbank exposure

Indian Canyon

Talus (0 – 15 cm)
Texture: ratio of sand/silt/clay = 70/23/7 (sandy loam)
Sodium absorption ratio: 2.0
Horizon: na
Dry Color: 2.5YR 5/3
Structure: 1-f-sbk
Gravel %: 10
Wet consistence: ss-ps
Dry consistence: so/sh
Notes: talus pile with open matrix; describing matrix only; talus is clast-supported and has high percentage of gravel; vfssi; effervesces; sparse bio-crust; not much varnish

Gullied middle section of site—sandy alluvium (capped by coppice dunes)
Texture: ratio of sand/silt/clay = 88/8/4 (sand)
Sodium absorption ratio: 2.0
Horizon: na
Dry Color: 2.5Y 6/3
Structure: sg-m-sbk
Gravel %: 0
Wet consistence: so-po
Dry consistence: so
Notes: vfU-fU sand; ripple cross-stratification to laminated; rooted and heavy biocrusts; mainstem sand of ap, mesquite and pda.

Misc. soil notes: in talus there is a slope-parallel pavement of pebbles; below pavement is Av horizon: good sign of eolian deposition

Arroyo Grande

Ap surface with biotic crust (0 – 25 cm)
Texture: ratio of sand/silt/clay = 76/19/5 (loamy sand)
Sodium absorption ratio: 1.8
Horizon: na
Dry Color: 2.5YR 6/3
Structure: 1-f-sbk

Gravel %: <10
Wet consistence: so-po
Dry consistence: so
Notes: lots of rooting/bioturbation; massive eolian; effervesces wildly; from trib bank of main e-most gully

Pleistocene debris fan (0 – 25 cm)
Texture: ratio of sand/silt/clay = 60/34/ (sandy loam/loamy sand)
Sodium absorption ratio: 2.2
Horizon: na
Dry Color: 10YR 6/4
Structure: 1-vf-sbk
Gravel %: 50-75%
Wet consistence: ss-ps
Dry consistence: vh
Notes: poorly-sorted; effervesces wildly; clast-supported, poorly-sorted conglomerate (pebble to boulder size); calcite cemented; no imbrication

Lower eolian with grass and biotic crust
Texture: sand (field)
Sodium absorption ratio: na
Horizon: na
Dry Color: na
Structure: 1-f-sbk
Gravel %: 0
Wet consistence: so-po
Dry consistence: so
Notes: well-sorted, medium sand; rooting; eolian; right next to 207-5 infiltration

Granite Park

Representative of hillslope-proximal material (base of bedrock/talus slope)
Texture: ratio of sand/silt/clay = 49/44/7 (loam)
Sodium absorption ratio: 21.9
Horizon: na
Dry Color: 10YR 6/3
Structure: 1-f/m-sbk
Gravel %: 0
Wet consistence: so-ps
Dry consistence: sh
Notes: massive vf sandy silt; unusually boring—very little rooting, vesicularity, etc.

Representative of lower catchment coppice dune sand
Texture: sand (field)

Sodium absorption ratio: na
Horizon: na
Dry Color: na
Structure: m/sg
Gravel %: 0
Wet consistence: so-po
Dry consistence: lo
Notes: massive? rooted, bioturbated, moderately-sorted, vf-f sand

Miscellaneous notes: northward flank of lower catchment (at toe of bedrock to slope to about 35 m riverward) includes buried Pleistocene pebble-cobble subrounded (clast-supported) gravel peeking out of lower cutbanks

223-mile

Ap/coppice sand below feature (roasting pit) next to gully with checks
Texture: ratio of sand/silt/clay = 65/30/5 (sandy loam)
Sodium absorption ratio: 7.7
Horizon: na
Dry Color: 2.5Y 6/3
Structure: 1-m-sbk
Gravel %: 0
Wet consistence: so-po
Dry consistence: so
Notes: silty and vf sand; some fU sand; bioturbated, rooted, trace ash? from roasting pit (or other organic litter?)

Debris fan sediment exposed in main wash walls
Texture: ratio of sand/silt/clay = 66/29/5 (sandy loam)
Sodium absorption ratio: 0.9
Horizon: na
Dry Color: 2.5Y 6/3
Structure: m/1-sbk
Gravel %: >75
Wet consistence: so-ps
Dry consistence: lo
Notes: clast-supported, pebble-boulder gravel; clasts subangular; matrix = (from interflow/wash) vf-m sandy silt; heterogeneous in places—imbricated, slightly sorted gravel, interbedded by sand layers; in other, open framework cobbles and boulders (rock avalanche)

Appendix D. Soil Shear Strength
(Reports mean soil shear strength; measured with a torvane; units are kg/cm^2)

Torvane (Shear Stress) Data Sheet

STUDY SITE

Date	Site Number	Site Name	River Mile
Worker	Time of Day	Weather	

MEASUREMENTS

Sample	Torvane Size	Soil type	Reading
1			
2			
3			
4			
5			
6			
7			
8			
9			
10			
11			
12			
13			
14			
15			
16			
17			
18			
19			
20			

Sample	Torvane Size	Soil type	Reading
21			
22			
23			
24			
25			
26			
27			
28			
29			
30			
31			
32			
33			
34			
35			
36			
37			
38			
39			
40			

General notes

Figure D.1. Soil shear strength data sheet.

Kwagunt

#1 : talus
silty w/ fine organic litter : 0.442
biotic crust (covers most of talus): 1.009

notes**:** near perm station; silty ground—largely disturbed areas, in hillslope gully bottoms, or under canopy of bushes and rocks; biotic crust—strength depends upon substrate = on old talus remnant face high-relief crust grows on fine eolian mantle (reading ~3.5-4.0); on younger colluvium, lower-relief crust on more compact fines (reading ~5.0-9.0)

#2: toe of slope, near arch sites
silt w/ weak biotic crust: 0.491

notes**:** pretty much same readings as talus slope soils w/ no biotics

60-mile

#1: high in catchment
more active/in gullies: 0.488
older, more stable colluvium: 0.802

notes: just of younger/more active colluvium and older varnished/paved colluvium; no bedrock itself; this is, in some cases, the τ of angle of sliding friction of pavement chips, in strongest τ cases, it is biotic crust

#2: lower in catchment, near arch sites
trail: 0.14
gully channel: 0.261
interfluve: 0.416
biotic crust: 0.95

notes: eolian; gully channel stronger b/c of rock fragments; also, gully channel stronger where people hadn't stepped, often b/w erosion control rocks; forms kind of crust, just like sed off of trail; most likely rainsplash seal

Palisades

#1: upper part of site (playa and salt crust)
playa: 3.423 (
salt: 1.276

notes: note deviation from torvane size, even though they are measuring essentially the same strength soil; thickest salt crusts were selected for measurement

#2: middle of catchment, near coppice dunes
sand, b/w veg, w/o biotic crust, not disturbed: 0.369
areas w/ biotic crust: 0.952 (0.2)

notes: two of the smaller veins in 0.2 are broken off, thus values are minimum τ; inevitably "break through" and detach crust in order to get vein penetration, thus these are minimum τ for biotic crust

#3: midsection of main gully
untrampled channel, often w/ mud drape/crust or smoothed (by flow) sand: 0.688
loose channel sand and gravel, or channel sand disturbed by trampling: 0.128

notes: all done within 20 m segment of gully channel

#4: upper part of site (playa and salt crust)
playa: 2.571
salt: 0.934

Basalt Cliffs

#1: alluvial fan
channel: 0.194
interfluve: 0.377
notes: na

#2: dune
channel : 0.439
interfluve: 0.864
notes: na

#3: alluvial fan
channel: 0.264
interfluve: 0.407
notes: na

#4: dune
channel: 0.595
interfluve: 0.524
notes: na

Parashant

#1: around gully channel

channel bottom (undisturbed): 0.32

non-channel: 0.49

Indian Canyon

#1: upper talus reach
channel (sand): 0.255
interfluve (sand w/ biotic crust): 1.474
notes**:** lot of raindrop sealing in non-channels

Arroyo Grande

#1: gullied area (middle part of site?)
channel (sand): 0.711
interfluve (sand w/ crust): 0.792
notes: na

#2: debris fan (upper catchment)
channel (sand and rock): 0.400
interfluve (rocky, crust): 1.980
notes: na

#3: lower section of site
channel (sandy): 0.448
interfluve (sandy): 0.653
notes: na

#4: middle reach of site
channel: 0.262
interfluve: 0.643

Granite Park

#1: gullied area (middle of site?)
channel (sand): 0.711
interfluve (sand w/ crust): 0.792
notes: na

#2: debris fan (upper catchment)
channel (sand and rock): 0.400
interfluve: (rocky, crust): 1.980
notes: from debris fan above gullies

#3: lower section of site
channel (sandy): 0.448
interfluve (sandy): 0.653
notes: none

#4: middle reach of site
channel: 0.262
interfluve: 0.643
notes: none

223-mile

#1: around 3 main gullies
interfluve (biotic crusts): 2.595
channel (sand): 0.451
notes: none

#2: E-most gully
stable interfluve: 0.419
deflated interfluve (dune): 0.148
channel: 0.271
notes: on active sand dune

Appendix E. Soil Permeability
(Equilibrium rate at zero head at which saturated soil can take in water; measured with a tension-disc infiltrometer; units are cm/s)

Guelph Permeameter Data Sheet

STUDY SITE

Date	Site Number	Site Name	River Mile
Worker	Time of Day	Weather	

MEASUREMENTS (USE EXTRA SHEETS IF NEEDED)

Reading	Time (min)	Time Interval (min)	Head Level (mm)	Reservoir Level (cm)	Water Level Change (cm)	Rate of Water Level Change (cm/min)
1						
2						
3						
4						
5						
6						
7						
8						
9						
10						
11						
12						
13						
14						
15						
16						
17						
18						
19						
20						

General notes (soil, vegetation, slope, etc.)

Figure E.1. Infiltrometer data sheet

Kwagunt

56-1: 0.006
notes: taken up on talus slope in silty soil; lot of biotic crust in vicinity, as well as mesquite, saltbrush, hedgehog cactus, and grass; taken on a slight slope

56-2: 0.003
notes**:** at small gully head in lower part of site

56-1a: 0.002
notes: October repeat of 56-1

56-2a: 0.004
notes: October repeat of 56-2

60-mile

60-1: 0.026
notes: on sand dune; run out of water, weird scatter in data, value not trustworthy

60-2: 0.002
notes**:** upper catchment—shale and colluvium

60-1a: 0.024
notes: October repeat of 60-1

60-2a: 0.003, 0.006, 0.002
notes: October repeat of 60-2 (3 repetitions)

60-3: 0.012, 0.005
notes: on cryptobiotic crust at mid-site

Palisades

65-1: na (virtually impermeable, infiltration did not change with tension)
notes: playa; flat, salt-crusted soil; little veg nearby; lot of mudcracks

65-2: 0.007
notes: mid-site; fine sand (eolian-derived); surrounded by bio-crusts; flat, right above small gully head

65-3: 0.023
notes: lower part of site, on Arroweed Terrace; low slope; arroweed, mesquite, and biotic crust immediately surrounding; medium-grain sand

65-4: 0.021
notes: lower part of site, on Arroweed Terrace; bank above main arroyo, near the outlet; med grain sand; instrument acting funny at time, but data plot looks good

65-1a: na (virtually impermeable, weird scatter in data)
notes: October repeat of 65-1

65-5: 0.004, 0.002
notes: talus slope, underneath a mesquite (two repetitions)

65-6: 0.000, 0.012, 0.001
notes: salty piping reach, on bare ground (three repetitions)

65-4a: 0.026
notes: October repeat of 65-4

65-7: 0.003
notes: Arroweed Terrace near 65-4, under a shrub

Basalt Cliffs

70-1: 0.023
notes: alluvial fan; pebbly alluvial fan with fine sand matrix; vegetation relatively sparse, mainly scrub brush with some grass and occasional mesquite; no biotic crust; on moderate slope; above all gullies

70-2: 0.014
notes: near (above) gully head on c:046; fine sand; take on bare ground, but area mesquite-dominated, plus grasses

70-3: 0.01, 0.005
notes: stony interspace-mid fan (above channel heads, 2 repetitions)

70-4: 0.001, 0.001
notes: alluvial fan, under bush, near 70-3 (2 repetitions)

70-5: 0.001, 0.014
notes: at gully heads, lower fan: coppice dune sand (2 repetitions)

70-6: 0.006, 0.005
notes: beneath mesquite tree at gully mouth (2 repetitions)

Parashant

198-1: 0.001
notes: talus, above gully heads, bare ground

198-2: 0.006
notes: footslope, near gully head, under shrub

198-3: 0.002
notes: lower footslope, near gully mouth, cryptobiotic crust

198-4: 0.001
notes: lower footslope, near gully mouth, grass/forb

198-5: 0.001
notes: lower footslope, near gully mouth; trampled bare soil

Indian Canyon

206-1: 0.004
notes: talus slope; fairly steep angle; very rocky, not much soil; ~70% rock cover

206-2: 0.003
notes: talus slope; same as 206-1

206-3: 0.014
notes: middle incised reach; adjacent to middle incised channel; have alluvial sand with scattered crypto, also creosote around; pretty level

206-4: 0.051
notes: lowest reach

206-1A: 0.003
notes: talus, bare ground

206-1B: 0.003
notes: talus, under shrub

206-1C: 0.002
notes: talus; crypto

206-1D: 0.006
notes: talus; grass

206-2A: 0.007
notes: lower talus, gully head region; bare ground

206-2B: 0.004
notes: lower talus, gully head region; under shrub

206-2C: 0.006
notes: lower talus, gully head region; crypto

206-2D: 0.001
notes: lower talus, gully head region; grass

206-3A: 0.039
notes: incised gully reach; bare ground

206-3B: 0.003
notes: incised gully reach; under shrub

206-3C: 0.007
notes: incised gully reach; crypto

206-3D: 0.015
notes: incised gully reach; on small blue grama plant

206-4A: 0.046
notes: upper unincised reach; dune, bare ground

206-4B: 0.009
notes: upper unincised reach; under prickly compound leaf shrub

206-4C: 0.062
notes: upper unincised reach; crypto

206-4D: 0.014
notes: upper unincised reach; on small forb

206-5A: 0.054
notes: lower unincised reach (’83 sand); bare ground

206-5B: 0.014
notes: lower unincised reach (’83 sand); under shrub

206-5C: 0.015
notes: lower unincised reach (’83 sand); crypto

206-5D: 0.052

notes: lower unincised reach (’83 sand); on large bunchgrass

Arroyo Grande

207-1: 0.018
notes: above gully head; little veg or rock cover nearby; on fine sand

207-2: 0.006
notes: debris fan; hillside above gullies; rocky; very little soil; pavement-like

207-3: 0.001
notes: debris fan; odd scatter in data; hard to trust

207-4: 0.011
notes: between two w-most, steep gullies; on biotic crust; crusty substrate beneath that

207-5: 0.037
notes: lower dune near main gully; sand

207-1A: 0.002
notes: debris flow; extremely gravely, bare ground

207-1B: 0.000
notes: debris flow; under acacia bush

207-1C: 0.002
notes: debris flow; on well-developed crust, on benchlet above acacia

207-1D: 0.001
notes: debris flow; on small blue grama (cut off at ground)

207-2A: 0.008
notes: gully heads; on level sandy bench (bare ground); raindrop crust

207-2B: 0.001
notes: gully heads; 2/3 in from edge of large creosote; hydrophobic

207-2C: 0.002
notes: gully heads; on crypto

207-2D: 0.001
notes: gully heads; on small blue grama

207-3A: 0.022
notes: gully mouths; raindrop crust on arroyo bank (bare ground)

207-3B: 0.001
notes: gully mouths; just in from edge of large prickly comp shrub; hydrophobic
207-3C: 0.022
notes: gully mouths; on well-developed but fragmented crust

207-3D: 0.001
notes: gully mouths; on dead bunchgrass base

207-4A: 0.058
notes: below gully mouths; bare ground

207-4B: 0.143
notes: below gully mouths; under shrub

207-4C: 0.002
notes: below gully mouths; crypto

207-4D: 0.007
notes: below gully mouths; grass

207-5A: 0.001
notes: debris-flow slope gravel surface

207-5B: 0.002
notes: gully mouths; under dead shrub; very slow to start

207-5C: 0.002
notes: gully heads; crypto

207-5D: 0.018
notes: below gully heads; cut off dead bunch grass; very slow to start; on dune

Granite Park

209-1: 0.019
notes: hillslope crest between drainages; sandy, stabilized, vegetated dune; bare ground with biotic crust and grasses nearby

209-2: 0.003
notes: bedrock upper catchment; steep slope above site; very rocky; scatter in data; cannot trust because taken on bedrock

209-3: 0.008

notes: south-facing slope in lower catchment; sparse vegetation; taken on crusted bare ground right next to trib gully

209-4: 0.009
notes: north-facing slope in lower catchment; very grassy; set on grass on flatter part of slope

209-1A: 0.007
notes: talus; bare ground

209-1B: 0.011
notes: talus; under shrub

209-1C: 0.001
notes: talus; crypto

209-1D: 0.004
notes: talus; grass

209-2A: 0.002
notes: near gully head; bare ground on small, sandy blowout

209-2B: 0.001
notes: near gully head; under large shrub canopy; very slow to start

209-2C: 0.000
notes: near gully head; crypto on NE-facing knoll

209-2D: 0.006
notes: near gully head; on small blue grama; surrounded by crust, in channel

209-3A: 0.005
notes: mid-catchment; bare ground with raindrop crust

209-3B: 0.005
notes: mid-catchment; under shrub; had to prime w/ 30 ml water

209-3C: 0.009
notes: mid-catchment; crypto

209-3D: 0.004
notes: mid-catchment; cheat grass

209-4A: 0.006
notes: near gully mouth; bare ground

209-4B: 0.006
notes: near gully mouth; under large shrub canopy

209-4C: 0.025
notes: near gully mouth; crypto

209-4D: 0.012
notes: near gully mouth; cheat grass

209-5A: 0.023
notes: non-vegetated south slope; bare ground on outer edge of laria

209-5B: 0.001
notes: non-vegetated south slope; under larria shrub; very slow to start

209-5C: 0.005
notes: non-vegetated south slope; crypto

209-5D: 0.001
notes: non-vegetated south slope; on new weeds

209-6A: 0.003
notes: grassy north slope; on small bare patch in large crust area

209-6B: 0.002
notes: grassy north slope; under large laria shrub canopy

209-6C: 0.007
notes: grassy north slope; on dry moss

209-6D: 0.004
notes: grassy north slope; cheat grass/litter

223-mile

223-1: 0.004
notes: debris fan catchment; very rocky; sparse vegetation; bare ground

223-2: 0.009
notes: near gully heads; bare ground

223-3: 0.004
notes: up from E-most gully head, near deflated dune; on sand

223-4: 0.005

notes: debris flow catchment above E-most gully; on slope above 223-3; very rocky; on bare ground

223-5: 0.047
notes: on deflated dune next to 223-3; had to refill reservoir; bare sand

223-6: 0.005
notes: debris fan, b/w 2 sub-sites; right by main tributary wash; set right on biotic crust

223-1A: 0.008
notes: western debris flow catchment; bare ground

223-1B: 0.000
notes: western debris flow catchment; under shrub

223-1C: 0.011
notes: western debris flow catchment; crypto

223-1D: 0.017
notes: western debris flow catchment; grass

223-2A: 0.002, 0.045
notes: western gully heads; bare ground

223-2B: 0.011, 0.021
notes: western gully heads; under mostly dead shrub with no litter

223-2C: 0.006, 0.026
notes: western gully heads; on level cryptobiotic crust

223-2D: 0.000, 0.007
notes: western gully heads; on cut off dry grass

223-3A: 0.000, 0.026
notes: western gully mouths; bare ground on very steep slope

223-3B: 0.002, 0.003
notes: western gully mouths; under dead bush

223-3C: 0.007, 0.033
notes: western gully mouths; crypto on very steep slope

223-3D: 0.002, 0.000
notes: western gully mouths; on dry cheat grass and acacia litter; steep bank; very slow start

223-4A: 0.000
notes: eastern debris flow catchment; on bare, fine soil with raincrust

223-4B: 0.010
notes: eastern debris flow catchment; under shrub

223-4C: 0.001
notes: eastern debris flow catchment; crypto

223-4D: 0.003
notes: eastern debris flow catchment; on small dead grass

223-5A: 0.077, 0.190
notes: eastern gully head; bare ground, side of blowout

223-5B: 0.000, 0.000
notes: eastern gully head; under shrub; extremely hydrophobic

223-5C: 0.036, 0.030
notes: eastern gully head; on remnant of cryptobiotic crust in blowout area above rock under ledge

223-5D: 0.002, 0.001
notes: eastern gully head; on cheatgrass remnant b/w blowout and big rock; sped up after 2 minutes

223-6A: 0.090, 0.020
notes: eastern gully mouth; bare ground

223-6B: 0.004, 0.002
notes: eastern gully mouth; under edge of mesquite; very hydrophobic

223-6C: 0.034, 0.030
notes: eastern gully mouth; crypto

223-6D: 0.005, 0.015
notes: eastern gully mouth; on small dry grass

Appendix F. Vegetation Transect Data
(Performed with an 8-pin frame along a 50 m transect; readings were taken every 2.5 meters for 20 total stations; nested frequency was determined by dividing the total number of cover type occurrence by 20 for a given transect; ground cover determined by totaling cover type occurrence using 8-pin frame).

Figure F.1. Vegetation transect data sheet.

TABLE F.1. VEGETATION TRANSECT DATA FOR KWAGUNT

	#1-a	#1-b	#2-a	#2-b	#3-a	#3-b
grass/forb	26	1	48	1	33	1
shrub	7	0.45	0	0.15	0	0.05
cactus	0	0	0	0	0	0
litter	34	1	48	1	84	1
soil	23	0.95	51	0.95	40	0.95
rock	32	0.95	6	0.25	0	0.05
crypto	42	1	10	0.25	3	0.3

a: nested frequency (ground), 50x50 cm quadrat size
b: ground cover from 8-pin frame
#1: talus
#2: near gully heads
#3: below gully mouths

TABLE F.2. VEGETATION TRANSECT DATA FOR 60-MILE

	#1-a	#1-b	#2-a	#2-b	#3-a	#3-b
grass/forb	1	0.8	20	0.95	21	0.9
shrub	3	0.25	1	0.05	0	0.05
cactus	4	0.1	3	0.3	4	0.25
litter	3	0.85	15	0.9	11	0.85
soil	14	0.85	59	1	113	0.95
rock	127	0.95	35	0.65	6	0.4
crypto	12	0.4	27	0.65	9	0.4

a: nested frequency (ground), 50x50 cm quadrat size
b: ground cover from 8-pin frame
#1: bedrock above gully heads
#2: near gully heads
#3: below headcuts, mid-site

TABLE F.3. VEGETATION TRANSECT DATA FOR PALISADES

	#1-a	#1-b	#2-a	#2-b	#3-a	#3-b	#4-a	#4-b
grass/forb	1	0.65	3	0.25	28	0.8	7	0.55
shrub	1	0.15	1	0.1	1	0.35	7	0.6
cactus	0	0	0	0	1	0.1	0	0
litter	47	0.9	1	0.45	5	0.95	26	1
soil	19	0.6	145	1	119	1	118	1
rock	88	0.95	3	0.5	1	0.15	0	0.1
crypto	2	0.35	7	0.15	6	0.3	2	0.15

a: nested frequency (ground), 50x50 cm quadrat size
b: ground cover from 8-pin frame
#1: talus upper catchment
#2: playa
#3: salty piping reach
#4: Arroweed Terrace

TABLE F.4. VEGETATION TRANSECT DATA FOR BASALT CLIFFS

	#1-a	#1-b	#2-a	#2-b	#3-a	#3-b
grass/forb	16	1	2	0.9	0	0.9
shrub	0	0.05	0	0.05	0	0.1
cactus	4	0.15	0	0	0	0
litter	6	0.8	9	1	20	1
soil	63	1	94	1	80	1
rock	72	1	55	0.95	5	0.45
crypto	0	0	0	0.1	55	0.85

a: nested frequency (ground), 50x50 cm quadrat size
b: ground cover from 8-pin frame
#1: alluvial fan upper catchment
#2: near gully heads
#3: below gully mouths

TABLE F.5. VEGETATION TRANSECT DATA FOR KWAGUNT

	#1-a	#1-b	#2-a	#2-b	#3-a	#3-b
grass/forb	1	0.2	3	0.25	0	0.2
shrub	12	0.4	1	0.1	0	0.1
cactus	0	0	0	0	0	0
litter	55	1	64	1	71	1
soil	8	0.55	21	0.7	2	0.2
rock	71	1	43	0.85	10	0.65
crypto	13	0.85	29	0.95	77	1

a: nested frequency (ground), 50x50 cm quadrat size
b: ground cover from 8-pin frame
#1: talus upper catchment
#2: near gully heads
#3: below gully mouths

TABLE F.6. VEGETATION TRANSECT DATA FOR INDIAN CANYON

	#1-a	#1-b	#2-a	#2-b	#3-a	#3-b	#4-a	#4-b	#5-a	#5-b
grass/forb	0	0.75	0	0.05	1	0.7	1	0.5	10	0.7
shrub	1	0.05	2	0.15	1	0.05	1	0.05	3	0.6
cactus	0	0.1	1	0.05	0	0	0	0	0	0
litter	7	1	55	1	19	1	8	0.95	34	0.8
soil	23	1	50	0.95	24	0.8	25	0.9	11	0.6
rock	107	1	9	0.2	0	0	3	0.2	43	0.7
crypto	20	0.7	43	0.7	114	0.95	122	0.95	59	0.85

a: nested frequency (ground), 50x50 cm quadrat size
b: ground cover from 8-pin frame
#1: talus upper catchment
#2: gully head
#3: middle incised reach
#4: upper unincised reach
#5: lower unincised reach (1983 sand)

TABLE F.7. VEGETATION TRANSECT DATA FOR ARROYO GRANDE

	#1-a	#1-b	#2-a	#2-b	#3-a	#3-b	#4-a	#4-b
grass/forb	6	0.65	7	1	2	0.3	5	0.55
shrub	1	0.1	0	0	0	0.1	19	0.55
cactus	2	0.1	2	0.05	0	0	0	0
litter	15	0.8	23	1	75	1	68	1
soil	0	0.45	0	0	7	0.2	34	0.85
rock	109	1	6	0.25	0	0.05	0	0
crypto	27	0.9	122	1	76	0.9	31	0.6

a: nested frequency (ground), 50x50 cm quadrat size
b: ground cover from 8-pin frame
#1: debris flow upper catchment
#2: gully heads
#3: gully mouths
#4: beyond gully mouths

TABLE F.8. VEGETATION TRANSECT DATA FOR GRANITE PARK

	#1-a	#1-b	#2-a	#2-b	#3-a	#3-b	#4-a	#4-b	#5-a	#5-b	#6-a	#6-b
grass/forb	6	0.75	15	1	12	0.95	2	0.4	4	0.9	12	0.95
shrub	3	0.2	0	0	0	0	5	0.05	0	0.05	0	0.05
cactus	1	0.1	3	0.05	5	0.1	0	0	1	0.05	0	0
litter	17	1	32	0.95	23	0.95	35	0.8	28	0.95	73	1
soil	2	0.25	8	0.45	1	0.15	17	0.2	6	0.45	7	0.85
rock	120	0.95	2	0.45	0	0	5	0.1	10	0.7	0	0
crypto	12	0.9	96	1	119	1	96	0.85	110	1	64	1

a: nested frequency (ground), 50x50 cm quadrat size
b: ground cover from 8-pin frame
#1: talus upper catchment
#2: gully head
#3: mid-catchment
#4: gully mouth
#5: south-facing slope
#6: north-facing slope

TABLE F.9. VEGETATION TRANSECT DATA FOR 223-MILE

	#1-a	#1-b	#2-a	#2-b	#3-a	#3-b	#4-a	#4-b	#5-a	#5-b	#6-a	#6-b
grass/forb	0	0.15	0	0.05	1	0.1	0	0.35	0	0.3	3	0.15
shrub	1	0.05	1	0.05	0	0.1	3	0.2	0	0.05	1	0.05
cactus	1	0.15	0	0.05	0	0	0	0.05	0	0	0	0
litter	4	1	25	1	39	0.95	23	1	10	1	34	1
soil	0	0.3	9	0.55	16	0.5	1	0.35	110	0.95	46	0.9
rock	122	1	46	0.75	51	0.6	94	1	0	0	18	0.5
crypto	32	1	79	0.95	51	0.6	39	0.95	38	0.3	55	0.75

a: nested frequency (ground), 50x50 cm quadrat size
b: ground cover from 8-pin frame
#1: western debris flow upper catchment
#2: western gully heads
#3: western gully mouths
#4: eastern debris flow upper catchment
#5: eastern gully head
#6: eastern gully mouth

Appendix G. Erosion-Control Photo Comparison
(Repeat photographs of select erosion-control structures taken in February and October, 2002)

60-mile

A

B

Figure G.1. 60-mile structures #2 (left) and #3 (right), at confluence in main channel. February (A) #3 is intact, but #2 needs repair due to minor flanking, scour, and undercutting; October (B) very little change overall.

A

B

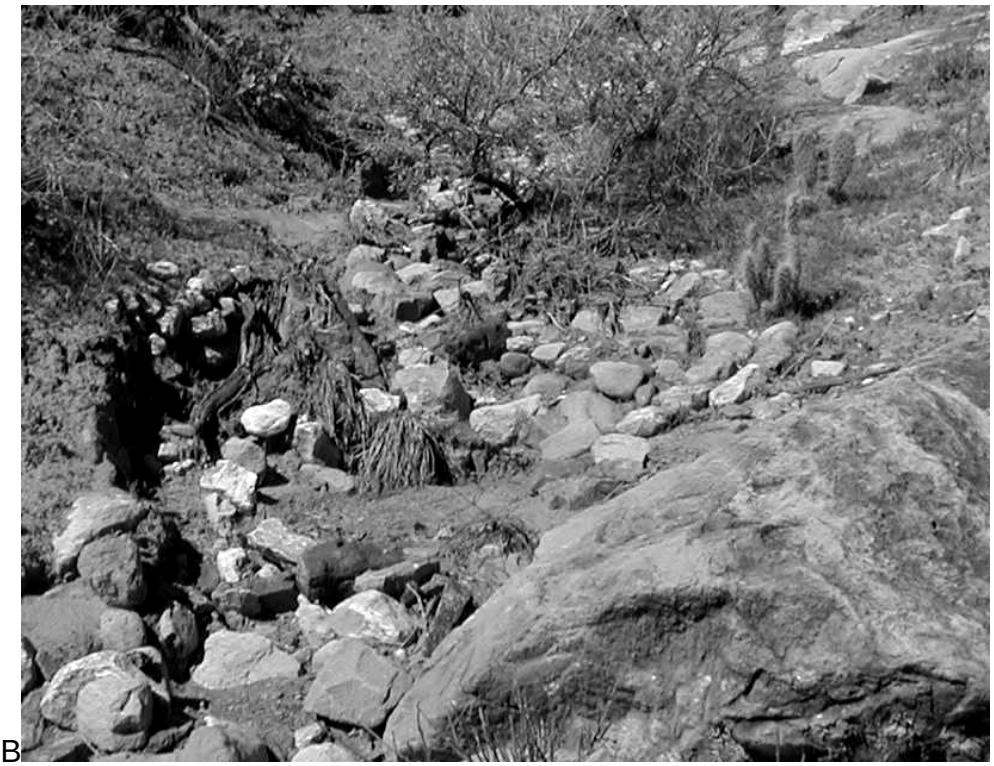

Figure G.2. 60-mile structure #6. February (A) right side is intact; left side features minor breaching at knickpoint; October (B) right side still intact, but left side flanked such that structure cobbles removed.

A

B

Figure G.3. 60-mile structure #8. February (A) completely intact; October (B) completely intact.

Palisades

A

B

Figure G.4. Palisades structure #42. February (A) flanked; October (B) up to 60 cm of lateral erosion (by arrow).

A

B

Figure G.5. Palisades structure #41. February (A) piping in channel bank; October (B) some deepening, widening, and retreat of erosion features in channel bank.

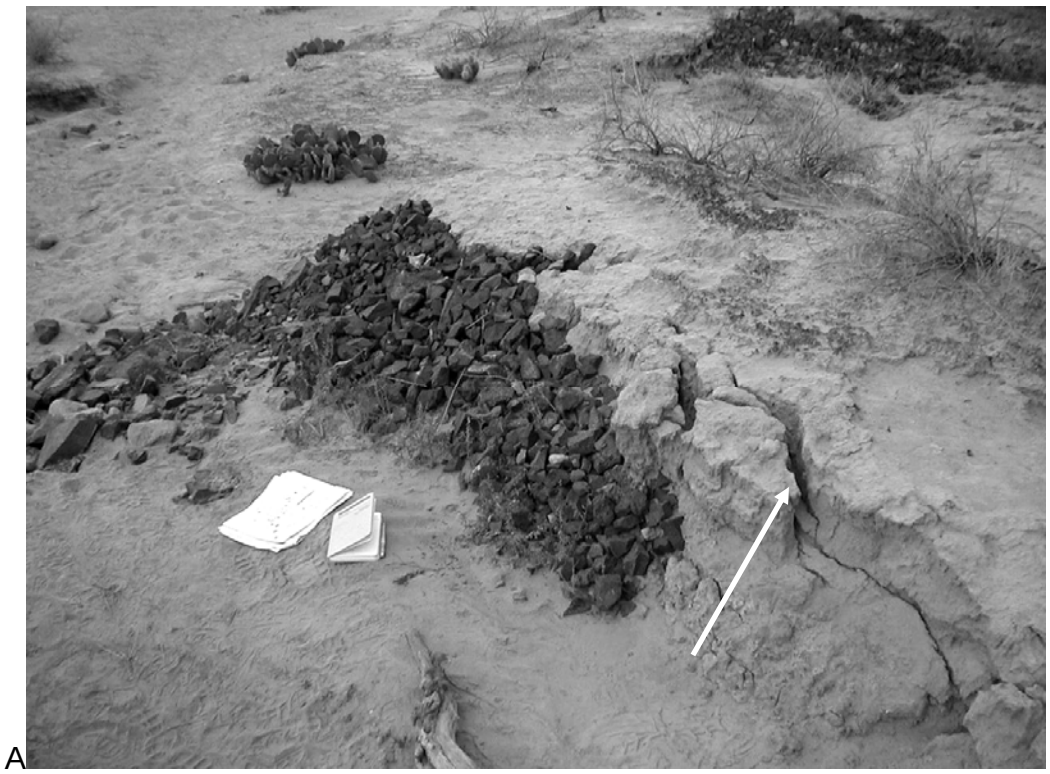

A

B

Figure G.6. Palisades structure #41. View downstream. February (A) note fracturing of bank (arrow); October (B) blocks in (A) have collapsed.

A

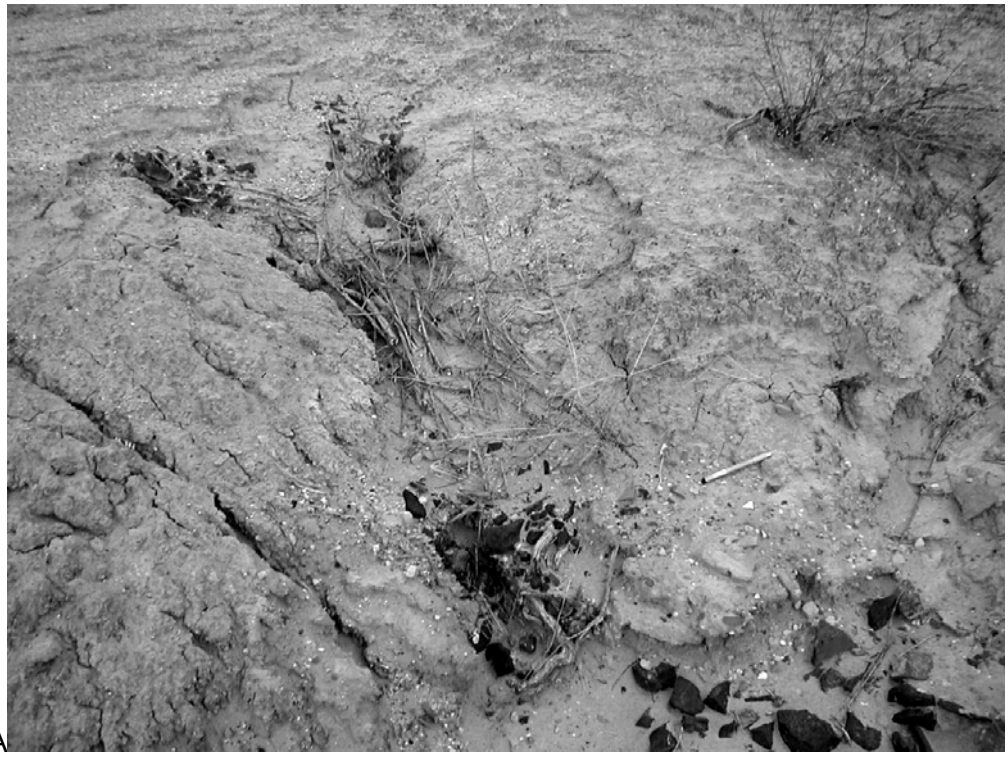

B

Figure G.7. Palisades small, unnamed structures. February (A) in high drainage density region with many rills nearby; October (B) 30-cm tall block of sediment below was undercut and failed (arrow), structures at top were flanked.

A

B

Figure G.8. Palisades small, unnamed structure in tributary gully. February (A) completely flanked; October (B) major channel widening and headcut retreat.

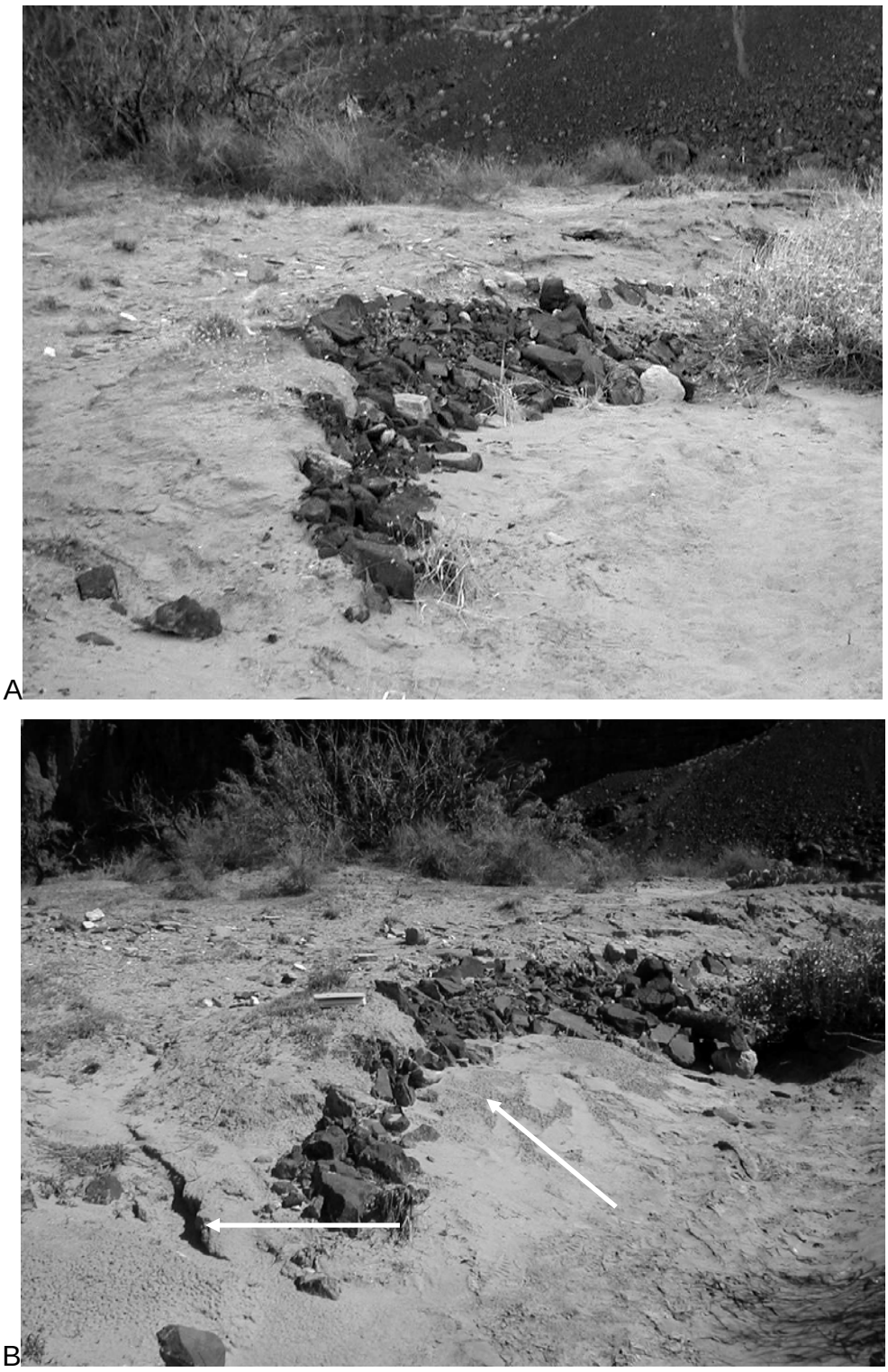

Figure G.9. Palisades structure #35N. February (A): completely intact. October (B): still fairly stable. Possible deposition to side of structure (arrow). Channel in foreground is new (arrow).

Figure G.10. Palisades structure #21, F7. February (A) woody debris has been incorporated into this structure through erosion. Flanked and scoured; October (B) left side of channel has been scoured out, nearly doubling channel width.

Figure G.11. Palisades structure #17N (?). February (A) intact, gully healed; October (B) still stable, except for slight scour near pen on left-central side.

Basalt Cliffs

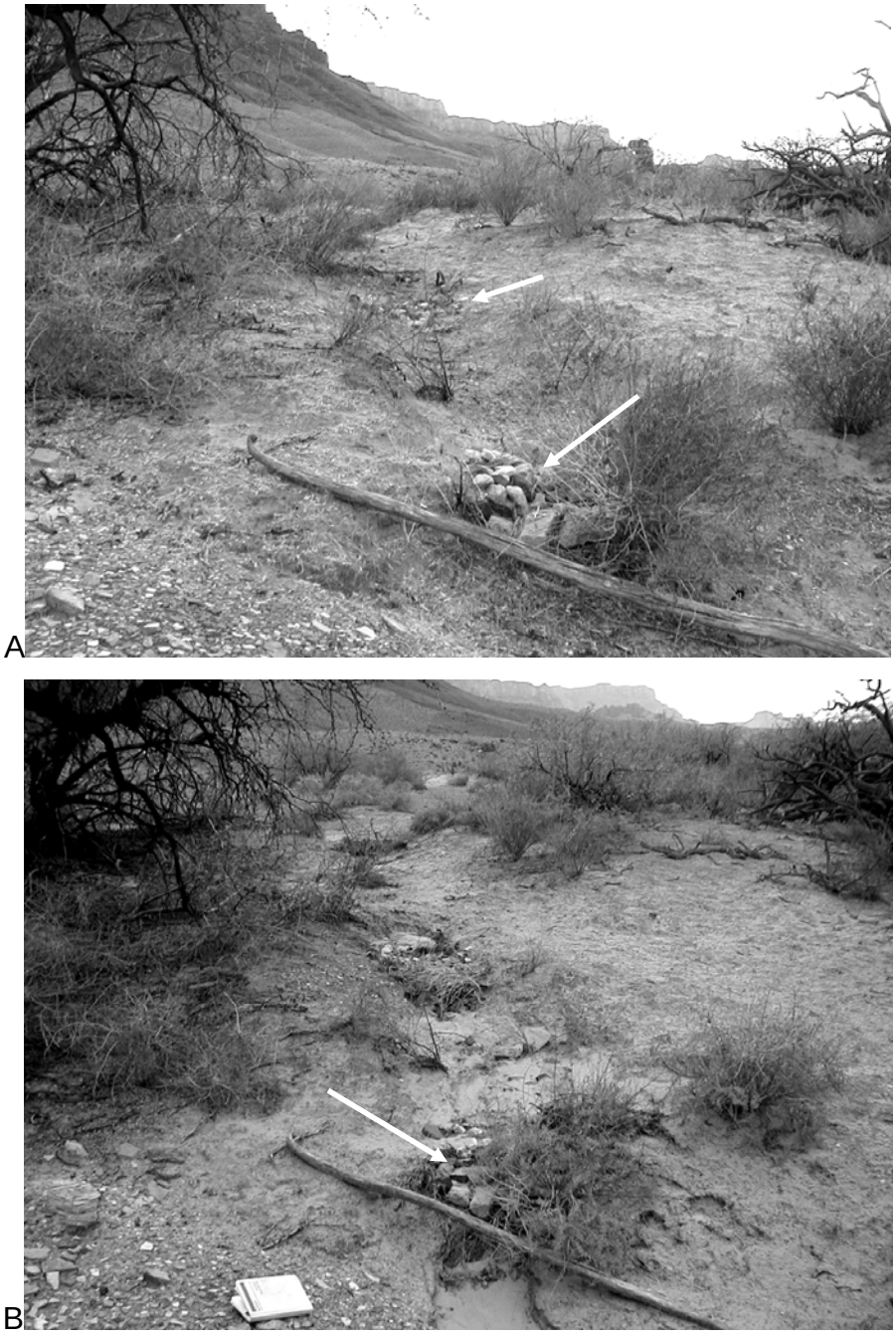

Figure G.12. Basalt Cliffs eastern gully with two structures (see arrows, #9 in foreground). February (A) all structures are intact; October gullies flowed, channels widened, knickpoint formed in front of structure #9. Some infilling within structure #9 (arrow).

A

B

Figure G.13. Basalt Cliffs structure in western gully. February (A) intact; October (B) knickpoint just below structure, some channel widening, sediment deposition in middle part of structure, some rocks removed.

A

B

Figure G.14. Basalt Cliffs wooden checkdam structures #2 (background) and #3 (foreground) in west gully in C:13:348. February (A) intact; October (B) not much change in #2, but #3 has filled in with sediment.

A

B

Figure G.15. Basalt Cliffs unnamed, wooden checkdam structure in east gully. February (A) intact; October (B) sediment deposition, still intact.

Indian Canyon

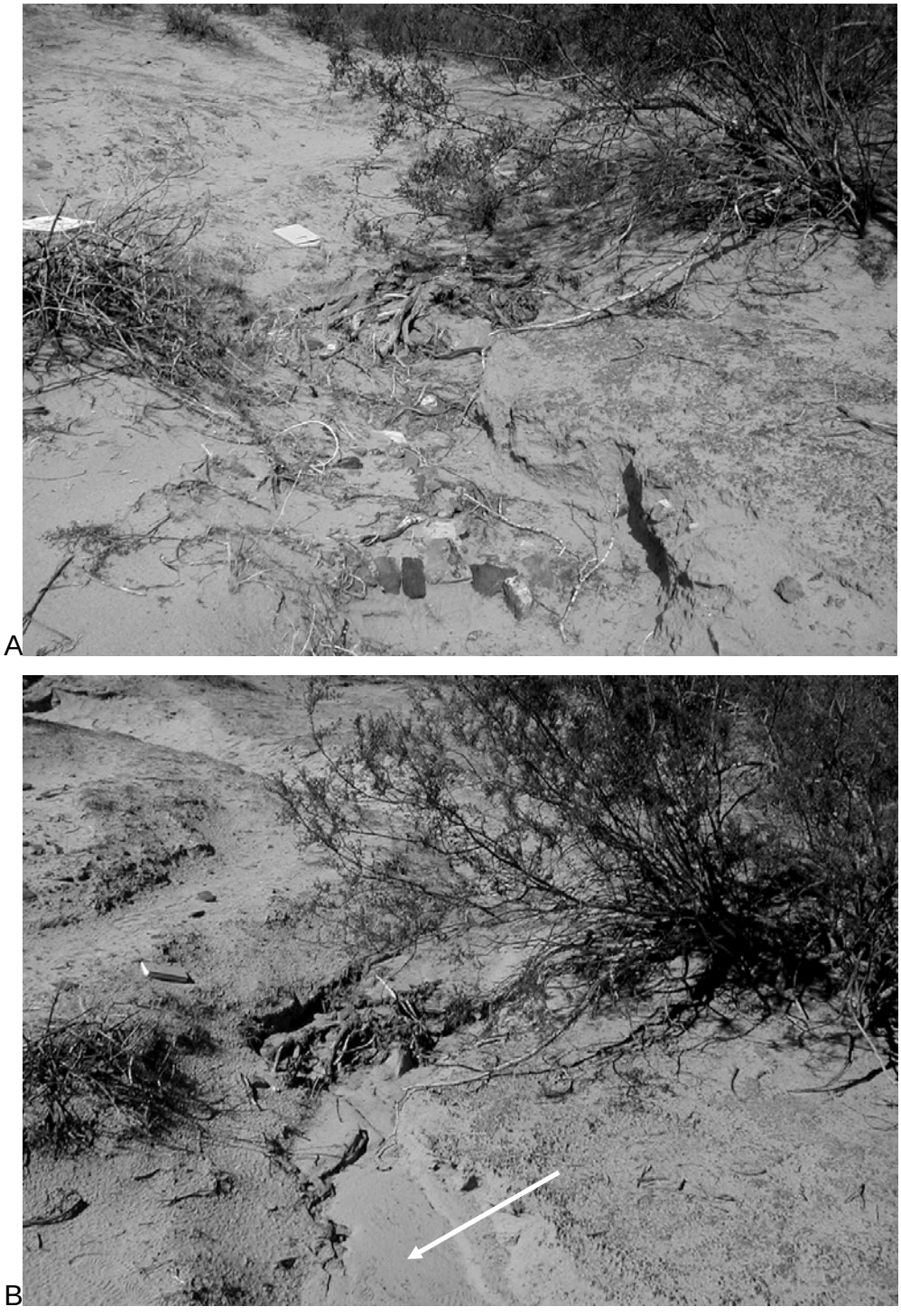

Figure G.16. Indian Canyon structure #4. February (A) flanked; October (B) widening, incision, and knickpoint retreat at structure, sediment deposition at base of photo (arrow).

A

B

Figure G.17. Indian Canyon structure #5. February (A) breached; October (B) incision and widening of smaller, rejuvenated thalweg cut evident.

Arroyo Grande

A

B

Figure G.18. Arroyo Grande structure #2. February (A) intact; October (B) no change.

Figure G.19. Arroyo Grande structures in western gully. February (A) most structures are flanked; October (B) partially filled with eolian sediment.

A

B

Figure G.20. Arroyo Grande structure #1. February (A) intact; October (B) no change.

Granite Park

A

B

Figure G.21. Granite Park structure #3. February (A) intact; October (B) no change.

A

B

Figure G.22. Granite Park structure #2. February (A) intact, although minor erosion near pen; October (B) minor erosion near pen filled in through rainsplash creep.

A

B

Figure G.23. Granite Park unnamed structures in foreground, structure #2 in background. February (A) intact, minor flanking around foreground boulders; October (B) little change.

A

B

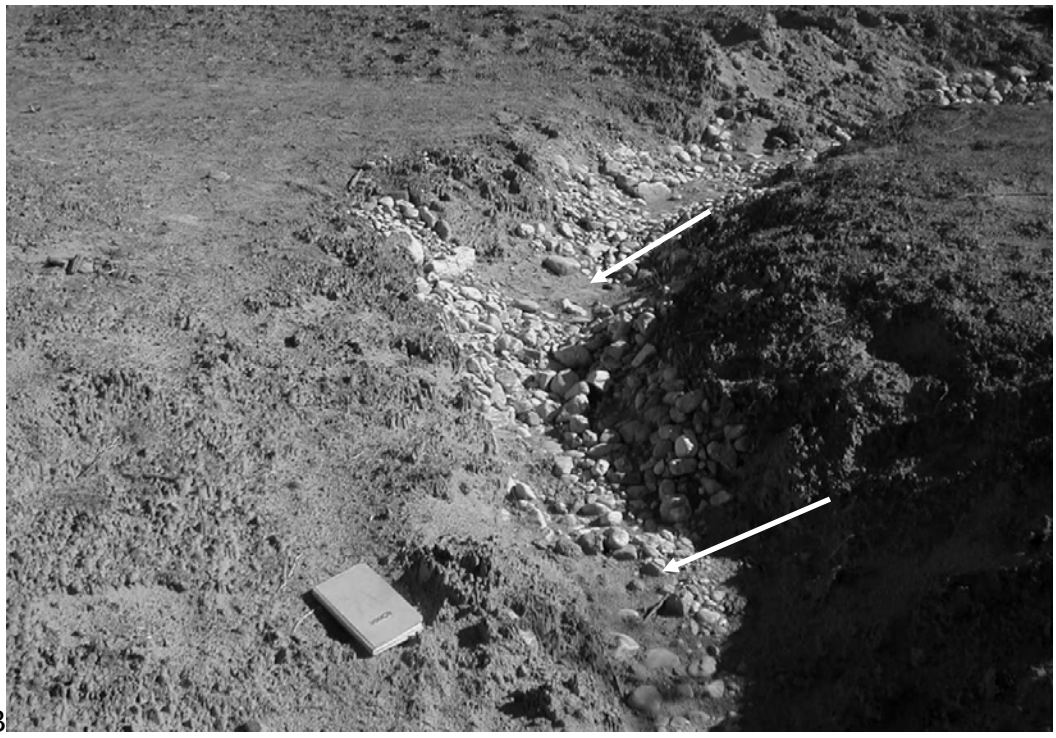

Figure G.24. Unnamed structures. February (A): intact. October (B): sediment filling at bottom and top of photograph (arrows).

Figure G.25. Granite Park series of unnamed structures. February intact; October sediment infilling in front checkdam (arrow).

A

B

Figure G.26. Granite Park structure #1. February (A) intact; October (B) no change.

A

B

Figure G.27. Granite Park structure #4. February (A) intact; October (B) no change.

223-mile

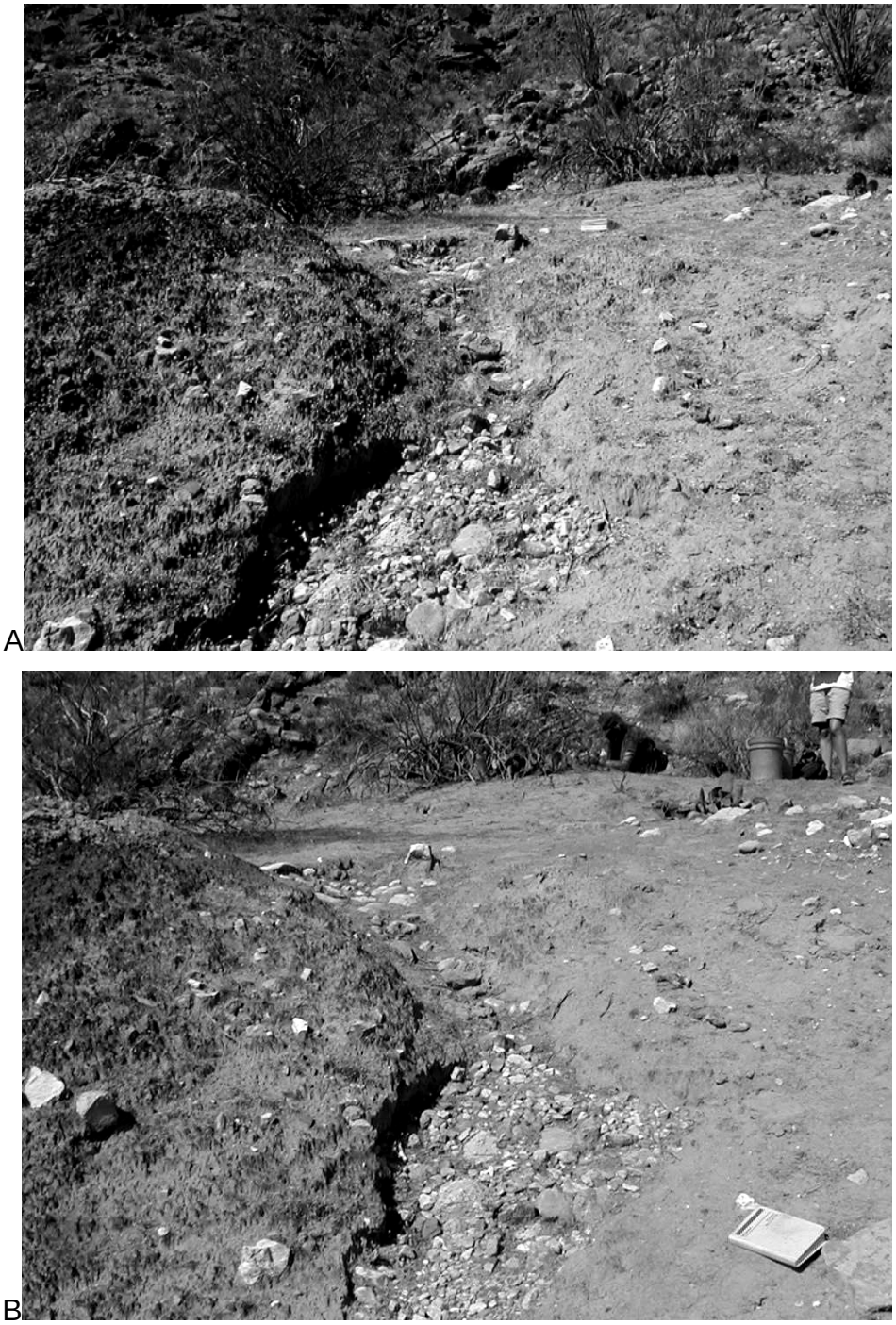

Figure G.28. 223-mile Structures #8 (top) and #10 (bottom). February (A) #8 is intact, but #10 is flanked; October (B) no change.

A

B

Figure G.29. 223-mile structure #10. February (A) some flanking; October (B) no change.

A

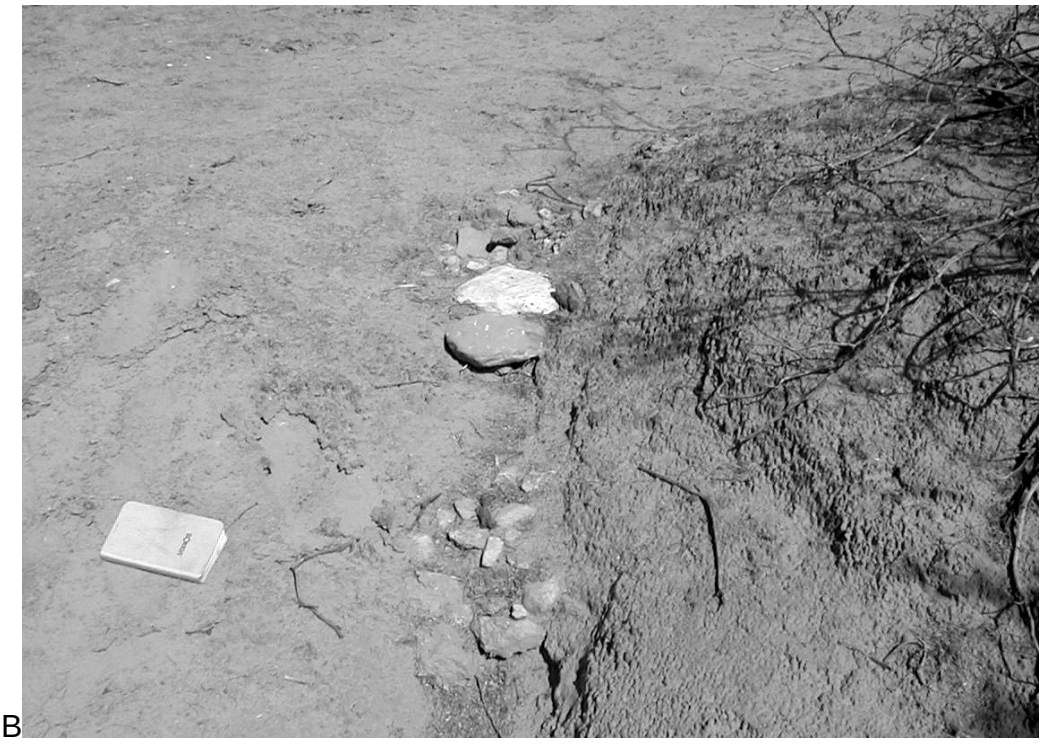

B

Figure G.30. 223-mile structure #5. February (A) minor breaching, but mostly intact; October (B) no change.

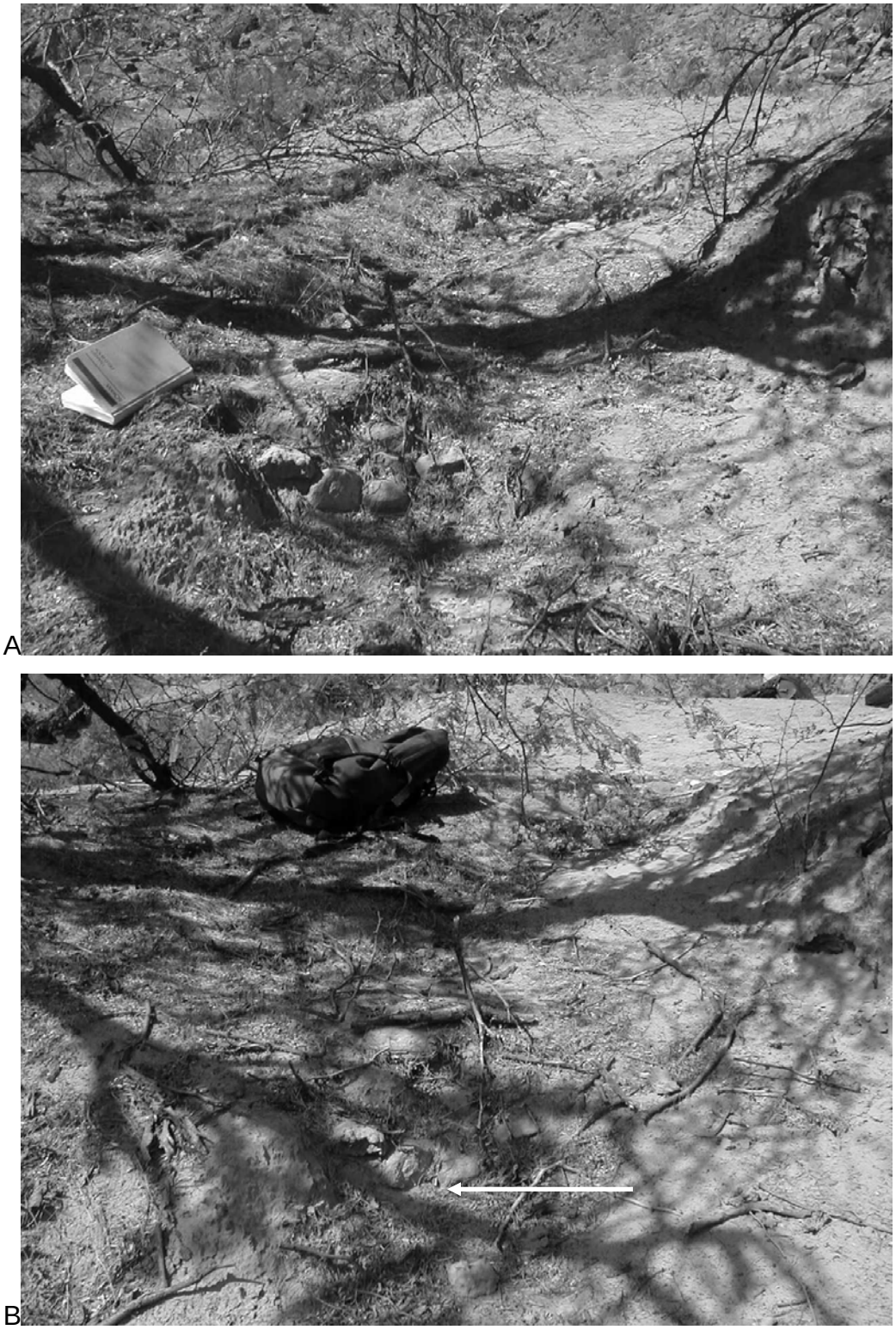

Figure G.31. 223-mile structures #7 (foreground) and #6 (background). February (A) both are intact; October (B) some deposition within structure #7 (arrow).

A

B

Figure G.32. 223-mile structure #16. February (A) flanked and breached; October (B) no change.

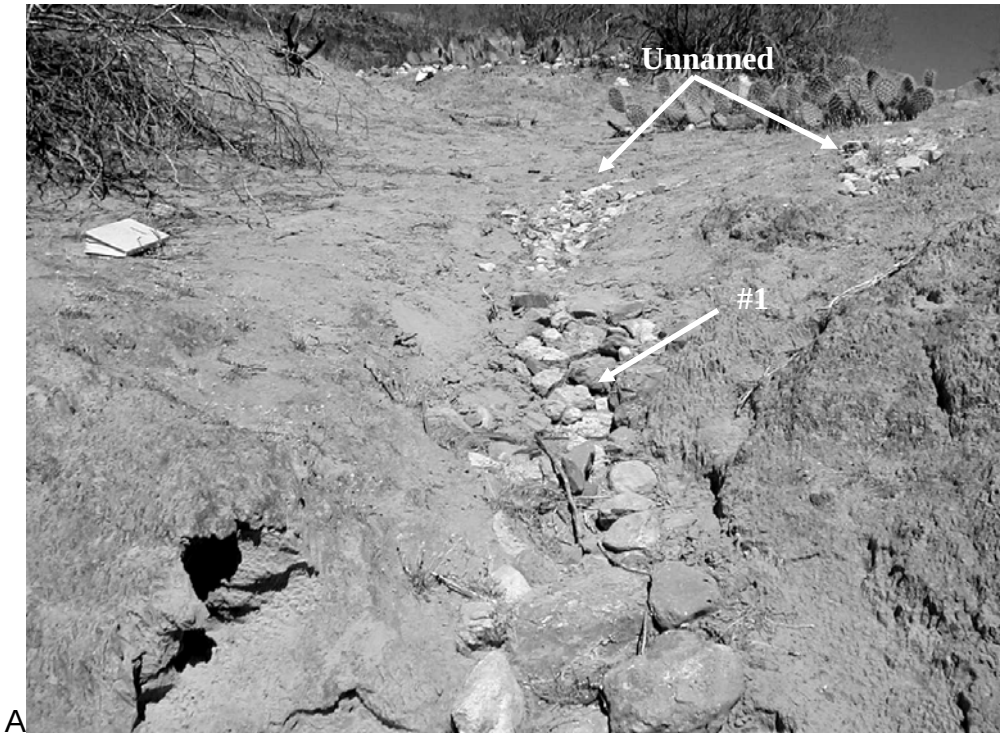

A

B

Figure G.33. 223-mile structure #1 (bottom), unnamed structures (top). February (A) #1 has minor breaching and flanking; unnamed structures intact; October (B) no change.

A

B

Figure G.34. 223-mile structure #2. February (A) minor breaching, rock displacement; October (B) little change.

A

B

Figure G.35. 223-mile structure #11. February (A) intact; October (B) infilled by eolian sand.

A

B

Figure G.36. 223-mile structure #14. February (B) minor breaching and flanking; October (B) no change.

Appendix H. Erosion-Control Structure Data Tables
(Properties and denudation associated with erosion-control structures measured by total-station ground surveys)

TABLE H.1. EROSION-CONTROL STRUCTURE ASSESSMENT

study site	ID	Year built	Year maintained	Local grade (m/m)	Contributing area (m^2)	on knpt?	Structure length (m)	Upstream structure $(m)^2$	Downstream knpt $(m)^2$	February Condition[1]	October Condition
60-mile	1	1996	na[3]	0.22	570	Y	0.39	nm[4]	nm	B	B
60-mile	2	1996	2000	0.27	597	N	0.84	5.00	nm	I	I
60-mile	5	1996	1998	0.24	424	Y	0.77	nm	7.43	B	F
60-mile	4	1996	na	0.12	455	Y	0.94	7.81	0.47	B	B, F
60-mile	3	1996	2000	0.25	748	N	2.59	1.74	3.94	I	F, B
60-mile	6	1996	2000	0.19	1358	Y	2.47	2.22	2.03	B	B, F
60-mile	7-2	na	na	0.12	1421	N	0.65	6.81	0.69	F	F
60-mile	7	1996	na	0.24	1427	N	0.75	2.19	3.76	I	I
60-mile	8	1996	na	0.20	1440	N	2.18	0.70	3.06	I	I
60-mile	9B	1996	na	0.24	1446	Y	0.81	0.29	1.82	I	I
60-mile	9A	1996	na	0.30	1455	N	0.66	0.39	0.77	F	F
60-mile	12A	1996	na	nm	1457	nm	nm	nm	nm	I	F
60-mile	12B	1996	na	0.25	1458	Y	2.51	0.77	nm	F	F
Pal (099)	42	1995	1998	0.04	54762	nm	nm	nm	nm	F	F
Pal (099)	41	1995	1998	0.03	56580	N	1.26	nm	30.20	I	F
Pal (099)	41N	na	1998	0.01	58212	N	2.14	25.33	2.73	I	I
Pal (099)	39	1995	1998	0.00	58632	N	0.88	1.85	0.76	I	I
Pal (099)	38	1995	1998	0.00	59171	N	1.68	7.38	41.46	I	I
Pal (099)	37	1995	1998	0.06	59433	N	1.17	7.24	33.05	nm	F
Pal (099)	37N	na	1998	0.03	59701	N	0.94	3.93	28.18	I	I
Pal (099)	35N	1998	na	0.02	60161	N	0.47	4.65	23.06	I	I
Pal (099)	35	1995	1998	0.04	60567	N	1.63	9.72	11.71	I	I
Pal (099)	18	1995	2000	0.01	61124	N	1.91	5.22	4.58	nm	B
Pal (099)	28	1995	1998	0.03	8171	Y	0.59	nm	32.67	nm	B, F
Pal (099)	27	1995	1998	0.02	8629	N	0.86	9.12	22.69	nm	F
Pal (099)	26	1995	2000	0.03	8700	N	1.21	2.89	18.59	nm	B, F
Pal (099)	25	1995	1998	0.04	8853	N	1.03	4.24	13.32	nm	F
Pal (099)	24	1995	1998	0.04	8897	N	0.76	3.92	8.64	nm	F
Pal (099)	23	1995	1998	0.04	8940	N	0.37	2.17	6.10	I	I
Pal (099)	22	1995	1998	0.05	9024	Y	2.95	5.21	nm	nm	B, F
Pal (099)	21	1995	1998	0.05	9354	N	2.88	2.16	nm	F	B, F
Pal (099)	19	1995	1997	0.05	9373	nm	nm	nm	nm	I	I
Pal (099)	16	1995	1998	0.10	9450	nm	nm	nm	nm	I	I
Pal (099)	15	1995	2000	0.01	84713	N	2.59	12.56	43.77	I	I
Pal (099)	14	1995	2000	0.03	84847	N	3.45	4.01	36.31	nm	F
Pal (099)	13	1995	1998	0.05	85193	N	2.04	9.14	27.17	nm	B, F
Pal (099)	12	1995	1998	0.06	85329	N	1.40	6.20	17.53	nm	B, F
Pal (099)	11	1995	1998	0.05	85465	N	3.00	3.12	11.41	nm	B, F
Pal (099)	10	1995	1998	0.11	85608	N	1.31	5.59	4.51	nm	B
Pal (099)	9	1995	1998	0.05	85749	Y	1.13	3.45	4.18	nm	B
Pal (100)	na	na	na	0.03	2618	N	0.79	na	4.76	I	I
Pal (100)	na	na	na	0.01	2667	N	na	3.34	1.42	I	I
Pal (100)	na	na	na	0.09	2762	N	0.94	2.05	5.80	I	I
Pal (100)	21	1995	1998	0.10	2832	Y	4.40	2.58	6.18	I	I
Pal (100)	na	na	na	0.16	2916	N	1.13	1.34	3.71	nm	F
Pal (100)	19	1995	1998	0.09	2989	N	1.06	2.65	0.29	I	I
Pal (100)	na	na	na	0.16	3024	Y	1.66	1.39	3.14	I	I
Pal (100)	20	1995	1998	0.04	3060	Y	0.88	3.37	nm	nm	B
Pal (100)	17	1995	1998	0.01	3171	N	0.88	1.06	nm	I	I
Pal (100)	18	1995	na	0.06	3285	N	0.96	4.95	nm	I	I
Pal (100)	25	1995	na	0.00	3144	N	0.24	nm	1.06	I	I
Pal (100)	26	1995	na	0.11	3237	N	0.96	6.75	32.41	I	I
Pal (100)	14	1995	1998	0.04	7304	N	2.75	12.09	17.57	nm	F
Pal (100)	13	1995	2000	0.05	7485	N	2.72	12.59	1.26	I	I
Pal (100)	12	1995	1998	0.12	7874	Y	3.05	1.22	22.81	nm	F
Pal (100)	11	1995	1998	0.05	7984	N	0.98	0.92	18.18	I	I
Pal (100)	10	1995	1998	0.04	8100	N	3.01	2.39	12.78	I	I

TABLE H.1 (CONTINUED). EROSION-CONTROL STRUCTURE ASSESSMENT

study site	ID	Year built	Year maintained	Local grade (m/m)	Contributing area (m^2)	on knpt?	Structure length (m)	Upstream structure (m)	Downstream knpt (m)	February Condition	October Condition
Basalt (348)	2	1997	na	0.07	3054	N	0.71	na	6.01	I	I
Basalt (348)	3	1997	na	0.12	3067	N	1.04	0.85	4.12	I	I
Basalt (348)	na	1997	na	0.11	3204	Y	1.50	3.33	1.05	I	I
Basalt (348)	4	1997	na	0.05	3354	Y	2.65	6.24	nm	I	I
Basalt (348)	na	1997	na	0.12	nm	N	2.76	nm	3.77	I	I
Basalt (346)	6	1997	na	0.06	3185	N	0.30	nm	9.69	I	B
Basalt (346)	5	1997	na	0.17	3327	N	1.01	5.35	3.33	I	B
Basalt (346)	4	1997	na	0.06	3358	Y	0.58	2.92	0.44	I	F
Basalt (346)	3	1997	na	0.14	3403	N	0.63	3.43	0.21	I	I
Basalt (346)	2	1997	na	0.07	3474	Y	0.57	3.43	1.42	I	F
Basalt (346)	1	1997	1998	0.11	3500	Y	0.52	1.54	nm	I	B
Basalt (346)	9	1997	1998	0.07	434	nm	0.09	nm	2.87	I	I
Basalt (346)	7	1997	1998	0.13	2521	N	0.25	22.33	1.10	I	B
Basalt (346)	8	1997	1998	0.08	2577	N	0.20	1.29	nm	I	I
Indian Can	6	1997	1998	0.06	1280	N	1.34	nm	10.45	B, F	B, F
Indian Can	5	1997	1998	0.33	2055	Y	0.07	39.24	5.55	B, F	B, F
Indian Can	4	1997	1998	0.10	2183	N	0.23	6.02	0.70	I	I
Indian Can	3	1997	1998	0.19	2189	Y	0.16	0.70	4.06	B, F	B, F
Indian Can	2	1997	1998	0.03	2409	N	0.43	13.74	2.00	B, F	B, F
Arroyo	2	1997	na	0.19	220	N	3.03	nm	0.68	I	I
Arroyo	3	1997	2000	0.40	256	Y	1.21	0.68	1.38	B, F	B, F
Arroyo	4	1998	2000	0.44	289	N	0.44	0.31	0.63	F	F
Arroyo	5	1998	na	0.46	296	Y	0.34	0.37	2.23	B, F	B, F
Arroyo	6	1998	2000	0.38	318	N	1.31	0.92	0.90	F	F
Arroyo	7	1998	2000	0.60	334	N	nm	0.41	0.49	B, F	B, F
Arroyo	8	1998	2000	0.31	342	N	0.29	1.42	nm	I	I
Arroyo	9	1998	2000	0.32	344	N	0.31	0.50	nm	F	F
Arroyo	1	1997	2000	0.10	3979	N	0.92	nm	3.41	I	I
Granite	3	1996	1999	0.06	6395	N	1.27	nm	6.67	I	I
Granite	2	1996	1999	0.07	6723	Y	1.19	6.44	1.72	I	I
Granite	na	1999	na	0.10	7145	N	1.25	1.84	29.86	I	I
Granite	na	1999	na	0.08	7169	N	0.86	0.6	28.4	I	I
Granite	na	1999	na	0.05	7197	N	2.98	0.32	25.1	I	I
Granite	na	1999	na	0.05	7377	N	0.9	1.97	22.23	I	I
Granite	na	1999	na	0.06	7449	N	0.92	0.99	20.32	I	I
Granite	na	1999	na	0.05	7517	N	0.81	5.11	14.4	I	I
Granite	na	1999	na	0.06	7574	N	0.77	2.35	12.05	I	I
Granite	na	1999	na	0.04	7586	N	1.38	0.7	10.4	I	I
Granite	na	1999	na	0.08	7603	N	2.63	0.23	7.06	I	I
Granite	na	1999	na	0.07	7619	N	1.11	1.22	4.73	I	I
Granite	na	1999	na	0.03	7818	N	nm	nm	nm	I	I
Granite	na	1999	na	0.18	7894	N	nm	nm	nm	I	I
Granite	1 (?)	1996	1999	0.11	7992	Y	3.1	4.73	3.66	I	I
Granite	4	1996	1999	0.10	8153	N	0.98	10.98	na	I	I
223-mile	3	1997	na	0.46	84	N	0.83	na	4.49	F	F
223-mile	2	1997	1998	0.59	69	N	0.9	0.86	2.73	I	I
223-mile	1	1997	na	0.32	61	Y	0.79	2.1	0.82	B	B
223-mile	na	na	na	0.32	6	nm	nm	nm	nm	I	I
223-mile	8	1997	na	0.19	140	N	0.88	nm	19.86	I	I
223-mile	10	1997	na	0.30	141	N	3.06	0.57	16.23	F	F
223-mile	5	1997	na	0.13	239	N	0.61	9.05	6.57	I	I
223-mile	6	1997	na	0.31	245	N	0.53	0.47	5.57	I	I
223-mile	na	na	na	0.20	248	N	0.52	0.68	4.37	I	I
223-mile	7	1997	na	0.46	254	N	0.53	1.49	2.35	I	I
223-mile	16	1998	2000	0.52	261	Y	2.28	2.35	0.18	F	F
223-mile	11	1997	na	0.06	745	N	nm	nm	10.63	I	I
223-mile	13	1997	na	0.13	928	N	0.55	15.61	2.76	B, F	B, F
223-mile	14	1997	na	0.43	956	Y	0.46	2.76	9.01	B, F	B, F
223-mile	na	na	na	0.32	1082	Y	0.56	15.81	nm	I	I

[1] F = flanked, B = breached, I = intact

[2] distances to particular features

[3] data not available

[4] data not measured

TABLE H.2. EROSION AND DEPOSITION AT EACH STRUCTURE BETWEEN SURVEYS

site	ID	structure erosion (m)	channel erosion (m)	condition
60-mile	ck1	0.029	0.014	B
60-mile	ck2	-0.056	0.014	I
60-mile	ck5	-0.021	-0.02	F
60-mile	ck4	-0.043	-0.02	B, F
60-mile	ck3	-0.109	-0.02	I
60-mile	ck6	0.000	-0.02	B, F
60-mile	ck7-2	0.002	-0.02	F
60-mile	ck7	-0.061	-0.02	I
60-mile	ck8	-0.082	-0.02	I
60-mile	ck9b	-0.026	-0.02	I
60-mile	ck9a	0.146	-0.02	F
60-mile	ck12b	-0.032	-0.02	F
Palisades	ck41	0.052	0.079	F
Palisades	ck41N	0.065	0.079	I
Palisades	ck39	0.034	0.079	I
Palisades	ck38	0.008	0.079	I
Palisades	ck37	0.042	0.079	F
Palisades	ck37N	0.003	0.079	I
Palisades	ck35N	0.033	0.079	I
Palisades	ck35	0.052	0.079	I
Palisades	ck18	0.025	0.079	B
Palisades	ck15	0.022	0.079	I
Palisades	ck14	0.006	0.079	F
Palisades	ck13	0.176	0.079	B, F
Palisades	ck12	0.002	0.079	B, F
Palisades	ck11	-0.005	0.079	B, F
Palisades	ck10	0.018	0.079	B
Palisades	ck9	-0.006	0.079	B
Palisades	ck28	0.040	0.045	B, F
Palisades	ck27	0.074	0.045	F
Palisades	ck26	0.032	0.045	B, F
Palisades	ck25	0.121	0.045	F
Palisades	ck24	0.066	0.045	F
Palisades	ck23	0.025	0.045	I
Palisades	ck22	0.089	0.045	B, F
Palisades	ck21	0.008	0.045	B, F
Palisades	ck25	-0.017	0.048	I
Palisades	ck26	0.030	0.048	I
Palisades	ck14	0.183	0.048	F
Palisades	ck13	0.015	0.048	I
Palisades	ck12	0.151	0.048	F
Palisades	ck11	-0.005	0.048	I
Palisades	ck10	-0.046	0.048	I
Palisades	unnamed	-0.006	0.03	I
Palisades	unnamed	0.080	0.03	I
Palisades	unnamed	0.071	0.03	I
Palisades	21	0.024	0.03	I
Palisades	unnamed	-0.061	0.03	F
Palisades	ck19	0.002	0.03	I
Palisades	unnamed	0.106	0.03	I
Palisades	20	0.106	0.03	B
Palisades	ck17	0.061	0.03	I
Palisades	ck18	0.047	0.03	I
Basalt	ck6	0.119	0.061	B
Basalt	ck5	0.114	0.061	B
Basalt	ck4	0.025	0.061	F
Basalt	ck3	-0.052	0.061	I
Basalt	ck2	0.018	0.061	F
Basalt	ck1	0.052	0.061	B
Basalt	ck9	0.044	0.032	I
Basalt	ck7	0.140	0.032	B
Basalt	ck8	0.024	0.032	I
Basalt	ck2	0.001	0.034	I
Basalt	ck3	-0.042	0.034	I
Basalt	unnamed	0.040	0.034	I
Basalt	ck4	-0.032	0.034	I
Basalt	unnamed	-0.044	0.018	I

TABLE H.3. EROSION STATISTICS FOR STRUCTURES[1]

	Intact	Damaged
n	35	34
mean	0.006	0.051
stdev	0.049	0.065
min (q_0)	-0.109	-0.061
q_1	-0.031	0.002
median (q_2)	0.012	0.032
q_3	0.038	0.106
max (q_4)	0.106	0.183

[1] Positive numbers represent denudation, negative numbers represent deposition

Appendix I. Photogrammetry DTM Error
(Spatial error maps resulting from point-to-model and model-to-model comparisons with ground surveys)

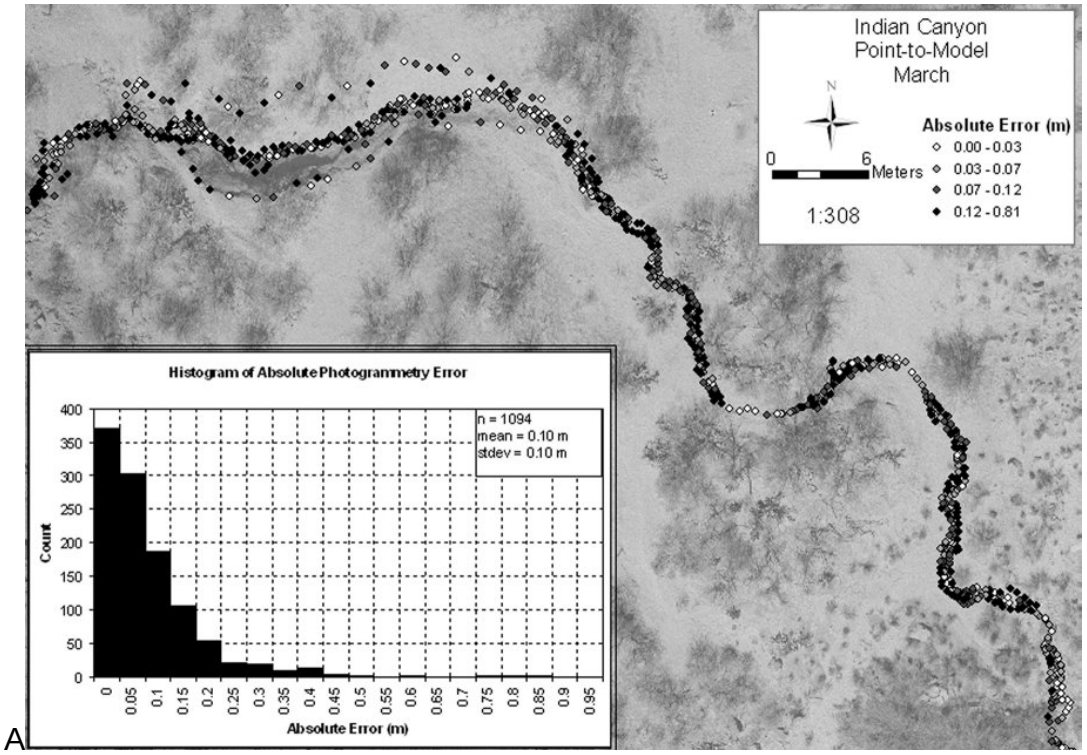

A

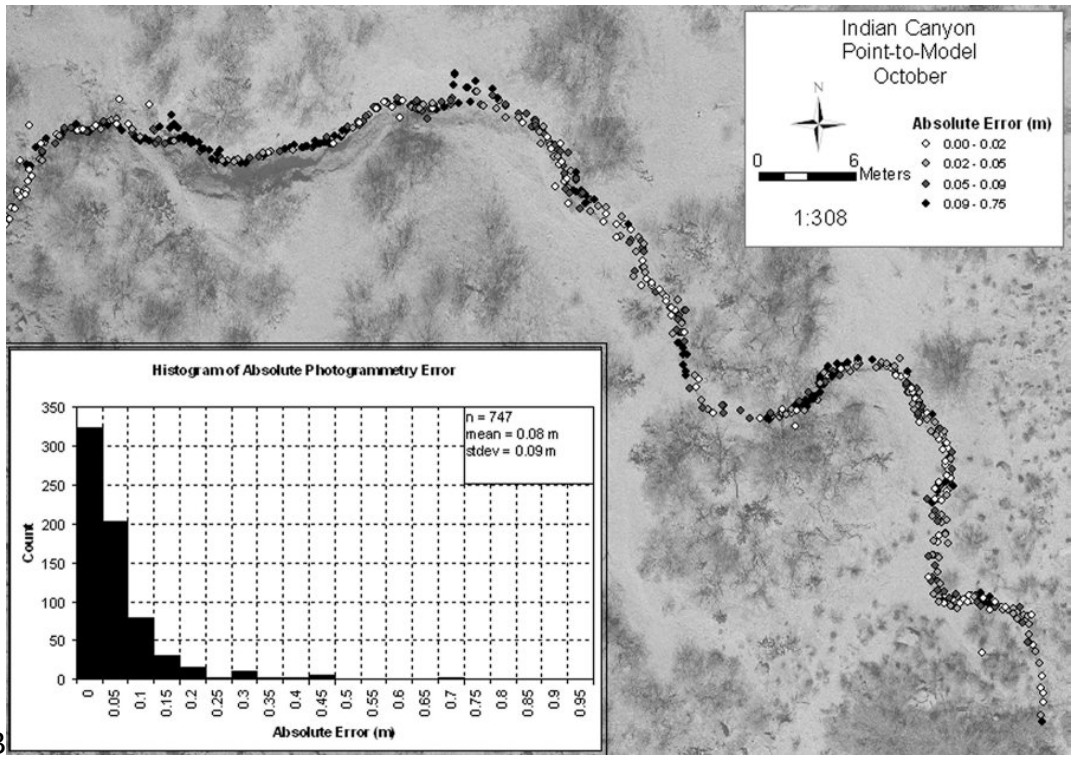

B

Figure I.1. Point-to-model manual photogrammetry DTM error for Indian Canyon in March (A) and October (B).

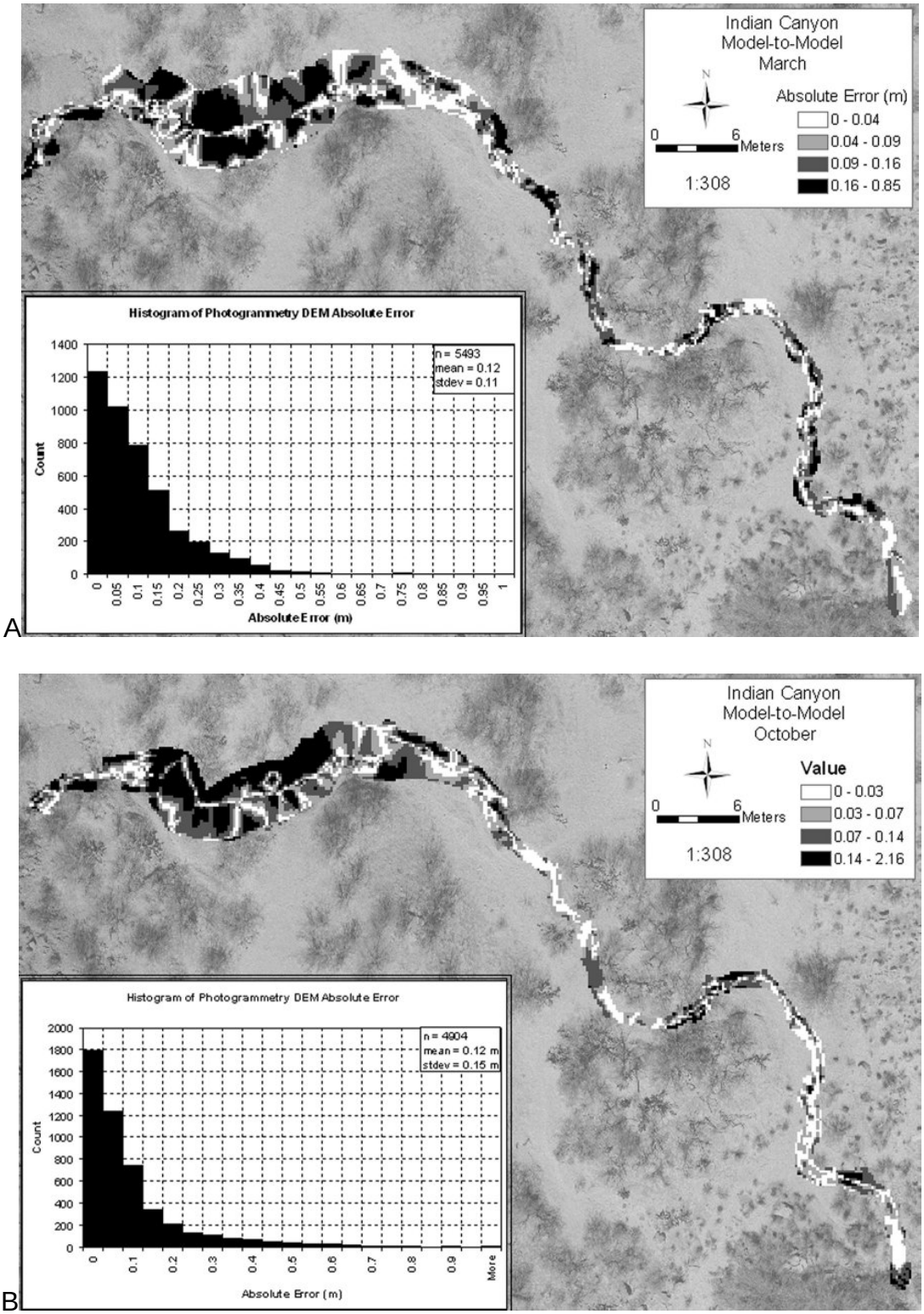

Figure I.2. Model-to-model manual photogrammetry DTM error for Indian Canyon in March (A) and October (B).

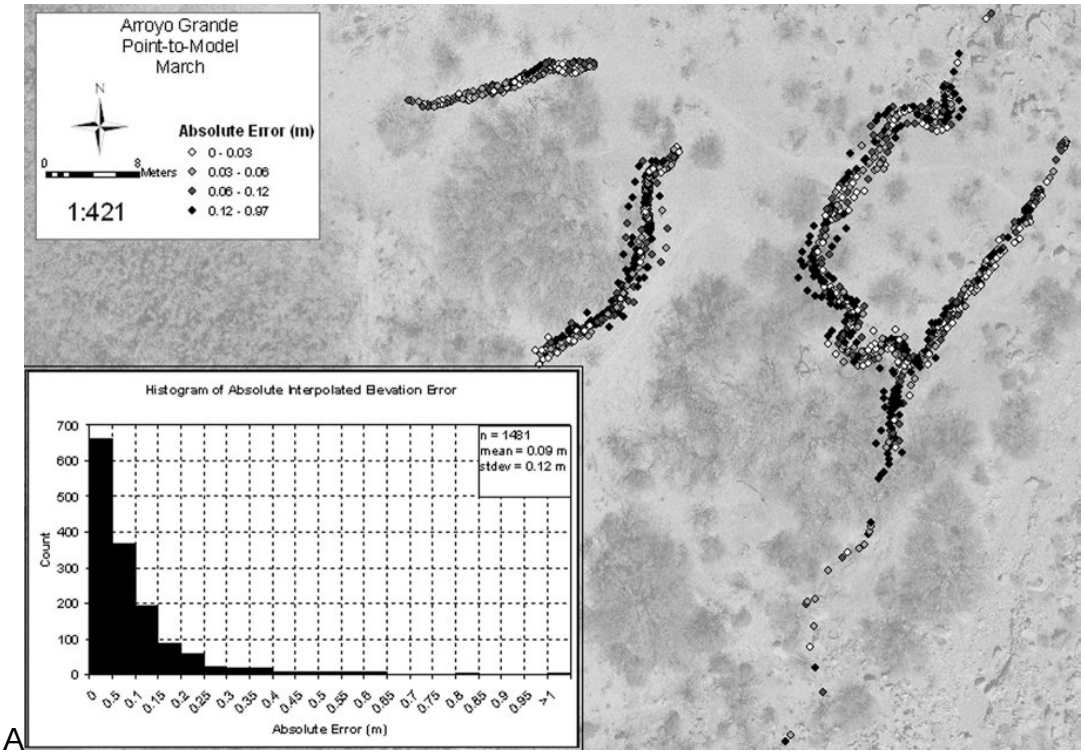

A

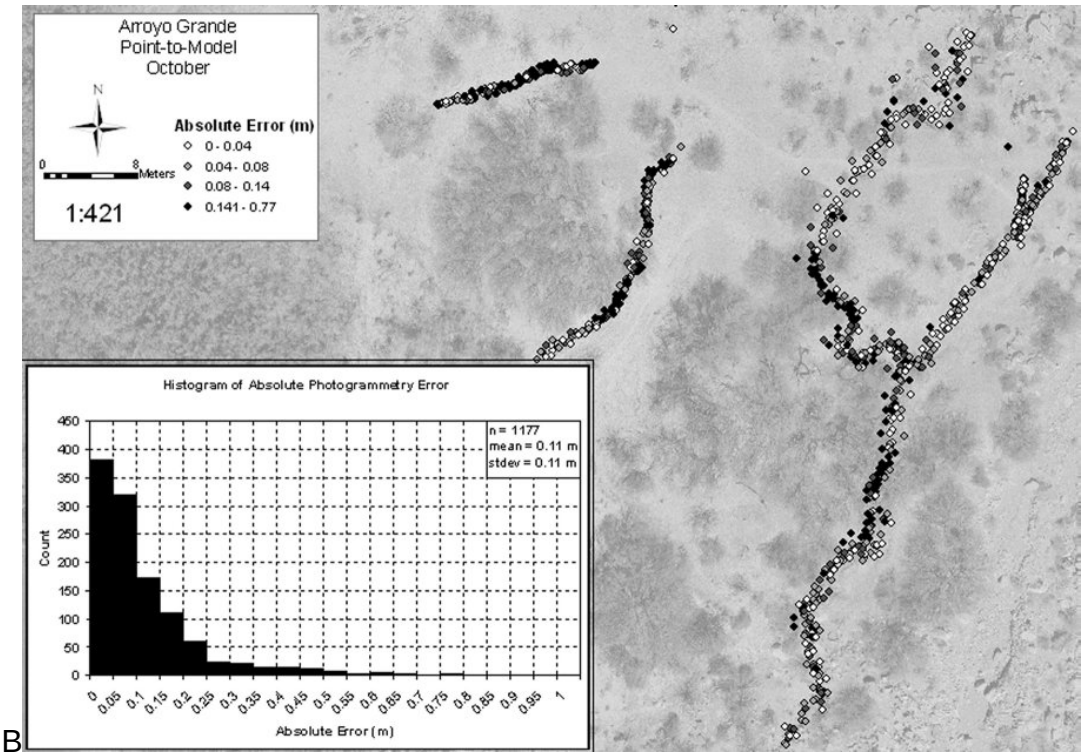

B

Figure I.3. Point-to-model manual photogrammetry DTM error for Arroyo Grande in March (A) and October (B).

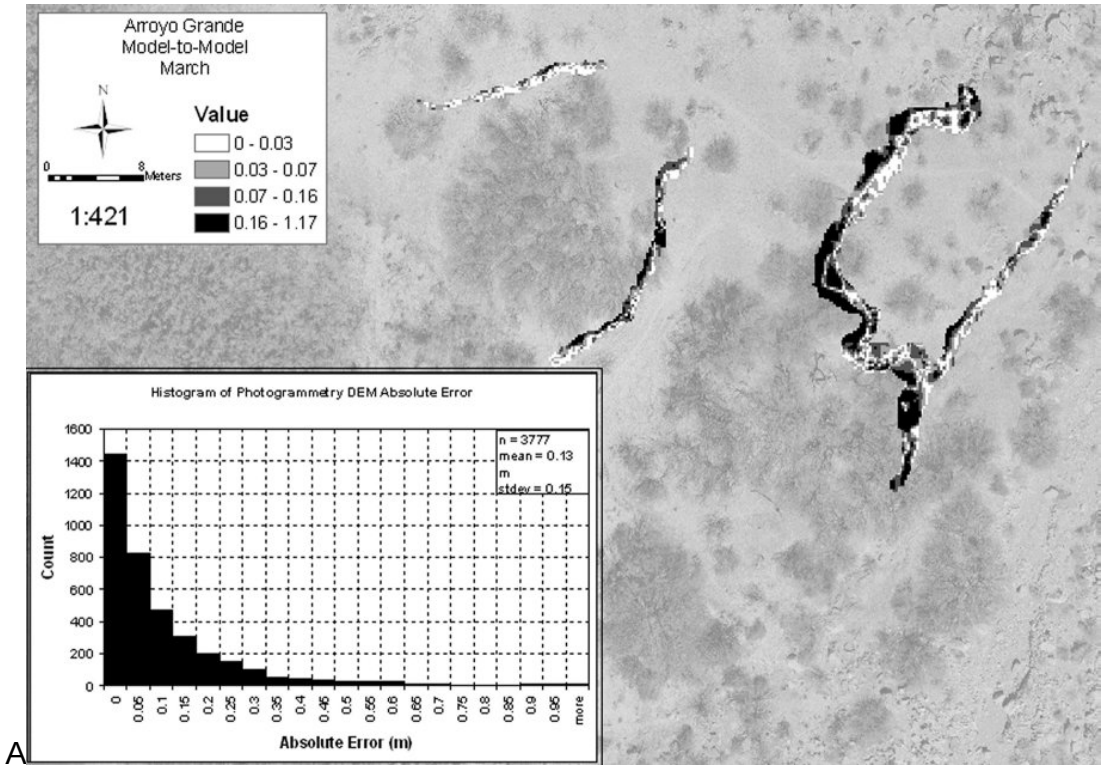

A

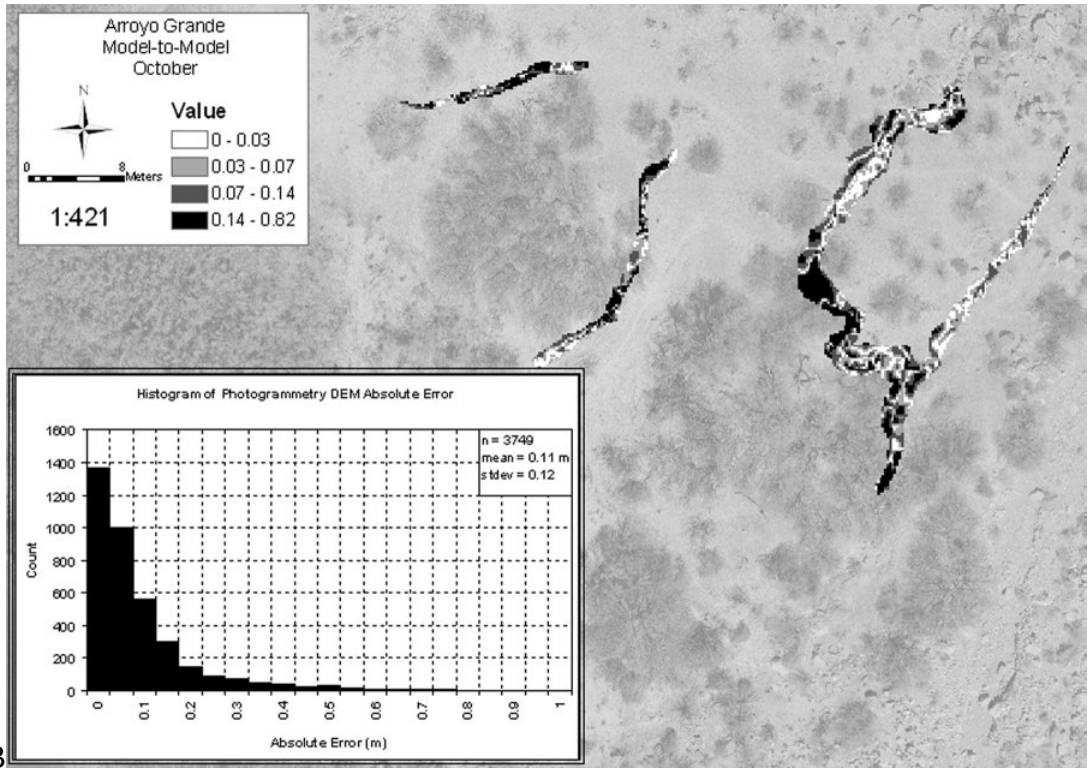

B

Figure I.4. Model-to-model manual photogrammetry DTM error for Arroyo Grande in March (A) and October (B).

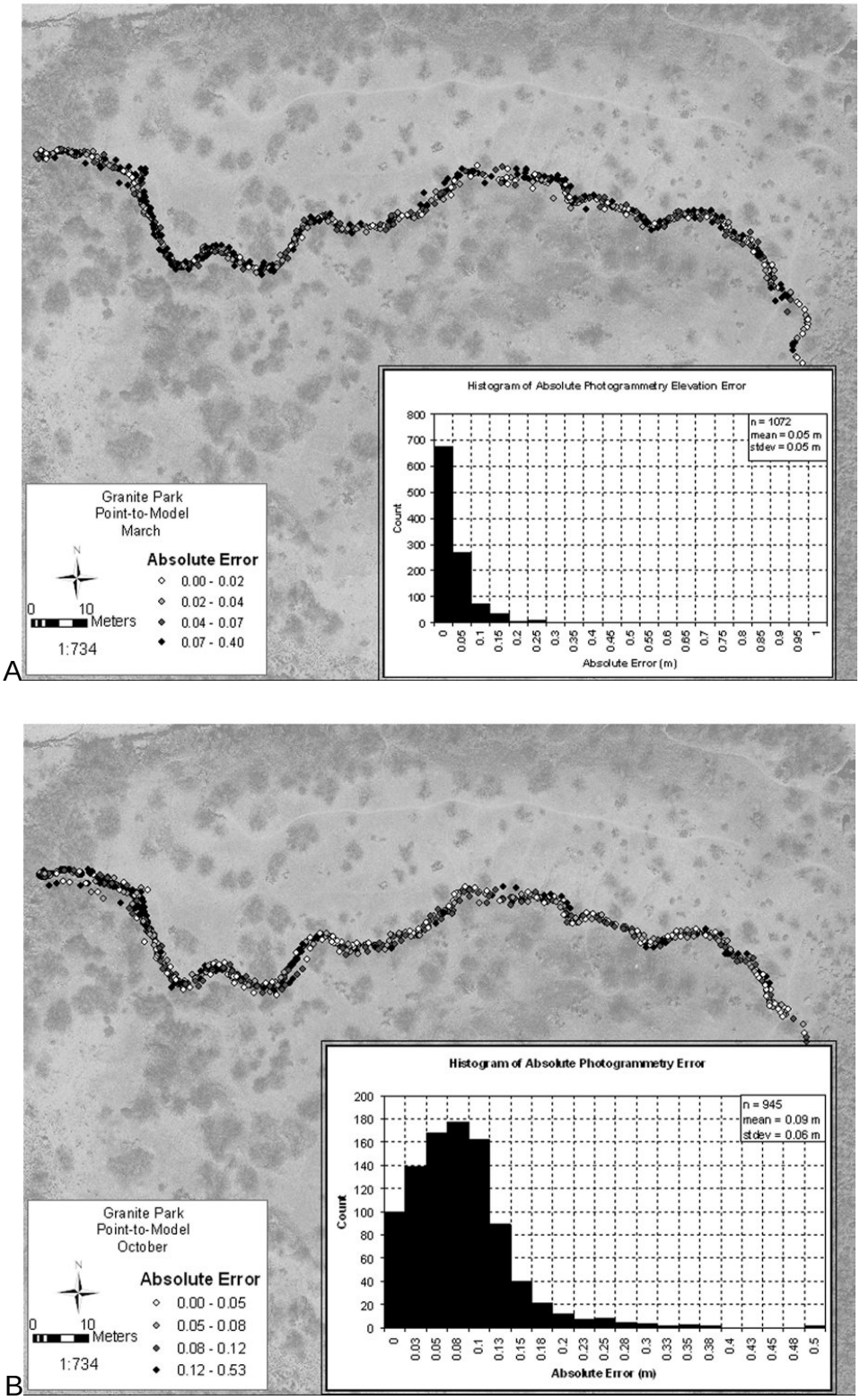

Figure I.5. Point-to-model manual photogrammetry DTM error for Granite Park in March (A) and October (B).

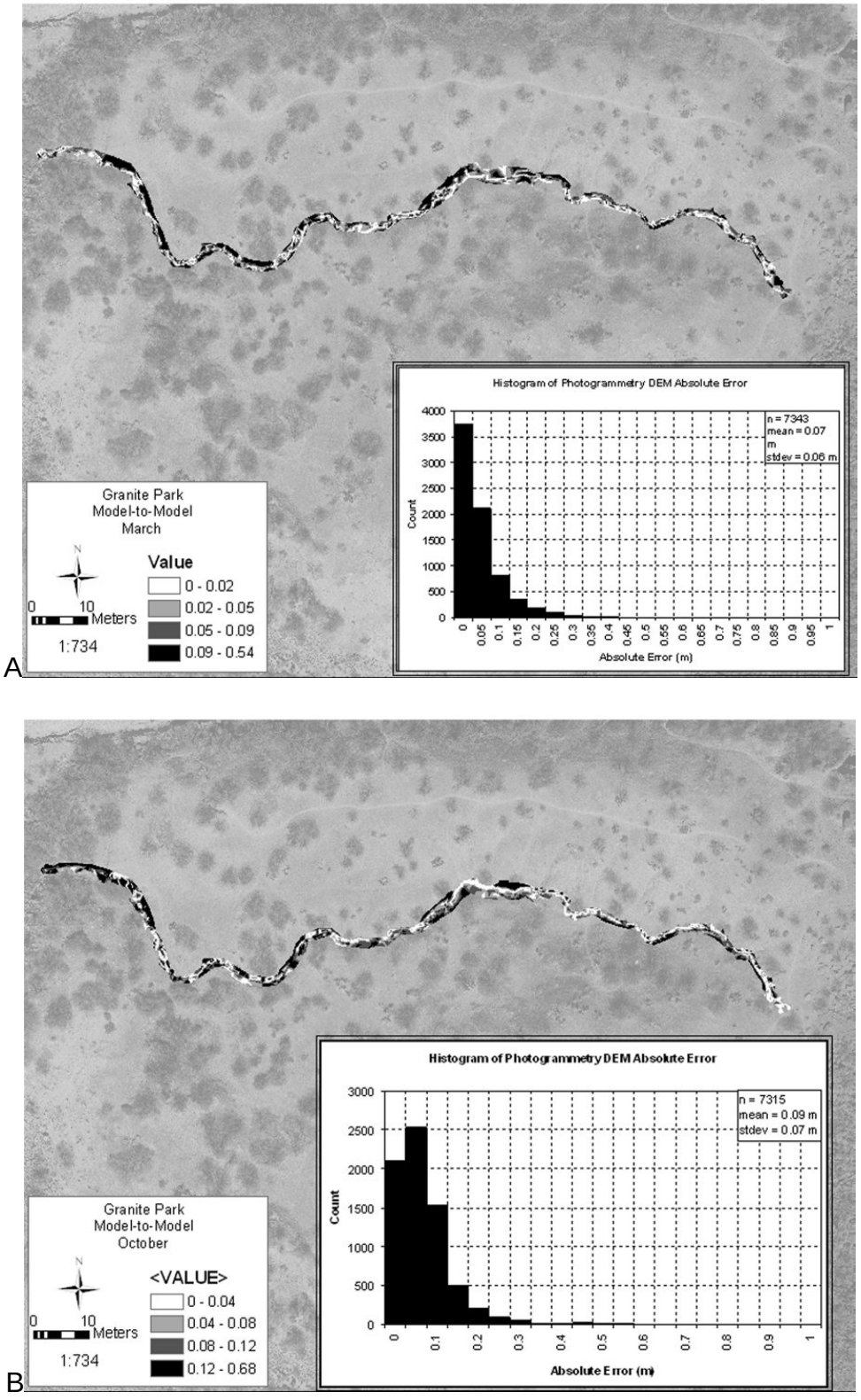

Figure I.6. Model-to-model manual photogrammetry DTM error for Granite Park in March (A) and October (B).

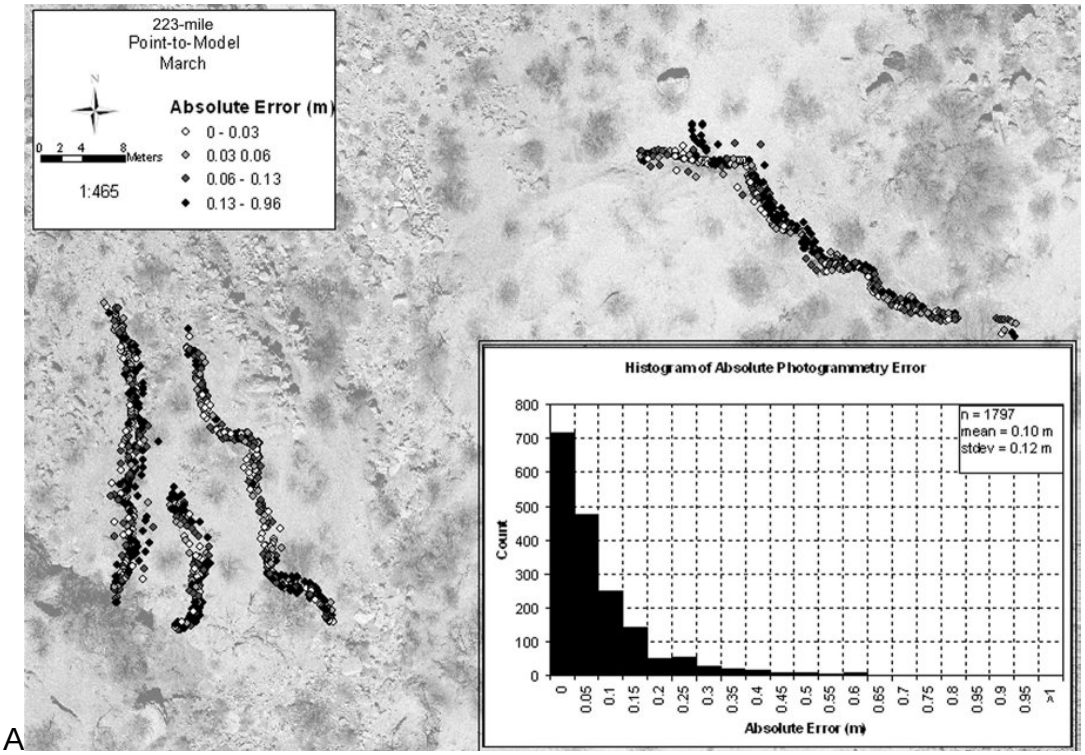

A

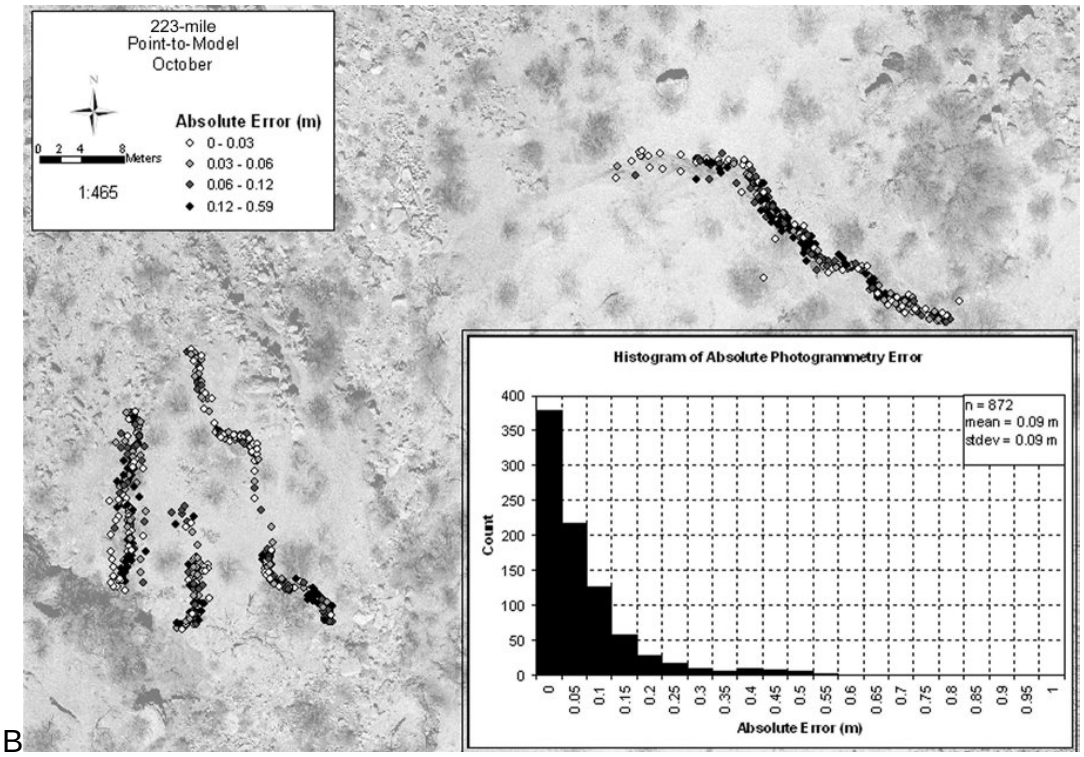

B

Figure I.7. Point-to-model manual photogrammetry DTM error for 223-mile in March (A) and October (B).

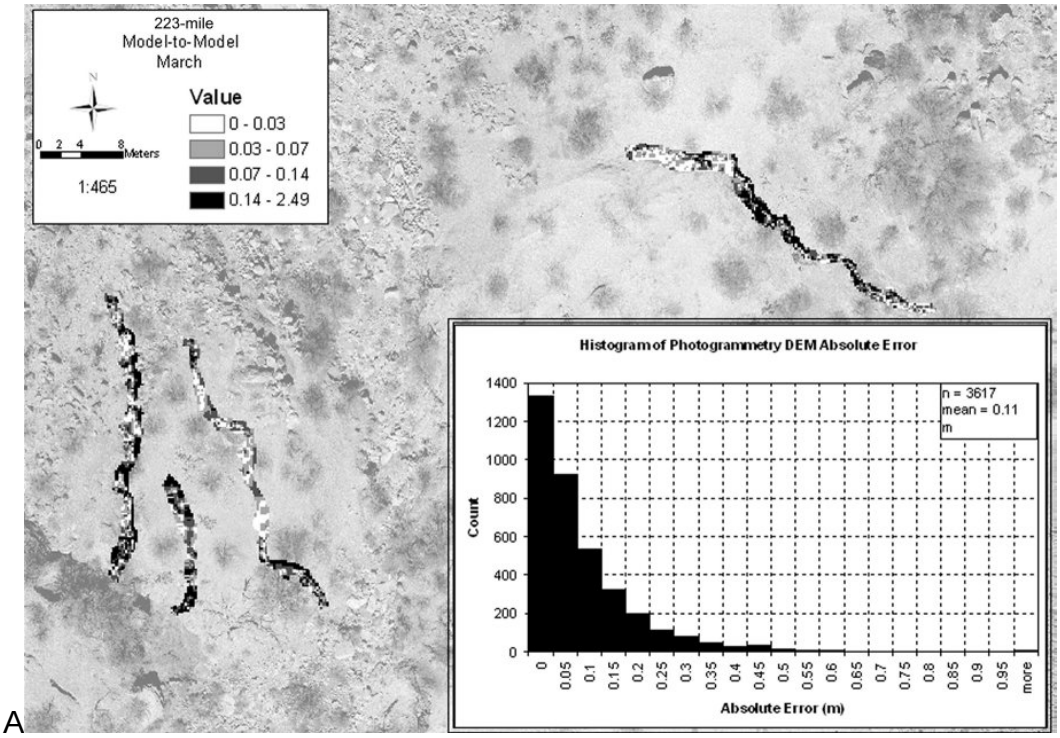

A

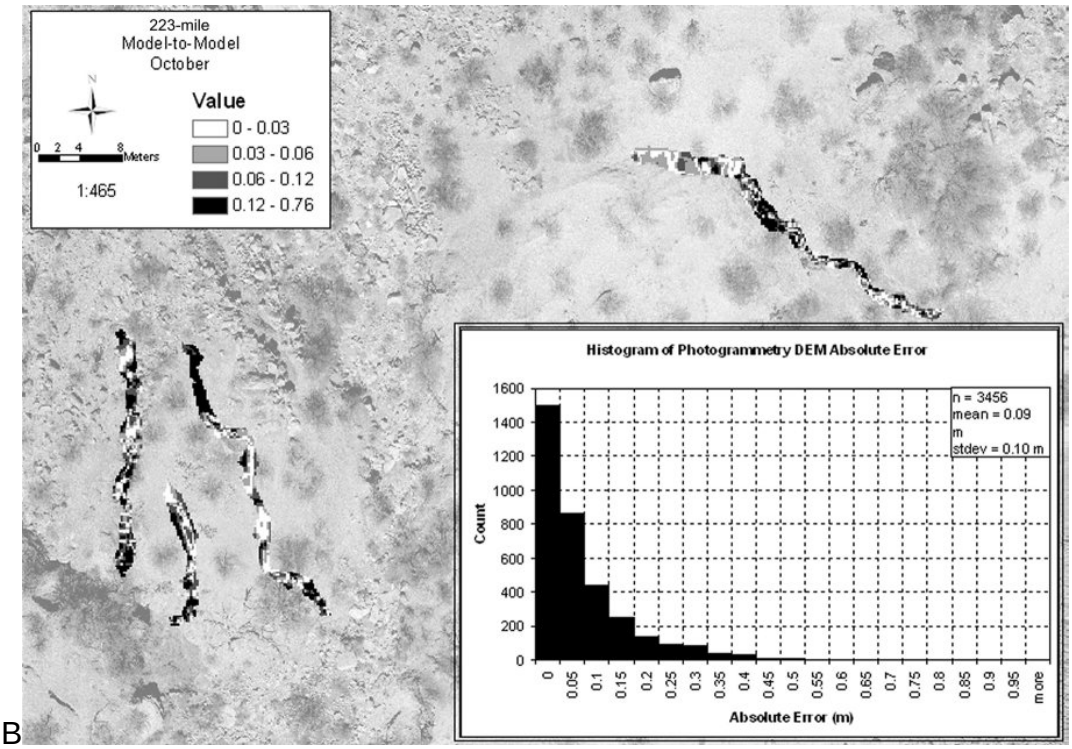

B

Figure I.8. Model-to-model manual photogrammetry DTM error for 223-mile in March (A) and October (B).

Appendix J. Photogrammetry Long Profiles and Cross Sections
(Compares photogrammetry gully long profiles and channel cross-sections to corresponding ground survey long profiles and cross-sections)

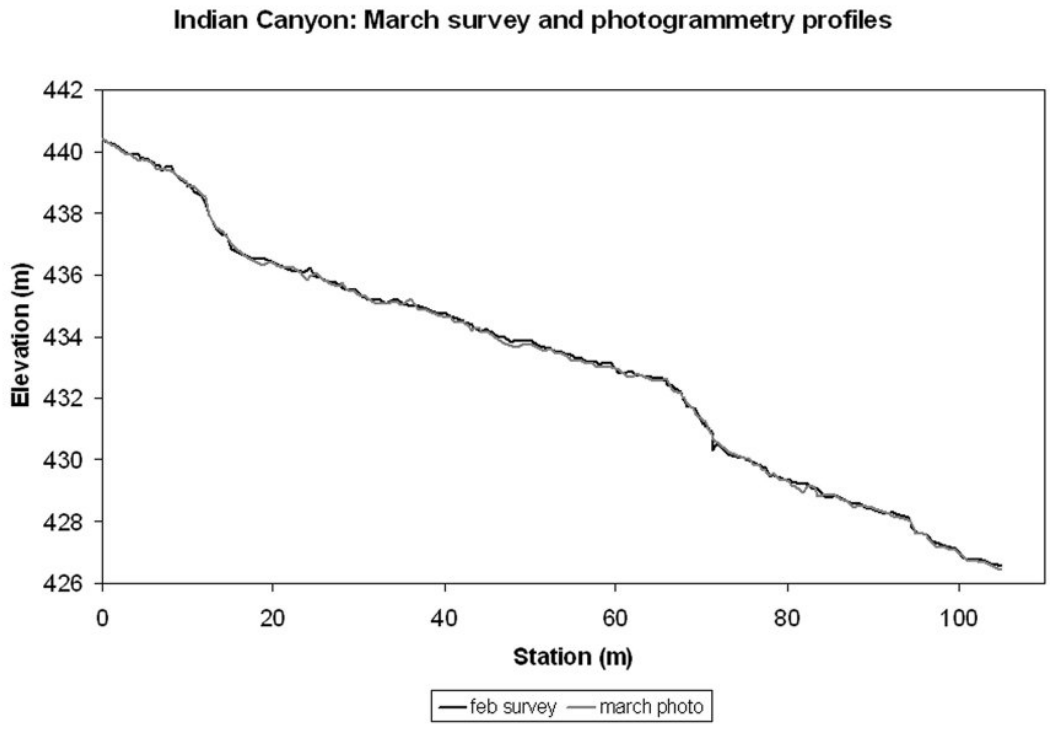

A

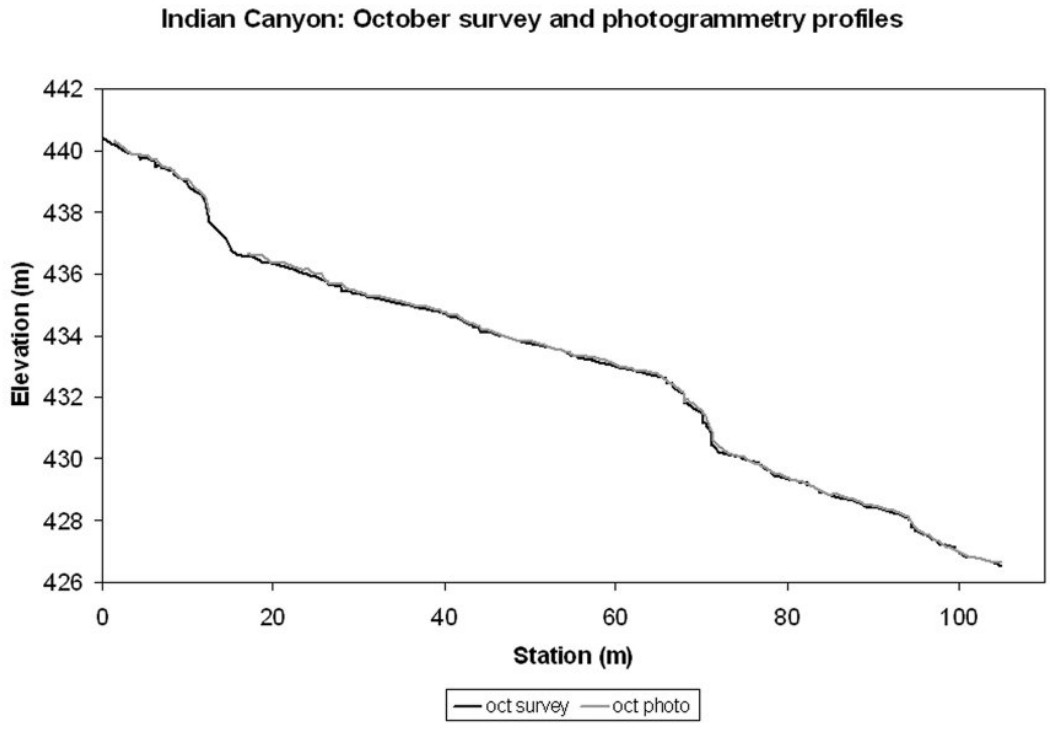

B

Figure J.1. Indian Canyon March (A) and October (B) long profiles.

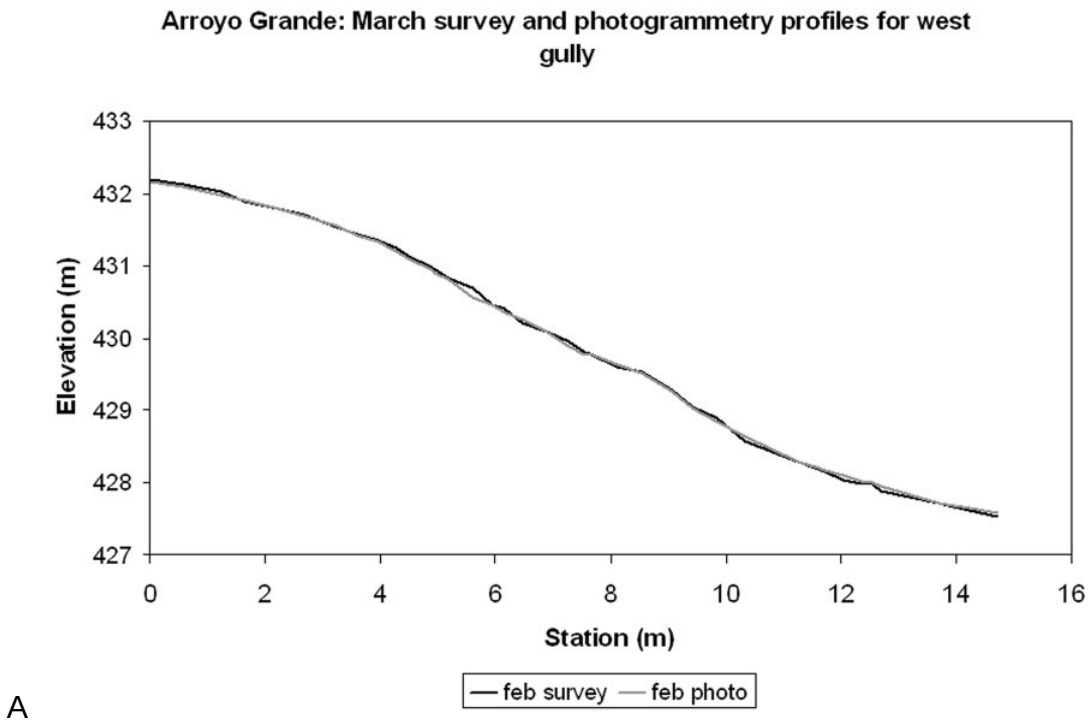

A

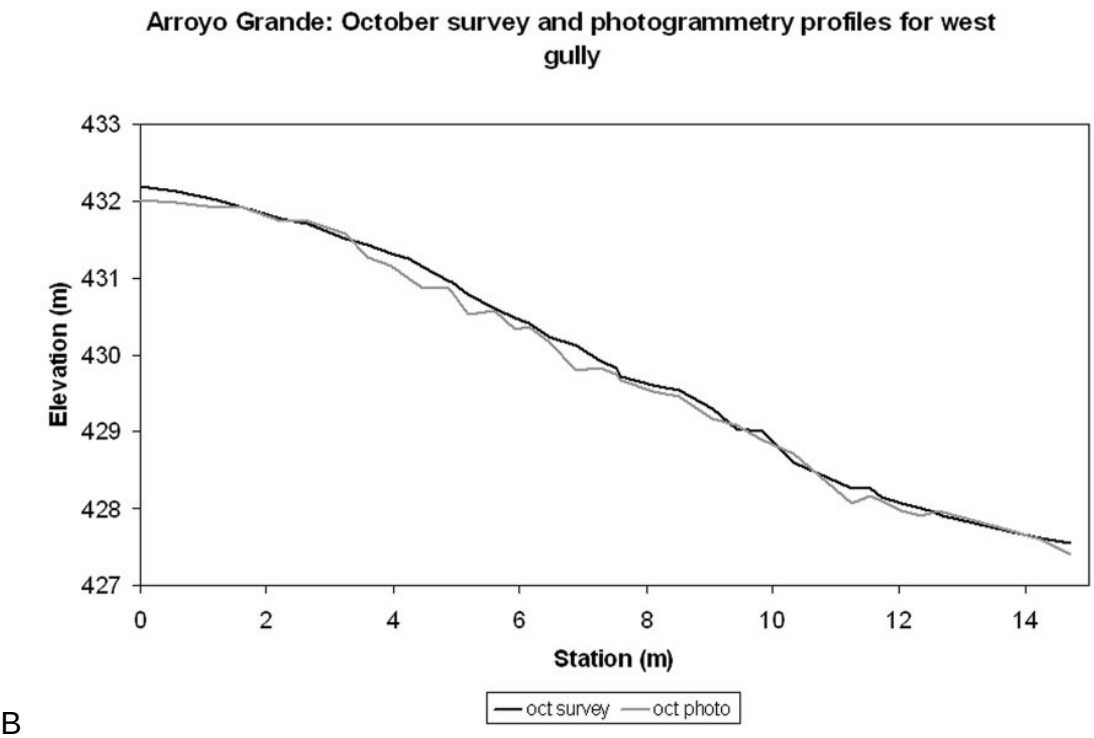

B

Figure J.2. Arroyo Grande west gully March (A) and October (B) long profiles.

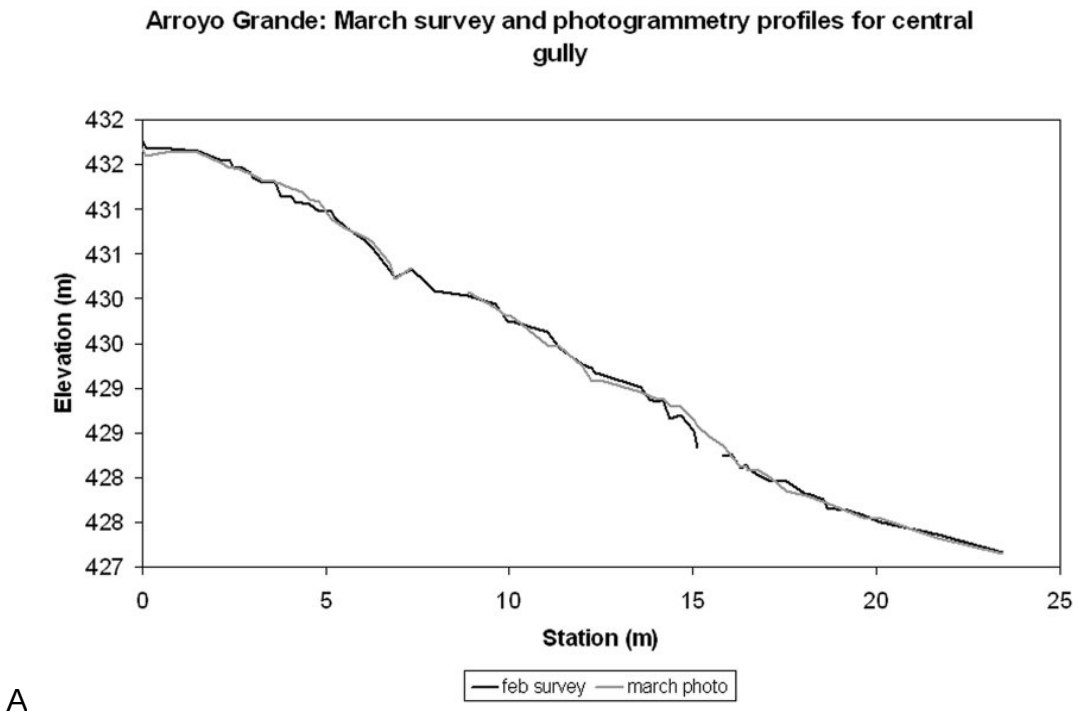

A

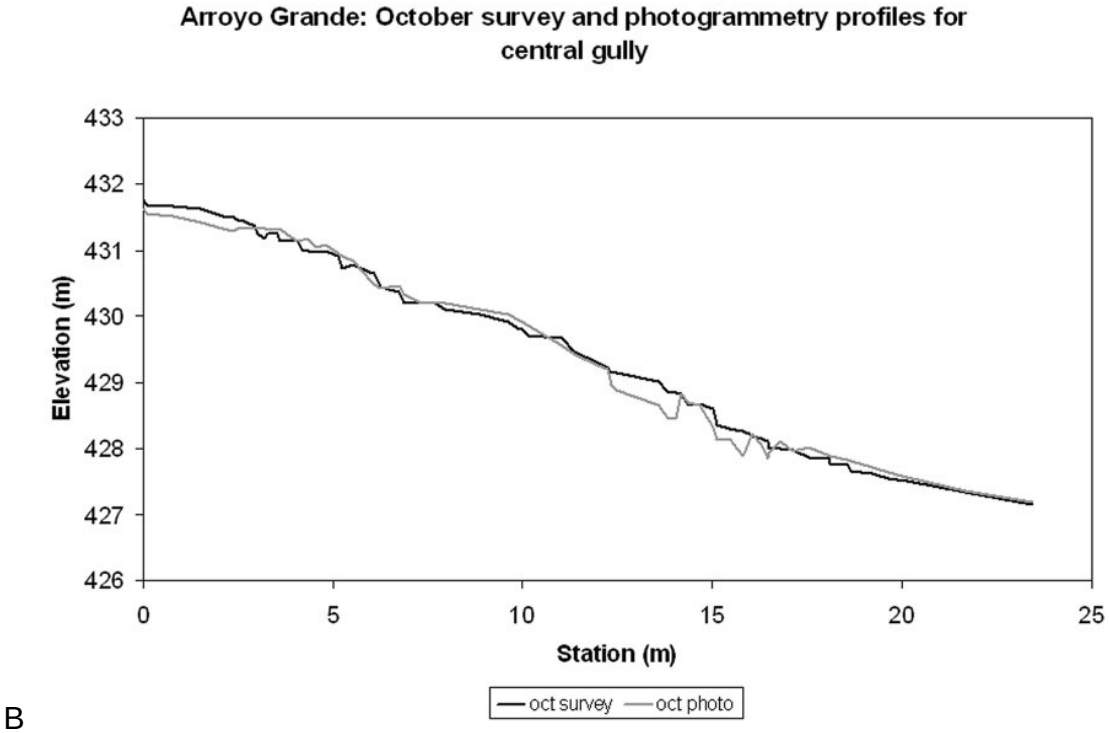

B

Figure J.3. Arroyo Grande central gully March (A) and October (B) long profiles.

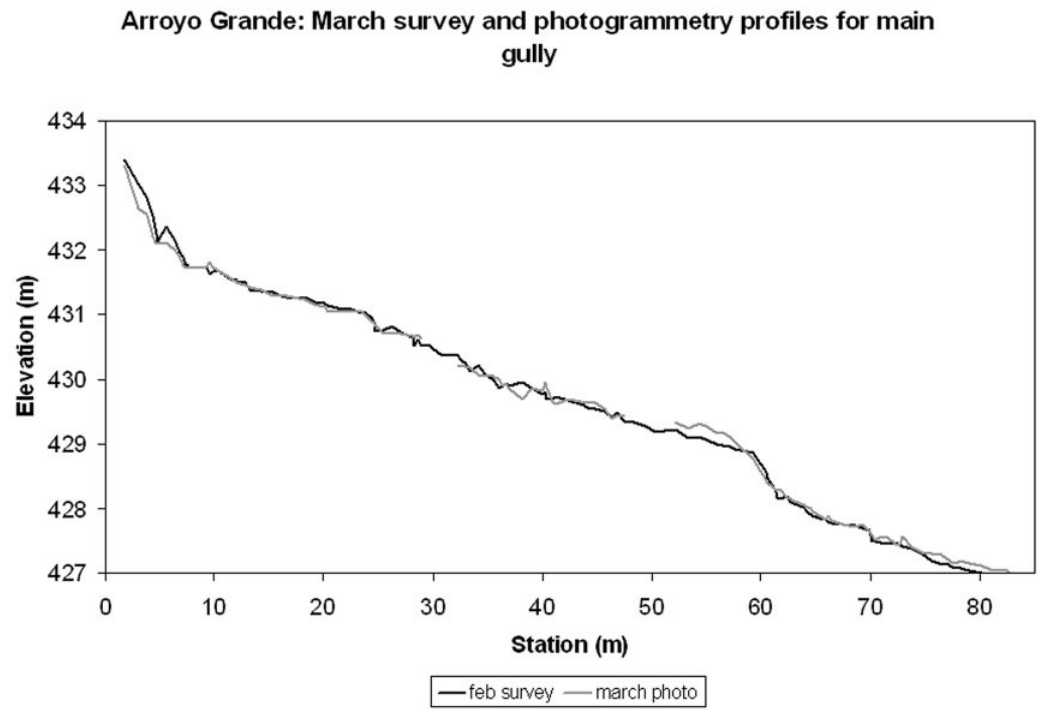

A

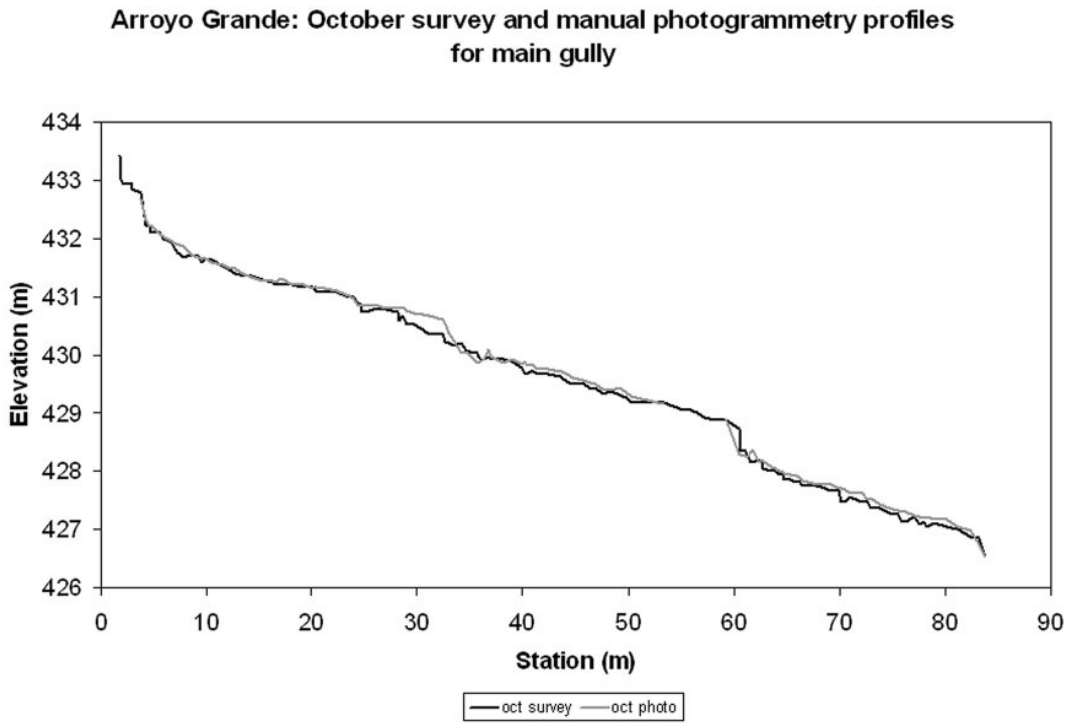

B

Figure J.4. Arroyo Grande main gully March (A) and October (B) long profiles.

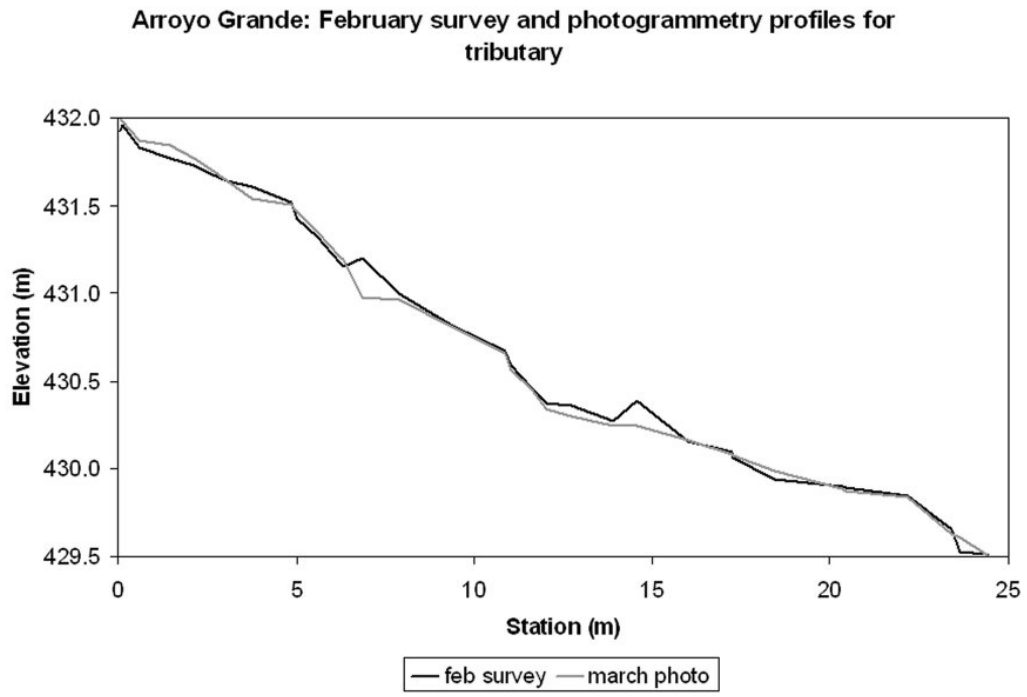

A

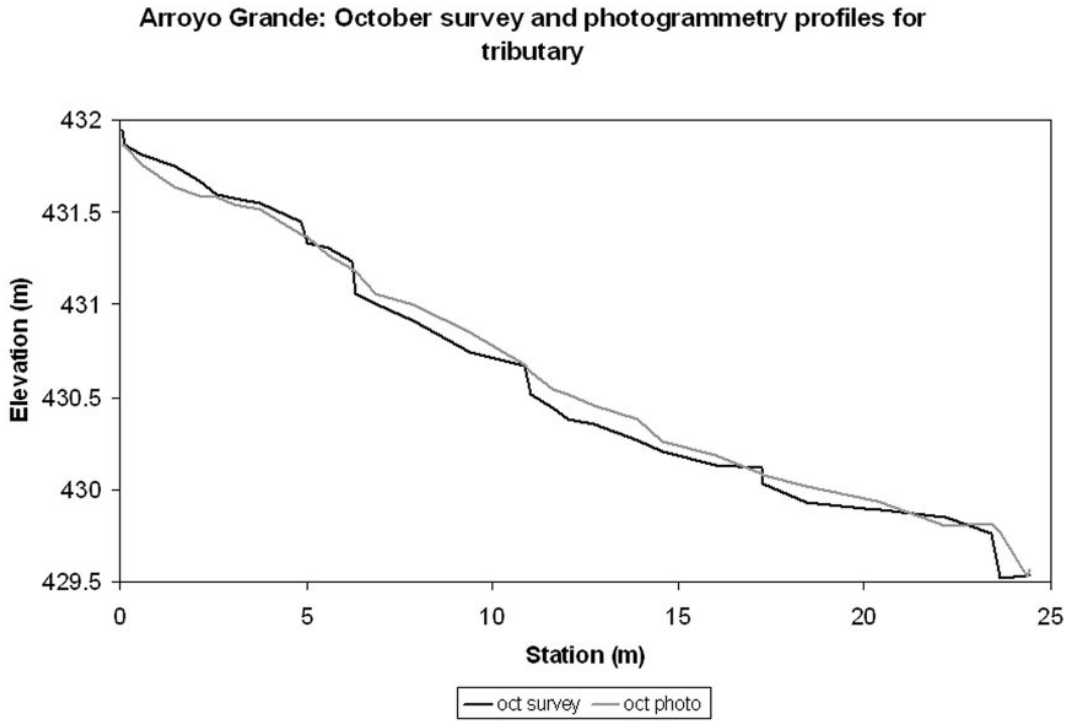

B

Figure J.5. Arroyo Grande tributary gully March (A) and October (B) long profiles.

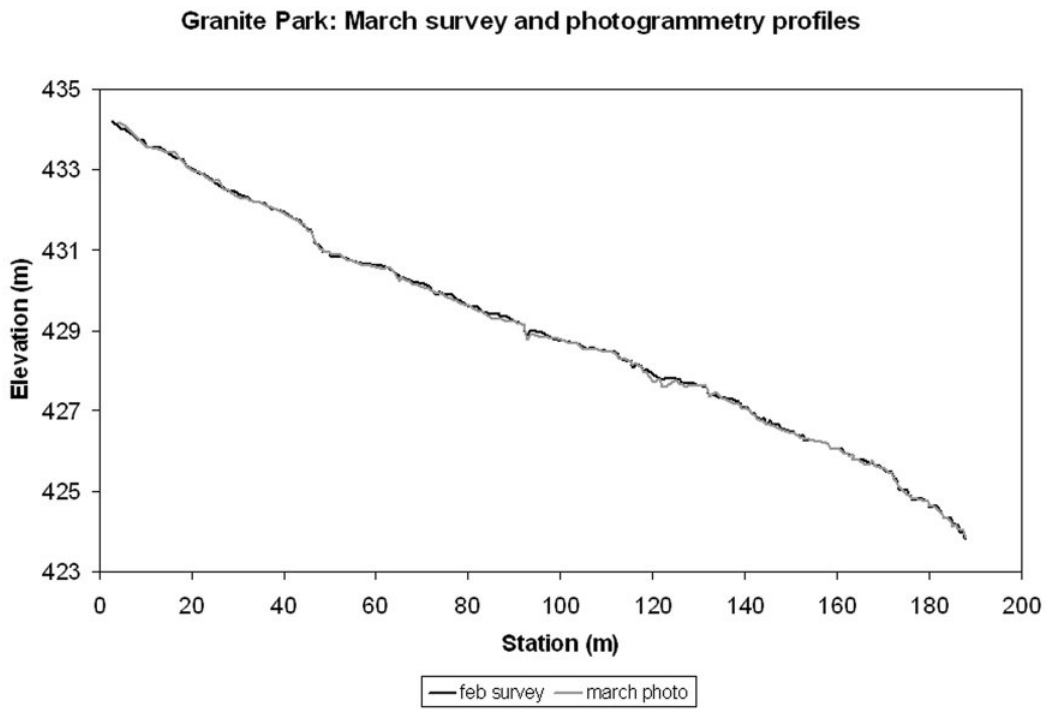

A

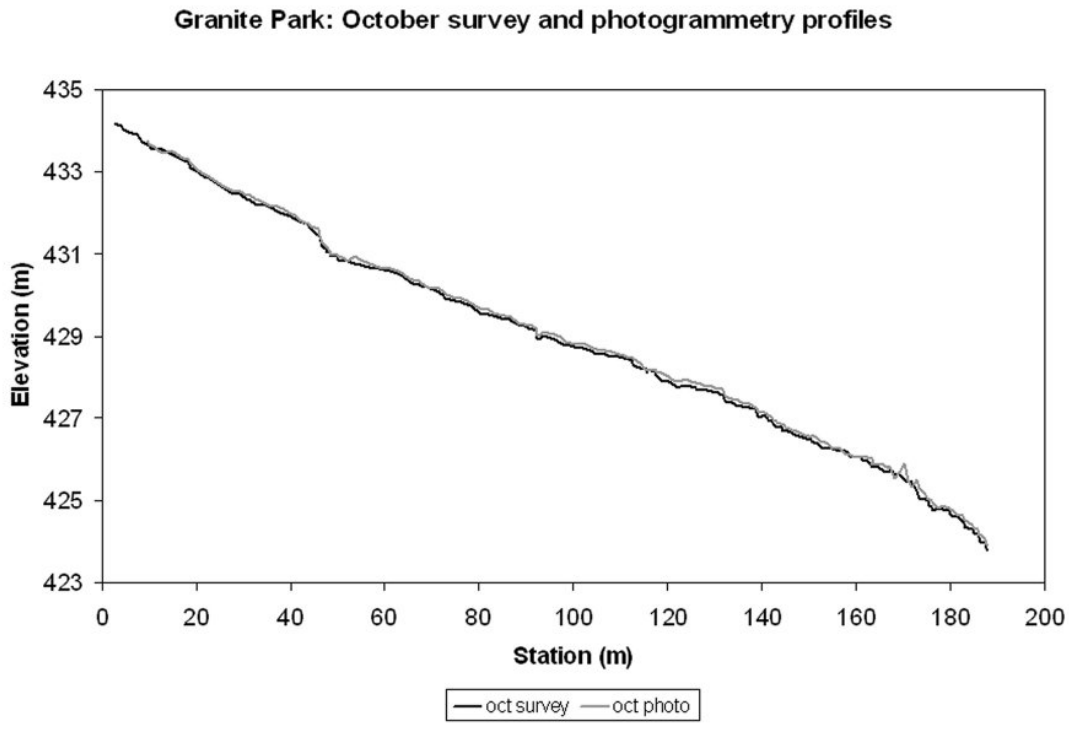

B

Figure J.6. Granite Park March (A) and October (B) long profiles.

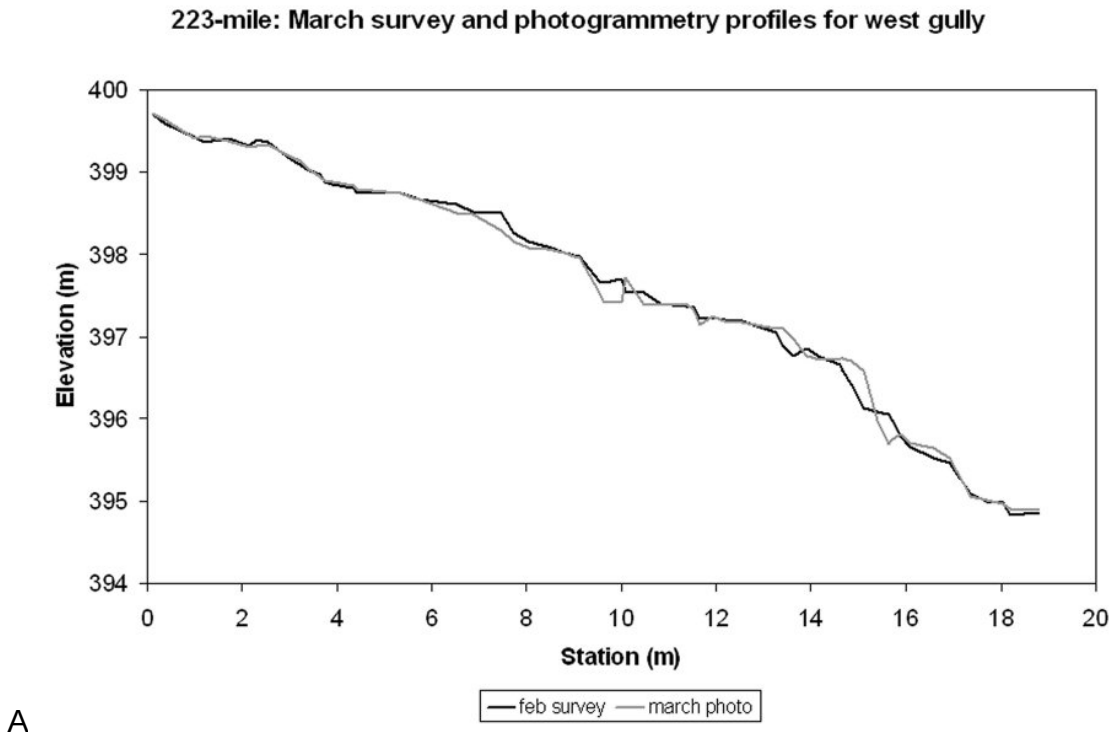

A

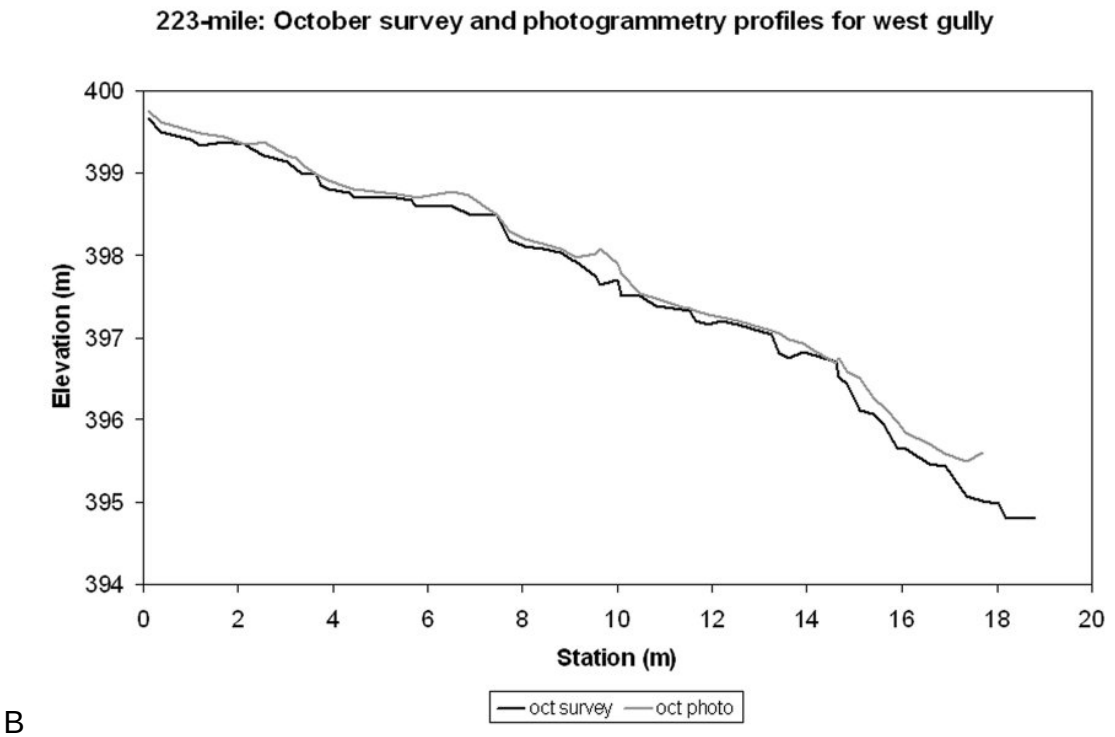

B

Figure J.7. 223-mile west gully March (A) and October (B) long profiles.

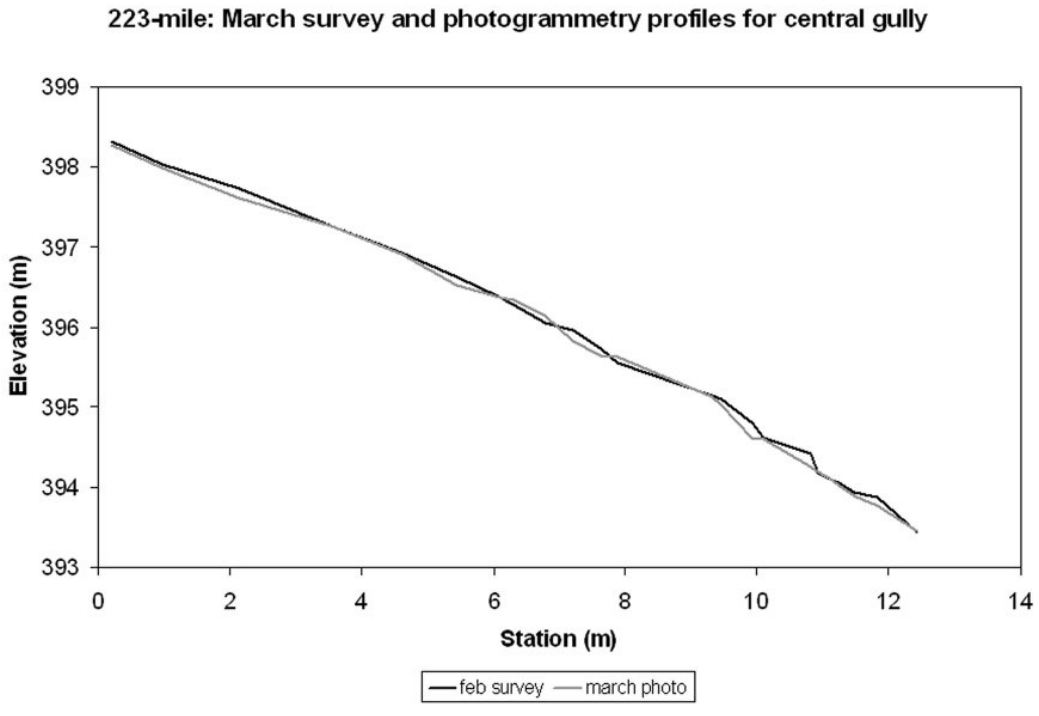

A

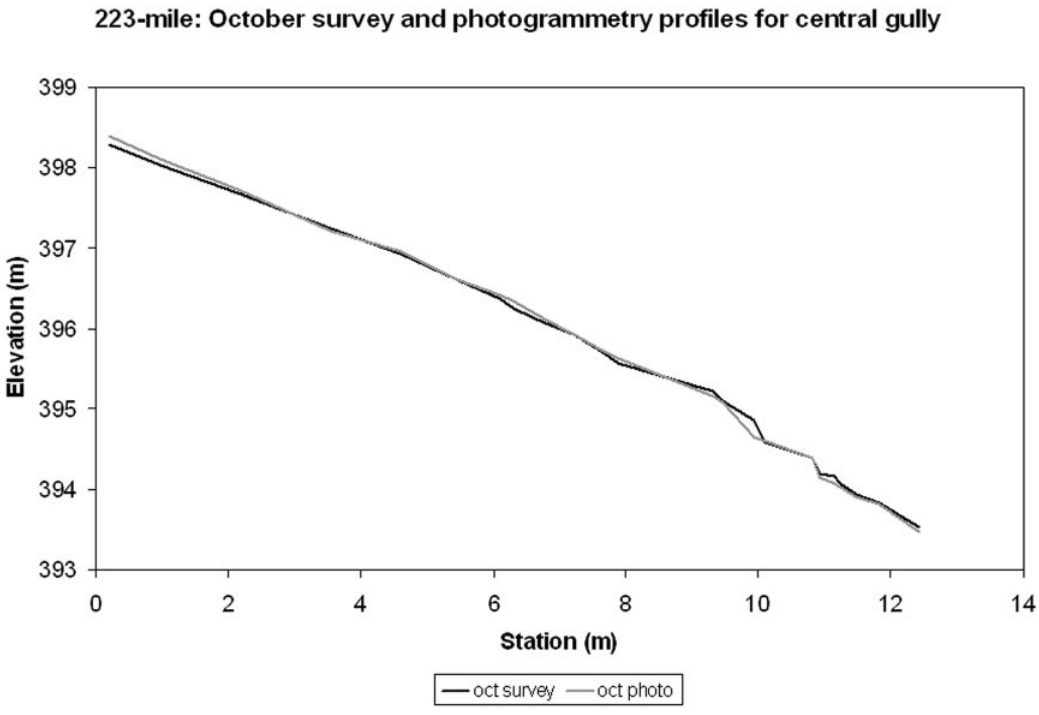

B

Figure J.8. 223-mile central gully March (A) and October (B) long profiles.

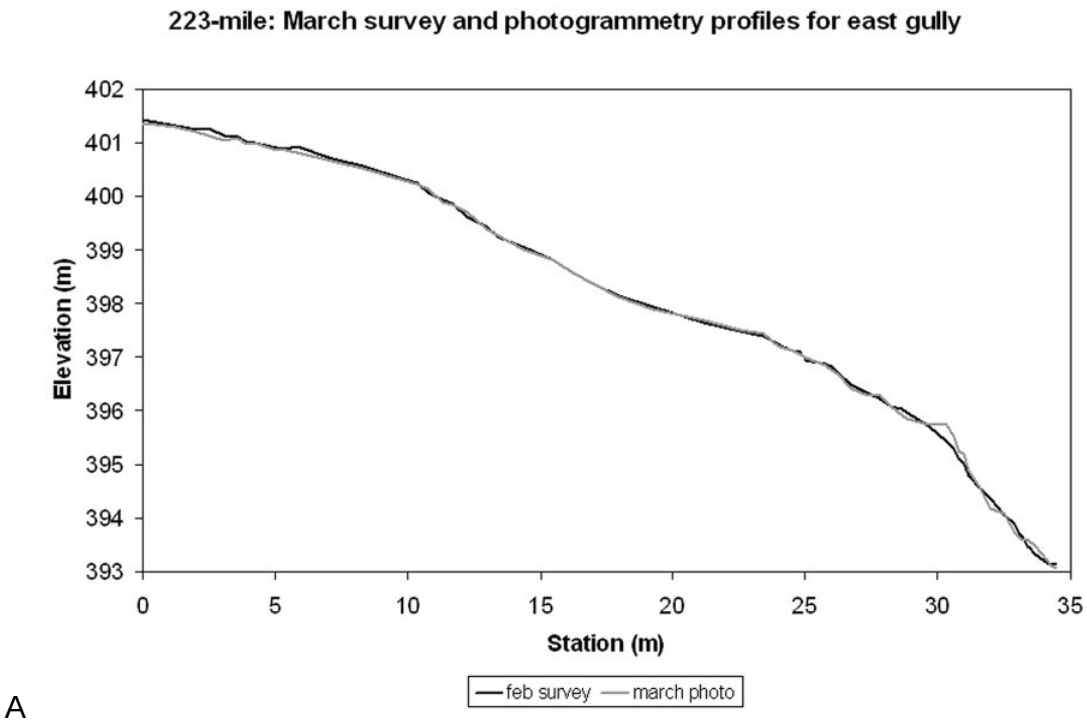

A

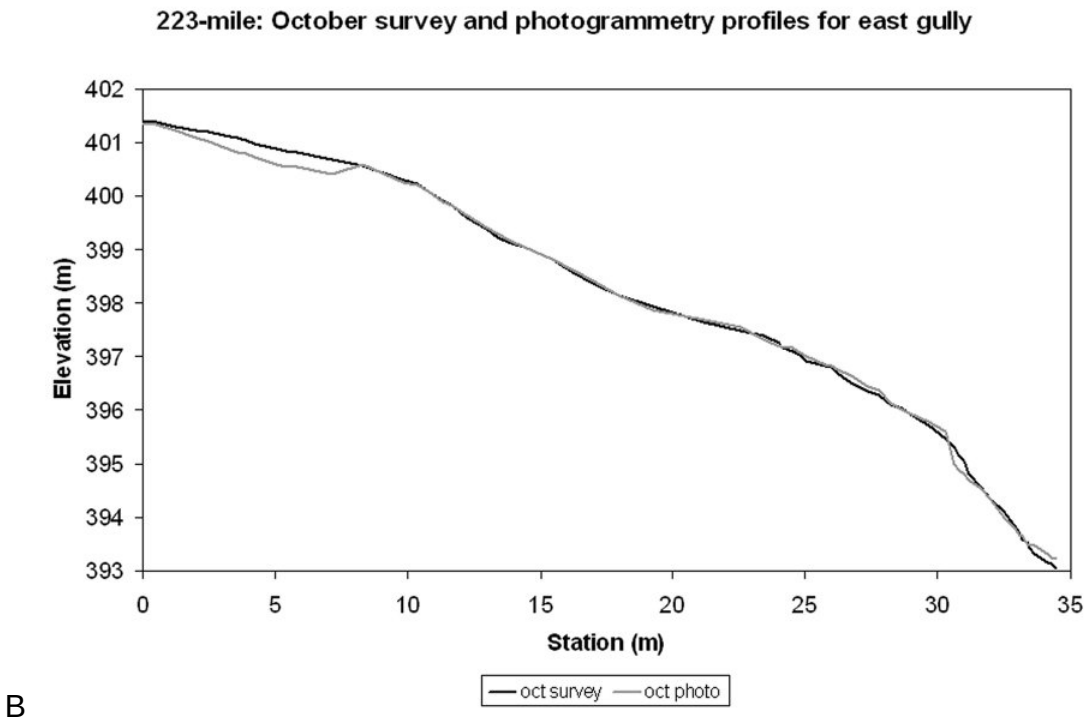

B

Figure J.9. 223-mile east gully March (A) and October (B) long profiles.

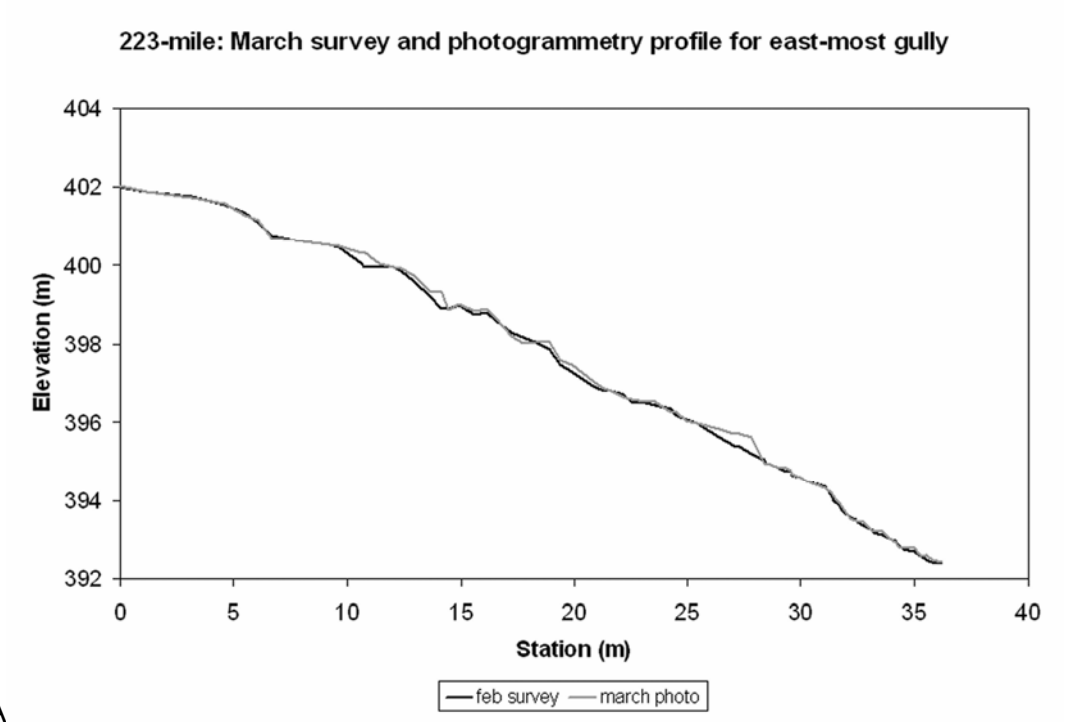

A

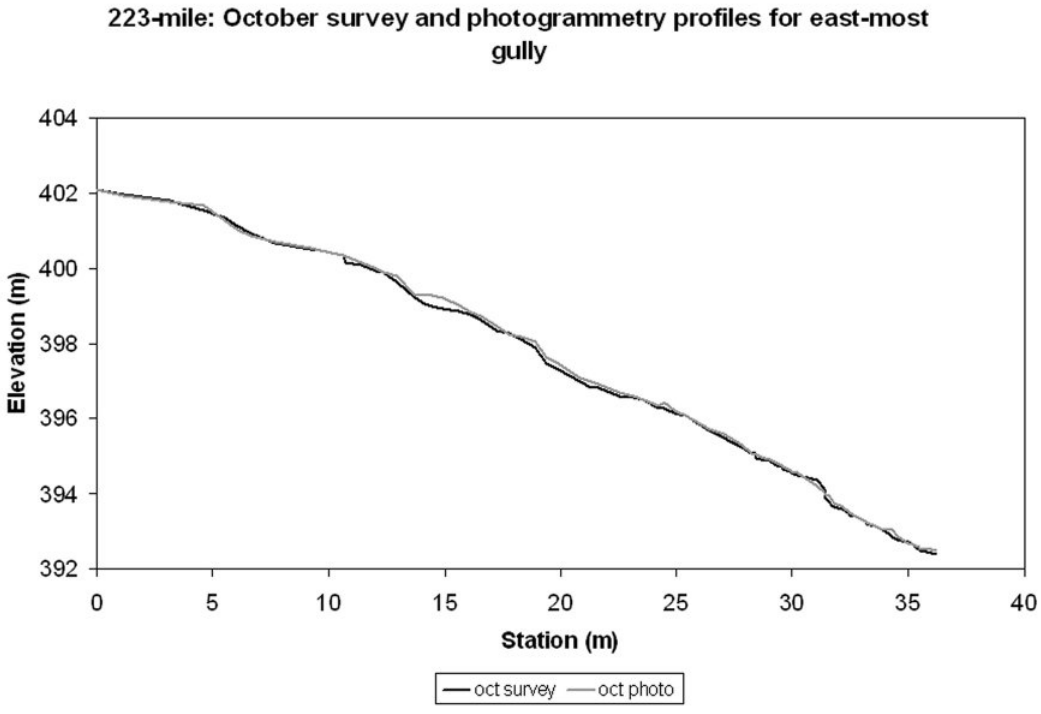

B

Figure J.10. 223-mile east-most gully March (A) and October (B) long profiles.

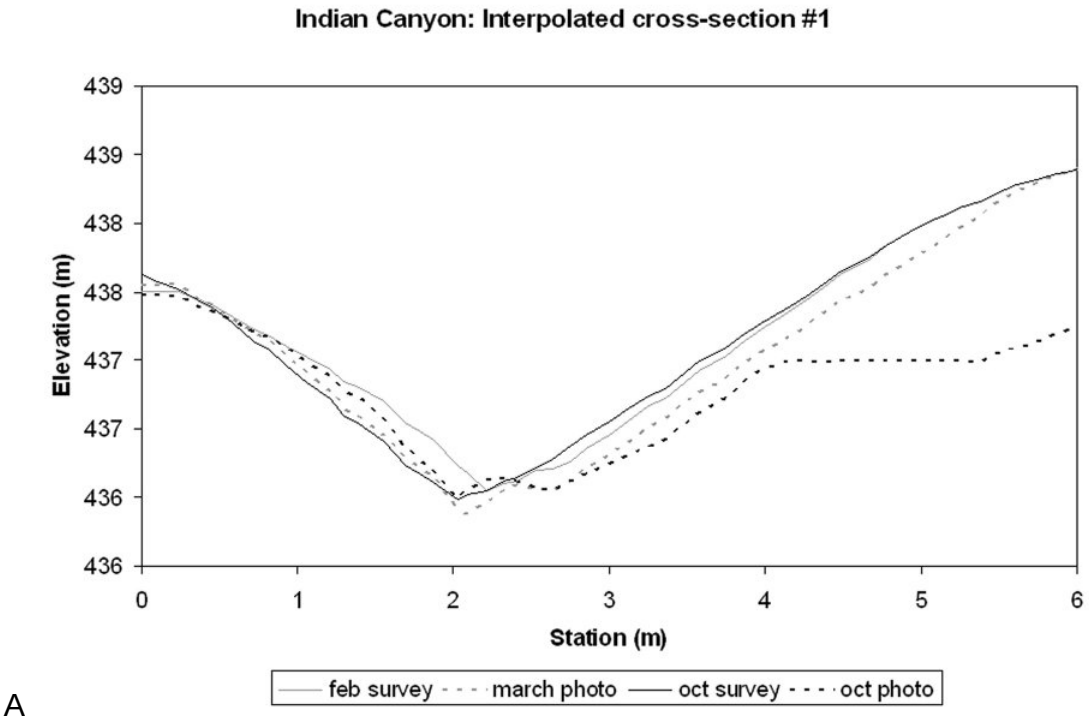

A

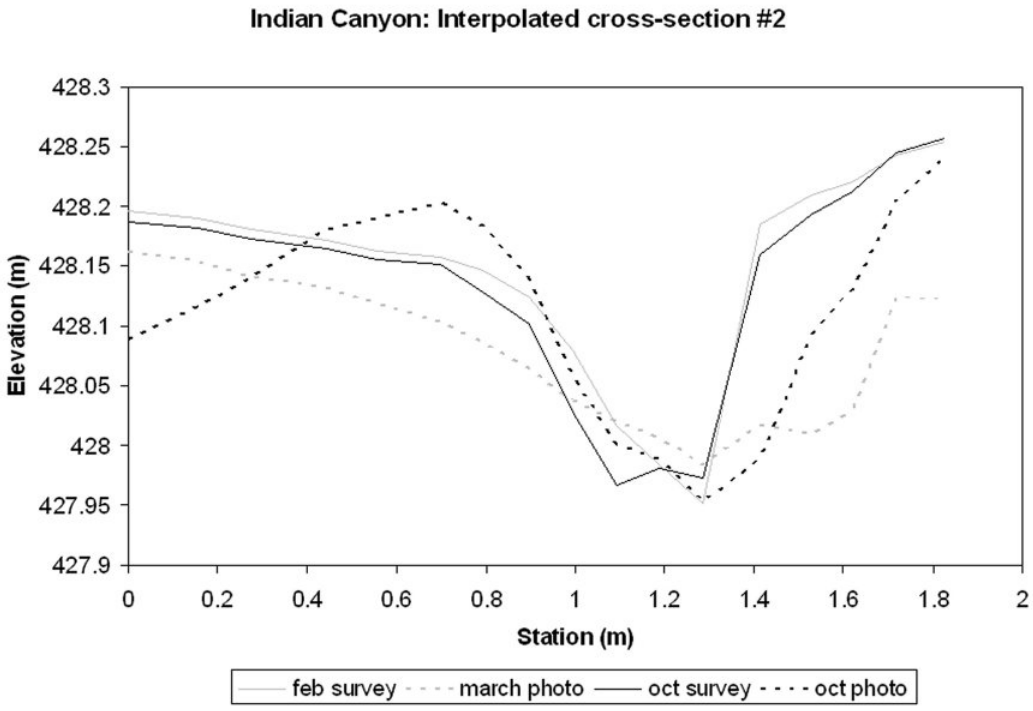

B

Figure J.11. Indian Canyon cross sections. #1 (A) is upstream of #2 (B).

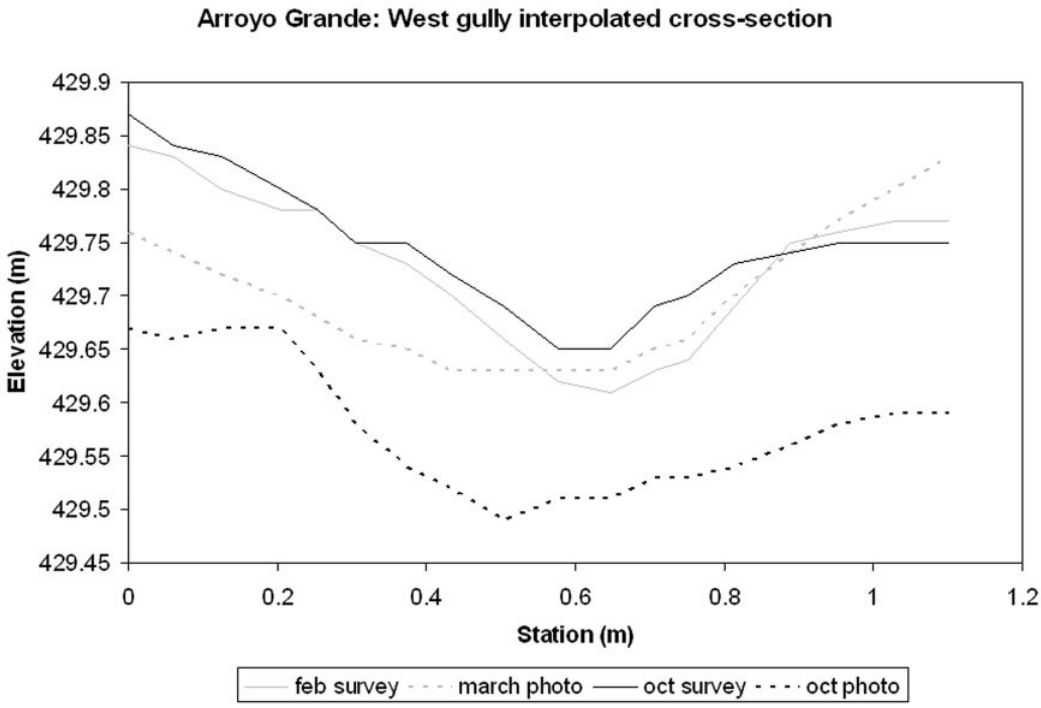
Arroyo Grande: West gully interpolated cross-section
Elevation (m)
429.9
429.85
429.8
429.75
429.7
429.65
429.6
429.55
429.5
429.45
0
0.2
0.4
0.6
0.8
1
1.2
Station (m)
feb survey
march photo
oct survey
oct photo

A

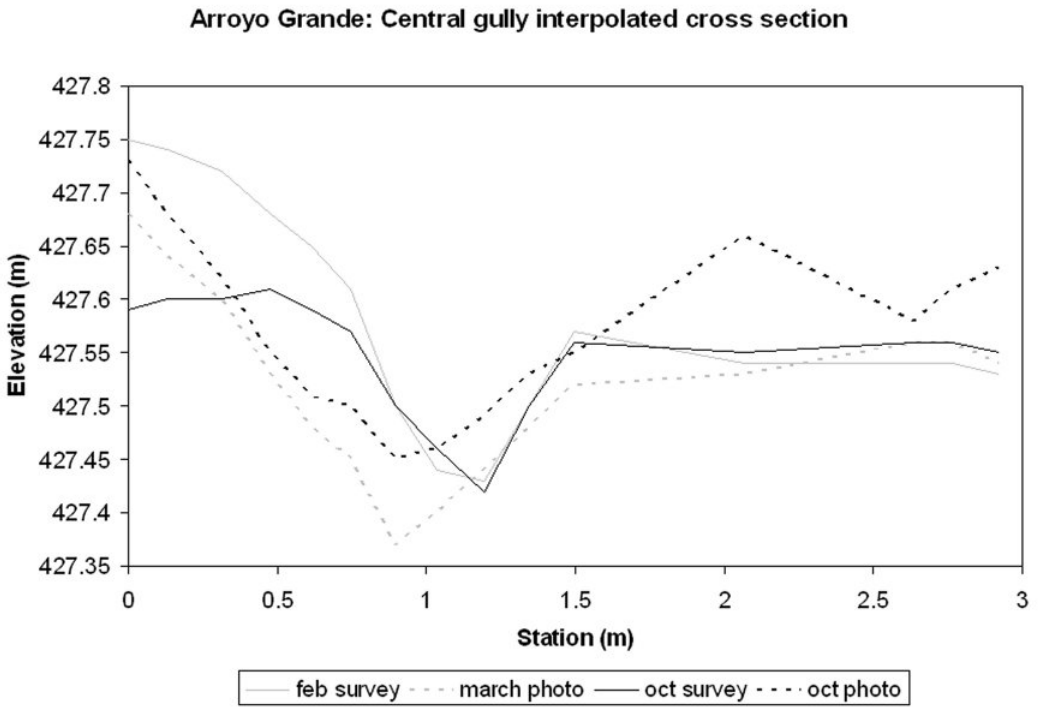
Arroyo Grande: Central gully interpolated cross section
Elevation (m)
427.8
427.75
427.7
427.65
427.6
427.55
427.5
427.45
427.4
427.35
0
0.5
1
1.5
2
2.5
3
Station (m)
feb survey
march photo
oct survey
oct photo

B

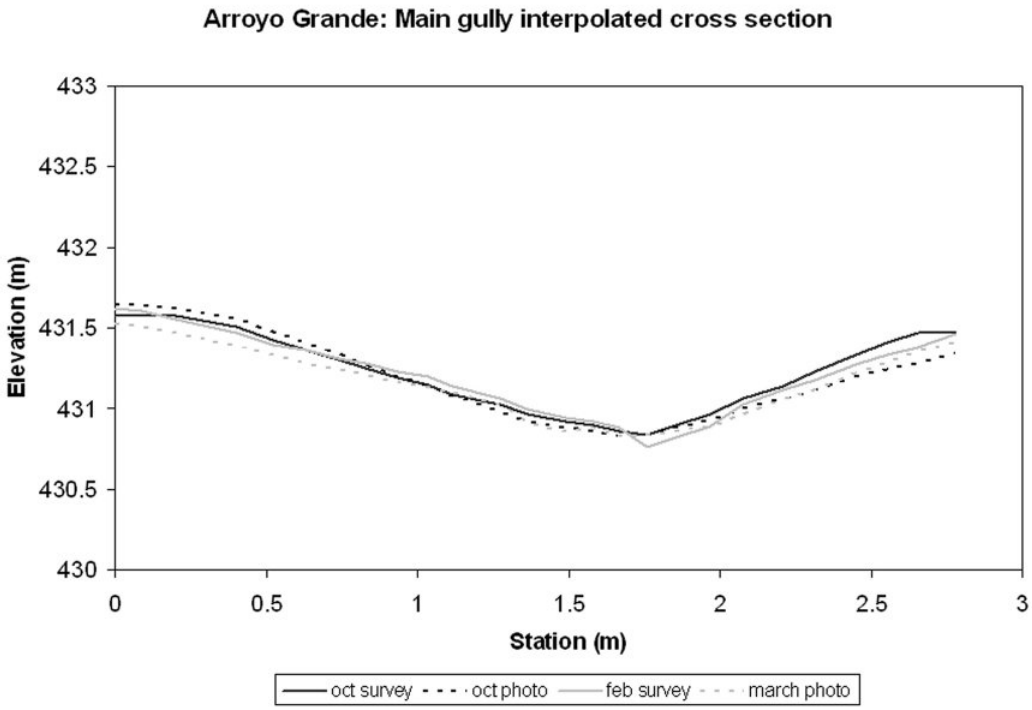

C

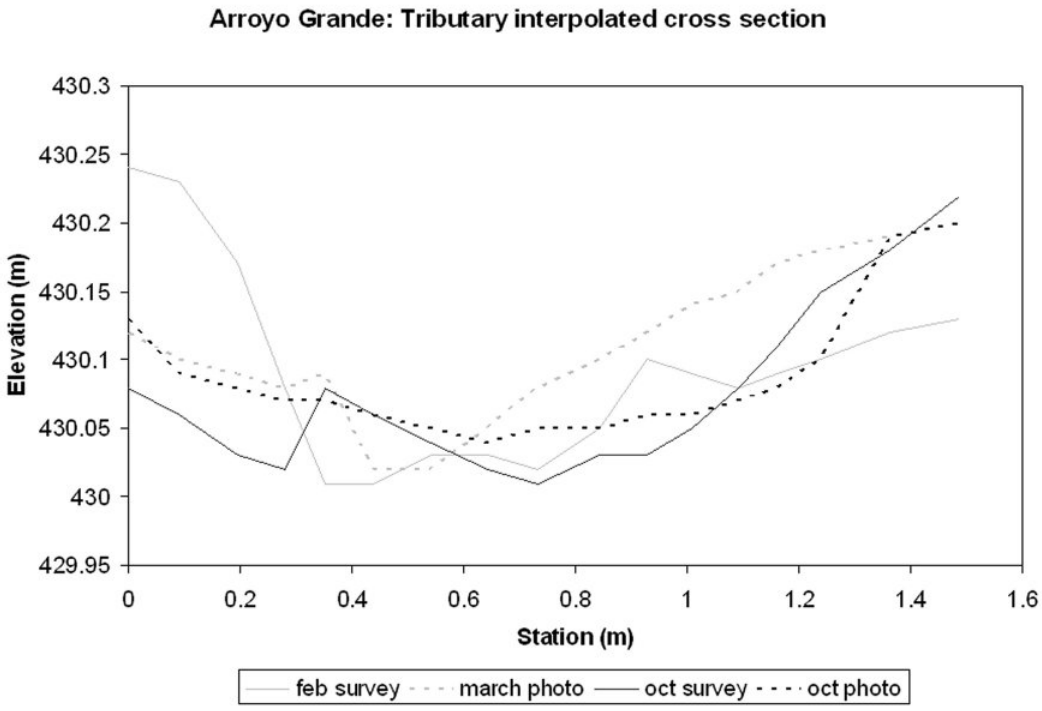

D

Figure J.12. Arroyo Grande cross sections for west (A), central (B), main (C), and tritutaries (D) gullies.

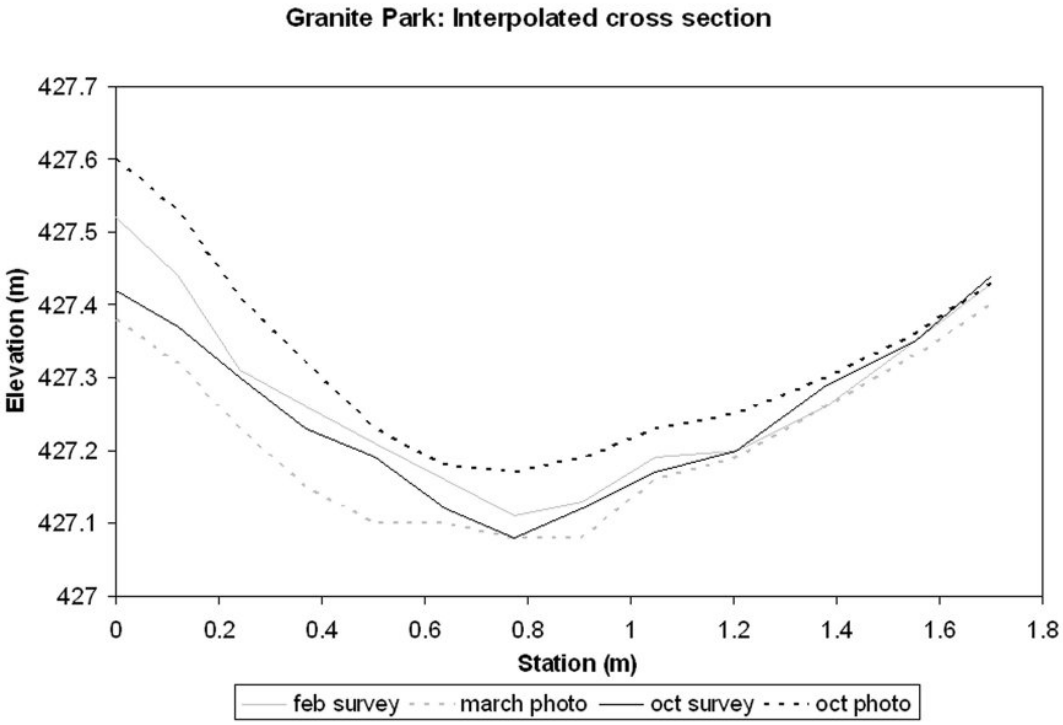

Figure J.13. Granite Park cross section.

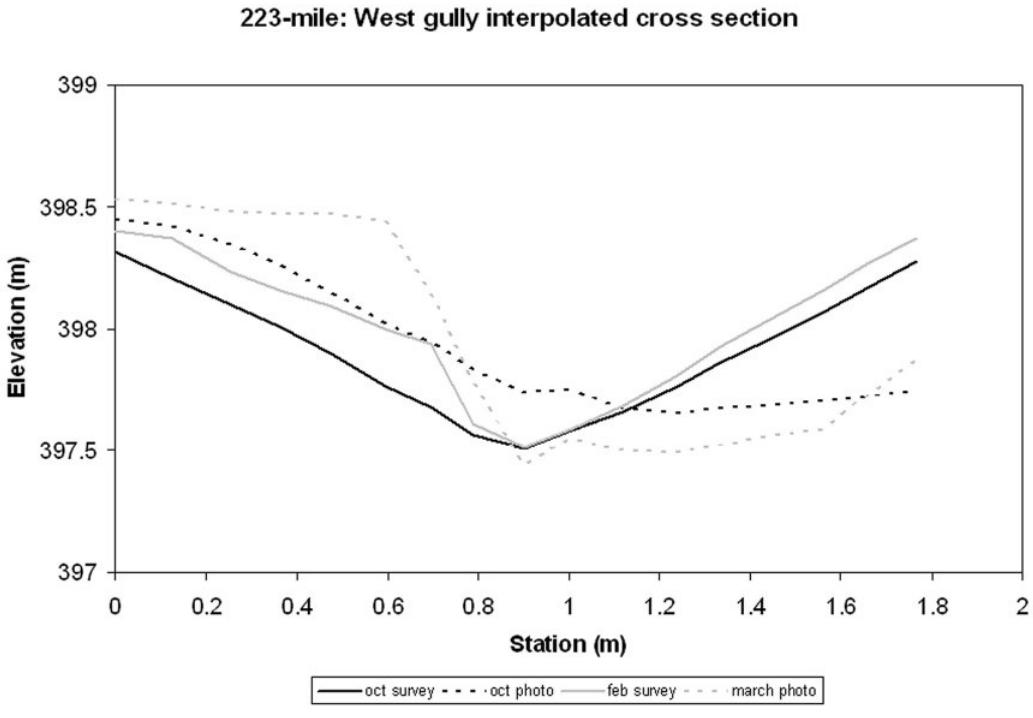

A

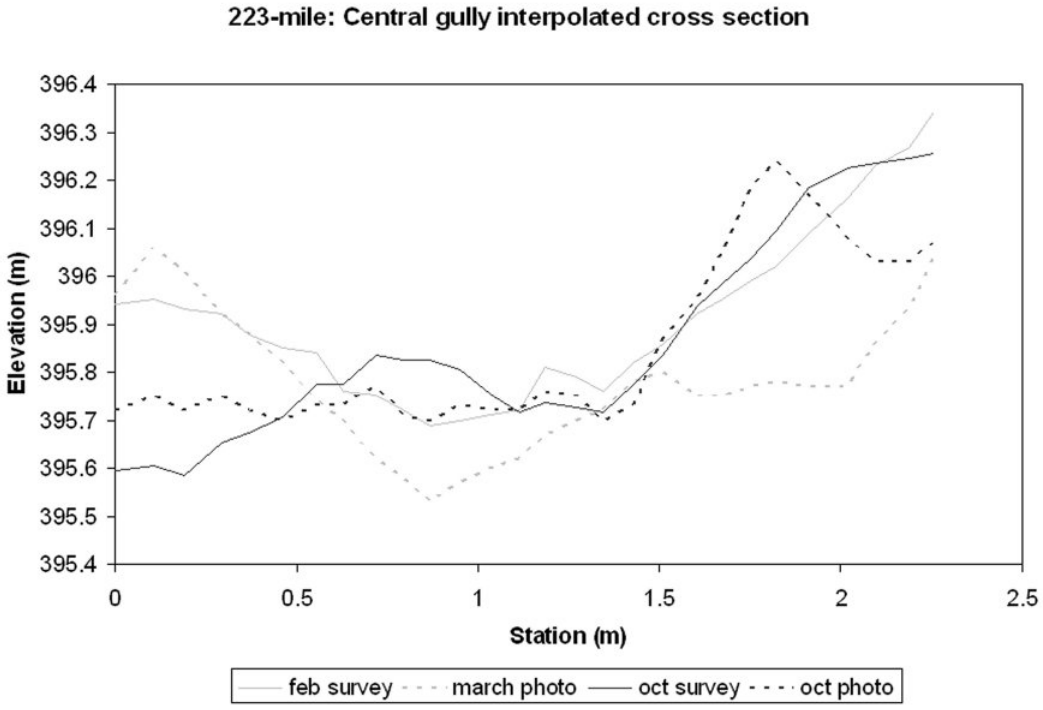
223-mile: Central gully interpolated cross section
Elevation (m)
396.4
396.3
396.2
396.1
396
395.9
395.8
395.7
395.6
395.5
395.4
0
0.5
1
1.5
2
2.5
Station (m)
feb survey
march photo
oct survey
oct photo

B

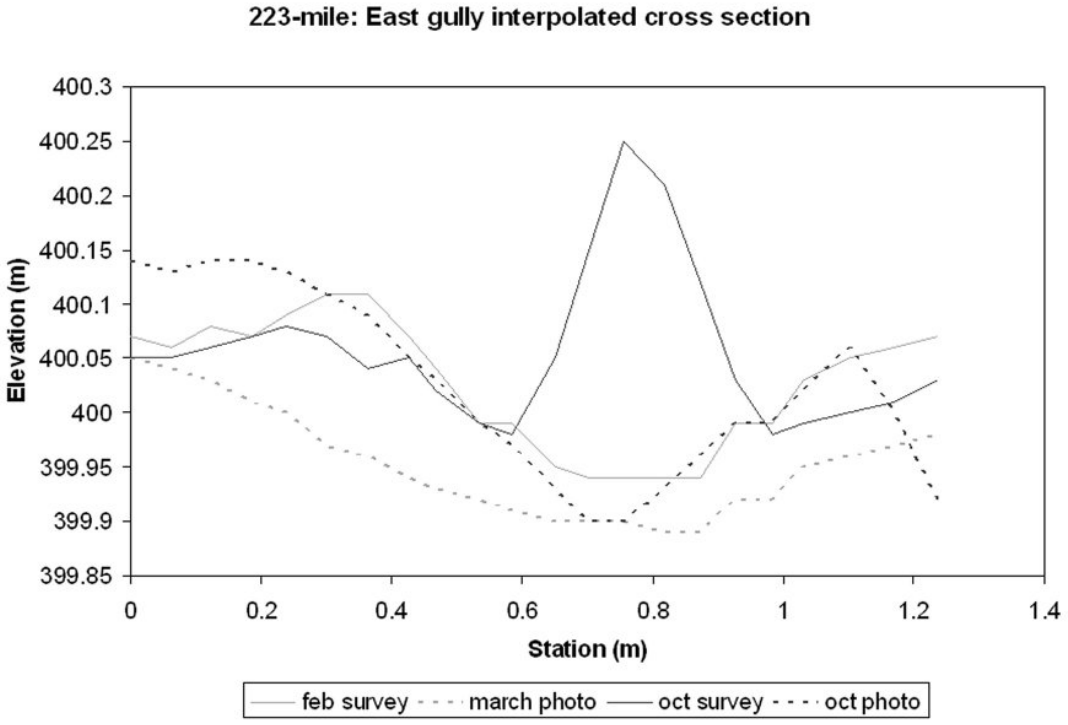
223-mile: East gully interpolated cross section
Elevation (m)
400.3
400.25
400.2
400.15
400.1
400.05
400
399.95
399.9
399.85
0
0.2
0.4
0.6
0.8
1
1.2
1.4
Station (m)
feb survey
march photo
oct survey
oct photo

C

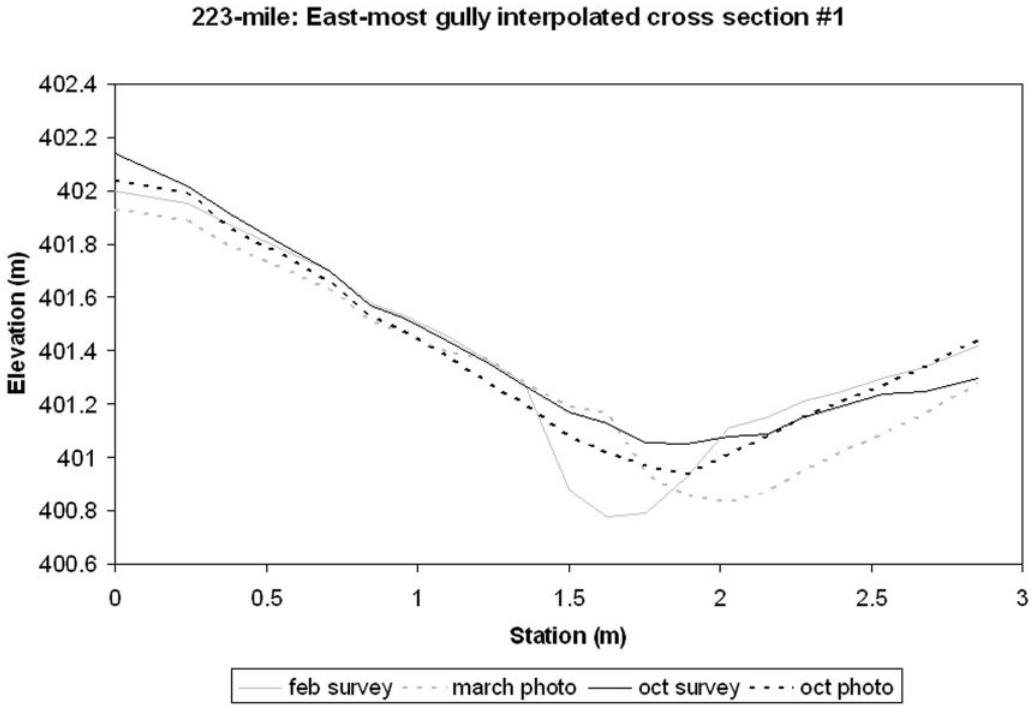

D

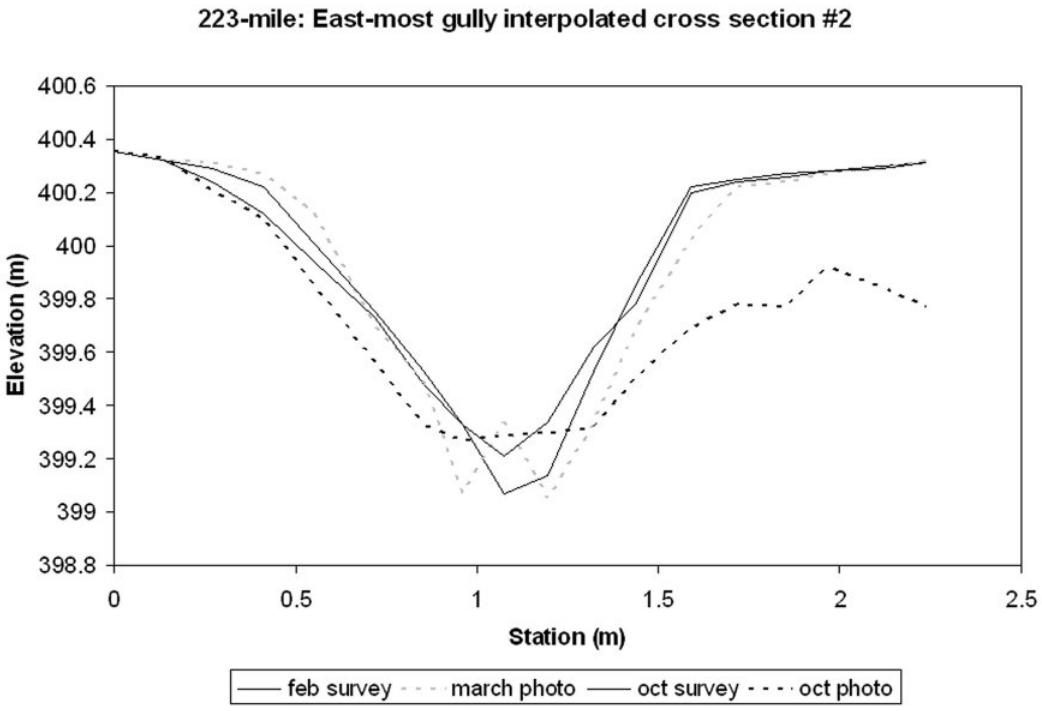

E

Figure. J.14. 223-mile cross sections for west (A), central (B), east (C), and east-most (D, E) gullies. For the east-most gully, cross section #1 (D) is upstream of #2 (E).

Appendix K. Optimal Photogrammetry Density Maps
(Estimates point density needed to achieve optimal photogrammetric accuracy)

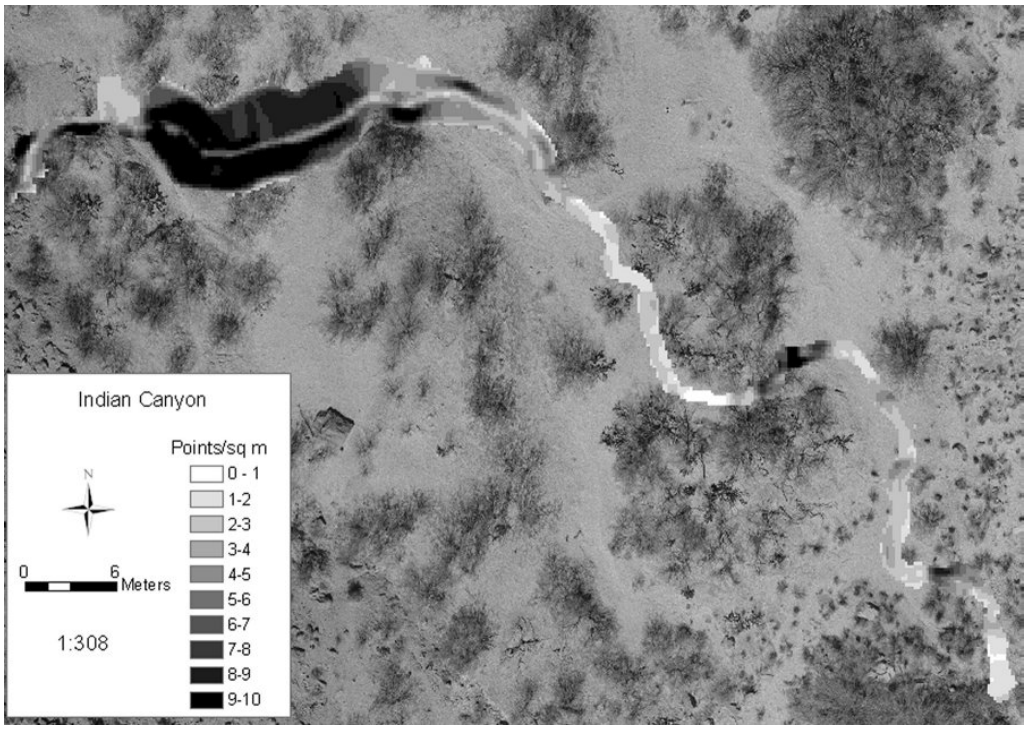

Figure K.1. Optimal photogrammetric density for Indian Camp.

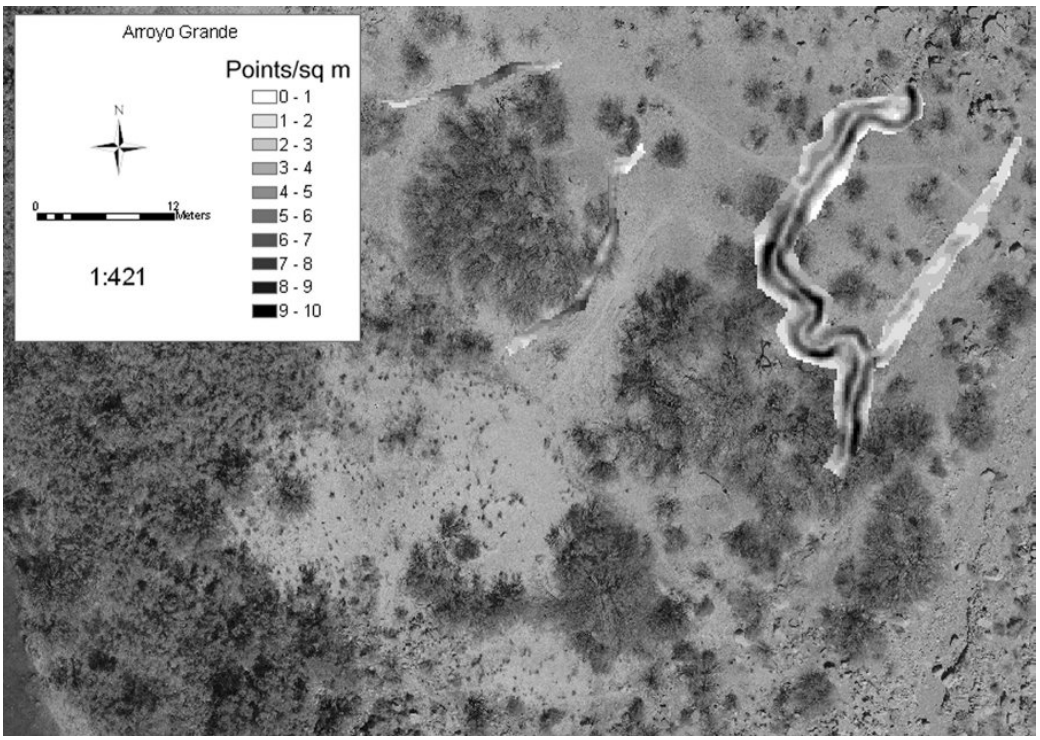

Figure K.2. Optimal photogrammetric density for Arroyo Grande.

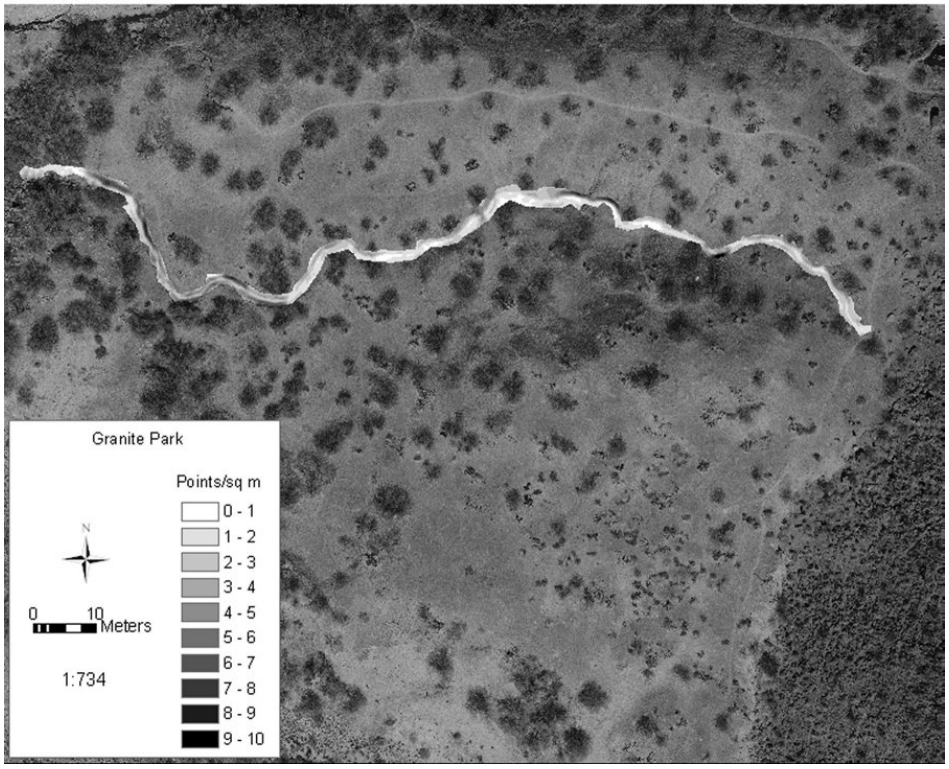

Figure K.3. Optimal photogrammetric density for Granite Park.

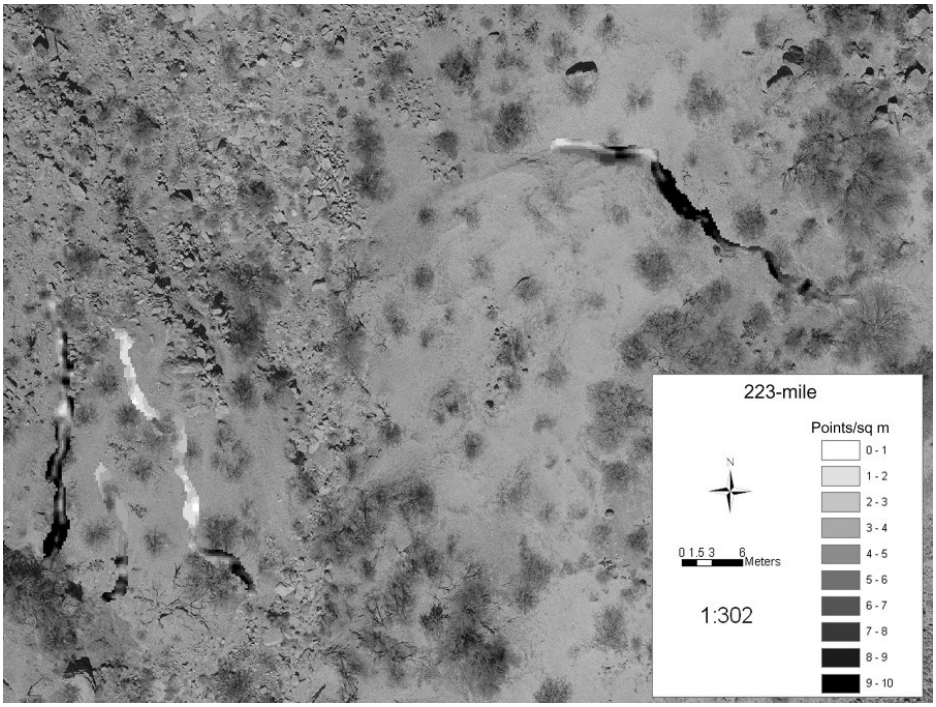

Figure K.4. Optimal photogrammetric density for 223-mile.

Appendix L. Eastern Grand Canyon Survey Profile Comparisons and Slope-Area Indices (Western Grand Canyon omitted due to lack of change)

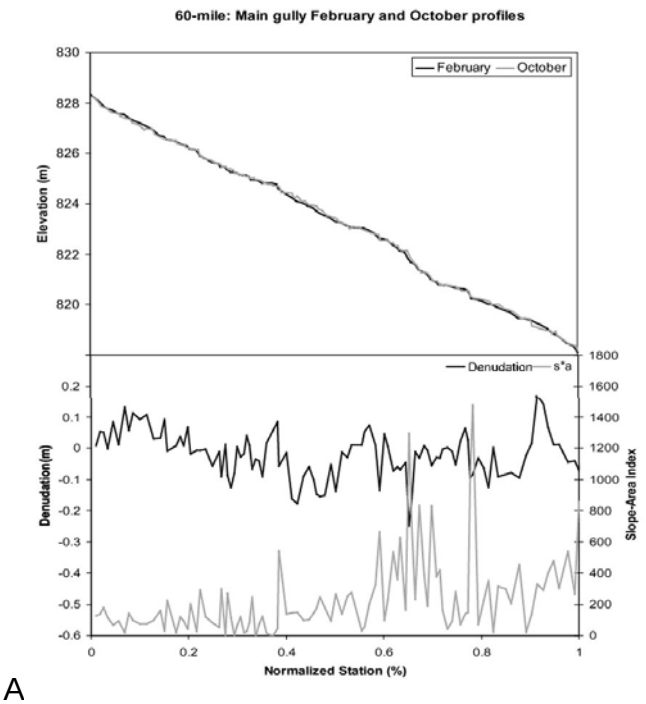

A

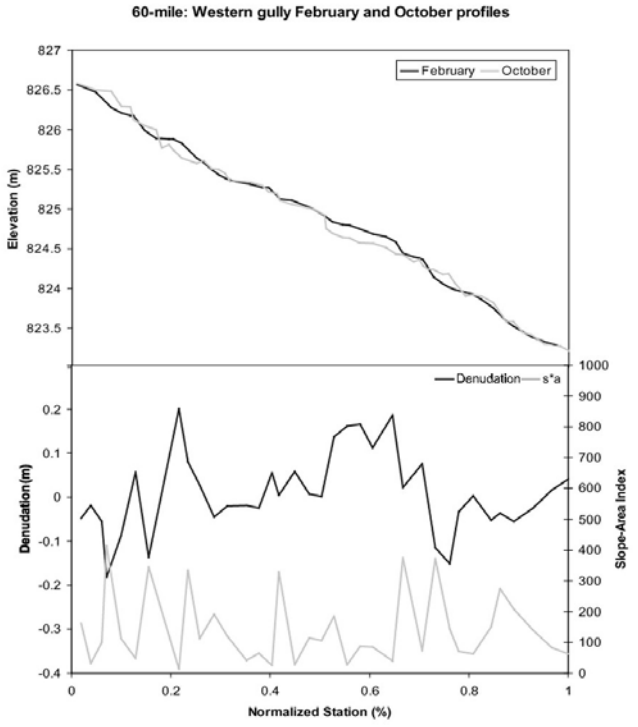

B

Figure L.1. February-October survey comparison and slope-area index values for main gully (A) and west gully (B) at 60-mile site.

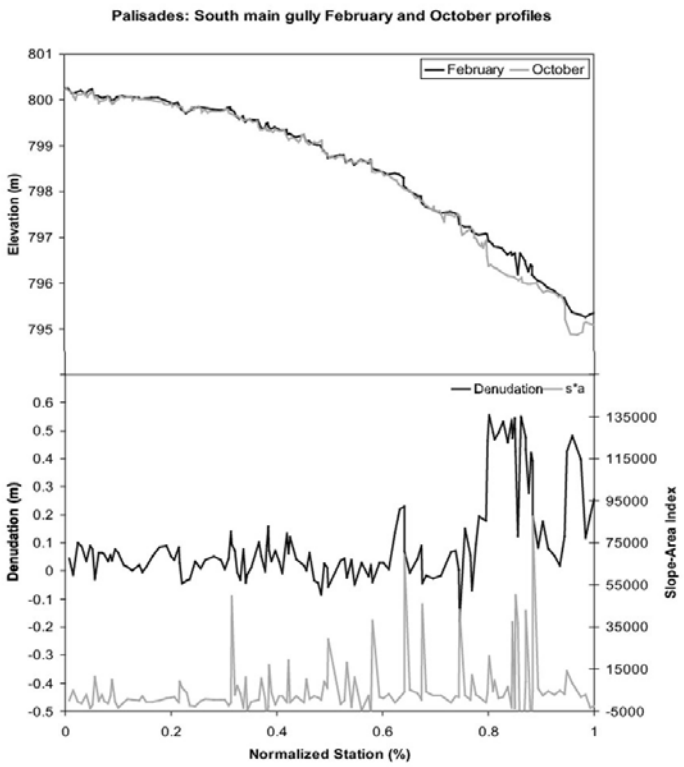
Palisades: South main gully February and October profiles
February
October
Elevation (m)
801
800
799
798
797
796
795
Denudation
s*a
Denudation (m)
0.6
0.5
0.4
0.3
0.2
0.1
0
-0.1
-0.2
-0.3
-0.4
-0.5
Slope-Area Index
135000
115000
95000
75000
55000
35000
15000
-5000
0
0.2
0.4
0.6
0.8
1
Normalized Station (%)

A

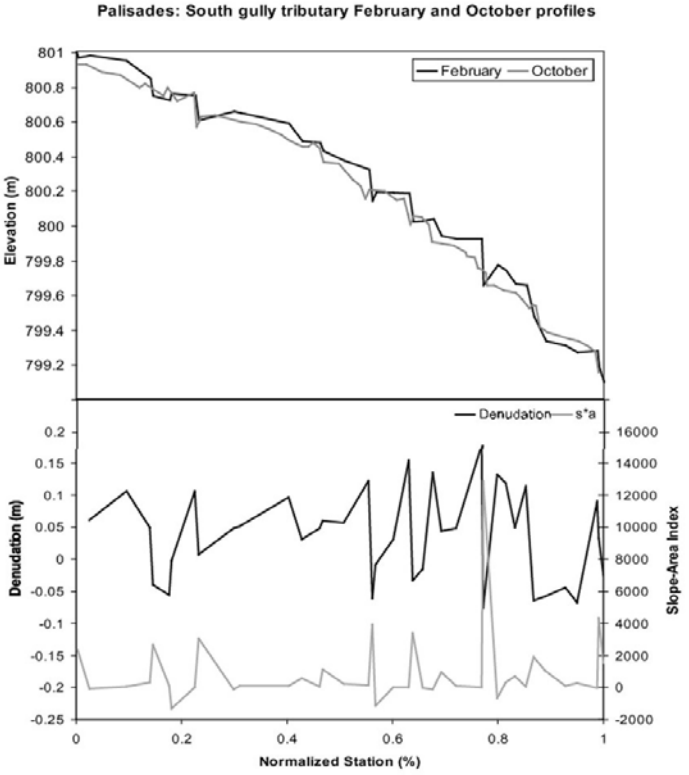
Palisades: South gully tributary February and October profiles
February
October
Elevation (m)
801
800.8
800.6
800.4
800.2
800
799.8
799.6
799.4
799.2
Denudation
s*a
Denudatbn (m)
0.2
0.15
0.1
0.05
0
-0.05
-0.1
-0.15
-0.2
-0.25
Slope-Area Index
16000
14000
12000
10000
8000
6000
4000
2000
0
-2000
0
0.2
0.4
0.6
0.8
1
Normalized Station (%)

B

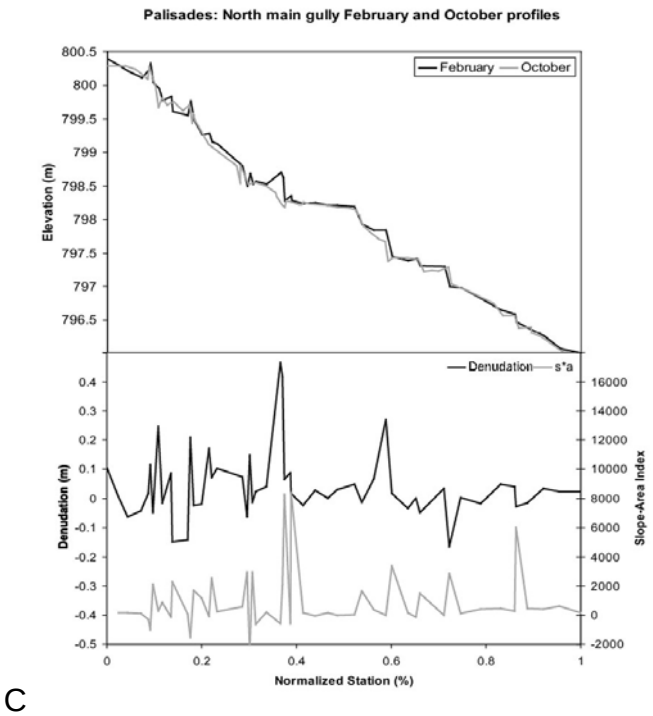

C

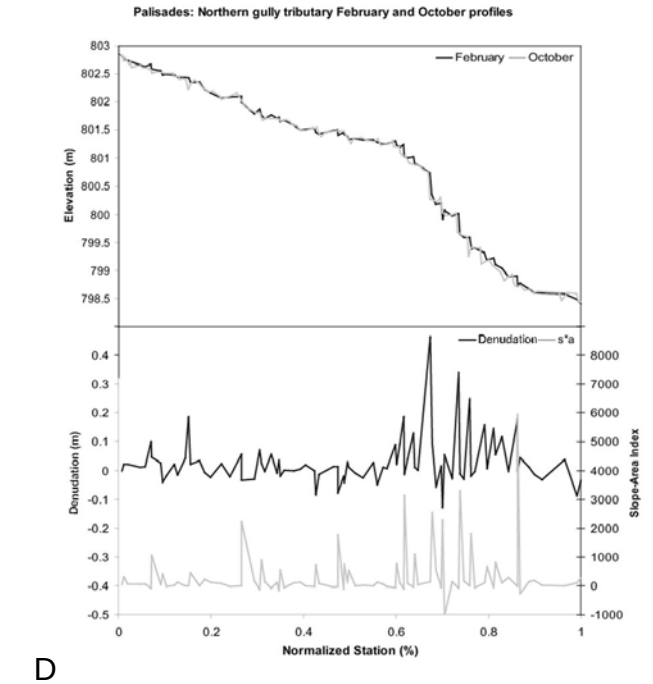

D

Figure L.2. February-October survey comparison and slope-area index values for south main gully (A), south tributary gully (B), north main gully (C), and north tributary gully (D) at Palisades site.

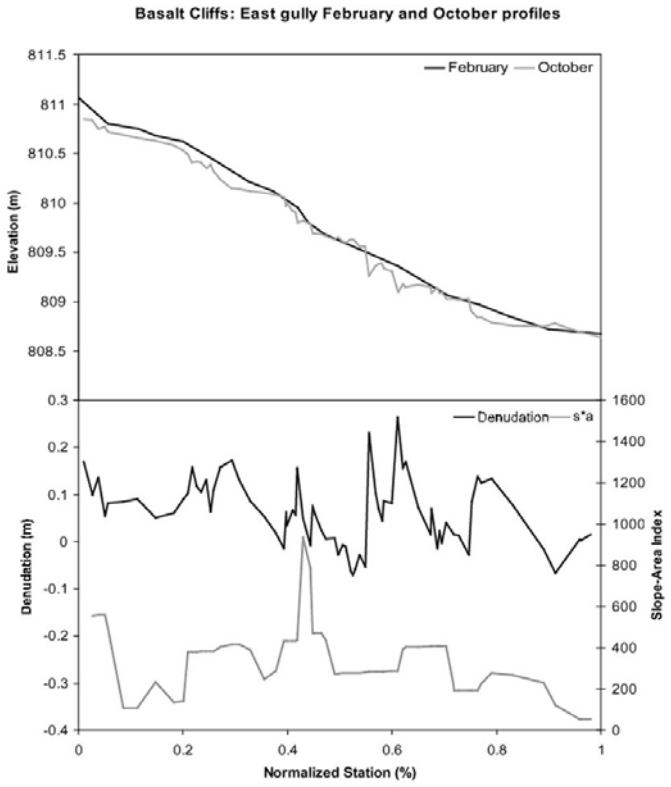
Basalt Cliffs: East gully February and October profiles
February
October
Elevation (m)
811.5
811
810.5
810
809.5
809
808.5
Denudation
s*a
Denudation (m)
Slope-Area Index
0.3
0.2
0.1
0
-0.1
-0.2
-0.3
-0.4
1600
1400
1200
1000
800
600
400
200
0
0
0.2
0.4
0.6
0.8
1
Normalized Station (%)

A

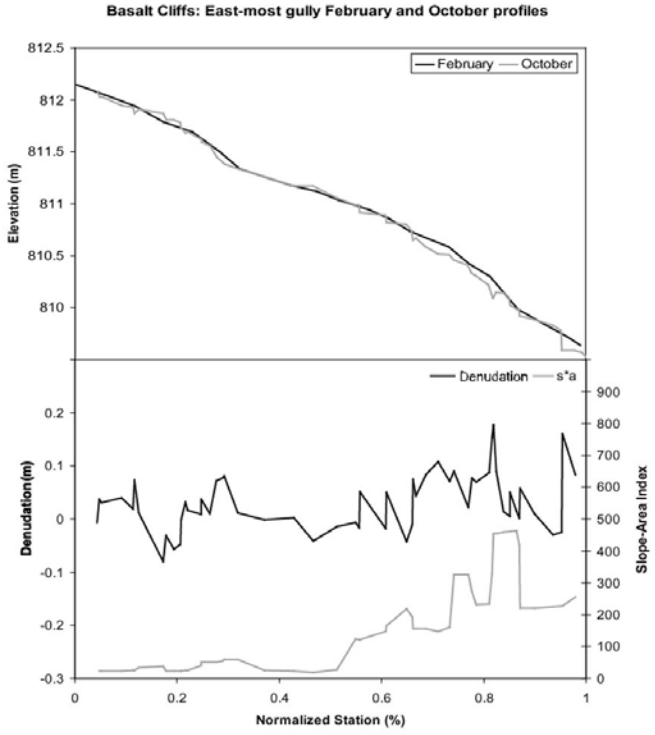
Basalt Cliffs: East-most gully February and October profiles
February
October
Elevation (m)
812.5
812
811.5
811
810.5
810
Denudation
s*a
Denudation(m)
Slope-Area Index
0.2
0.1
0
-0.1
-0.2
-0.3
900
800
700
600
500
400
300
200
100
0
0
0.2
0.4
0.6
0.8
1
Normalized Station (%)

B

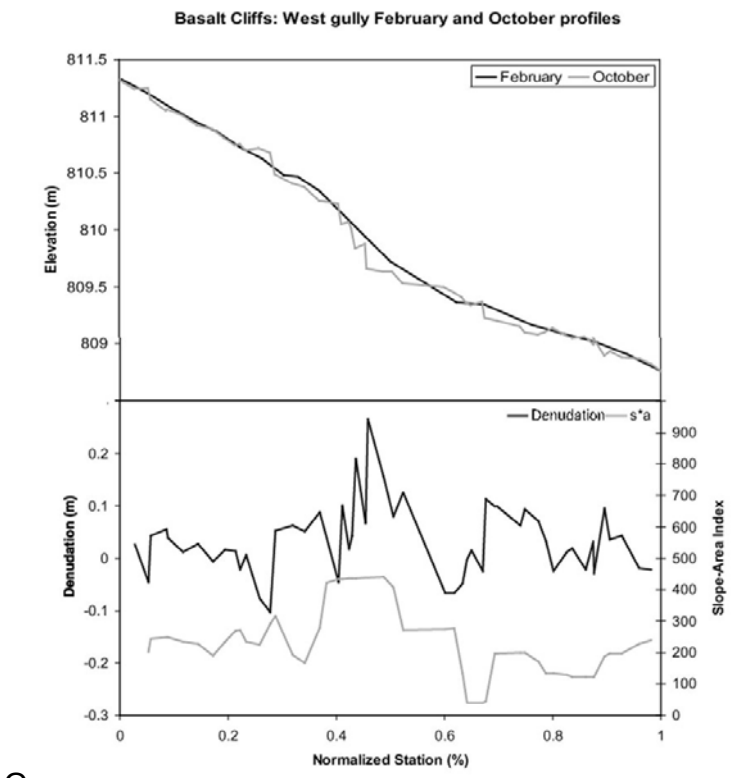

C

Figure L.3. February-October survey comparison and slope-area index values for east gully (A), east-most gully (B), and west gully (C) at Basalt Cliffs site.

Appendix M. Gully Sensitivity Maps
(GIS-based model showing locations that exceed a slope-area erosion threshold)

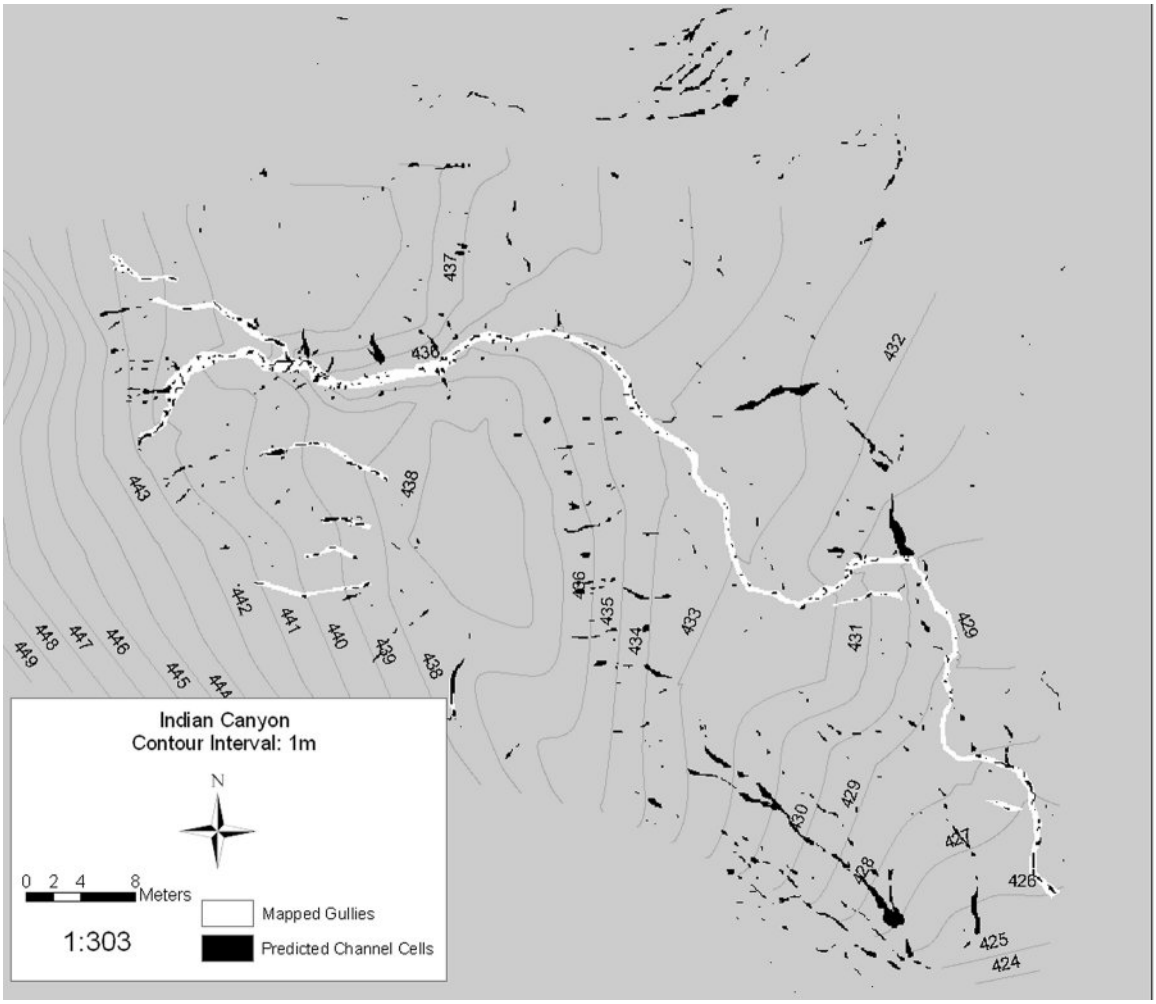

Figure M.1. Gully threshold map for Indian Canyon.

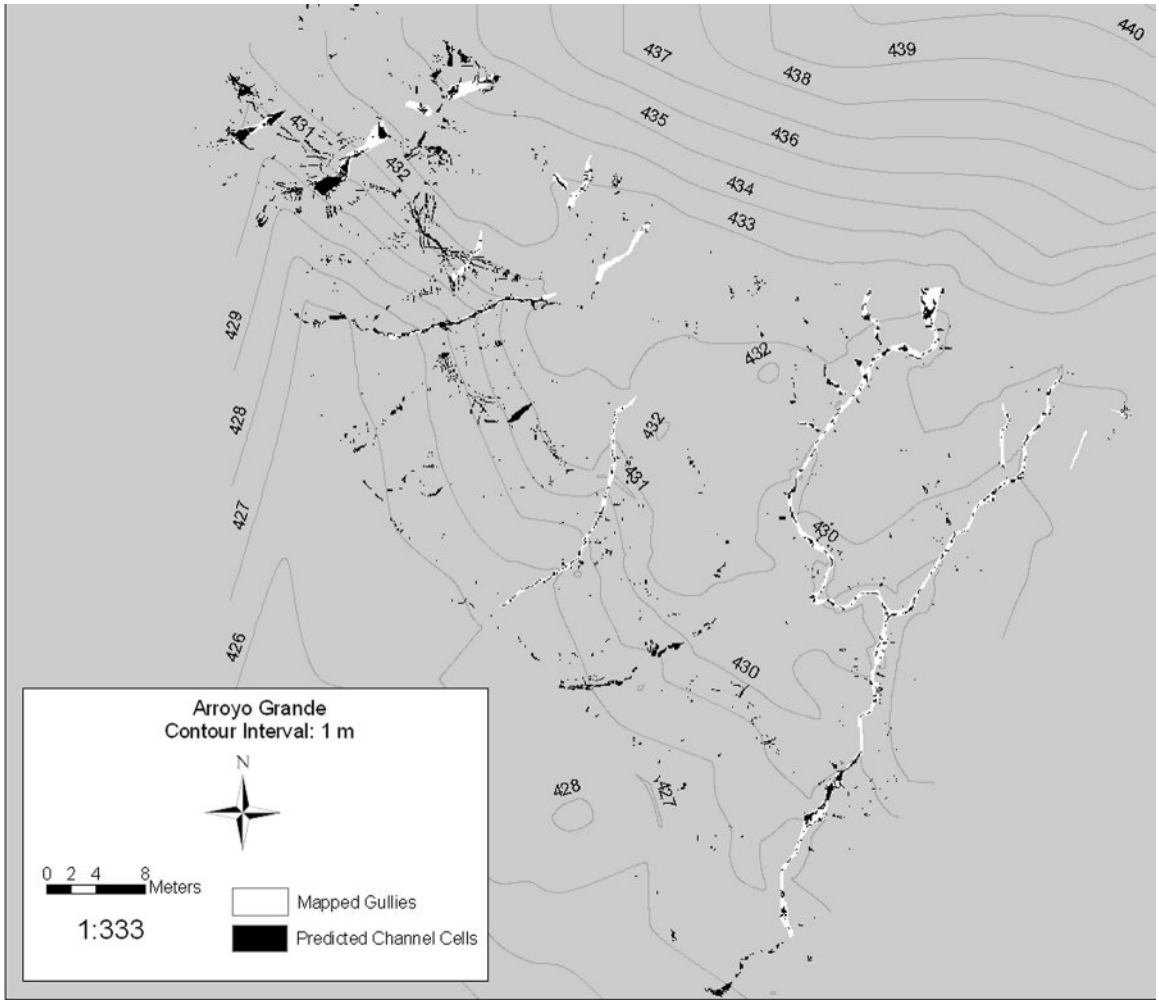

Figure M.2. Gully threshold map for Arroyo Grande.

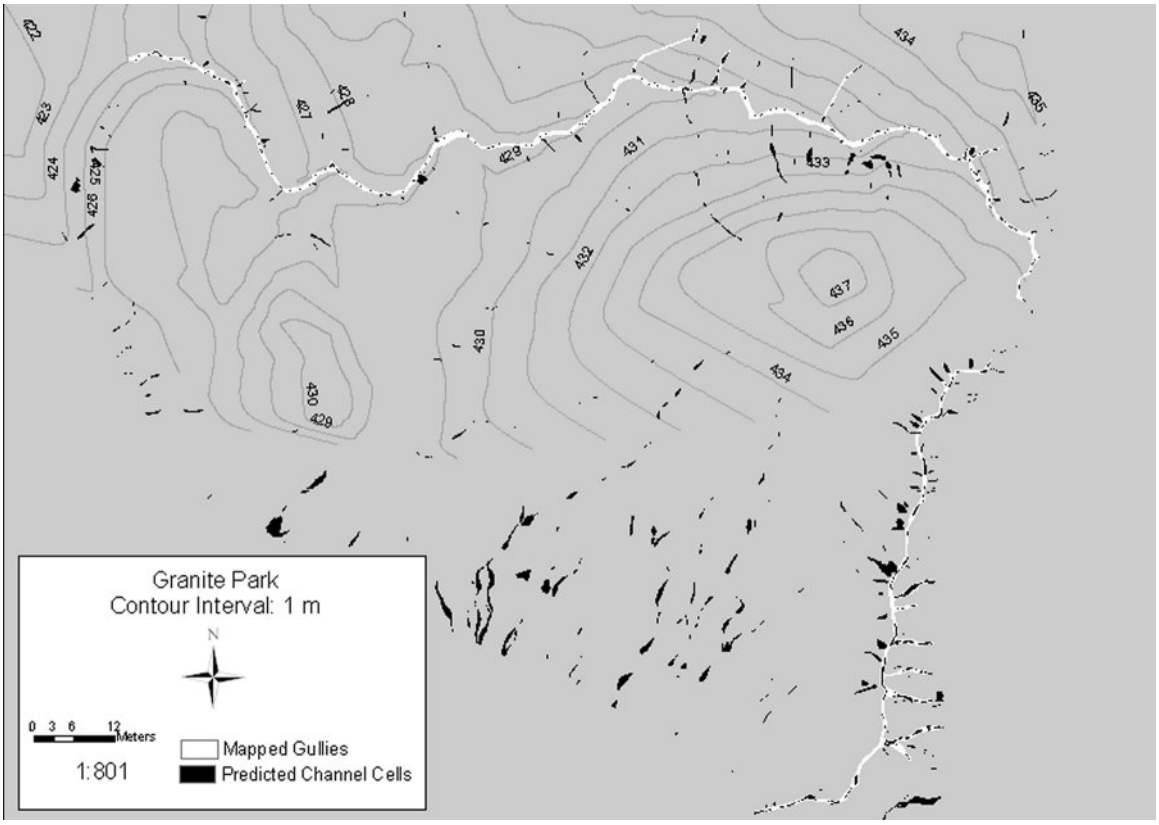

Figure M.3. Gully threshold map for Granite Park.

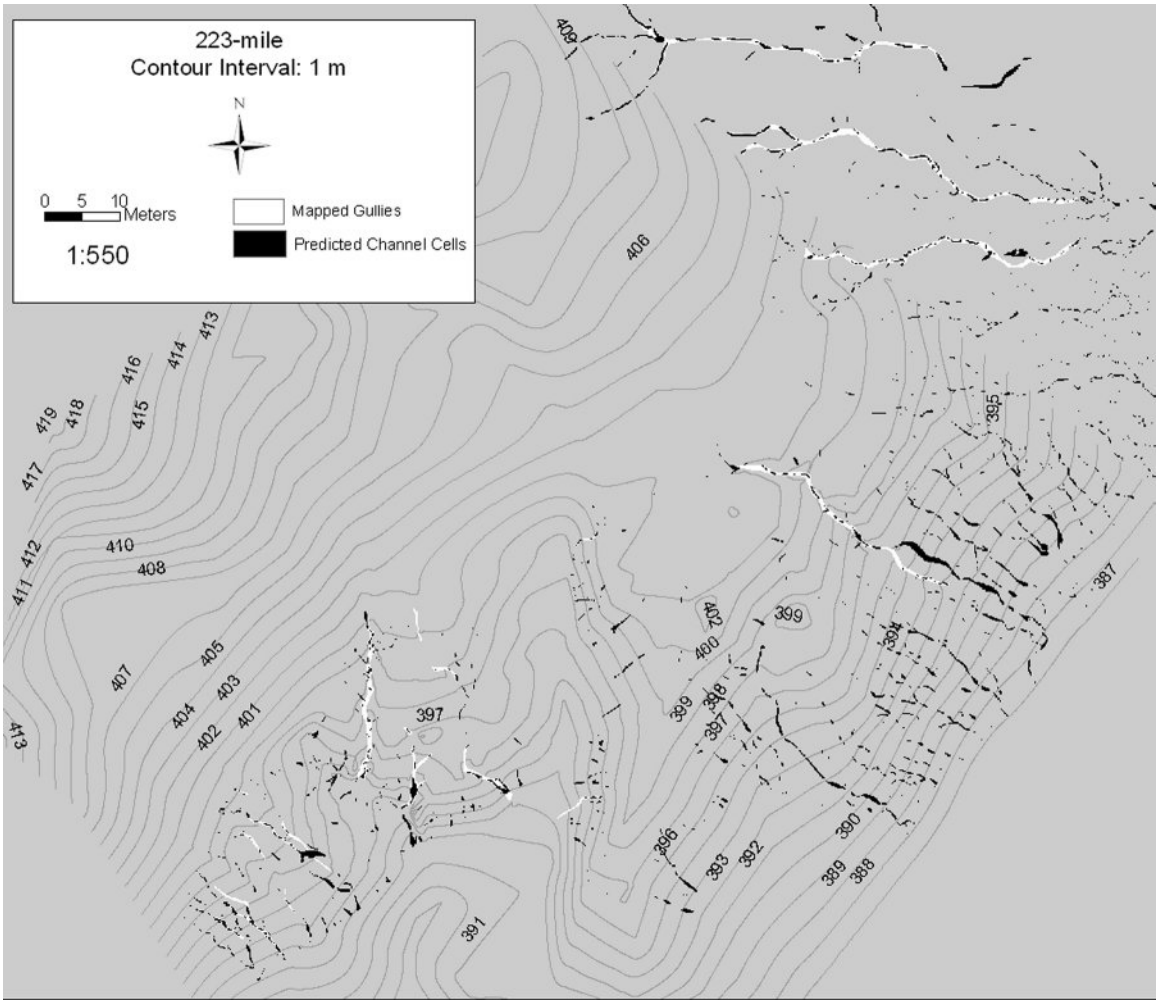

Figure M.4. Gully threshold map for 223-mile.